1949

THE PHYSICAL REVIEW

VOLUME 75 Second Series NUMBER 7

APRIL 1, 1949

Published for the

AMERICAN PHYSICAL SOCIETY

by the

AMERICAN INSTITUTE OF PHYSICS

[illegible] New York, N. Y.

A journal of exp

Published by the American Institute of Ph
for the
AMERICAN PHYSICAL SOCIE

Officers

President

F. W. Loomis
University of Illinois
Urbana, Illinois

Vice-President

I. I. Rabi
Columbia University
New York, New York

Secretary

K. K. Darrow
Bell Telephone Laboratories
Office:
Columbia University
New York 27, New York

Treasurer

G. B. Pegram
Columbia University
New York 27, New York

Local Secretary
for the Pacific Coast

J. Kaplan
University of California at
Angeles
Los Angeles, California

Managing Editor

John T. Tate
University of Minnesota
Minneapolis, Minnesota

The Physical Revie
Entered as second-class matter
Acceptance for mailing at special rate

VIEW

Established by E. L. Nichols in

BOARD OF EDITORS

Associate Editors

S. A. Goudsmit
E. M. Purcell
V. F. Weisskopf

Manuscripts for publication should be submitted to John
Minneapolis, Minnesota. The authors
to pay a publication charge of $4 per page which
to 500 free reprints. Instructions will be sent with

All correspondence concerning papers in the process
addressed to the Publication Manager, American
East 38 Street, New York 22, New York.

Subscription Price

Back Numbers

Vol. 1, 1913–Vol. 74, 1948
prior to July, 1929;
July, 1929–December, 1941;
January, 1942–December, 1946.

for back numbers should be
Pennsylvania, or to the
New York 22, New York.

the case of members of the
Treasurer; in the case of
Institute of Physics.

Physics Department, Cornell University,

Printed by the Lancaster Press, Inc., Prince and Hillman Streets, Lancaster, Pennsylvania
Entered as second-class matter at the Post Office at Lancaster, Pennsylvania, under the Act of
Acceptance for mailing at special rate of postage provided for in paragraph (d-2), section 538, P. L. & R., authorized

THE
PHYSICAL REVIEW

A journal of experimental and theoretical physics established by E. L. Nichols in 1893

SECOND SERIES, VOL. 75, NO. 7 APRIL 1, 1949

The Disintegration of Se^{75}

MICHEL TER-POGOSSIAN, J. EUGENE ROBINSON, AND C. SHARP COOK
Department of Physics, Washington University, St. Louis, Missouri
(Received December 20, 1948)

The photoelectrons produced in both lead and uranium radiators by the gamma-rays following K-capture in Se^{75} have been investigated using a uniform field, semi-circular magnetic spectrometer. The gamma-rays thus found have energies of 76 kev, 123 kev, 137 kev, 267 kev, 283 kev, and 405 kev with a possible radiation at approximately 99 kev. A tentative decay scheme is proposed.

I. INTRODUCTION

THE 125-day activity which has been assigned[1-2] to Se^{75} and which decays by K-capture to As^{75} has been studied in order to determine the energies of the gamma-rays present in its disintegration. A possible decay scheme has also been proposed.

A somewhat similar investigation using a lens spectrometer reports[3] gamma-rays having energies of 0.097, 0.122, 0.137, 0.265, and 0.400 Mev.

II. APPARATUS

The uniform field semicircular magnetic spectrometer used for these investigations has been previously described in some detail.[4] The radius of curvature of the electron path between source and counter is 14 cm. Baffles have now been placed at 30°, 90°, and 150° from the source in order to reduce possible errors caused by scattering.

The magnetic field is measured by the flip coil and ballistic galvanometer arrangement previously described.

The counter is of the end window type, the opening for the window being in the form of a narrow slit which serves also as the exit slit of the spectrometer.

Windows used in this experiment were made either of Nylon or Zapon, the former having a lower cut-off energy of 26 kev (550 gauss-cm of momentum) and the latter a similar cut-off energy of 2 kev (150 gauss-cm). Pressure in the thin Zapon window counter was kept constant by means of a pressure control device described elsewhere.[5] Both counters were normally operated with an argon-ethylene mixture ratio of four to one and a total pressure of 8 cm Hg.

III. EXPERIMENTAL DETAILS AND RESULTS

The Se^{75} measured in this investigation was obtained through slow neutron bombardment of selenium powder in the pile at Oak Ridge. A spectrographic analysis (as furnished by Oak Ridge) of the selenium used in the bombardment indicates nothing more than traces of any impurity, with the lines of selenium being very strong. A careful study indicates that the chances are very small that any of the gamma-rays found are the result of impurities in the sample bombarded. Since no selenium isotope other than Se^{75} has a comparatively long half-life,[6] the investigation of the gamma-rays was not begun until approximately one month after the active sample had been received from Oak Ridge. For this reason all gamma-rays found should be associated with the decay of the single isotope Se^{75}.

Because of the large number of lines which

[1] H. N. Friedlander, L. Seren, and S. H. Turkel, Phys. Rev. 72, 23 (1947); Phys. Rev. 72, 888 (1947).
[2] W. S. Cowart, M. L. Pool, D. A. McCowan, and L. W. Woodward, Phys. Rev. 73, 1454 (1948).
[3] E. N. Jensen, L. J. Laslett, and W. W. Pratt, AECD-1836 (1948); E. N. Jensen, AECD-2399 (1948).
[4] F. N. D. Kurie and M. Ter-Pogossian, Phys. Rev. 74, 677 (1948).
[5] M. Ter-Pogossian, J. Townsend, and J. E. Robinson, Rev. Sci. Inst., in press.
[6] G. T. Seaborg and I. Perlman, "Table of the isotopes," Rev. Mod. Phys. 20, 585 (1948).

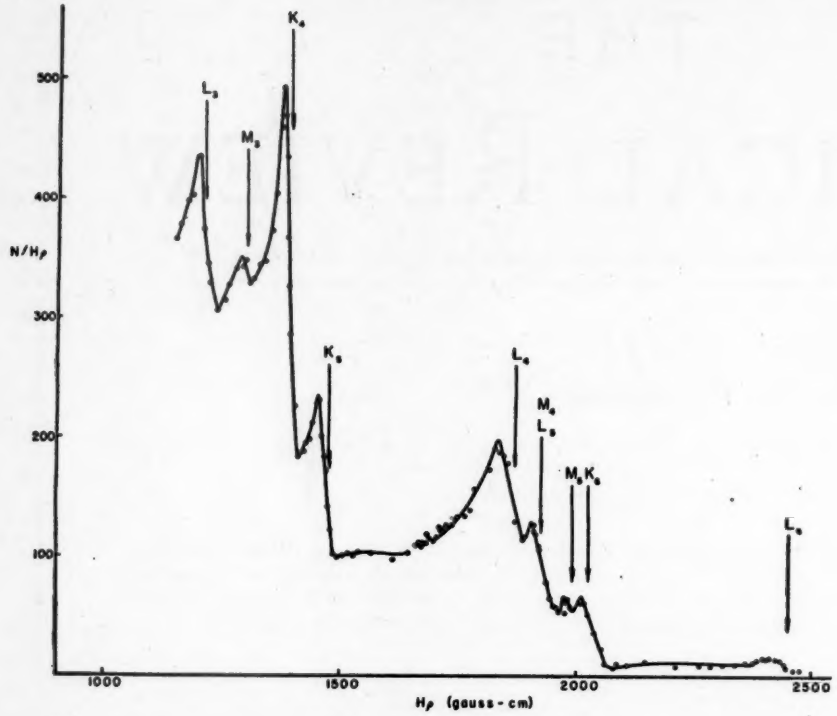

FIG. 1. Spectrum of the Compton and photoelectrons ejected from a 50-mg/cm² uranium radiator by the gamma-rays of Se^{75}.

required analysis both uranium and lead foils were used as radiators of photoelectrons. The use of both uranium and lead radiators greatly facilitates the assignment of the observed photoelectron lines to their respective gamma-rays, since the relative position of any one line in the two cases will depend markedly upon whether it is produced by the ejection of an electron from the K, L, or M shell of the atom. The thickness of both lead and uranium radiators was 50 mg/cm². The selenium source was placed immediately behind the radiator in either a copper or Lucite capsule.

The relative numbers of Compton and photoelectrons ejected from the uranium radiator are indicated in Fig. 1. Here the total number of electrons per unit momentum interval ($N/H\rho$) is plotted against momentum ($H\rho$ in gauss-cm). The window used in this case was the Nylon window. A similar result using the lead radiator and the Nylon window is shown in Fig. 2. In order to make a more accurate study of the low energy gammas the results shown in Fig. 3 were obtained using the same source and lead radiator as used to obtain Fig. 2, but this time with the thin Zapon window counter.

The photoelectron lines found have been analyzed as indicated in Table I into six distinct groups whose gamma-energies are: 76 kev, 123 kev, 137 kev, 267 kev, 283 kev, and 405 kev. These gammas have been indicated by the numbers 1 through 6, respectively, in the table and in the figures and their K, L, and M lines are indicated in the figures with appropriate subscripts. In addition to the lines thus analyzed there is a slight protuberance discernible in Fig. 3 at approximately 350 gauss-cm. If this slight rise is assumed to be produced by photoelectrons projected from the K shell of the lead atom, then the energy of the gamma-ray which produces these electrons must be approximately 99 kev. This is in agreement with the energy of 97 kev reported by Jensen *et al.*[3] for one of the gamma-rays from Se^{75}. Its proximity to the Zapon window cut-off energy will reduce its intensity by a considerable factor and thereby make it difficult to observe.

These results are in relatively good agreement with the results reported[3] by the Iowa State group. Two additional gammas have however been found, these being at 76 kev and 283 kev. Both of these radiations have more recently been observed[7] by the Iowa State group as indicated in Table I.

IV. POSSIBILITY OF A METASTABLE STATE

Laslett[7] has also indicated that in their work the 99-kev gamma-ray has been found as an internal conversion line but only weakly in the photoelectron spectrum. This, in conjunction with the current results showing a very weak photoelectron line, means that for this particular radiation the coefficient of internal conversion is quite large. There are in this region of the periodic table several cases where a large coefficient of internal conversion exists because of the high multipole order and

[7] L. J. Laslett, private communication.

small energy of the gamma-rays.[8] A nucleus which emits such a high multipole order low energy radiation is, in general, metastable with a half-life appreciably long in comparison to the lifetime of a nuclear state producing the more common dipole or quadrupole radiation.

In order to test for a metastable state in As^{75} a chemical separation of the type described by Friedlander *et al.*[1] was carried out with arsenic carrier being added to the active selenium. A check of the activities after separation revealed all the activity in the selenium fraction. From this, one concludes that a metastable state in As^{75}, *if it exists*, has a half-life sufficiently short that it cannot be measured by these techniques; that is of the order of magnitude of 20 seconds or less. Another investigation[9] reports that As^{75} has no metastable state whose half-life is in the range 10^{-6} second to 10^{-3} second. This narrows considerably the possible range of half-life values available to an As^{75} metastable state. The only other alternative is that the metastable state, *if it exists*, occurs in the parent nucleus, Se^{75}.

That the isomeric state should occur in Se^{75} seems quite reasonable in view of recent work[10] on the shell structure theory of the nucleus. It has been pointed out in this work that isomerism should in general be correlated with the odd member of the pair N, Z, where N represents the number of neutrons in a nucleus and Z the number of protons. For Se^{75} the odd member is $N=41$ whereas for As^{75} the odd member is $Z=33$. Two general islands of isomerism have been found in the regions $39 \leqslant (Z \text{ or } N) \leqslant 51$, and $63 \leqslant (Z \text{ or } N) \leqslant 81$. No such case of isomerism has been reported in the region $31 \leqslant (Z \text{ or } N) \leqslant 37$.

Experimental evidence for such a metastable state in Se^{75} is however non-existent. Using a Cauchois bent crystal spectrograph, Stokes[11] has studied the K_α radiation emitted by the active selenium. No trace of radiation having a wavelength corresponding to the K_α lines of selenium could be found whereas a strong arsenic K_α line was obtained.

TABLE I. Gamma-ray energies as calculated from photoelectron lines in the three sets of data compiled in the current investigation with comparative energies as reported by Jensen, Laslett, and Pratt.*

Gamma	Fig. 1	Fig. 2	Fig. 3	Jensen, Laslett and Pratt
1	—	76	76 (99?)	77** 99**
2		124	122	122
3	139	137	137	137
4	267	267		265
5	283	283		281**
6	407	404		400

* See reference 3.
** Private communication from Dr. L. J. Laslett.

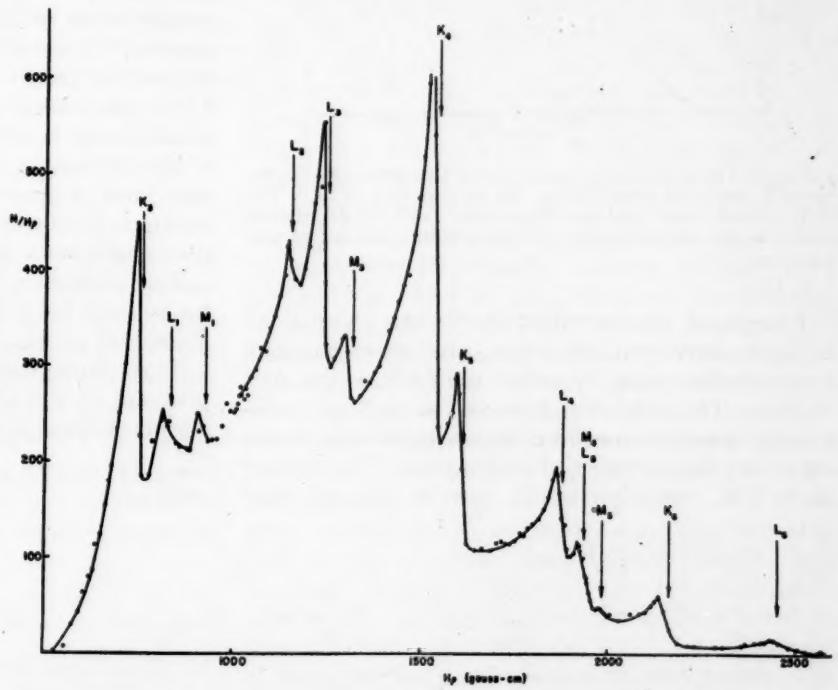

FIG. 2. Spectrum of the Compton and photoelectrons ejected from a 50-mg/cm² lead radiator by the gamma-rays of Se^{75}. The G-M counter used to obtain these data had a Nylon window which passed electrons whose energies were greater than 26 kev (550 gauss-cm of momentum).

[8] A. C. Helmholz, Phys. Rev. **60**, 415 (1941). Bradt, Gugelot, Huber, Medicus, Preiswerk, and Scherrer, Helv. Phys. Acta **XVIII**, 351 (1945).
[9] S. De Benedetti and F. K. McGowan, Phys. Rev. **74**, 728 (1948).
[10] E. Feenberg and K. C. Hammack, Phys. Rev. **75**, 332 (1949) and private communication.
[11] R. H. Stokes, AECD-1943 (1948) and private communication from Professor L. J. Laslett.

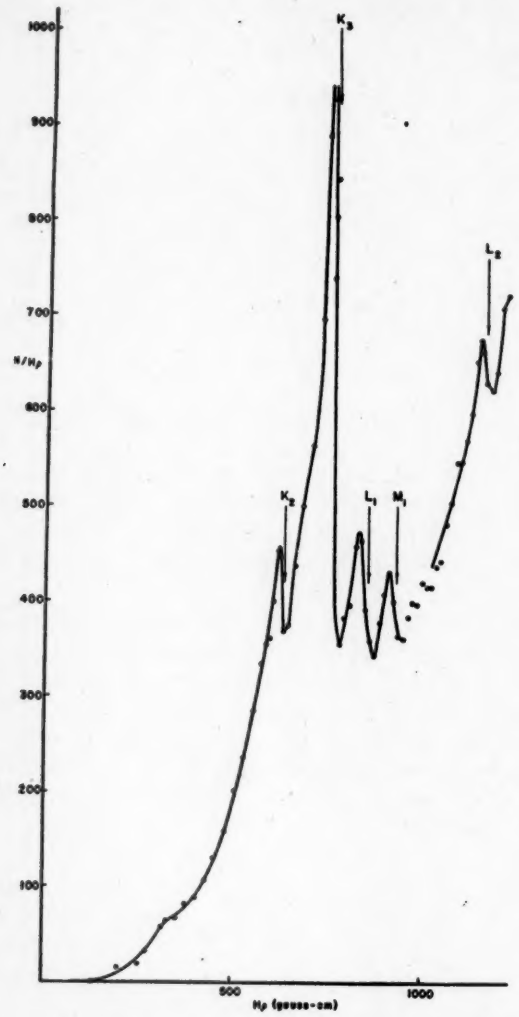

FIG. 3. The low energy region of the Compton and photoelectron spectrum produced by the gamma-rays of Se^{75}. The G-M counter used to obtain these data had a Zapon window with a lower cut-off energy of 2 kev (150 gauss-cm of momentum).

Except for the fact that the 99-kev gamma-ray is highly converted, there is no positive evidence of a metastable state in either the Se^{75} or the As^{75} nucleus. The evidence, however, is not yet sufficiently complete to make any definite conclusions regarding the existence of such a state. The absence of Se^{75} K_α radiation would seem to indicate that the metastable state, if it exists, is present in the daughter element, As^{75}.

Using the formula derived by Dancoff and Morrison[12] relating the conversion coefficient in the K shell and the multipole order (l) of the radiation:

$$\alpha_K = Z^3\alpha^4(l/l+1)(2/E)^{l+5/2},$$

where α is the fine structure constant, one finds that a multipole order $l=2$ would yield approximately 2 internal conversion electrons for every gamma-ray corresponding to the 99-kev transition. A half-life[8] of about 10^{-7} second would be expected for such a multipole order. For a multipole order $l=3$ about 25 internal conversion electrons are predicted for each gamma-ray with an expected half life of about 10^{-2} second. These half-lives are in the regions yet unexplored as indicated above and one of these half-lives may well be found upon the development of new techniques.

V. A TENTATIVE DISINTEGRATION SCHEME

It is of interest to note that the 123-kev and 283-kev gammas and the 137-kev and 267-kev gammas add, respectively, to 406 and 404 kev. These sums are identical within experimental errors with the single quantum transition producing the 405-kev gamma. It therefore seems quite reasonable to assume that the 137-kev and 267-kev gammas are in cascade as well as the 123-kev and 283-kev gammas, both of these groups then going to the ground state of As^{75} in parallel with the 405-kev gamma. One cannot immediately fit either the 76-kev nor the 99-kev gamma into such a scheme. Their positions in any tentatively proposed scheme would be quite arbitrary.

In addition to the ones reported here there has also been a gamma-ray at 10.3 kev reported by Stokes.[11] No attempt has been made to fit it into the level scheme here.

The authors wish to express their appreciation for several helpful discussions with Professors H. Primakoff and E. Feenberg.

This work has been supported by the joint program of the Office of Naval Research and the Atomic Energy Commission.

[12] S. M. Dancoff and P. Morrison, Phys. Rev. **55**, 122 (1939).

Some Excitation Functions of Bismuth

E. L. KELLY AND E. SEGRÈ
Radiation Laboratory, Department of Physics, University of California, Berkeley, California
(Received December 17, 1948)

Excitation functions have been measured, using a 38-Mev alpha-beam and a 19-Mev deuteron beam for the following reactions: Bi(α,2n)At^{211}, Bi(α,3n)At^{210}, Bi(d,p)RaE, Bi(d,n)Po^{210}, and Bi(d,3n)Po^{209}. The results are summarized in Figs. 4 and 5 and Tables I and II. A new isotope of astatine, At^{210}, has been identified; this isotope has a half life of 8.3 hr., decaying by K-capture to Po^{210} with the emission of a 1.0-Mev gamma-ray and a few conversion electrons.

BISMUTH has long been a favorite element for excitation function work. This is due in part to the fact that bismuth has a single stable isotope, is abundant, and is easily evaporated to form thin uniform films. Also, many of the products of bismuth bombarded with deuterons or alphas are alpha-active, which is convenient for determination of absolute counting rates. Early investigators[1–3] in this field had available deuterons up to 9-Mev energy. In later work deuterons up to 14 Mev[4] and alphas up to 28-Mev energy[5] were used. In spite of the excellence of the work that already had been done on bismuth, the availability of the 19-Mev deuteron beam and the 38-Mev alpha-beam of the 60-in. Crocker Radiation Laboratory cyclotron made further work seem worth while. The method used in the present work is the well-known stacked foil technique with some improvement in the definition of the energy and the measurement of the beam current. A stack of aluminum foils, each having a thin film of evaporated bismuth on one side, was exposed to the collimated beam of the Crocker 60-in. cyclotron. The stack was not thick enough to stop the beam which was caught in a Faraday cup, amplified, and fed into a recording milliameter. The mean range of the cyclotron beam was found by determining the amount of aluminum absorber required to reduce the beam intensity to one-half. The activity induced in the bismuth films was counted by means of a parallel plate ionization chamber. Figure 1 gives a schematic diagram of the apparatus used for the bombardments. Tables I and II and Figs. 4 and 5 give the final results, i.e., the cross sections for the various processes as a function of the energy of the bombarding deuteron or alpha-particle.

EXPERIMENTAL DETAILS

The aluminum foil used as backing for the evaporated bismuth, and for the energy determination absorbers, was punched on a die whose area was accurately measured. The dimensions of several foils were also measured with a traveling microscope. The areas of the various foils agreed to better than 3 parts in a thousand. Each backing foil, which was 0.001 inch thick, was thoroughly cleaned in CCl_4 and absolute alcohol, and weighed on an assay balance to the closest 0.01 mg. Next, the foils were placed in a high vacuum chamber and bismuth evaporated onto them to the desired thickness. (Most runs were made with 1 to 1.5 mg cm^{-2} of bismuth.) The foils were then reweighed and the thickness of bismuth determined with an estimated accuracy of 1 part in 200 or better.

The raw beam of the 60-in. Crocker cyclotron had enough inhomogenity in energy so that a better definition of the energy was required. This was obtained with a collimation system which consisted of the deflector channel of the cyclotron and the $\frac{1}{8}$-inch slit shown in Fig. 1. Because of the fringing magnetic field of the cyclotron, this collimation system served as a velocity selector producing a beam of very homogeneous energy. Tests of energy *versus* deflector voltage showed a dependence of 0.04 Mev per kilovolt on the deflector. In practice the deflector voltage was held constant within 2 kilovolts for the entire run. Since this collimation reduced the primary beam intensity by a factor of approximately one hundred (from 10^{-5}–10^{-6} to 10^{-7}–10^{-8} amp.) a sensitive beam current integrator was necessary. The current to the Faraday cup of Fig. 1 (10^{-7} to 10^{-8} amp.) was amplified to 1 milliampere by a modified version of the current amplifier described by Vance,[6] and recorded on an Esterline Angus recording milliameter. The integrated beam current was found by planimetering the area under the trace. The trace of each run was planimetered by two people, and the agreement was 1 part in 200 or better. Allowance was made for the peculiar form of the Esterline Angus trace.

[1] D. G. Hurst, R. Lantham, and W. B. Lewis, Proc. Roy. Soc. **174**, 126 (1940).
[2] J. M. Cork, J. Halpern, and H. Tatel, Phys. Rev. **57**, 348 (1940); **57**, 371 (1940).
[3] R. S. Krishnan and E. A. Nahum, Proc. Roy. Soc. **A180**, 321 (1942).
[4] J. M. Cork, Phys. Rev. **70**, 563 (1946).
[5] D. R. Corson, K. R. MacKenzie, and E. Segrè, Phys. Rev. **58**, 672 (1940).
[6] A. W. Vance, Rev. Sci. Inst. **7**, 489 (1936).

The range of the collimated beam was determined in a manner similar to that described by Wilson.[7] The foil wheel shown in Fig. 1 contained aluminum absorbers differing in thickness by approximately 1 mg cm^{-2}. Each of these absorbers in turn was placed in the path of the beam, while the amount of beam current stopped and the amount transmitted were determined simultaneously by current amplifiers.[6] This gave the fraction of the total beam current transmitted for various thicknesses of aluminum absorber. From this data the mean beam range was at once determined. The position of the foil wheel could be changed by remote control, and since the stacked bismuth foils were contained in the wheel it was possible to determine the beam range, bombard the stacked bismuth foils, and redetermine the beam range without turning off the cyclotron. The range data for a typical run are plotted in Fig. 2. It will be noted that there was little change in the beam range during the run. The straggling of 1.1 percent compares favorably with the theoretical minimum of 0.9 percent given by Livingston and Bethe.[8] The range in aluminum was converted to energy using the table of Smith.[9]

The activity induced in the bismuth films was followed by counting each sample in a parallel plate ionization chamber having a depth of 1.5 cm and filled with argon at a pressure of 1.7 atmospheres. The pulses from electron collection in the chamber were fed into a preamplifier and then into an amplifier whose time of rise was 0.2 microsecond. The amplified pulses were discriminated and counted on a 256 scaling circuit and mechanical register. The counter was checked against a standard alpha-particle source (a thin uranium sample electro-deposited on platinum) at the beginning and end of each counting period, and was found to remain constant to one percent over the entire period of 2 years during which these studies were made. The background was 1 to 2 counts per minute. The counting rate of the uranium alpha-standard as a function of discriminator bias is shown in Fig. 3. The counting efficiency at the operating bias of 14 has been taken to be 0.50. This round number takes into account the absorption in the sample itself and the back-scattering from the support.

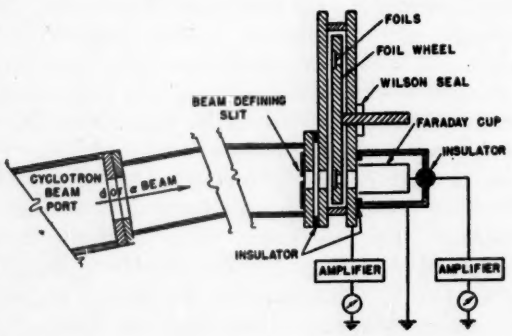

FIG. 1. Schematic diagram of the collimating tube, foil holder, and current amplifiers. This apparatus connects directly to the cyclotron tank and becomes therefore an integral part of the cyclotron vacuum system, obviating the need for any windows or separate pumps.

The possibility of error in the beam current measurements as a result of gas ionization or secondary electron emission was investigated. The space around the Faraday cup and the foil wheel was connected to the cyclotron tank during normal operation, as shown in Fig. 1. Since the pumping speed of the opening of the defining slits was small, a leak in this region could cause a substantial increase in pressure with a resulting increase in gas ionization along the path of the beam between the slits and the Faraday cup. Any selective collection of these gas ions would, of course, introduce an error. To test this effect, the pressure in the region of the Faraday cup was gradually increased until the cyclotron tank pressure showed a 50 percent increase. At this juncture the pressure in the region of the Faraday cup was approximately 10 microns of mercury, but no evidence of gas ionization was observed on the beam current meters. Since in normal operation no observable change in cyclotron tank pressure was produced by our apparatus, this source of error must be ruled out. The effect of possible secondary emission of electrons is also ruled out. The fringing magnetic field of the cyclotron is 2500 gauss in the region where the Faraday cup was located. The resulting curvature in the path of any secondary electron formed by the beam striking the bottom of the Faraday cup would be more than sufficient to prevent the escape of the electron.

Bi(α,2n) AND Bi(α,3n) EXCITATION FUNCTIONS

At bombarding alpha-energies below 29 Mev the only alpha-particle activity observed in the bombarded bismuth was that of At^{211}, which has a half-life of 7.5 hr. At higher bombarding alpha energies another alpha-activity was observed after the 7.5-hr. activity had died out. This was found to be due to Po^{210}. No other alpha-activity was detected. This made the separation of activities extremely simple. Alpha-counts 5 or 6 days after bombardment gave only the Po^{210} activity; correcting this for decay and subtracting from alpha-counts made within 24 hours after bombardment, we obtained the activity resulting from At^{211}, which could then easily be extrapolated back to the time of the end of bombardment. This method of sepa-

[7] R. R. Wilson, Phys. Rev. 60, 749 (1941).
[8] M. Stanley Livingston and H. A. Bethe, Rev. Mod. Phys. 9, 285 (1937).
[9] J. H. Smith, Phys. Rev. 71, 32 (1947).

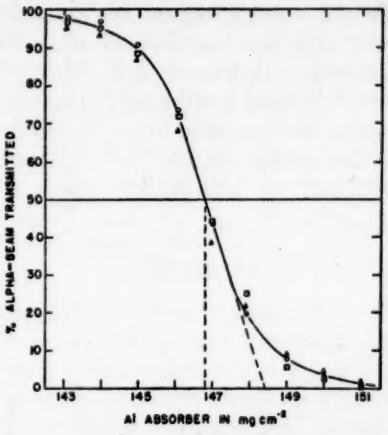

FIG. 2. The percent of the α-beam transmitted by the Al absorber plotted as a function of the absorber thickness. The three sets of points represent data taken before bombardment, at the middle of bombardment, and after bombardment of the bismuth foils. The straggling, given by the difference between the extrapolated range and the mean range divided by the mean range, is 1.1 percent.

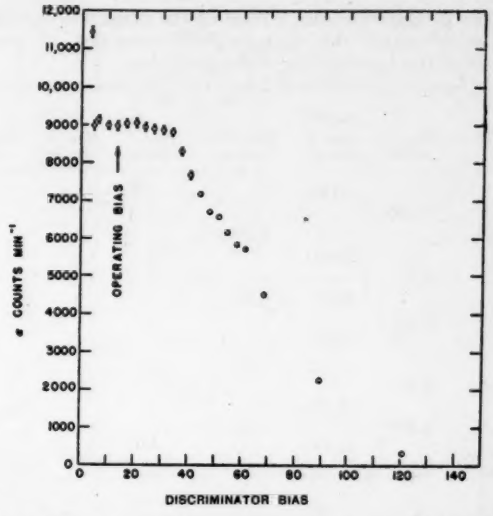

FIG. 3. Counts per minute of the thin U α-standard plotted as a function of the pulse discriminator bias voltage. The operating bias was kept constant to within 2 units.

rating the activities was quick and accurate.* The question immediately arose, however, as to the origin of the Po^{210}. Careful investigation, which will be discussed in detail later, showed that the Po^{210} came from the Bi(α,3n) reaction producing At^{210} which in turn decays to Po^{210} by orbital electron capture, with a half-life of 8.3 hr. Thus the At^{210} which had no alpha-activity decayed to an alpha-emitter which was readily counted on an absolute scale. The results of three runs were analyzed in this way and reduced to absolute cross section *versus* energy of the bombarding alphas. One run was made with bismuth films of 0.3 mg cm^{-2}, one with 1.5 mg cm^{-2}, and one with 2.0 mg cm^{-2}. When the results of these runs were first compared, a dispersion of a few percent was found, which was felt to be outside the experimental error. After thorough checking, this dispersion was tentatively laid to the inaccuracy in the stopping power ratio of bismuth to aluminum, which had been extrapolated from the value for gold given by Bethe.[8] A subsequent experimental determination of this stopping power ratio removed the apparent dispersion. The results of the three runs are shown in Fig. 4 and Table I.

Bi(d,p), Bi(d,n), AND Bi(d,3n) EXCITATION FUNCTIONS

The activities resulting from deuterons on bismuth are more difficult to separate than those from alphas on bismuth. Early work has established the production of RaE(Bi^{210}) and Po^{210} from the Bi(d,p) and Bi(d,n) reactions. Recent work[10] shows that the Bi(d,2n) reaction is not ordinarily observed and that the only alpha-activity at these energies, other than that due to the Bi(d,n) and Bi(d,p) reactions, is due to the Bi(d,3n) reaction which results in Po^{208} with a half-life of about 3 years. This is in agreement with the results of two deuteron on bismuth runs made by the authors.

For the separation of the Po^{210} with a 140-day half-life, the Po^{208} with a 3-year half-life, and the RaE, which goes by 5-day β-decay to Po^{210}, the following procedure was adopted.** Each sample was alpha-counted within several hours after bombardment and daily for a week; each sample was counted again after 2 months when all of the 5 day RaE had decayed into Po^{210}, and thereafter once every 3 months for a year. In order to determine the Po^{208} half-life, ten samples were analyzed by trial and error into 140-day Po^{210} and Po^{208}, such that when the Po^{210} activity was subtracted, the resulting activity fell on a straight line on semilog paper. The slope of this line gave the Po^{208} half-life. The result was 3.0 ± 0.2 years where the error given is based on internal consistency only. Each bombarded sample was then analyzed by the same method except that the resulting activity after Po^{210} subtraction was required to fit a straight line with a slope corresponding to a half-life of 3.0 years. This yielded the Po^{208} activity, which was extrapolated back to the time of the end of bombardment, and the total Po^{210} activity which was also extrapolated back to the time of the end of bombardment. Sub-

* This method neglects the 8.3-hr. half-life for formation of the Po^{210} mentioned below, but the resulting error introduced was found to be negligible in all cases.

[10] D. H. Templeton, J. J. Howland, and I. Perlman, Phys. Rev. 72, 758 (1947).

** It is not practical to use the difference in energy between the alphas of Po^{208} and Po^{210} to distinguish between the two because the difference is too small (5.298–5.14 Mev).

TABLE I. Experimental values of the cross section for the Bi(α,2n)At^{211} and the Bi(α,3n)At^{210} reactions at various energies of the bombarding alpha-particles.

α-energy Mev	$\sigma_{At^{211}}$ Run I barns	Run II barns	Run III barns	$\sigma_{At^{210}}$ Run I barns	Run II barns	Run III barns
18.8		0.000				
19.9	0.000					
20.0			0.000			
20.2		0.001				
21.2	0.01					
21.6		0.01	0.03			
22.4	0.10					
23.0		0.11				
23.1			0.16			
23.5	0.25					
24.2		0.29				
24.6	0.40		0.35			
25.4		0.45				
25.7	0.55					
26.1			0.57			
26.5		0.58				
26.7	0.67					
27.4			0.71			0.000
27.6		0.69			0.000	
27.7	0.75			0.000		
28.6	0.83		0.81	0.004		0.004
28.7		0.78			0.003	
29.6	0.90			0.013		
29.7		0.85			0.007	
29.9			0.90			0.015
30.5	0.89			0.06		
30.7		0.89			0.05	
31.0			0.91			0.10
31.4	0.86			0.17		
31.7		0.85			0.16	
32.2			0.81			0.28
32.3	0.75			0.35		
32.6		0.75			0.37	
33.1	0.62			0.53		
33.3			0.63			0.53
33.6		0.61			0.61	
34.0	0.48			0.73		
34.5			0.46			0.75
34.6		0.47			0.82	
34.8	0.39			0.93		
35.5		0.37			1.01	
35.6	0.30		0.33	1.03		0.94
36.4	0.24	0.29		1.14	1.16	
36.7			0.25			1.11
37.2	0.20	0.23		1.20	1.21	
38.0	0.17			1.24		
38.8	0.15			1.27		

tracting the extrapolated Po^{208} from the activity measured immediately after bombardment gave the Po^{210} due to the Bi(d,n) reaction. From the extrapolated total Po^{210} activity and the Po^{210} activity due to the Bi(d,n) reaction, the amount of RaE was found. The amount of RaE was also found by the growth of the total alpha-activity in the first week after bombardment. These two determinations of RaE agreed within one percent. The results of two runs of deuterons on bismuth reduced to absolute cross section *versus* energy of the bombarding deuterons are shown in Fig. 5 and Table II.

The Po^{208} activity seemed to be produced by deuterons of an energy too low to make a (d,3n) reaction. A further close examination of the alpha-activity in the energy region between 10 and 15 Mev showed that we had also another Po isotope present, emitting alphas of 4.95 Mev. This substance is Po^{209} formed by the (d,2n) reaction. If we assume that it decays only by α-emission and that the maximum cross section for its formation is about 10^{-24} cm^2, a half-life of about 200 years results.

ASTATINE^{210}

Bismuth bombarded with alpha-particles of 37-Mev energy yields the 7.5-hr. alpha-activity of At^{211}, and the 140-day alpha-activity of Po^{210}, as was mentioned above; in addition, there is an easily distinguishable gamma-ray activity. The Po^{210} alpha-activity was found to decrease with decreasing energy of the bombarding alphas, disappearing with alpha-energies below 29 Mev (see Fig. 4). The gamma-activity likewise disappeared with bombarding alpha-energies below 29 Mev. The gamma-activity was found to follow the At^{211} alpha-activity quantitatively through a chemical separation and through a vacuum distillation over to a cold platinum plate.[11] In the separated astatine fraction Po^{210} alpha-activity could be observed after the relatively short-lived At^{211} alpha-activity had decayed out. These results suggested that Po^{210} was formed as a decay product of a new isotope of astatine, probably by capture of an orbital electron of At^{210} which had been formed by an (α,3n) reaction on bismuth.

In order to study the formation of the Po^{210} more carefully, a G-M counter was constructed having an optimum x-ray counting efficiency in the region of the K x-rays of polonium. This counter was a Chicago type, having a cyclindrical aluminum wall 0.25 mm thick lined with tin foil 0.08 mm thick.

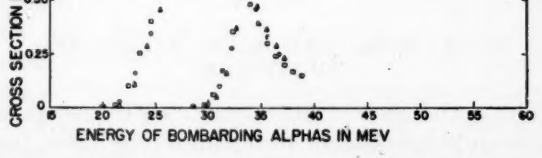

FIG. 4. Absolute cross section for the Bi(α,2n) reaction and the Bi(α,3n) reaction plotted as a function of the energy of the bombarding alphas.

[11] For the separation methods see Johnson, Leininger, and Segrè, "Chemical properties of astatine. I," J. Chem. Phys. 17, 1 (1949).

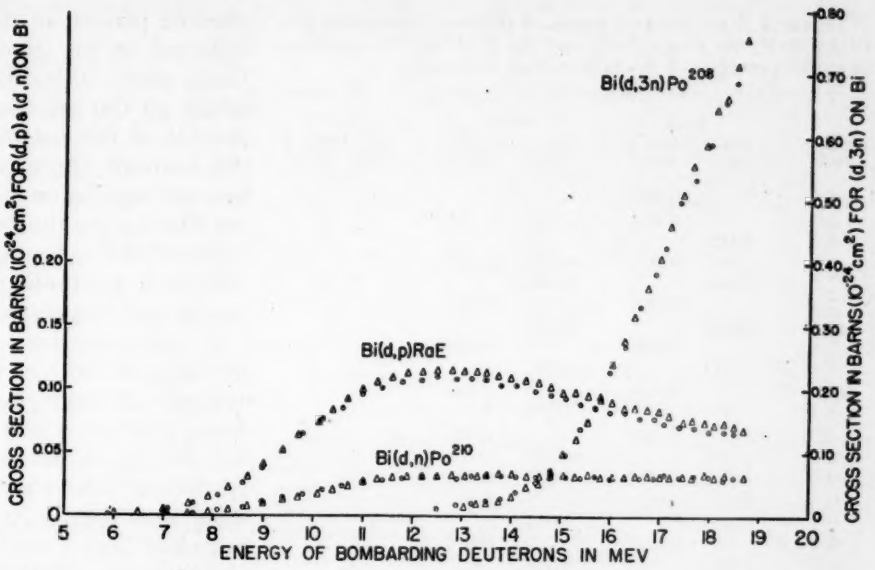
CROSS SECTION IN BARNS (10^{-24}cm^2) FOR (d,p) & (d,n) ON Bi
CROSS SECTION IN BARNS (10^{-24}cm^2) FOR (d,3n) ON Bi
Bi(d,3n)Po^{208}
Bi(d,p)RaE
Bi(d,n)Po^{210}
ENERGY OF BOMBARDING DEUTERONS IN MEV

FIG. 5. Absolute cross sections for the Bi(d,p), Bi(d,n), and the Bi(d,$3n$) reactions plotted as a function of the energy of the bombarding deuterons.

The counter was filled with argon plus 10 percent of alcohol to a pressure of 10 cm of mercury.

Two samples of astatine were studied with this G-M counter and with the alpha-counter. Sample A was prepared by bombarding thin bismuth with alphas of 25-Mev energy and then extracting the astatine by a vacuum distillation over to a cold platinum plate; sample B was prepared in the same way except that the bombarding alphas had an energy of 37 Mev rather than 25 Mev. Absorption in lead indicated that a gamma-ray of 1.0-Mev energy was present in sample B but was not present in sample A, as is shown in Fig. 6. This gamma-ray was found to decay with a half-life of 8.3 hours. Absorption in aluminum showed that some 0.9-Mev electrons accompanied the gamma-rays; these were in all probability conversion electrons of the 1.0-Mev gamma-rays. Absorption in platinum and tungsten revealed that both samples emitted x-rays showing the absorption properties to be expected for the K lines of polonium. The ratio of the K x-ray counting rate to the alpha-counting rate was 10 to 14 times as large in sample B as in sample A. In sample A the half-life of the K x-rays was 7.5 hours; in sample B the half-life of the K x-rays was slightly more than 8 hours. Po^{210} was found in sample B but not in sample A. Clearly, sample B contained a new isotope of astatine, most if not all of which decayed into Po^{210} with the emission of K x-rays and gamma-rays.

The existence of At^{210} and its decay by orbital electron capture to Po^{210} being thus established, the question arises as to whether all the Po^{210} found in our alpha-bombardment was produced through the decay of At^{210} or whether some was formed directly by a Bi(α,$2np$) reaction. This question could be settled in several ways. The method we chose consisted, in principle, in dividing a thin bombarded bismuth foil into two equal parts and extracting all the astatine from one part immediately after bombardment. A week later only the Po^{210} activities were left and were readily determined by alpha-counting each sample. If all the Po^{210} formed is a daughter of At^{210}, the unextracted sample and the extracted astatine sample must each have the same activity. On the other hand, if some of the Po^{210} is formed directly at bombardment then the unextracted sample must have a greater activity than the extracted astatine sample.

In practice this procedure requires enough time so that an extrapolation must be made back to the time of the middle of the bombardment. In order to make this extrapolation the procedure was repeated allowing various time intervals between the bombardment and the astatine extraction. To eliminate the effect of unequal division of the bombarded bismuth foil and variation of the extraction yield, the amount of At^{211} alpha-activity in each sample was used for normalization. The ratio of the Po^{210} resulting from the decay of the extracted astatine to the total Po^{210} formed plotted as a function of extraction time is shown in Fig. 7. The decay is seen to agree quite well with the 8.3-hour half-life found for the gamma-rays. The zero time intercept (the time of the middle of the bombardment) shows that within the experimental error all the Po^{210} was formed by the decay of the At^{210}.

Clearly, the results shown in Fig. 7 are valid only if the astatine extractions are free from polonium contamination. For this reason the extraction process[11] employed here will be described briefly. When an alpha-bombarded sample of bismuth on aluminum is heated in the presence of silver in an evacuated glass vessel, the astatine vapor is selectively adsorbed by the silver. Careful tests have shown that after 10 minutes at 310°C more

TABLE II. Experimental values of the cross section for the Bi(d,p)RaE, the Bi(d,n)Po^{210}, and the Bi($d,3n$)Po^{208} reactions at various energies of the bombarding deuterons.

	σRaE		σPo^{210}		σPo^{208}	
d-energy Mev	Run I barns	Run II barns	Run I barns	Run II barns	Run I barns	Run II barns
5.3		0.0002				
5.9		0.001				
6.0	0.001					
6.5	0.002	0.002	0.0003	0.0003		
7.0	0.004		0.0006			
7.1		0.005		0.001		
7.5	0.008		0.001			
7.6		0.009		0.002		
7.9	0.014		0.002			
8.1		0.016		0.004		
8.3	0.021		0.004			
8.6		0.026		0.007		
8.7	0.030		0.006			
9.0	0.040	0.037	0.009	0.010		
9.4	0.051	0.051	0.011	0.013		
9.7	0.062		0.014			
9.8		0.064		0.017		
10.1	0.073		0.016			
10.2		0.076		0.020		
10.4	0.082		0.019			
10.6		0.084		0.023		
10.7	0.091		0.023			
11.0	0.099	0.095	0.026	0.026		
11.3	0.104		0.028			
11.4		0.100		0.028		
11.6	0.108		0.029			
11.8		0.105		0.029		
11.9	0.111		0.030			
12.2	0.112	0.107	0.030	0.031		
12.5	0.114	0.109	0.030	0.031		0.01
12.8	0.114		0.031			
12.9		0.108		0.029		0.02
13.1	0.113		0.030		0.01	
13.2		0.108		0.031		0.02
13.3	0.113		0.030		0.02	
13.5	0.112	0.107	0.031	0.031	0.02	0.02
13.7	0.110		0.033		0.02	
13.8		0.102		0.031		0.03
14.0	0.109		0.032		0.03	
14.1		0.102		0.030		0.04
14.3	0.106		0.030		0.04	
14.5	0.104	0.098	0.031	0.030	0.05	0.05
14.8	0.101	0.095	0.031	0.031	0.07	0.07
15.1	0.096	0.093	0.032	0.031	0.10	0.10
15.3	0.097		0.030		0.12	
15.4		0.088		0.030		0.14
15.5$_5$	0.094		0.032		0.15	
15.7		0.086		0.031		0.17
15.8	0.091		0.030		0.19	
16.0		0.082		0.029		0.23
16.0$_5$	0.089		0.030		0.24	
16.3	0.084	0.081	0.030	0.030	0.27	0.27
16.5	0.084		0.031		0.31	
16.6		0.078		0.030		0.33
16.7$_5$	0.084		0.031		0.36	
16.9		0.077		0.030		0.38
17.0	0.082		0.031		0.41	
17.1		0.073		0.032		0.43
17.2	0.079		0.031		0.46	
17.4	0.074	0.071	0.031	0.031	0.51	0.50
17.7	0.075	0.070	0.030	0.032	0.55	0.53
17.9	0.074		0.032		0.59	
18.0		0.067		0.032		0.59
18.1	0.072		0.030		0.64	
18.3	0.073	0.067	0.032	0.029	0.66	0.66
18.5	0.070	0.066	0.032	0.031	0.71	0.69
18.7	0.068		0.030		0.75	

than 85 percent of the astatine alpha-activity was collected on the silver foil. Under the same conditions, using a bombarded bismuth sample from which all the astatine had decayed out, only 0.07 percent of the polonium alpha-activity present in the bismuth appeared on the silver foil. For this astatine separation method neither the temperature nor the heating time was very critical; however, the bismuth had to be melted (273°C or more), and the polonium contamination increased slowly with increasing temperature.

If there were any appreciable alpha-branching in the decay of At^{210}, as there is in At^{211}, one should see evidence of this alpha-activity and evidence of the decay product, which would be Bi^{206} with a 6.4-day half-life. Examination of extracted astatine in the 48-channel pulse analyser[12] showed no alpha-activity other than that of At^{211} and Po^{210}. If the branching ratio had been 1 part in 100 or larger the resulting alpha-activity could have been observed. Examination of the astatine extracted from a thick bismuth target bombarded with 200-microampere hours of alpha-particles having an energy of 37 Mev showed no evidence of 6.4-day activity. If 1 part in 10^4 of the At^{210} had decayed by alpha-emission, the 6.4-day Bi^{206} would have been observable.

CONCLUSIONS

The (d,p) and (d,n) reactions have recently been treated in a paper by Peaslee. In this paper he

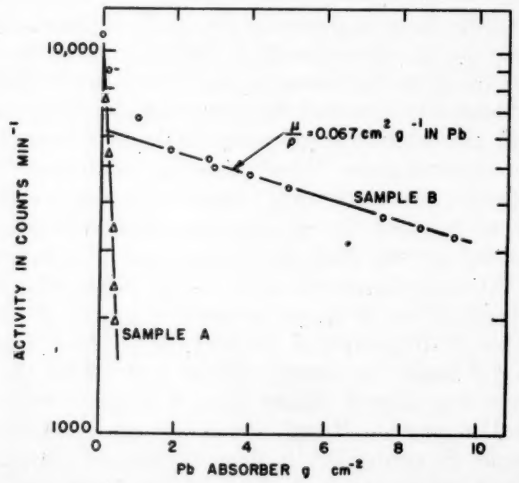

FIG. 6. The counting rate on a G-M counter of astatine samples plotted as a function of the thickness of lead absorber. Sample A consisted of the At extracted from a foil of Bi bombarded with alphas of 25-Mev energy; sample B consisted of the At extracted from a foil of Bi bombarded with alphas of 37 Mev. As a check of the geometry the mass absorption coefficient of a Co^{60}-γ-standard was measured and found to be 0.055 cm^2g^{-1} in Pb.

[12] Ghiorso, Jaffey, Robinson, and Weissbourd, "An alpha-pulse analyser apparatus," *Plutonium Project Record* **14B**, 17.3 (1948), to be issued.

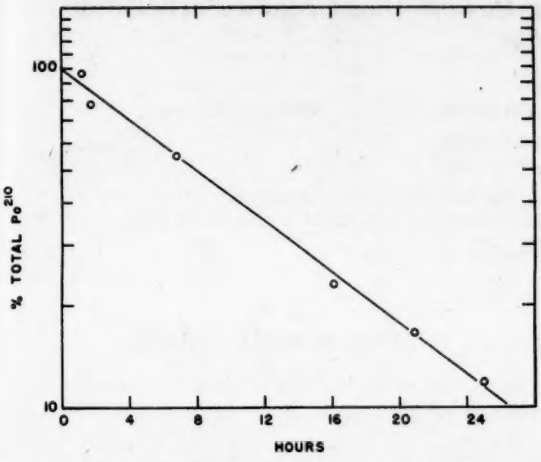

FIG. 7. The amount of Po^{210} formed by the decay of the extracted At^{210}, expressed as percent of the *total* Po^{210} formed, plotted as a function of the time from the middle of bombardment until the At extraction.

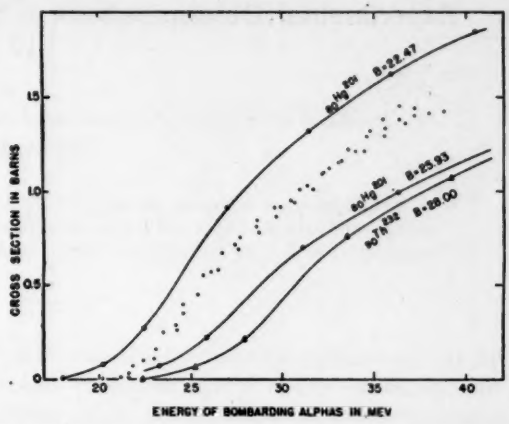

FIG. 8. The cross section of the compound nucleus (At^{213}) as a function of the energy of the bombarding nucleus. The solid lines represent the computed data of Weisskopf. The scattered points are experimental values of the sum of σ for Bi(α,2n) and σ for Bi(α,3n).

interprets our experimental material, and we refer to it for details.[13] The main qualitative conclusions are that the stripping processes of the deuteron as opposed to the formation of a compound nucleus in which the whole deuteron is absorbed are mainly responsible for the observed cross sections. In the (d,p) case the stripping process is the well-known Oppenheimer-Philips reaction; in the (d,n) case it is an analogous reaction.

The interpretation of the (α,2n) and the (α,3n) reactions can be made in a very simple semi-empirical way as follows.

Consider first the cross section σ_α for formation of the compound nucleus. This cross section has been calculated in some typical examples by V. F. Weisskopf.[14] In Fig. 8 the solid lines give Weisskopf's values for $_{80}Hg^{201}$ for two values of the barrier height, 25.93 Mev and 22.47 Mev corresponding to $r_0=1.3\times10^{-13}$ cm and 1.5×10^{-13} cm; the values are also given for $_{90}Th^{232}$ for a barrier height of 28.00 Mev corresponding to $r_0=1.3\times10^{-13}$ cm.

If we sum our (α,2n) and (α,3n) cross sections, we find passable agreement with Weisskopf's curve. See Fig. 8. This we interpret as meaning that all other competing reactions—(α,p), (α,pn), (α,γ), (α,α), etc.,—have small cross sections compared with (α,2n) and (α,3n) in the energy region considered. Exception to this is the (α,n) reaction which in the energy region around 20 Mev may have a cross section which, although small on an absolute scale, exceeds appreciably the (α,2n) cross section. Hence until experiments on this point are completed it will be impossible properly to fit the theoretical curve for the compound nucleus formation to our experimental data in the region near the threshold. An investigation of the (α,n) cross section is in progress.

It is interesting to consider the excitation energy of the compound nucleus above its ground state. The compound nucleus At^{213} in its fundamental state would certainly be alpha-radioactive. By comparison with neighboring known nuclei—At^{211}, AcC′, At^{212}, etc.,—one would make a fair guess of half-life of about 5×10^{-3} sec. and an alpha-energy of 7.5 Mev. Hence the excitation energy of the compound nucleus is approximately equal to the energy of the impinging alpha-particle minus 7.5 Mev. Thus to release 2 neutrons it takes at least $21.5-7.5=14$ Mev and to remove a third neutron an additional 8.5 Mev or at least $30-7.5=22.5$ Mev to remove 3 neutrons.

The cooperation of Dr. J. G. Hamilton, Mr. T. Putnam, Mr. B. Rossi, and other members of the 60-inch cyclotron group in making the bombardments for this work is gratefully acknowledged. Thanks are due Dr. R. F. Leininger for assistance in the preparation of the separated samples and also Mr. H. P. Robinson for help with the pulse analysis. The authors are indebted to Mr. R. W. Birge for the design and construction of some of the apparatus used and for some of the preliminary work on this problem.

This work was done under the auspices of the AEC.

[13] D. C. Peaslee, Phys. Rev. **74**, 1001 (1948).
[14] AEC Declassified Document MDDC 1175 (1947), *Lecture Series in Nuclear Physics*, LA24, Chapter 36, p. 105.

Experimental Determinations of Stopping Powers Using Alpha-Particles of 15 to 37 Mev

E. L. KELLY
Radiation of Laboratory, Department of Physics, University of California, Berkeley, California
(Received December 17, 1948)

The integrated stopping power relative to aluminum has been measured for copper, silver, tantalum, bismuth, and thorium using alpha-particles of approximately 15- to 28-Mev and 28- to 37-Mev energies. The results are summarized in Table II.

FOR the excitation function work described in the preceding article it was necessary to know the stopping power of bismuth for alpha-particles having energies between 20 and 40 Mev. Since the existing data were not sufficiently accurate for this work an experimental determination of the relative stopping power of various elements from thorium to aluminum was undertaken, using the alpha-particle beam of the Crocker 60-inch cyclotron. For reasons of convenience, only metallic elements were investigated, using aluminum as a standard of comparison. Beryllium, copper, silver, tantalum, bismuth, and thorium were originally chosen for investigation; unfortunately, suitable beryllium foil was unobtainable and this element had to be omitted.

The stopping power was determined in the following way. The range of the alpha-beam in aluminum was first determined. Next an absorber of the element to be investigated was placed in the path of the alpha beam, reducing the energy of the emergent alpha-particles. Then the range in aluminum of the reduced energy alphas was determined. The difference in the two measured ranges in aluminum represents the thickness of aluminum absorber which would produce the same energy loss (at the alpha-particle energy used) as would the absorber under investigation. This procedure was carried out at two alpha-particle energies, approximately 28 Mev and 37 Mev. The results are summarized in Table I.

TABLE I. Absorbers of equivalent stopping power. Each absorber "sandwich" reduced the alpha-beam to half-intensity —the alpha-beam traversing all "sandwiches" from left to right. "Sandwiches" of equivalent stopping power are indicated by equal signs.

62.7 Cu + 60.5 Al + 33.3 Al = 60.5 Al +	62.7 Cu + 34.5 Al = 144.0 Al
91.2 Ag + 54.1 Al + 28.7 Al = 54.1 Al +	91.2 Ag + 30.6 Al = 144.0 Al
90.9 Ta + 65.1 Al + 29.1 Al = 65.1 Al +	90.9 Ta + 32.0 Al = 144.0 Al
112.0 Th + 60.8 Al + 31.5 Al = 60.8 Al +	112.0 Th + 29.8 Al = 144.0 Al
62.7 Cu + 60.5 Al + 36.5 Al = 60.5 Al +	62.7 Cu + 37.4 Al = 147.0 Al
91.2 Ag + 54.1 Al + 31.6 Al = 54.1 Al +	91.2 Ag + 33.4 Al = 147.0 Al
90.9 Ta + 65.1 Al + 32.4 Al = 65.1 Al +	90.9 Ta + 34.8 Al = 147.0 Al
99.0 Bi + 60.8 Al + 34.5 Al = 60.8 Al +	99.0 Bi + 37.2 Al = 147.0 Al
99.1 Bi + 59.1 Al + 36.5 Al = 59.1 Al +	99.1 Bi + 39.1 Al = 147.0 Al
90.9 Th + 67.4 Al + 33.9 Al = 67.4 Al +	90.9 Th + 36.4 Al = 147.0 Al
90.9 Th + 66.6 Al + 35.0 Al = 66.6 Al +	90.9 Th + 37.5 Al = 147.0 Al

EXPERIMENTAL DETAILS

The set of absorbers first used in the experiment consisted of elements that were readily available in the form of thin foil, i.e., aluminum, copper, silver, tantalum, and thorium. The Th absorber was a single foil accurately ground to size. The Al, Cu, Ag, and Ta absorbers were cut to size on a die and consisted of three or more foils each, so that any slight thickness variation in the individual foils would tend to average out. In the second run of this experiment two bismuth absorbers of three foils each were added to the set. Also, thinner thorium foil was secured and two thorium absorbers of three foils each were also added to the set.

The apparatus used was a modification of that described in the preceding article and is shown schematically in Fig. 1. The wheel *A* contained the absorbers of the various elements to be studied together with suitable aluminum absorbers. Wheel *B* contained only aluminum absorbers differing by 1.0 mg cm^{-2}. The various alpha-ranges in aluminum were determined in a manner similar to that described in the preceding article. With wheel *A* in position 1 (112.5 mg cm^{-2} Al in the beam), readings were taken of the current stopped by wheels *A* and *B* and of the current to the Faraday cup; this was repeated for several positions of wheel *B*. In this way the mean beam range in Al was determined. Then wheel *A* was turned to position 2 (62.7 mg cm^{-2} Cu + 60.5 mg cm^{-2} Al) and the currents again read for suitable positions of wheel *B*. This procedure was followed for a cycle in the order 1, 2, 1, 2, 1, 3, 1, 3, ··· where the numbers refer to the position of wheel *A*. Thus the full alpha-energy

TABLE II. Values of the stopping power relative to aluminum computed from the data of Table I.

		Cu	Ag	Ta	Bi	Th
37-Mev alpha-beam	1st run	0.801	0.671	0.548		0.505
	2nd run	0.797	0.672	0.545	0.520	0.501
	Mean	0.799$_0$	0.671$_5$	0.546$_5$	0.520	0.503
Reduced energy beam	1st run	0.781	0.650	0.516		0.477
	2nd run	0.783	0.652	0.518	0.494	0.474
	Mean	0.782	0.651	0.517	0.494	0.475$_5$

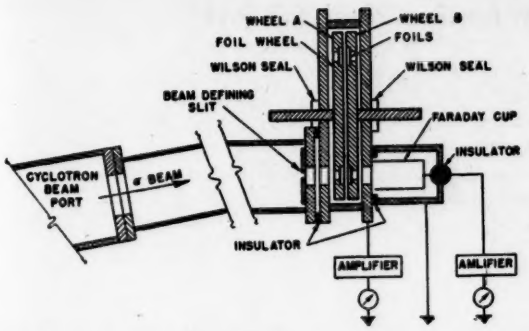

FIG. 1. Schematic diagram of the collimating tube, foil holders, and current amplifiers.

beam range was determined immediately before and after each reduced alpha-energy beam range determination.

To determine the stopping power for alpha-particles of 27 Mev in energy, the stack of foils in each position of wheel *A* was turned over (i.e., position 2 was changed from 62.7 mg cm^{-2} Cu+60.5 mg cm^{-2} Al to 60.5 mg cm^{-2} Al+6.27 mg cm^{-2} Cu). In this way the energy of the alpha-beam was lowered before the beam entered the various absorbers being investigated.

The α-beam was found to be remarkably constant in energy, the mean range remaining within $\pm\frac{1}{2}$ mg cm^{-2} Al for each cycle of data taken and within ± 1 mg cm^{-2} Al for the entire run. The 3-mg cm^{-2} difference in the range of the alpha-beam used in the two runs can be traced to changes made on the cyclotron. The resultant change in the relative stopping power, however, is too small to be observed, being about 1 part in 500.

RESULTS

The results of the two runs are summarized in Tables I and II. Each sandwich in Table I represents the average of 8 or more determinations. If the relative mass stopping power data of Table II is reduced to stopping power per electron as a function of log$Z$, the results fall very nearly on a straight line for each energy range. This is shown in Fig. 2. The deviation of thorium, although small, is felt to represent a real effect since the over-all error of this data is estimated to be less than one percent.

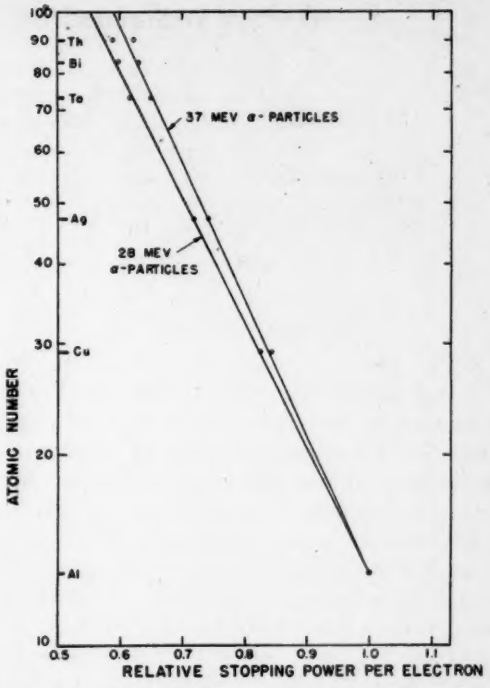

FIG. 2. Relative stopping power per electron as a function of the atomic number Z.

The cooperation of Dr. J. G. Hamilton, Mr. T. Putnam, Mr. B. Rossi, and other members of the 60-inch cyclotron group is gratefully acknowledged.

Neutron Diffraction Studies of Order-Disorder in Alloys*

C. G. SHULL AND SIDNEY SIEGEL**
Oak Ridge National Laboratory, Oak Ridge, Tennessee
(Received December 27, 1948)

Neutron diffraction techniques have been used to study order in the substitutional solid solutions FeCo, Ni_3Mn, and Cu_3Au. Superlattice effects have been found in the first two examples, which are difficult to study by x-rays.

INTRODUCTION

MANY alloy systems contain substitutional solid solution areas in which an atom A of one constituent merely substitutes at random for an atom B of the other species on the available sites of the lattice. When this substitution is random, the system is described as a disordered solid solution. In some systems, by suitable thermal treatment such a structure can be transformed into an ordered solid solution or superlattice, in which the A atoms are preferentially located with respect to neighboring B atoms, but still on the same lattice sites occupied in the disordered states. X-ray diffraction studies have been extremely instructive in revealing the facts of superlattice formation in such alloys.

A simple example of the order-disorder effects is shown in Fig. 1 for an AB alloy containing equal atomic percentages of the two atoms and crystallizing in a body-centered cubic structure. In the disordered state, B atoms have merely substituted at random for A atoms, whereas in the ordered state there are discrete planes of A atoms and discrete planes of B atoms.

Transformations from a disordered to an ordered state can be studied directly by x-ray diffraction techniques and indirectly by resistivity, specific heat, etc., measurements. Excellent reviews[1] of work performed in this field have been given by Nix and Shockley and by Barrett. The sensitivity of the x-ray diffraction method in detecting such changes depends upon the difference in scattering power of the atoms involved in the structure. Since this difference becomes unfavorably small in certain applications (in FeCo, for instance), it was thought that neutron diffraction techniques might usefully supplement the x-ray procedures. Neutron scattering cross sections do not vary as regularly or in the same manner as x-ray scattering cross sections; hence there are cases where the necessary differences are obtained with one technique and not with the other. This was recognized in early studies of neutron scattering from samples of ordered and disordered alloys by Nix, Beyer, and Dunning.[2] These investigators measured the change in transmission of Fe-Ni samples for a heterogeneous neutron beam obtained from a Ra-Be source. The experimental conditions under which these studies were performed were of necessity rather crude because of the very limited neutron intensity available at that time. Differences were obtained, however, in the transmission by samples of different heat treatment, and these were ascribed to the ordering of the lattice in certain cases.

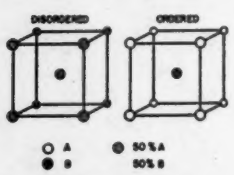

FIG. 1. Typical structure showing order-disorder effects for an alloy AB.

The two structures illustrated in Fig. 1 will produce markedly different diffraction patterns. A pattern characteristic of a simple body-centered cubic lattice and containing reflections (110), (200), (211), (220), (310), etc., will be obtained for the disordered sample while the ordered sample will show not only all of these reflections but the extra ones (100), (111), (210), (300) as well. In its simplest form then, the detection of superstructure is merely to search for the presence of the extra superstructure lines and the ease with which this can be done depends upon the relative intensities of the superstructure lines and the normal lattice lines.

In the Debye-Scherrer-Hull powder technique the intensity in a diffraction line (hkl) as obtained from a powder briquet plate is given by

$$I_{hkl}=\kappa(j_{hkl}F_{hkl}^2/\sin^2\theta_{hkl}), \quad (1)$$

where j_{hkl} is the multiplicity factor, F_{hkl} is the structure factor, θ_{hkl} the Bragg angle of scattering for the (hkl) reflection, and κ is a constant. For a completely disordered sample of AB having the structure shown in Fig. 1

$$F_{hkl}=f_A+f_B \quad (2)$$

* This document is based on work performed under Contract No. W-7405-eng-26 for the Atomic Energy Project at Oak Ridge National Laboratory.
** On leave from Westinghouse Research Laboratories, Pittsburgh, Pennsylvania.
[1] F. C. Nix and W. Shockley, Rev. Mod. Phys. 10, 1 (1938). C. S. Barrett, *Structure of Metals* (McGraw-Hill Book Company, Inc., New York, 1943), Chapter XII.
[2] F. C. Nix, H. G. Beyer, and J. R. Dunning, Phys. Rev. 58, 1031 (1940).

TABLE I. X-ray and neutron scattering amplitudes for various atoms.

	X-rays ($\sin\theta/\lambda=0.2$)	Neutrons
Mn	$4.17\cdot10^{-12}$ cm	$-0.32\cdot10^{-12}$ cm
Fe	4.33	+0.91
Co	4.54	+0.37
Ni	4.74	+1.04
Ni^{58}	4.74	+1.41
Ni^{60}	4.74	+0.3
Cu	4.95	+0.76
Au	14.90	+0.77

per AB molecule, whereas for the ordered sample the structure factors of the extra superstructure lines will be

$$F_{hkl}^{ss}=f_A-f_B \tag{3}$$

and the structure factors for the normal b.c.c. reflections from the ordered sample will be the same as (2). In these expressions f_A represents the scattering amplitude for an atomic center A. It is of interest to compare the scattering amplitudes for the x-ray and neutron cases and some typical values of use in the present studies are shown in Table I.

The x-ray scattering amplitudes vary in a regular fashion approximately as the atomic number and show a pronounced angular variation (form factor). For this reason they are shown evaluated at the angle corresponding to $(\sin\vartheta)/\lambda=0.2$. In contrast, the neutron scattering amplitudes show no regular variation with atomic number and are, moreover, independent of scattering angle since the scattering of slow neutrons is isotropic. The neutron wave-length (~1A) is much larger than the dimensions of the scattering nucleus (~10^{-4}A) and this results in isotropic scattering. The signs of the scattering amplitudes for the neutron case are generally positive but sometimes negative as in the case of manganese. For the x-ray case these are invariably positive except in the close vicinity of an absorption resonance when intermediate phases of scattering may be encountered. It is to be noted that different isotopes of the same element can possess drastically different neutron scattering properties, whereas this difference would not be present with x-rays.

The scattering amplitudes given in Table I can be used to compare the relative usefulness of x-ray or neutron diffraction in establishing the presence of superstructure. In illustrating this, the case of FeCo which crystallizes in a structure of the type shown in Fig. 1 will be used. Table II compares the intensities to be expected for the (100) superstructure reflection and the (110) normal lattice reflection for the two cases. These have been calculated using the x-ray amplitudes and scattering angles obtained with CoKα x-radiation and with a neutron wave-length of 1.06A. Suitable substitution in Eq. (1) provides the relative intensities. From these calculated values it is seen that neutron

TABLE II. Relative diffraction line intensities characterizing order and disorder in FeCo.

	X-rays	Neutrons
I_{100}	1	1
I_{110}	1390	6.0

scattering techniques would be much more sensitive for the detection of structural order. For other systems, the reverse may be true, depending upon the relative amplitudes of scattering for the constituent atoms.

Jones and Sykes[3] have extended the usefulness of the x-ray technique in these unfavorable cases by taking advantage of the anomaly in x-ray scattering power for radiation of wave-length near to that of an absorption edge. Thus when copper atoms are irradiated by ZnKα x-rays, the x-ray scattering amplitude is altered somewhat from its normal value and this may assist in establishing the presence of order in a copper alloy. They were able to show by this procedure that β-brass (CuZn) did exist in an ordered state at room temperature. Likewise, Ellis and Greiner[4] have shown the ordering which can be produced in FeCo.

EXPERIMENTAL RESULTS

For initial study, the three alloys FeCo, Ni_3Mn, and Cu_3Au appeared to possess exemplary scattering properties. The former two are extremely difficult to study with x-radiation for reasons discussed above, while the latter is quite amenable to x-ray techniques and has been extensively investigated. Details of the neutron diffraction techniques have been given in the literature[5] so these will not be discussed here. A monochromatic beam of neutrons (wave-length 1.06A) was diffracted by samples of loose powder held in position by parallel windows of thin aluminum. The powder diffraction pattern was obtained by counting the number of scattered neutrons at various angular positions of the detecting counter. The neutron counting rate

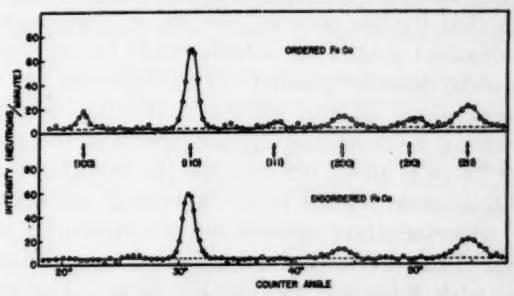

FIG. 2. Neutron diffraction patterns for ordered and disordered samples of FeCo.

[3] F. W. Jones and C. Sykes, Proc. Roy. Soc. **161**, 440 (1937).
[4] W. E. Ellis and E. S. Greiner, Trans. Am. Soc. Metals 29, 415 (1941).
[5] E. O. Wollan and C. G. Shull, Phys. Rev. **73**, 830 (1948).

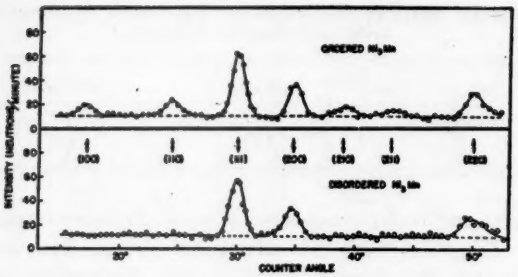

FIG. 3. Neutron diffraction patterns for ordered and disordered samples of Ni_3Mn.

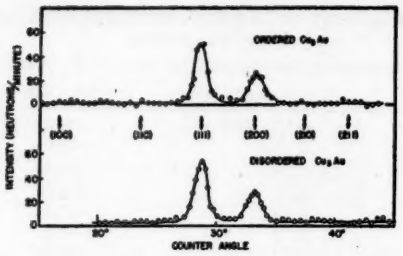

FIG. 4. Neutron diffraction patterns for ordered and disordered samples of Cu_3Au.

in the diffraction pattern was, at most, of the order of one neutron per second and, since this is only about five times normal counter background, it was necessary to scan the pattern a number of times to smooth out statistical fluctuations. All of the data have been corrected for counter background.

Figure 2 shows the patterns obtained for ordered and disordered samples of FeCo. The disordered sample had been quenched in water from 850°C, whereas the ordered sample had been slowly cooled from 750°C during a period of 100 hours. Extra diffractive features are to be noted at the superstructure line positions (100), (111), and (210) for the ordered sample in contrast to their absence for the disordered sample. Thus, ordering of the type shown in Fig. 1 is indicated for the slowly cooled sample.

The relative intensities of the (100) and (110) reflections of the ordered sample are about 1:5 by experiment and this compares not unfavorably with the calculated ratio 1:6 as shown in Table II. No great accuracy was sought for in the intensity evaluations but the data as such would indicate a fairly high degree of ordering in the sample. Accurate intensity measurements would, of course, permit a calculation of the degree of ordering. A second point of interest in the patterns is the presence of disorder scattering which is discernible in the pattern differences. The diffuse scattering for the disordered sample is about 20 percent larger than that for the ordered sample. A calculation of the disorder scattering (which would be isotropic if complete disorder existed) to be expected for this system gives as the diffuse scattering intensity about 0.6 neutron per minute, whereas the measured value is about 0.8 neutron per minute.

The system Ni-Mn is an interesting one because the superstructure intensities are enhanced as a result of the reversed phase of scattering for manganese with reference to that for nickel. The usual algebraic difference in the superstructure structure factors becomes a numerical sum in this case and the superstructure line intensities become comparable to the ordinary line intensities and can even exceed them in cases of favorable atomic ratio.

Figure 3 shows the patterns obtained for ordered and disordered samples of Ni_3Mn. Extra diffraction features are obtained at the superstructure line positions corresponding to (100), (110), (210), and (211) reflections for the ordered sample. The intensities of the extra lines turn out to be about 50 percent of those expected on the basis of the nuclear scattering amplitudes and this indicates that this particular sample was about 50 percent ordered and 50 percent disordered. The ordered preparation was given a slow cooling for 100 hours from 550°C. The ordered structure corresponds to a face-centered cubic lattice with Mn atoms at the corners and Ni atoms at the face-centered positions.

It has been mentioned earlier that different isotopes of an element can possess different neutron scattering amplitudes. The two major nickel isotopes illustrate this, as shown in Table I, with the Ni^{58} scattering amplitude being nearly five times that for Ni^{60}. This suggests that certain alloy systems can be best studied by selectively using one or the other (or a combination) of particular isotopes. The alloy $MnNi^{60}$ would show, for instance, very unusual patterns: the regular diffraction lines could be made vanishingly weak in comparison to the superstructure line intensities. Ni^{60} would be most suitable for study of the Ni-Fe system whereas Ni^{58} or normal Ni would be preferred in studying Ni-Co combinations.

Patterns for ordered and disordered samples of Cu_3Au are shown in Fig. 4 and here it is to be seen that the superstructure effects are undetectable. This is not unexpected since the neutron scattering amplitudes for Cu and Au are so close in value as listed in Table I. When the patterns of Fig. 4 were obtained, the Au amplitude was unknown and hence these patterns yielded the first value for this amplitude. Subsequent examination of the neutron diffraction pattern for metallic gold confirmed this value. In contrast to the results of the neutron diffraction examination, x-ray diffraction patterns for the ordered and disordered samples, kindly taken for us by Dr. M. A. Bredig, showed pronounced intensity differences indicative of ordering.

Helpful assistance in the task of data accumulation by Mr. M. C. Marney is acknowledged.

A New Measurement of the Packing Fractions of the Nickel Isotopes

A. E. SHAW
Argonne National Laboratory, Chicago, Illinois
(Received December 8, 1948)

The packing fractions of the nickel isotopes have been measured by comparison with known hydrocarbon lines using a double-focusing mass spectrograph. A new constant source of positive ions was used which produces mass spectra as high as the eighth order. The values of the packing fractions were determined to be: ^{58}Ni(-8.29×10^{-4}); ^{60}Ni(-8.69×10^{-4}); ^{61}Ni(-8.75×10^{-4}); ^{62}Ni(-9.01×10^{-4}); ^{64}Ni(-8.62×10^{-4}). The binding energies of the neutrons added to form the heavier isotopes are tabulated. An explanation is suggested for the differences in the packing fractions reported here and those given by Okuda and his associates.

INTRODUCTION

THE first determination of the packing fraction of nickel was made by Aston,[1] who used the doublets given by the approximate ratios ^{58}Ni:CO_2 and CH_4:^{12}C. These measurements led to a value of -10×10^{-4} MU for the packing fraction of ^{58}Ni. In 1938 Aston repeated his measurements[2] using his new spectrograph and the doublets ^{58}Ni:CO_2 and ^{16}O:^{12}C. These measurements gave a value of -8.35×10^{-4} MU for ^{58}Ni. In these early measurements the source of ions was a high voltage discharge through a vapor of $Ni(CO)_4$, modified by the introduction of CO_2 to reduce the tendency of the discharge to decompose the $Ni(CO)_4$. In other experiments, the $Ni(CO)_4$ was cooled to -20°C and the pure vapor was passed continuously into the discharge tube. Notwithstanding the various precautions that were taken, the discharge was unsteady and spectra beyond the first order were not sufficiently intense to be useful.

In 1941 a new determination of the packing fractions of the nickel isotopes was reported.[3] The source of positive ions for this measurement was a high voltage discharge through a vapor mixture of $Ni(CO)_4$ and normal heptane, $n-C_7H_{16}$. No further details were given on the source but in a previous paper,[4] it was stated that a cylindrical discharge tube was used with an aluminum bar anode and a concave iron cathode. In the absence of more details it is difficult to judge the constancy or reproducibility of this source of positive ions.

Generally speaking, a high voltage gaseous discharge tends to produce an intermittent and fluctuating beam of ions. This occurs in many cases because of the tendency of the discharge to decompose the chemical compounds that are introduced and because of the accumulation of sputtered material. In view of the uncertainties of this type of source and the apparent rapid and irregular variation in the binding energy of the nickel isotopes, as deduced from the packing fraction measurements of Okuda[4] and his associates, it was deemed desirable to make new measurements under completely different conditions.

SOURCE

The positive ions of nickel were derived from a new ion source,[5] the schematic representation of which is shown in Fig. 1. The tungsten crucible, which holds the metal to be vaporized, was made by drilling a hole 2.5-mm diameter, and 5-mm deep in a pure tungsten rod 5-mm diameter and 9.5-mm long. A flat spot was ground on the opposite end of this tungsten rod and a one-mm support rod of pure tungsten spotwelded to this point. The material to be vaporized was introduced into the crucible after which a tight fitting, pure tungsten cap was placed over the hole in the crucible. This cap as provided with an axial hole 0.25-mm diameter which limited the cross section of the beam of emerging vapor.

The crucible thus prepared was supported in the axis of a pure tungsten filament in the form of a circular loop. The filament was made of wire 0.425-mm diameter and operated at approximately 15 amperes. The plane of this filament was located 1.5-mm back from the plane of the tungsten cap. In this way electrons from the filament performed the double function of vaporizing the material within

TABLE I. Packing fractions f_1 of nickel isotopes.

Doublet	Number of doublets	$(f_2-f_1)\times10^4$ MU	$f_1\times10^4$ MU
^{58}Ni$^{+2}-{}^{12}C_2H_4$	7	24.96	-8.29 ± 0.07
^{60}Ni$-{}^{12}C_5$	10	11.90	-8.69 ± 0.08
^{61}Ni$-{}^{12}C_5H$	9	13.24	-8.75 ± 0.08
^{62}Ni$-{}^{12}C_5H_2$	10	14.74	-9.01 ± 0.05
^{64}Ni$-{}^{12}C_4{}^{13}CH_3$	7	16.02	-8.62 ± 0.08

Note: The masses of ^{12}C and H used in the calculations of the packing fractions f_2, and the mass of the neu on used in the calculation of the binding energies are values recommended by K. T. Bainbridge, *Isotopic Weights of the Fundamental Isotopes*, Preliminary Report No. 1, National Research Council, June 1948, p. 19. The mass of ^{13}C was that given by S. Flügge-J. Mattauch, Physik. Zeits. 44, 192 (1943).

[1] F. W. Aston, Nature 120, 956 (1927); cf. also *Mass Spectra and Isotopes* (Edward Arnold & Co., London, 1933).
[2] F. W. Aston, Nature 141, 1096 (1938).
[3] T. Okuda, K. Ogata, H. Kuroda, S. Shima, and S. Shindo, Phys. Rev. 59, 104 (1941).
[4] T. Okuda, K. Ogata, K. Aoki, and Y. Sugawara, Phys. Rev. 58, 578 (1940).
[5] A. E. Shaw, Phys. Rev. 73, 1222 (1948).

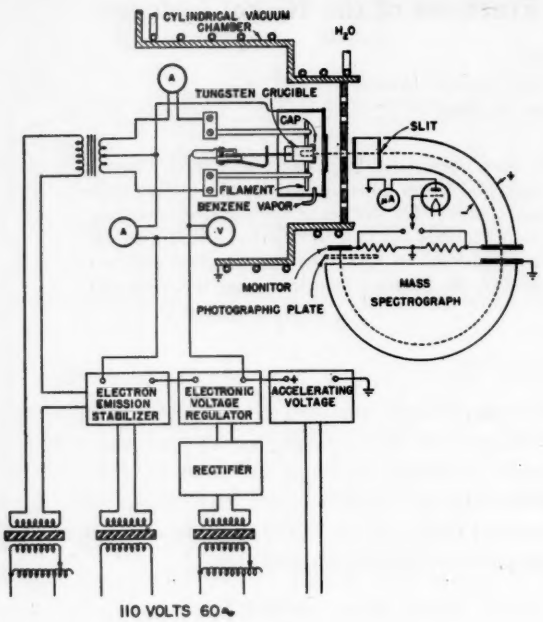

FIG. 1. Schematic diagram of positive ion source.

the crucible and ionizing it as it emerged through the hole in the cap. *It was found that this source produces spectra as high as the eighth order when the bombarding voltage is approximately 600.*

The thermal radiation given off by the hot crucible upsets the equilibrium of the filament by raising its temperature beyond the point corresponding to the power dissipated in it. Although the filament power may be controlled manually, for the best stability and reproducibility it is desirable to employ electronic regulating and stabilizing circuits. These are shown in block diagram in Fig. 1. Complete details of these circuits and the source will be published elsewhere.

The supply voltages for the source enter through 30-kv isolation transformers since the source proper is above ground by the magnitude of the accelerating voltage. The coarse controls are provided by the variacs shown, whereas the fine controls are attached to the individual emission stabilizer and voltage regulator. The product of the electron current to the crucible and the bombarding voltage is taken as a measure of the power dissipated in the crucible. This is only approximate but it serves as a convenient means for reproducing a fixed set of conditions.

EXPERIMENTS

In order to utilize this source for packing fraction measurements of nickel, it was necessary to provide a standard hydrocarbon comparison line for each of the nickel isotope lines. This was accomplished by introducing benzene vapor (C_6H_6) directly into the ionization chamber through a small tantalum tube (see Fig. 1). Thus both the nickel vapor from the hot crucible and the benzene vapor were ionized simultaneously by the same 600-volt electrons. The hydrocarbon lines were sufficiently intense with pressure of the order of 5×10^{-5} mm Hg. The nickel lines were brought out with comparable intensity by 30 watts of electron power dissipated in the crucible. The photographs were made with a double-focusing mass spectrograph,[6] in which the principal slit was set at 0.020 mm. Exposure times varied from three minutes to five minutes. The monitor shown in Fig. 1 provided a check of the intensity and constancy of the ion beam. When desired, the photographic plate is moved into the path of the beam by means of an externally controlled Wilson Seal.

RESULTS

Second-order spectra were photographed to obtain a comparison line for ^{58}Ni, since no ion corresponding to $m/e=58$ has been observed with benzene. First order spectra contained the four doublets which were used for the measurements of ^{60}Ni, ^{61}Ni, ^{62}Ni, and ^{64}Ni. The hydrocarbon comparison line for ^{64}Ni was the ^{13}C isotope peak.[7] In Fig. 2 is shown a photographic enlargement of a typical triplet from which the doublet $^{58}Ni^{+2}$–$^{12}C_2H_5$ was obtained. Figure 2 also shows the four doublets in the first order.

All measurements of doublet separation were made on a Gaertner Comparator whose scale read directly in thousandths of a millimeter. Each final value of doublet separation was the result of five separate measurements that were generally reproducible to within ±0.002 mm. All measured values were given equal weight and expressed in terms of the probable error in the arithmetic mean. The packing fractions are given in Table I.

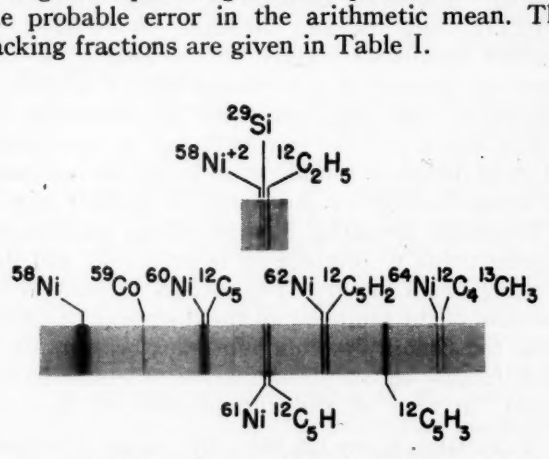

FIG. 2. Typical doublets used in calculation of packing fractions of nickel isotopes.

[6] A. J. Dempster, Phys. Rev. **53**, 64 (1938).
[7] "Mass Spectral Data," National Bureau of Standards, Washington, D. C., Serial No. 175, June 30, 1948.

TABLE II. Binding energies of n added neutrons.

Mass No. A	Atomic mass M	ΔM	n	Binding energy Mass units	Mev
58	57.9519				
		1.9960	2	0.0218	20.3
60	59.9479				
		0.9987	1	0.0102	9.5
61	60.9466				
		0.9975	1	0.0114	10.6
62	61.9441				
		2.0007	2	0.0171	16.0
64	63.9448				

DISCUSSION OF RESULTS

The packing fractions in Table I differ in several respects from those obtained by Okuda[8] and his associates, whose results were as follows:

^{58}Ni($f_1=-6.97\times10^{-4}$), ^{60}Ni($f_1=-8.37\times10^{-4}$), ^{61}Ni($f_1=-7.5\times10^{-4}$), ^{62}Ni($f_1=-8.14\times10^{-4}$) and

$$^{64}\text{Ni}(f_1=-8.22\times10^{-4}).$$

The largest discrepancy between their results and the values in Table I occurs at ^{58}Ni. The source of ions for their measurements was a high voltage discharge through a vapor mixture of $Ni(CO)_4$, and normal heptane, $n-C_7H_{16}$, the latter providing the standard hydrocarbon comparison lines. The ^{58}Ni mass was compared with a hydrocarbon mass that was assumed to be $^{12}C_4H_{10}$. In the case of many hydrocarbon compounds, the ion whose $m/e=58$, occurs as a peak with the isotope ^{13}C, for ionizing electrons of 50 and 70 volts. However, there are also numerous hydrocarbons in gaseous form such as 1, 2-diisopropylbenzene, n-butyl mercaptan and 2, 2-dimethylbutane whose mass spectra reveal the existence of normal peaks at $m/e=58$. In the case[8] of $n-C_7H_{16}$, the ion formed by electron impact corresponding to $m/e=58$ is $^{12}C_3{}^{13}CH_9^+$ and not $^{12}C_4H_{10}^+$, although it is conceivable this latter ion may occur in the high voltage discharge through the vapor mixture used.

If one compares the ^{58}Ni mass with the mass $^{12}C_3{}^{13}CH_9$, their value of f_1 is increased to -7.72×10^{-4}. In the case of ^{60}Ni, Okuda and his associates used a comparison mass which was assumed to be $^{12}C_5^+$. There is no evidence for the formation of this ion by electron impact,[8] although it may occur under the conditions of the high voltage discharge through the vapor mixture of $Ni(CO)_4$ and $n-C_7H_{16}$. The hydrocarbon ions corresponding to $m/e=61$, 62, and 64 do occur normally[8] under impact of 50 and 70-volt electrons.

The values of the packing fractions deduced by Okuda and his associates are all slightly smaller than those obtained in the present observations. The differences may be due to the fact that in their experiments as in all previous observations, except for recent experiments reported by Dempster,[9] an intermittent gas discharge was used as a source of ions.

The packing fractions in Table I enable one to calculate the true atomic mass of each of the nickel isotopes. Each of these isotopes is formed from the preceding one by the addition of neutrons, hence the binding energy of the added neutrons can be calculated from the actual increment in mass. Table II gives the values of binding energy for the n added neutrons in terms of mass units and Mev. The mass increase ΔM is in each case less than the neutron mass. Table II also reveals that the two neutrons involved in the formation of ^{60}Ni from ^{58}Ni are most firmly bound, while the additional pair added to ^{62}Ni to form ^{64}Ni are least firmly bound.

The atomic masses given in Table II enable one to calculate the atomic weight of the element nickel. Combining these masses and the relative abundances[10] of the nickel isotopes the atomic weight is found to be 58.70, referred to the chemical scale.

ACKNOWLEDGMENT

The author is deeply grateful to Dr. A. J. Dempster, Division Director, for many helpful suggestions and advice, and to Dr. Mark Inghram for the use of a Nier-Inghram gas leak, for his friendly interest and occasional suggestion.

[8] "Mass Spectral Data," National Bureau of Standards, Washington, D.C., Serial No. 14, October 31, 1947.

[9] A. J. Dempster, Phys. Rev. **74**, 1225 (1948).

[10] J. R. White and A. E. Cameron, Phys. Rev. **74**, 991 (1948).

Microwave Investigations of Methyl Fluoride, Fluoroform, and Phosphorus Trifluoride

O. R. GILLIAM, H. D. EDWARDS, AND WALTER GORDY
Department of Physics, Duke University, Durham, North Carolina*

(Received December 27, 1948)

From measurements on pure rotational transitions in the microwave region the moments of inertia, I_B in g cm$^2\times10^{-40}$, have been determined as follows: 32.8544 for $C^{12}H_3F$, 33.7444 for $C^{13}H_3F$, 81.0693 for $C^{12}HF_3$, and 107.286 for $P^{31}F_3$. The molecular dimensions determined are: for CH_3F, $d_{CH}=1.109$A, $d_{CF}=1.385$A, and $\angle HCH=110°\,0'$; for CHF_3, $d_{CF}=1.326$A, with $d_{CH}=1.111$A (assumed) and $\angle FCF=110°$ (assumed); for PF_3, $d_{PF}=1.546\pm0.008$A with $\angle FPF=104\pm3°$ (assumed). The line breadth parameters, $\Delta\nu$, normalized to 1 mm of Hg pressure are for CH_3F 20 mc, for CHF_3 18 mc, and for PF_3 16 mc. Confirming evidences for the nuclear spin values, $\frac{1}{2}$ for P^{31} and F^{19} have been obtained.

MEASUREMENTS have been made on pure rotational transitions of methyl fluoride, fluoroform, and phosphorus trifluoride occurring in the millimeter wave region. The experimental methods used have been described in previous publications.[1] The frequencies were measured by harmonics of a 10-mc signal monitored by radio station W W V, of the Bureau of Standards.

Table I lists the measured frequencies, B values, and moments of inertia. Each of these molecules has a strictly symmetric-top structure. For the low rotational states which are involved here the effects of centrifugal distortion are not very significant, and the rotational frequencies are given quite accurately by the simple formula,

$$\nu(\text{cm}^{-1})=2B(J+1)=[2h(J+1)/8\pi^2cI_B],$$

where J is the rotational quantum number for the lower state involved. However, for the $J=2\rightarrow3$ transition of PF_3, the $K=2$ line was resolved, and the centrifugal distortion constants D_J and D_{JK} in the more general equation,[2]

$$\nu(\text{cm}^{-1})=2B(J+1)-2D_{KJ}K^2(J+1)-4D_J(J+1)^3,$$

were evaluated as $+7$ Kc/sec. and -8 Kc/sec., respectively. The moment of inertia for CHF_3 recently determined from optical spectra,[3] $I_B=81.08\times10^{-40}$ g cm^2, is in remarkably good agreement with the present results. The I_B value obtained for $C^{12}H_3F$ lies between 32.95 and 32.21, the two values[4,5] previously obtained from infra-red spectroscopy. No previous spectral evaluation of the PF_3 moment of inertia has been made.

TABLE I. Pure rotational frequencies and molecular constants for ground vibrational state.

Molecule	Transition	Observed frequencies in mc/sec.	Absorption coefficients (cm^{-1})	B_0	$I_B^{(0)}$*
$C^{12}H_3F$	0→1	51071.69±0.18	1.4×10^{-4}	25535.85	32.8544
$C^{13}H_3F$	0→1	49724.73±0.18		24862.37	33.7444
HCF_3	1→2	41394.95±0.18	2.2×10^{-5}	10348.74	81.0693
PF_3	1→2	31279.60±0.10		7819.900	107.286
	2→3	46918.82±0.18 ($K=0$ or 1) 46919.02±0.18 ($K=2$)			
PF_3	2→3	46940±10 47010±10 47033±10 47040±10	excited vibration states		

* The value of h is taken as 6.624×10^{-27} erg-sec.

The value 5.52 g cm$^2\times10^{-40}$ was calculated from the Johnston-Dennison formula[6]

$$\sum\Delta\nu=[(6/I_A)-(7/I_B)](h/8\pi^2c),$$

with the I_B for $C^{12}H_3F$ determined in the present measurement and with $\sum\Delta\nu=24.44$ cm^{-1} obtained by re-averaging the data of Bennett and Meyer[4] on the three perpendicular type infra-red vibration-rotation bands. Bennett and Meyer give $\sum\Delta\nu=24.30$. This would require that $I_A=5.49$. In our re-averaging, we have omitted lines of high J at the ends of the observed bands. Possible error in the I_A makes uncertain the last figure quoted for d_{CH} and the bond angle, but it is not probable that the value given for d_{CF} will be significantly affected by this error since the determination of this dimension depends only slightly on I_A.

The surprisingly short d_{CF} distance in fluoroform

* This research was supported by U. S. Air Force Contract No. W-19-122-ac-35 with the Air Materiel Command, Watson Laboratories.

[1] (a) W. Gordy and M. Kessler, Phys. Rev. **72**, 644 (1947); (b) R. Unterberger and W. V. Smith, Rev. Sci. Inst. **19**, 580 (1948); (c) W. Gordy, Rev. Mod. Phys. **20**, 668 (1948).

[2] Z. I. Slawsky and D. M. Dennison, J. Chem. Phys. **7**, 509 (1939); G. Herzberg, *Infrared and Raman Spectra of Polyatomic Molecules* (D. Van Nostrand Company, Inc., New York, 1945), p. 400.

[3] H. J. Bernstein and G. Herzberg, J. Chem. Phys. **16**, 30 (1948).

[4] W. H. Bennett and C. F. Meyer, Phys. Rev. **32**, 888 (1928).

[5] K. P. Yates and H. H. Nielsen, Phys. Rev. **71**, 349 (1947).

[6] M. Johnston and D. M. Dennison, Phys. Rev. **48**, 868 (1935).

found by Bernstein and Herzberg[3] is confirmed. Fortunately, the moments of inertia of CHF_3 and PF_3 are not very sensitive to small variations in the parameters which must be assumed. Though the limits of error cannot be established definitely, the probable errors in d_{CF} and d_{PF} are indicated by the changes produced when the assumed angle is changed by $\pm 3°$. The electron diffraction values[6a] for PF_3 are $d_{PF}=1.52\pm0.04$A and $\angle FPF=104°\pm4°$. To our knowledge, no electron diffraction studies of fluoroform have been made.

Table III compares the CF and PF distances measured here with the added single bond covalent radii and with this sum corrected by the Schomaker-Stevenson rule[7] for the shortening caused by resonance with ionic structures. Bond lengths in some similar molecules recently measured with microwaves are listed for comparison. The Pauling[8] radii are here employed with the revised radius for carbon, 0.79A, suggested by Gordy,[9] and the fluorine radius, 0.72A, proposed by Schomaker and Stevenson.[7] For methyl fluoride, the Schomaker-Stevenson correction for resonance caused by ionic character provides a reasonably good explanation for the observed bond shortening, though for methyl chloride, bromide, and iodide this correction makes agreement with observation slightly worse. Pauling[10] has suggested resonance with double bonded structures as well as with ionic structures as a possible cause of the anomalously short bonds in molecules of the PF_3 type.

Unfortunately the determinations of the molecular structures are still not sufficiently accurate to establish the relative differences of the bond angles and CH lengths in the methyl halides. The latest values are: for the HCH angles, 110° 0′, 110° 0′, 109° 22′, and 110° 58′; for the CH lengths 1.109A, 1.109A, 1.111A, and 1.100A, for methyl fluoride, chloride, bromide, and iodide, respectively. The values for the last three are taken from the paper by Gordy, Simmons, and Smith.[11] In this paper an arithmetical error was made in the calculations for methyl bromide.* The corrected value is given here. It seems unlikely that the methyl bromide would fall out of sequence. Microwave studies on the methyl halides containing other isotopes are being undertaken by James W. Simmons. Thus these difficulties should soon be cleared up.

[6a] L. Pauling and L. O. Brockway, J. Am. Chem. Soc. **57**, 2684 (1935).

[7] V. Schomaker and D. P. Stevenson, J. Am. Chem. Soc. **63**, 37 (1941).

[8] L. Pauling, *The Nature of the Chemical Bond* (Cornell University Press, Ithaca, New York, 1940), p. 164.

[9] Walter Gordy, J. Chem. Phys. **15**, 81 (1947).

[10] L. Pauling, reference 8, p. 216.

[11] W. Gordy, J. W. Simmons, and A. G. Smith, Phys. Rev. **74**, 243 (1948).

* We are indebted to Mr. A. H. Sharbaugh for calling our attention to this error.

TABLE II. Molecular dimensions.

Molecule	Bond	Internuclear distance*	Bond angles
CH_3F**	CF	1.385A	
	CH	1.109	$\angle HCH=110°\,0'$
CHF_3	CF	1.326 ± 0.013	$\angle FCF=110°\pm3°$ (assumed)
	CH	1.111 (assumed)	
PF_3	PF	1.546 ± 0.008	$\angle FPF=104°\pm3°$ (assumed)

* Values of constants used are: $h=6.624\times10^{-27}$ erg-sec., $M_H=1.00813$ a.m.u., $M_{C^{13}}=12.00386$ a.m.u., and $M_1=1.6599$ g, all from R. T. Birge, Rev. Mod. Phys. 13, 233 (1941); $M_{Cl^3}=13.00761$ a.m.u. from M. S. Livingston and H. A. Bethe, Rev. Mod. Phys. 9, 373 (1937); $M_F=19.0045$ and $M_{P^{31}}=30.9836$ from F. W. Aston, Proc. Roy. Soc. **A163**, 391 (1937).

** The values 1.106A for d_{CH} and 109° 42′ for $\angle HCH$ are obtained if $I_A=5.49$ g cm^{-40} is used for CH_3F. However, d_{CF} remains 1.385A. With $I_A=5.55$ the values $d_{CH}=1.111$A, $d_{CF}=1.385$A, and $\angle HCH=110°\,6'$, are obtained.

It is of interest to compare the HCH bond angle found for CH_3F, 110° 0′, with that for SiH_3Cl, 103° 57′, recently determined from microwave spectroscopy by Sharbaugh.[12] The CH_3F angle, also that for the other methyl halides, is slightly greater than the tetrahedral angle 109° 28′, while that for SiH_3Cl is significantly less. In most of these molecules, particularly in SiH_3Cl, there is appreciable ionic character of the bond linking the halogen. This ionic character would tend to make the bond angle larger than tetrahedral because of sp^2 hybridization in C^+H_3 or Si^+H_3. On the other hand, contributions from double-bonded structures

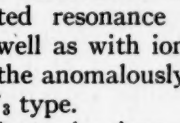

of the type $H-C^-=F^+$ would presumably decrease $\angle HCH$. The latter structure would probably not be very important in the methyl halides because, in addition to putting a plus charge on the electronegative halogen, it also requires one of the CH bonds to be broken. The latter effect would be partly offset by the Coulomb attraction between the H^- and the F^+. This attraction would again

TABLE III. Comparison of some calculated and observed interatomic bond lengths.

Molecule	Bond	Observed bond length	Added covalent radii	Added radii corrected for ionic character*
CH_3F	CF	1.385[a]	1.51	1.38
CHF_3	CF	1.326[a]	1.51	1.38
PF_3	PF	1.546[a]	1.82	1.65
AsF_3	AsF	1.712[b]	1.93	1.75
CH_3Cl	CCl	1.779[c]	1.78	1.75
CH_3Br	CBr	1.932[c]	1.93	1.91
CH_3I	CI	2.139[c]	2.12	2.12
SiH_3Cl	SiCl	2.035[d]	2.16	2.05

[a] Present work.
[b] Dailey, Rusinow, Shulman and Townes, Bull. Am. Phys. Soc. **23**, No. 3, 53 (1948).
[c] W. Gordy, J. W. Simmons, and A. G. Smith, Phys. Rev. **74**, 243 (1948).
[d] A. H. Sharbaugh, Phys. Rev. **74**, 1870 (1948).
* Calculated with the Schomaker-Stevenson rule,

$$d_{AB}=r_A+r_B-0.09|X_A-X_B|.$$

J. Am. Chem. Soc. **63**, 37 (1941).

[12] A. Harry Sharbaugh, Phys. Rev. **74**, 1870 (1948).

TABLE IV. Line breadth parameters.*

Molecule	$2\Delta\nu$ measured	Pressure mm of Hg	Temp.	$\Delta\nu$ for 1 mm Hg**
CH_3F	3.0 mc	7.5×10^{-2}	27°C	20 mc
CHF_3	0.82	2.3×10^{-2}	27°C	18
PF_3	1.1	3.4×10^{-2}	27°C	16

* Line breadth, $\Delta\nu$, here is half the width of the line measured between half-intensity points.
** Conversion of the data to 1-mm Hg pressure assumes a linear variation of $\Delta\nu$ with pressure.

tend to make the HCH angle large. Because of the d orbitals available in the valence shell of Si, contributions from structures of the type

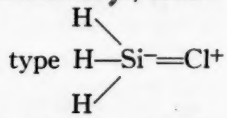

are possible in chlorosilane. Significant contributions from the latter structure could account for the abnormally small H Si H bond angle and the short Si—Cl distance in SiH_3Cl as contrasted with the corresponding dimensions in CH_3Cl. This explanation is in harmony with the fact that the dipole moment of SiH_3Cl is appreciably lower than that for any of the methyl halides, whereas purely electronegativity considerations would imply a greater dipole moment for H_3SiCl than for CH_3Cl. Significant contributions of

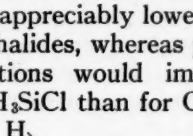

in addition to the larger amount of

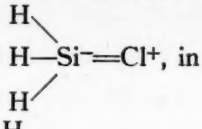

expected, could account for the fact that the nuclear quadrupole coupling of Cl in SiH_3Cl is only 53 percent of its value in CH_3Cl.

Line breadths obtained for CH_3F and CHF_3 are listed in Table IV. These are comparable in value to those of other molecules with similar dipole moments.

The observed line breadth parameters have been used with the dipole moments 1.83 and 1.59 for CH_3F and CHF_3 to calculate the peak absorption coefficients listed in Table I. No dipole moment value is available for PF_3. The procedure for the calculations is outlined in reference 1(c). For symmetric molecules of the type considered here (three identical corner atoms with nuclear spin $\frac{1}{2}$) the formula giving the resonant frequency absorption coefficient can be reduced to the form,

$$\alpha(\text{cm}^{-1})=0.140\frac{BA^{\frac{1}{2}}F_v\nu^2\mu^2g}{(\Delta\nu)_1T^3}\times\left[\frac{(J+1)^2-K^2}{J+1}\right]\exp\left(\frac{-E_r}{kT}\right),$$

where F_v = fraction of molecules in the vibration state considered; μ = molecular dipole moment in Debye units; $g=1$ for $K=0, 1, 2, 4, 5, 7$ etc., $=2$ for $K=3, 6, 9$, etc.; $(\Delta\nu_1)$ = line breadth in cm^{-1} for 1 mm of Hg pressure and for $T=300$; ν = resonant frequency in cm^{-1}; T = temperature in degree Kelvin; k = Boltzmann's constant; $B=(h/8\pi^2cI_B)$, $A=(h/8\pi^2cI_A)$; and $E_r=hc[BJ(J+1)+(A-B)K^2]$. Here A and B are in cm^{-1} and E_r is in ergs. J is the rotational quantum number for the lower state of the transition.

Nuclear spins of $\frac{1}{2}$ for P^{31} and for F^{19} are supported by the fact that no nuclear quadrupole hyperfine structure was detected in the molecules containing these atoms. From the rather large nuclear coupling observed[13] for As in AsF_3, one would expect to detect quadrupole coupling in PF_3 if the quadrupole moment of the P nucleus were not zero or very nearly zero. The spin $\frac{1}{2}$ for P^{31} is also indicated by the relative intensities of the lines of different K in the $J=2\rightarrow3$ transition of PF_3, which are separated by centrifugal distortions.

Theoretical considerations indicate that a nucleus of spin $\frac{1}{2}$ would have spherical symmetry and hence no electrical quadrupole moment. Since $(\partial^2V)/(\partial z^2)$ is large for the F in CH_3F and can be evaluated approximately from the Townes[14] theory, it follows from the present measurement that the quadrupole moment of F must indeed be very small. The doublet separation, $\Delta\nu=407\ \text{cm}^{-1}$, with $Z_i=7.2$ yields with the formula,[14]

$$\partial^2V/\partial z^2=(8e\Delta\nu/15Z_iR\alpha^2a_0^3),$$

a value for $(\partial^2V)/(\partial z^2)$ of 17×10^{15} e.s.u. Our observations with $I=\frac{3}{2}$ indicate $|eQ(\partial^2V/\partial z^2)|<0.5$ mc. Hence, $|Q|<0.0003\times10^{-24}\ \text{cm}^2$. This upper limit shows that the quadrupole moment, if not zero, must be less than about 1/10 of that of the small deuterium nucleus, and less than 1/200 that of the Cl^{35}.

We are attempting to obtain samples of $P^{32}F_3$, DCF_3, and $HC^{13}F_3$ for similar studies so that the structures of phosphorus trifluoride and fluoroform can be completely determined and the nuclear spin and quadrupole coupling of P^{32} can be evaluated.

We wish to thank Dr. A. F. Benning, of the Jackson Laboratories, of the E. I. du Pont de Nemours Company, for the sample of fluoroform, also Professor L. A. Bigelow and Mr. F. F. Holub, of the Duke Chemistry Department, for a sample of methyl fluoride.

[13] B. P. Dailey, K. Rusinow, R. G. Shulman, and C. H. Townes, Bull. Am. Phys. Soc. **23**, No. 3, 53 (1948).
[14] Charles Hard Townes, Phys. Rev. **71**, 909 (1947).

The Characteristic Radiations of Praseodymium (142)*

C. E. MANDEVILLE
Bartol Research Foundation of the Franklin Institute, Swarthmore, Pennsylvania
(Received December 20, 1948)

The nineteen-hour Pr^{142} emits 2.22-Mev nuclear beta-rays (aluminum absorption) and gamma-rays having a maximum energy of 1.74 Mev as determined by coincidence absorption. Evidence is considered which leads to a somewhat lower value for the energy of this gamma-ray. Lead absorption indicated a soft component at 0.17 Mev. Beta-gamma-coincidence data revealed the presence of a soft beta-ray spectrum of low intensity having an end point at 215 kev. The hard beta-rays are non-coincident with gamma-radiation and are thus considered to be associated with a ground state transition. Gamma-gamma-coincidences, denoting cascade emission of gamma-rays by the excited residual nucleus, were observed, but no beta-beta-coincidences were found.
See note added in proof.

INTRODUCTION

IT seems well established[1–3] that slow neutron bombardment of praseodymium gives rise to a 19.3-hour period. This activity has been assigned to Pr^{142}, since Pr^{141} appears to be the only stable isotope of praseodymium. Recent measurements[3] seem to indicate the presence of long lived activities. These would have no effect upon the results of the present investigation, since PrO_2 was irradiated for only two hours in the Oak Ridge pile, and the measurements were completed within five days after removal of the irradiated material from the pile. The data herein reported were compiled with the use of absorption and coincidence counting methods which have been previously described.[4] No chemical separations were performed. However, the effects of impurities were thought to be small because of the short exposure time. The ordinates of all of the curves presented in the text of the paper were observed to decay with the nineteen-hour period.

RESULTS

The absorption in aluminum of the beta-rays of Pr^{142} is shown in Fig. 1 where the upper limit is seen to occur at 1.04 g/cm² or 2.22 Mev as calculated by Feather's equation.[5] This value is in good agreement with earlier reports.[1,2]

Coincidence absorption of the secondary electrons of the gamma-rays of Pr^{142} is shown in Fig. 2. The end point, according to the calibration curve of the coincidence counting set,[4] corresponds to a quantum energy of 1.74 Mev. Lead absorption measurements have previously indicated a value of 1.9 Mev[2] and 2.1 Mev.[3] The presence of this gamma-ray was also noticed by the writer in 1943.[6] The momentum distribution of the recoil electrons ejected by this gamma-ray from a thick aluminum radiator in a magnetic spectrograph was found to have a curve shape and extrapolated end point[7] identical with that of the 1.61-Mev[8] gamma-ray of La^{140}. The energy value obtained by this com-

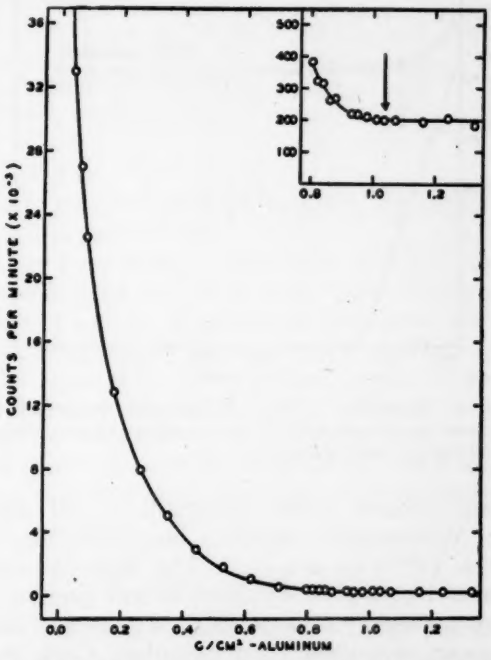

FIG. 1. Absorption in aluminum of the beta-rays of Pr^{142}. The absorption limit occurs at 2.22 Mev.

* Assisted by the Joint Program of the ONR and the AEC.
[1] C. S. Wu and E. Segrè, Phys. Rev. **61**, 203 (1942).
[2] J. W. DeWire, M. L. Pool, and J. D. Kurbatov, Phys. Rev. **61**, 544 (1942).
[3] J. M. Cork, R. G. Shreffler, and C. M. Fowler, Phys. Rev. **74**, 1657 (1948).
[4] C. E. Mandeville and M. V. Scherb, Nucleonics **3** (No. 4), 2 (1948).
[5] N. Feather, Proc. Camb. Phil. Soc. **34**, 599 (1938).
[6] C. E. Mandeville, unpublished data, 1943.
[7] The momentum distribution of the recoil electrons of the gamma-rays of lanthanum (140) [Phys. Rev. **63**, 387 (1943)] exhibits a high energy "tail" arising from the presence of gamma-rays of energy greater than 2 Mev and probably also from scattering. However, extrapolation at the point of maximum slope as recommended by Itoh [Proc. Phys. Math. Soc. Japan **23**, 605 (1941)] and by Siegbahn [Proc. Roy. Soc. **A189**, 527 (1947)] gives identical end points for the recoils of the high energy gamma-rays of La^{140} and Pr^{142}.
[8] R. K. Osborne and W. C. Peacock, Phys. Rev. **69**, 679 (1946).

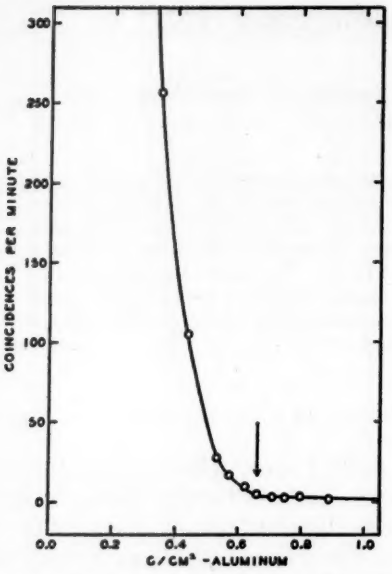

FIG. 2. Coincidence absorption of the recoil electrons of the gamma-rays of Pr^{142}. The end point corresponds to a quantum energy of 1.74 Mev.

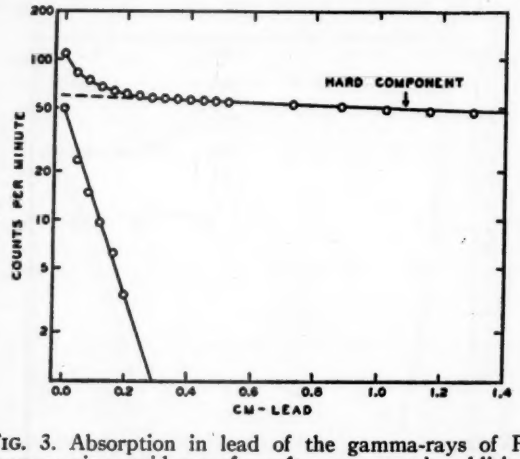

FIG. 3. Absorption in lead of the gamma-rays of Pr^{142}. The curve gives evidence of a soft component in addition to the well-known hard radiation.

parison method seems preferable to all others, since Wattenberg[9] reported no photo-neutrons from a Pr^{142}+Be source.** The lead absorption curve of Fig. 3 gives evidence of soft gamma-rays having an energy of about 0.17 Mev as well as the previously discussed hard radiation. Cork *et al.*[3] have reported conversion lines from Pr^{142} corresponding to gamma-ray energies of 133.7, 328.9, 489.6, and 623.6 kev.

The beta-gamma-coincidence rate of Pr^{142} is shown in Fig. 4, where it is seen to decrease from an extrapolated value of 0.05×10^{-3} coincidence

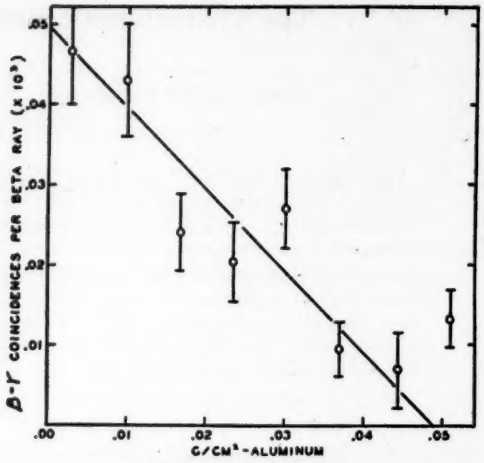

FIG. 4. The beta-gamma-coincidence rate of Pr^{142} as a function of the surface density of aluminum placed before the beta-ray counter. This curve shows that a soft spectrum is present having an end point at 215 kev and that the 2.22-Mev beta-rays lead to the ground state of the residual nucleus.

per beta-ray at zero absorber thickness to zero at 0.049 g/cm² in aluminum placed before the beta-ray counter.[10] This shows that a soft spectrum, coupled with gamma-rays, having an end point at 215 kev is present in the decay of Pr^{142}. It follows also that the 2.22-Mev beta-rays lead to the ground state of the Nd^{142} residual nucleus. A source of Pr^{142} was placed between two gamma-ray counters each shielded by 1.5 g/cm² of aluminum. A gamma-gamma-coincidence rate of 0.25×10^{-3} coincidence per gamma-ray was observed. The data of Cork *et al.*[3] also suggest cascade emission of gamma-rays. The conversion lines reported by them also sug-

[9] A. Wattenberg, Phys. Rev. 71, 497 (1947).

** Other reports of the energy of the intense gamma-ray of La^{140} are 1.63 Mev [L. C. Miller and L. F. Curtiss, Phys. Rev. 70, 983 (1946)] and 1.65 Mev [W. Rall and R. G. Wilkinson, Phys. Rev. 71, 321 (1947)]. Lens type spectrometers were employed in both cases.

[10] The "low Z" gamma-ray counter of the beta-gamma-coincidence counting arrangement was calibrated with the beta-gamma-coincidence rate of Sc^{46} (2 Mev of de-excitation energy, 2.66×10^{-3} coincidence per beta-ray). Knowing this, the difficulties related to detection of the small coincidence rate of Pr^{142} can be understood. To detect small beta-gamma-coincidence rates, counting rates as high as two-hundred thousand counts per minute have been used in the beta-ray counter. The beta-gamma-coincidences per beta-ray are unaffected as long as dead-time losses in the *gamma-ray counter* remain inappreciable. This more or less obvious fact has been verified by observing that the number of beta-gamma-coincidences per beta-ray recorded in the beta-ray counter remained unchanged for many different radioactive elements when the beta-ray counting rate was varied from twenty thousand to two-hundred thousand counts per minute.

If it is assumed that the soft spectrum of Pr^{142} is followed by about 2 Mev of gamma-ray energy, the beta-gamma-coincidence rate at zero absorber thickness, 0.05×10^{-3} coincidence per beta-ray, shows that the soft spectrum has an intensity about one-fiftieth as great as the 2.22-Mev spectrum. This estimate is in reasonably good agreement with the findings of the Ohio State group (reference 2) who report one high energy gamma-ray per twenty-five nuclear beta-rays.

It was stated in a footnote of a previous paper concerning Cd^{115}, Phys. Rev. 75, 221 (1949), that the calculated intensity of the softer spectrum constitutes a lower limit, since the low energy beta-rays are heavily absorbed and scattered in the thin window of the beta-ray counter. This comment was without meaning, since at *zero absorber thickness*, all correction factors are unity and the estimate of relative intensity should be exact.

gest the possible existence of beta-beta-coincidences. A search was made for them, but after carefully eliminating all scattering effects arising from the 2.22-Mev beta-rays, none were found. This is not surprising, because the conversion electrons and associated soft nuclear beta-rays are very few in number as compared to the 2.22-Mev nuclear beta-rays.

Note added in proof: The "Table of Isotopes" compiled by G. T. Seaborg and I. Perlman [Rev. Mod. Phys. **20**, 585 (1948)], has appeared since this paper was presented for publication. In the table, reference is made to a report having only a restricted distribution by W. C. Peacock, J. W. Jones, and R. T. Overman [Plutonium Project Report Mon N-432, p. 56 (Dec. 1947)]. Their value of 1.65 Mev is quoted in the isotopic table as the energy of the hard gamma-ray of Pr^{142}. This is in agreement with the deductions of the present paper.

ACKNOWLEDGMENTS

The writer wishes to express his particular appreciation to Henrietta Fricke of Bartol for having made the drawings for this paper and for the entire preceding series of papers dealing with pile-induced activities. He also acknowledges the continued interest of Dr. W. F. G. Swann, director of this laboratory.

PHYSICAL REVIEW VOLUME 75, NUMBER 7 APRIL 1, 1949

Radioactive Isotopes of Platinum and Gold

GEOFFREY WILKINSON

Radiation Laboratory and Department of Chemistry, University of California, Berkeley, California

(Received December 13, 1948)

Using the 60-inch Crocker Laboratory cyclotron, bombardments have been made of iridium and platinum with 19-Mev deuterons, of iridium with 38-Mev α-particles, and of platinum and gold with fast and thermal neutrons. Radioactive isotopes of iridium, platinum, and gold were chemically separated and the radiation characteristics studied.

THE results of a survey of the radioactive isotopes of platinum and gold have been reported previously.[1] Table I summarizes present knowledge of these isotopes. The present paper describes in more detail the experimental techniques used and the radiation characteristics of the radioactive isotopes observed.

I. EXPERIMENTAL

A. Bombardment

Using the 60-inch cyclotron at the Crocker Laboratory, bombardments were made of iridium with 38-Mev helium ions and 18-Mev deuterons, of platinum with 18-Mev deuterons, fast and thermal neutrons, and of gold with fast neutrons.

In all bombardments, reagent quality metals were used. Platinum and gold were bombarded as 2- and 5-mil foils. Iridium was bombarded as the powdered metal, in order to facilitate subsequent solution; in short bombardments where no chemical separations were made, iridium foil was used. The metal powder was tamped into the trough of a water-cooled copper "interceptor" target, which received about one-third of the total beam from the cyclotron. The iridium was protected by wrapping the target with 0.2-mil tantalum foil.

After bombardment, platinum and gold targets were dissolved in boiling aqua regia. Iridium was dissolved by the procedure of Wichers *et al.*[2] The metal powder (100 mg) was transferred to a thick-walled glass tube, and an equal weight of sodium chlorate was added. While the tube was cooled in liquid air to prevent chemical reaction, 5 ml of fuming hydrochloric acid were added. After sealing, the tube was allowed to warm and then heated at 300°C for about three hours.

B. Chemical Separations

The chemical methods used in both the initial separations and in the separation of daughter activities were variants on the procedures outlined below. The steps were carried out in the given order, the usual radiochemical techniques being employed with milligram amounts of carriers present. "Holdback" and "scavenger" carriers were used at appropriate points, and separations were repeated until acceptable radiochemical purity was obtained.

[1] Geoffrey Wilkinson, Phys. Rev. **73**, 252 (1948).

[2] E. Wichers, W. G. Schlect, and C. L. Gordon, J. Nat. Bur. Stand. Research **33**, 363 (1944).

TABLE I. Summary of present knowledge on gold and platinum isotopes.

Isotope	Type of radiation	Half-life	Energy of radiation in Mev: Particles	Energy of radiation in Mev: γ-rays	Produced by
Pt^{191}	K, ϵ^-, γ	3.00±0.02 days	0.5 ϵ^-	L, K x-rays 0.57, 1.5	Ir-d-2n Au^{191} decay Pt-n-2n
Pt^{193}	K, ϵ^-, γ	4.33±0.03 days	0.11 ϵ^-	L, K x-rays 1.5, 0.18	Ir-d-2n Pt-n-γ Pt-n-2n Au^{193} decay Pt-d-p
Au^{191}	K	~1 day			Pt-d-3n Ir-α-4n
Au^{192}	K, ϵ^-, $\gamma\beta^+$	4.7±0.1 hr.	~0.4, ~15ϵ^- ~1.9 β^+	K x-rays, 2–3	Pt-d-2n Ir-α-3n
Au^{193}	K, ϵ^-	15.8±0.3 hr.	<0.2 ϵ^-	L, K x-rays	Pt-d-n, 3n Ir-α-2n
Au^{194}	K, ϵ^-, γ β^+(~3%)	39.5±0.5 hr.	0.3 ϵ^- 1.8 β^+	L, K x-rays ~0.4 ~1.8	Ir-α-3n Pt-d-2n, 3n
Au^{195}	K, ϵ^-, γ	185±3 days	0.1 ϵ^-	L, K x-rays ~1.6, ~0.19	Ir-α-2n Pt-d-n, 2n, 3n
Au^{196}	K, $\gamma\beta^-$(~20%)	5.55±0.05 days	0.34 β^-	L, K x-rays 0.41, ~1.6	Pt-d-n, 2n Au-n, 2n
Au^{196}	K or I.T.	14.0±0.3 hr.		x-rays	Au-n-2n

1. Osmium was separated by distillation of the volatile tetroxide from nitric acid solutions, followed by reduction of the collected distillate to the metal by magnesium. This step was performed only in deuteron bombardments of iridium. Experiments showed that no osmium produced was from impurities in platinum bombardments.

The absence of any ruthenium activities resulting from impurities in iridium and platinum was shown by distillation of the tetroxide from boiling perchloric acid solutions after removal of osmium. The collected distillate was reduced to the oxide by alcohol.

2. Gold was extracted by ethyl acetate from 2–6N hydrochloric acid solutions containing nitric acid. After removal of the solvent by evaporation, gold was precipitated as the metal by saturation of a hot 2N nitric acid solution with sulfur dioxide.

3. After removal of gold contamination by repeated solvent extractions, excess stannous chloride was added to the cold hydrochloric acid solution, and the orange-red platinum complex, presumably H_2PtCl_4, which is immediately formed, was extracted with ethyl acetate.[3] The solvent was evaporated and platinum reduced to the metal by magnesium. Iridium and gold do not extract or interfere in this procedure even when present in large quantities. Palladium, however, behaves like platinum and is extracted, while rhodium reacts very slowly and extracts in small quantities. The absence of palladium contaminations was shown by the specific precipitation by dimethylglyoxime in 4N acid solution.

4. After removal of other activities, iridium was finally precipitated as the dioxide by the bromate oxidation method.[4] Rhodium reacts similarly, but contaminating rhodium activities were shown to be absent by solution of the oxide in hydrochloric acid and reduction of rhodium to the metal by titanous chloride.

In iridium bombardments, where large amounts of the element were present, separation was made by the sparingly soluble ammonium iridium chloride; the solution, after removal of platinum, was re-oxidized with nitric acid and saturated with ammonium chloride.

[3] H. Wöbling, Berichte 67, 773 (1934).
[4] R. Gilchrist and E. Wichers, J. Am. Chem. Soc. 57, 2565 (1935).

C. Measurements

The final precipitates were either washed with acetone and mounted as the metal or were dissolved in acid and aliquots of the solution evaporated for counting. Samples were mounted on microscope cover slides or on very thin mica.

"End on" type counters 7.5 cm high, 3 cm diameter, with 2- to 3-mg/cm² mica windows, filled with 10 cm argon and 0.5 cm alcohol were used; a Lauritsen type quartz fiber electroscope was used to measure some very active samples. Measured counting rates were corrected for coincidences and for variations in counter efficiency by use of a uranium reference. The geometry of the shelves of the counter were calibrated using a UX_2 standard.

Radiation characteristics were studied by absorption methods using aluminum, beryllium, and lead foils. For the reported ranges of electrons, the total absorber thickness for removal was computed, i.e., added absorbers plus air gap and counter window. Electrons and soft electromagnetic radiation were distinguished by their differential absorption in aluminum and beryllium. The average energy of L x-radiation in this region is of the order of 10 kev with an absorption half-thickness in beryllium of ~800 mg/cm². Unless the electrons are very energetic and require several L x-ray half-thicknesses of beryllium for their removal, electrons can be removed by a beryllium absorber and the absorption of residual soft quantum radiation then

measured in aluminum. The absorption curve of electrons in aluminum is obtained by subtraction from the measured aluminum curve of the electromagnetic radiation background. This, in turn, is obtained from the measured aluminum absorption curve of this radiation; in appropriate correction for reduction in the measured intensity of L x-rays by the beryllium filter is made and the true absorption curve constructed. If the electrons have a range much less than the half-thickness of the L x-rays in beryllium, the former are most easily determined from a direct absorption measurement with beryllium screens. When the electrons and L x-rays have comparable absorption in beryllium, the problem of resolution is more complicated, requiring complete absorption measurements in both aluminum and beryllium and a knowledge of the expected energy of L radiation.

Harder electromagnetic radiation was determined by lead absorbers. The active sample was placed between beryllium absorbers sufficient to remove electrons, and a third beryllium foil, of adequate thickness to remove all secondary electrons emitted from the lead absorbers, was placed immediately below the counter window. The lead absorbers were sandwiched between the beryllium foils. In addition, the whole counter set-up was removed from the usual lead housing in order to minimize scattering effects of γ-rays and secondary electrons from the walls.

For comparison with measured values, x-ray absorption half-thicknesses in beryllium, aluminum, and lead absorbers were calculated from the energies and relative intensities of the various L and K x-ray components, together with the absortpion coefficients given by Compton and Allison.[5] Because the critical absorption edges of iridium, platinum, and gold lie in the region of the heavy rare earths, hafnium and tantalum, measurements to distinguish between x-rays of these elements were not made, inasmuch as absorber materials were not available.

In the determination of ratios of electrons and electromagnetic radiation, corrections were made for absorption of electrons in the air gap and counter window and for counting efficiencies of quantum radiations. For radiations of energies between 30 kev and 0.5 Mev a counting efficiency of 0.5 percent was taken, with an increase of one percent per additional Mev energy. For softer radiations the efficiency was calculated for the counters used from the absorption coefficients in argon; the efficiencies at 7, 10, and 15 kev were respectively 12 percent, 2 percent, and 1 percent. No allowance was made for fluorescence yields of

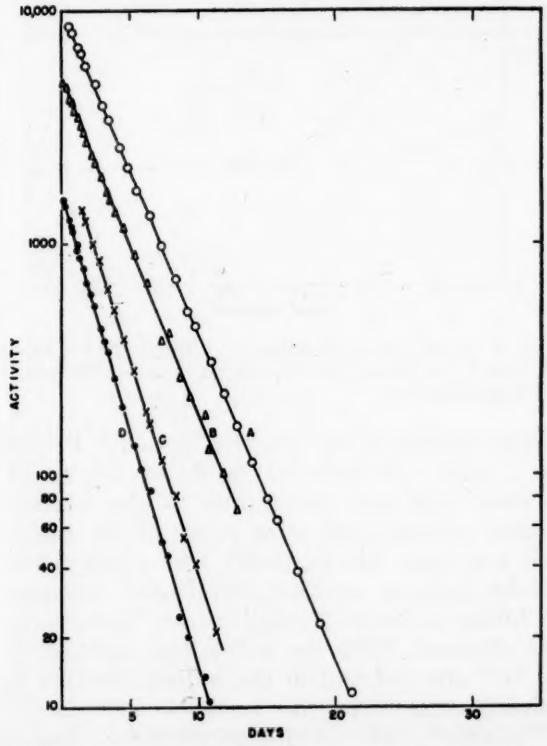

FIG. 1. Decays of 4.33-day Pt^{193} and 3.0-day Pt^{191}. (A) Gross decay of 4.33-day Pt^{193} from Pt+d bombardment. (B) Decay of soft electron radiation from Ir+d, half-life 4.33 days. (C) 3.0-day Pt^{191} from Ir+d, γ-decay through 5 g/cm² lead. (D) Decay of hard electron radiation from Ir+d, half-life 3.0 days.

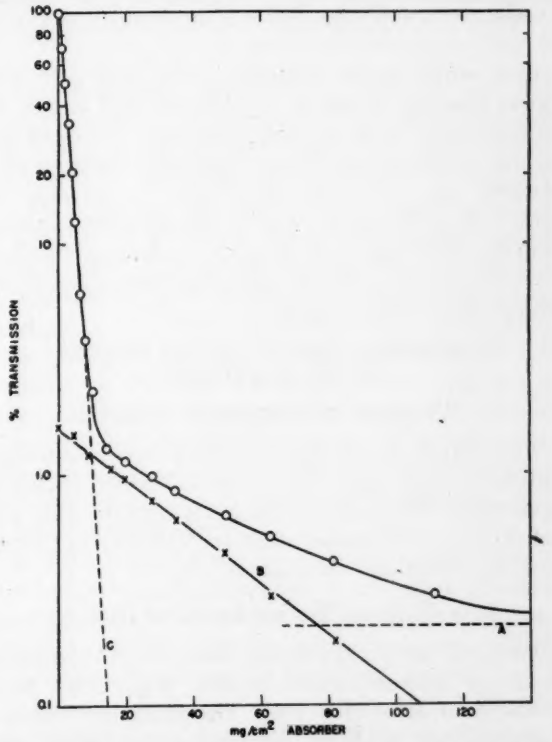

FIG. 2. Aluminum absorption of 4.33-day Pt^{193} from Pt+d. (A) K x-ray bacgkround. (B) L x-rays 28 mg/cm² Al half-thickness. (C) Electrons, total range 17 mg/cm².

[5] A. H. Compton and S. K. Allison, *X-rays in Theory and Experiment* (D. Van Nostrand Company, Inc., New York), second edition 1935.

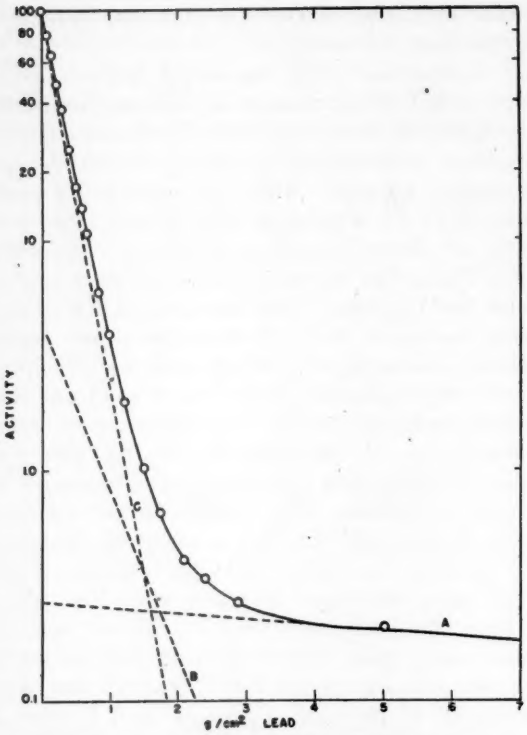

FIG. 3. Lead absorption of 4.33-day Pt^{193} from Pt+d. γ-ray half-thicknesses 15 g/cm² (A), 530 g/cm² (B), 185 mg/cm² (C) lead.

x-rays, which were assumed to be unity in the region studied. While it is realized that ratios so obtained may be in considerable error in view of the various assumptions made regarding counting efficiencies, etc., it seems justifiable to attempt to obtain an approximate idea of the radiations arising from one disintegration in order to allow calculation of reaction yields. Beam intensities were taken from the cyclotron instruments.

II. GENERAL SURVEY OF THE LONGER LIVED ACTIVITIES

A. Deuteron Bombardment of Iridium

Two platinum isotopes, with half-lives of 3.0 days and 4.33 days only are observed after chemical separation. The iridium fractions contain only the well-known Ir^{192}(60-day) and Ir^{194}(19-hr.)[6] activities from d,p reactions on iridium.

B. α-Particle Bombardment of Iridium

Osmium and iridium fractions from bombardments of iridium with 38-Mev α-particles were almost completely inactive. The platinum fraction contained the 4.33-day activity with a small proportion of the 3.0-day isotope. The chemically separated gold fraction which contained most of the activity gave a complex decay (Fig. 6), which was resolvable into activities of 4.0 hours, 15.8 hours, 39.5 hours, and 185 days. Chemical separations of platinum from the bulk of the gold fraction showed that the 4.33-day activity grows from a gold parent of half-life 16±1 hours. Very low activities of the 3.0-day platinum were also found to grow in the gold sample and appeared to have a parent with a half-life of approximately 1 day.

[6] Glenn T. Seaborg, Rev. Mod. Phys. 16, 1 (1944).

C. Deuteron Bombardment of Platinum

Gold, platinum, and iridium fractions were chemically separated from platinum foils bombarded with 19-Mev deuterons for various times from a few seconds to several hours. The platinum

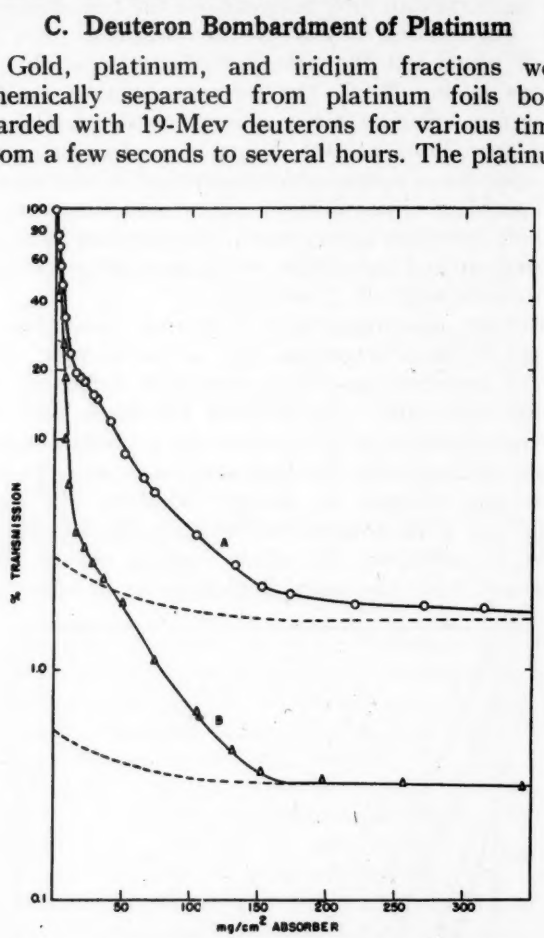

FIG. 4. Aluminum absorption of 4.33-day Pt^{193}+3.0-day Pt^{191} from Ir+d. Measured at 0.5 day (A) and at 16 days (B) after bombardment.

fraction contained the β-active isotopes[6] Pt^{199}(31-min.), and Pt^{197}(18-hour) produced by the d,p reaction. Chemical separation of the platinum fraction was repeated after decay of the shorter-lived activities. The platinum then contained the 4.33-day activity together with a small amount of the 3.0-day activity. No longer-lived isotopes have been observed. Both the well-known isotopes Ir^{192} and Ir^{194} are observed in the iridium fraction and probably arise from the reactions $Pt^{194}(d,\alpha)Ir^{192}$, $Pt^{196}(d,\alpha)Ir^{194}$. The saturation activities are approximately equal, in agreement with the abundances of Pt^{194} and Pt^{196}; further, the activities are too large to be due to iridium impurity in the platinum used.

The resolution of the decay and absorption curves of the gold fraction from deuteron bombardment of platinum is complicated by the presence of β-emitting Au^{198} and Au^{199}. Short bombardments, however, produce the shorter-lived activities in a relatively greater yield and allow comparatively simple resolution. In long bombardments, the decay of hard γ-radiation shows the 39.5-hour activity; after decay of this isotope and also Au^{198} and Au^{199}, the gold fraction contains only 5.5-day and 185-day activities. Separation of daughter activities from the gold fraction confirms the data in α-bombardment of iridium.

D. Neutron Bombardments of Platinum and Gold

The only gold activities observed from $n,2n$ reaction were the previously reported[8] 5.5-day isotope, together with a low yield of an isotope with a 14-hour half-life which is presumably an isomer.

Fast and thermal neutrons on platinum form the 4.33-day isotope but only in the fast bombardment was any evidence of the 3.0-day isotope seen.

III. PLATINUM ISOTOPES

A. 4.33-Day Pt^{193}

This isotope is formed both in deuteron and α-particle bombardments of iridium, in the deuteron bombardment of platinum, and in both fast and thermal neutron bombardments of platinum. It has been also found to grow from a gold parent isotope with a 16-hour half-life. The radiations, all of which decay (Fig. 1) with the same half-life, are as follows:

1. Electrons of range 16.5±1 mg/cm², which corresponds to an energy of 110 kev. The absorption curve of these electrons together with the soft electromagnetic radiation background is shown in Fig. 2.

2. The electromagnetic radiation consists of four components. Aluminum absorption shows soft radiation of half-thickness 29±1 mg/cm², which corresponds well with the energy of 10.3 kev which would be expected for L x-rays of iridium or platinum. In the lead absorption of the harder components (Fig. 3), there is a small percentage of a very hard γ-ray of half-thickness 14±0.5 g/cm² lead, corresponding to an energy of 1.5 Mev. After subtraction of this component, the residue was still complex, having a noticeable tail. If it is assumed that the "tail" is attributable to a γ-ray of energy ~180 kev (350 mg/cm² Pb), a half thickness of 185±5 mg/cm² is obtained for the softer component. This agrees with that expected for iridium K radiation, which has an energy of 67 kev.

The ratios of electrons and electromagnetic radiation were determined from an "infinitely thin" sample mounted on mica and from lead absorption measurements. After making the corrections discussed above, the following ratios were obtained:

$$\text{Electrons}: L \text{ x-rays}: K \text{ x-rays}: 170 \text{ kev } \gamma : 1.5 \text{ Mev } \gamma = 0.3 : 2 : 1 : 1\times10^{-2} : 5\times10^{-3}.$$

The measured energies of electrons and soft quantum radiation agree well with values reported by Krishnan and Nahum[7] for a "2.9-day" activity produced by deuteron bombardment of platinum. A similar isotope has also been reported[8] as having a half-life of 3.3 days. These activities were unquestionably due to the same isotope as is here observed. The gross decay was, however, measured through fourteen half-lives, the gross electromagnetic radiation through 8.5 half-lives, and the hard γ-radiation through 6.5 half-lives. A half-life of 4.33±0.03 days was deduced from the various measurements. Similar values of the half-life were obtained for the isotope produced in neutron bombarments of platinum and in the deuteron bombardment of iridium.

In order to calculate the cross sections for formation in the various reactions, it has been assumed that the isotope decays by orbital electron capture and that one K x-rays quantum represents one disintegration. However, the observed ratio of L to K x-radiation of 2:1 is abnormally high and may indicate decay by L electron capture in addition to K capture, or γ-ray conversion in the L shell.

The isotope has been allocated to mass 193.

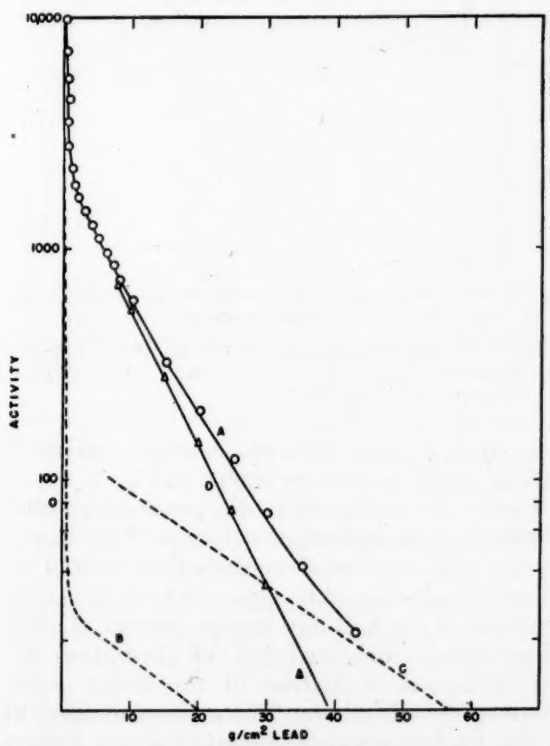

FIG. 5. Lead absorption of 4.33-day Pt^{193}+3.0-day Pt^{191} from Ir+d. (A) Measured absorption curve. (B) Calculated 4.33-day Pt^{193} contribution. Estimated hard γ-ray (C) and γ-ray of half-thickness 5.4 g/cm² lead (D) of 3.0-day Pt^{191}.

[7] R. S. Krishnan and E. A. Nahum, Proc. Camb. Phil. Soc. 37, 422 (1941).

[8] E. M. McMillan, M. Kamen, and S. Ruben, Phys. Rev. 52, 375 (1937).

It is produced in a yield comparable with that of the 3.0-day activity (see below) by deuteron bombardment of iridium. Assuming one K x-ray per disintegration and a counting efficiency of 0.5 percent for this x-ray, the cross section for Ir^{193}-d-$2n$ reaction is ~0.07 barn; with the same assumptions, the cross section for formation of the 3.0-day activity by Ir^{191}-d-$2n$ reaction is ~0.09 barn.

In the deuteron bombardment of platinum, the cross section for the production of Pt^{193} by d,p reaction on Pt^{192} is ~0.05 barn. This value compares reasonably, in view of the unavoidable assumptions, with values of 0.08 to 0.1 barn for d,p reactions in iridium and platinum, where β^--active isotopes Ir^{192}, Ir^{194}, and Pt^{197} are formed.

No iridium daughter of half-life greater than a few minutes has been detected, which is in agreement with the assignment to Pt^{193}.

B. 3.00-Day Pt^{191}

In the platinum fraction from deuteron bombardment of iridium, the isotopes Pt^{191} and Pt^{193} are to be expected in high yield from $d,2n$ reaction. The aluminum absorption curves (Fig. 4), after subtraction of electromagnetic radiation backgrounds, show electrons of ranges ~16 mg/cm², 145±5 mg/cm², and ~400 mg/cm², corresponding to energies of 0.1, 0.5 Mev, and ~1 Mev, respectively. The decay of the soft electron was obtained by subtraction of electromagnetic and hard electron radiation from the gross activity, and a value of 4.35 ±0.05 days measured through eight half-lives was obtained. The decay and electron energy of this radiation corresponds closely with the values obtained for the 4.33-day Pt^{193} described above and formed in the deuteron bombardment of platinum. The decay of the 0.5-Mev electron, obtained by subtraction of electromagnetic radiation background from the gross activities measured through a 20 mg/cm² beryllium absorber was 3.05±0.05 days through seven half-lives. Since no 1-Mev electron was observed in the radiation of the 4.33-day activity, the small fraction of this electron present is assumed to arise from the 3.0-day activity. The various decay curves are shown in Fig. 1.

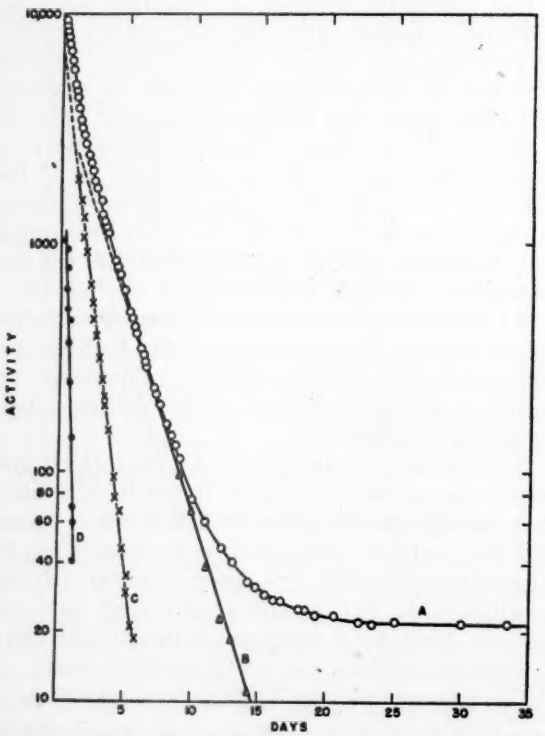

FIG. 6. Gross decay of gold fraction from Ir+α bombardment. A, B, C, and D are, respectively, the resolved decays of half-lives 185 days, 39.5 days, 15.8 hours, and 4.0 hours.

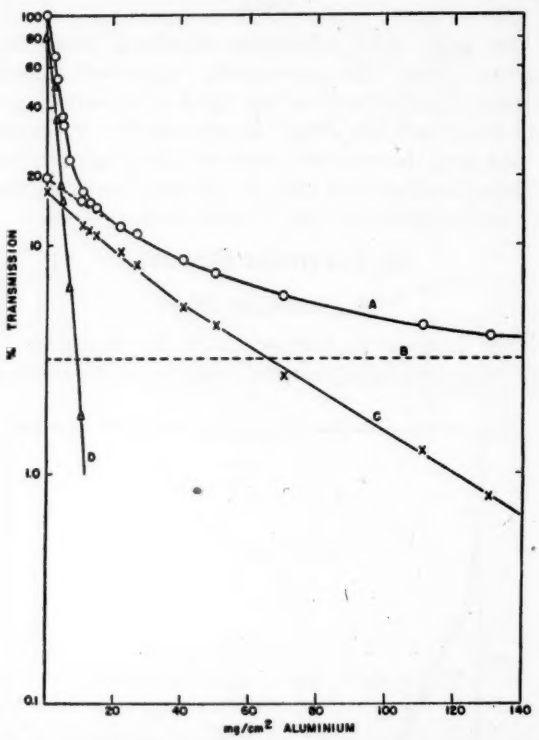

FIG. 7. Aluminum absorption of 185-day Au^{195} from Pt+d. (A) Measured curve. (B) K x-ray and γ-ray background. (C) L x-rays. (D) Electrons.

The hard γ-radiation had a gross decay of 3.00 ±0.05 days through eight half-lives. This was consistent with the small contribution to the total quantum radiation to be expected from the electron activities of the 4.33-day isotope present. This contribution was computed and the absorption of the electromagnetic radiation of the 3-day activity obtained by subtraction. The aluminum absorption of the 3.0-day activity showed L x-rays while the lead absorption curve (Fig. 5) showed components of half-thicknesses ~190 mg/cm², 5.4±0.2 g/cm², and 15 g/cm². With the heavier absorbers there was

a marked divergence from linearity of the 5.4-g/cm² line. The assumption of a small background of a γ-ray of $\sim$15 g/cm² half-thickness corrected this, and it would seem that the 3-day isotope also has a hard γ-ray similar to that of the 4.3-day isotope. This assumption is supported by the fact that the contribution to the hard γ-radiation computed for the 4.33-day isotope is less than 0.2 of the activity which has to be subtracted to give a linear absorption for the 5.4-g/cm² ray. The latter, which corresponds to 0.57-Mev energy, is undoubtedly the unconverted γ-rays corresponding to the 0.5-Mev electrons.

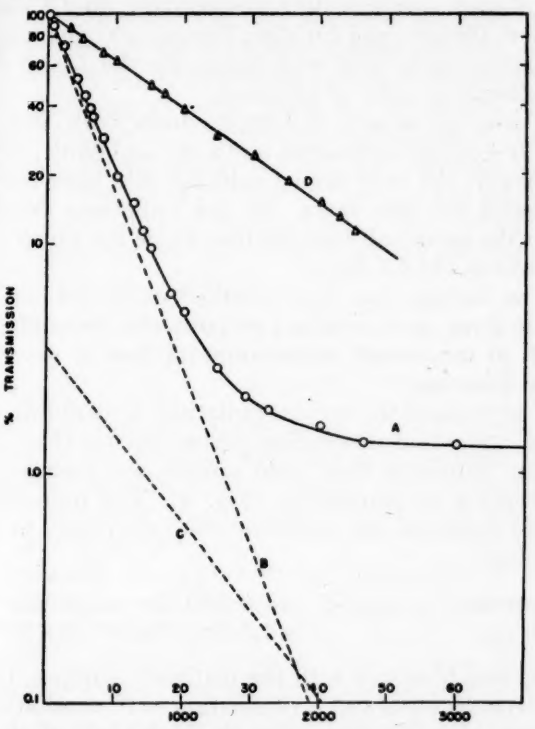

FIG. 8. Lead absorption of 185-day Au^{195} from Pt+d. A, B, C are components of half-thicknesses of 15 g/cm², $\sim$400 g/cm², and 185 g/cm² lead. D is the measured absorption of hard γ-ray.

The ratio of electrons to quantum radiation for the 3.0-day activity has been computed from measurements on an "infinitely thin" sample mounted on very thin mica and from the lead absorption. The following ratios were obtained after all corrections had been made:

0.1-Mev electron:0.5-Mev electron:L x-rays:
K x-rays:0.57 Mev γ:1.7 Mev γ
$=2\times10^{-3}:0.2:\sim1:1:0.2:1\times10^{-2}$.

The 3.0-day platinum activity is allocated to mass 191. It is produced with a cross section of $\sim$0.09 barn assuming Ir^{191}-d-2n reaction with 19-Mev deuterons; no iridium daughter of half-life greater than a few minutes has been detected. It is

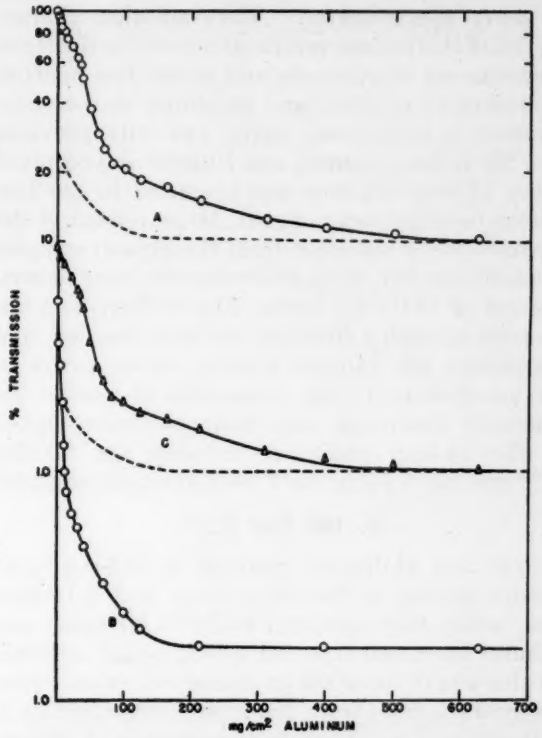

FIG. 9. Aluminum absorption of 39.5-hour Au^{194} and 185-day Au^{195} from Ir+α. (A) Measured absorption of mixture at 8.5 days after bombardment. (B) Contribution of 185-day activity at 8.5 days after bombardment obtained from subsequent measurements. (C) Resolved absorption of 39.5-hour Au^{194}.

not observed in the thermal neutron bombardment of platinum. In the bombardment of platinum with fast neutrons from a Be+d source, the platinum fraction, after decay of the shorter-lived 31-min. and 19-hour activities, showed a complex decay caused by a mixture of the 4.33-day activity with a small yield of the 3.0-day activity.

For 19-Mev deuterons, the d,3n reaction on Ir^{191} might be expected to form Pt^{190}, since the d,3n reaction with platinum and other elements in this region has a cross section $\sim$0.1 that of the d,2n reaction. However, no activity other than the 3.0- and 4.33-day activities were observed in the platinum fraction from deuteron bombardments of iridium, nor was the 10.7-day Ir^{190},[9] which would be the daughter of Pt^{190}, found in the iridium fraction. From general considerations of nuclear stability, Pt^{190} is expected to be stable or very long-lived; from the present data, the half-life is greater than five hundred years.

IV. GOLD ISOTOPES

A. 5.55-Day and 14-Hour Au^{196}

The 5.55-day gold activity has been previously reported[8] and its radiations have been studied by

[9] L. J. Goodman and M. L. Pool, Phys. Rev. 71, 288 (1947).

the β-ray spectrometer.[10] The radiation characteristics of this isotope produced here in the deuteron bombardment of platinum and in the fast neutron bombardment of gold, and measured in the same geometry in both cases, agree well with previous data. McMillan, Kamen, and Ruben[8] also reported that a 14-hour activity was produced in the fast neutron bombardment of gold. Measurement of the electromagnetic radiation from the present samples with sufficient beryllium to remove electrons showed a period of 14.0 ± 0.3 hours. The activity was not observed through a 2000-mg/cm^2 lead absorber, and presumably the 14-hour activity emits x-rays or soft γ-radiation. It was impossible to resolve the aluminum absorption and lead absorption curves for the 14-hour radiations because the 5.5-day Au^{196} and the 3.7-day Au^{198} formed simultaneously.

B. 185-Day Au^{195}

Cork and Halpern[11] reported a 164-day gold activity having a 0.45-Mev β-ray and 0.11-Mev γ-ray which they allocated to Au^{199}. Krishnan and Nahum[7] have also reported a long period activity, but this was in too small an amount to characterize. The gold fractions from deuteron bombardments of platinum and α-particle bombardments of iridium measured in the same geometry, show, after decay of the shorter periods, a long-lived activity whose radiation characteristics are identical in the two cases. A very active sample of the gold activity was obtained from a platinum target which had received a total of 490 microampere hours of 19-Mev deuterons and which had decayed for five months prior to separation. A sample of about 0.4 millicurie was obtained on four milligrams of gold carrier.

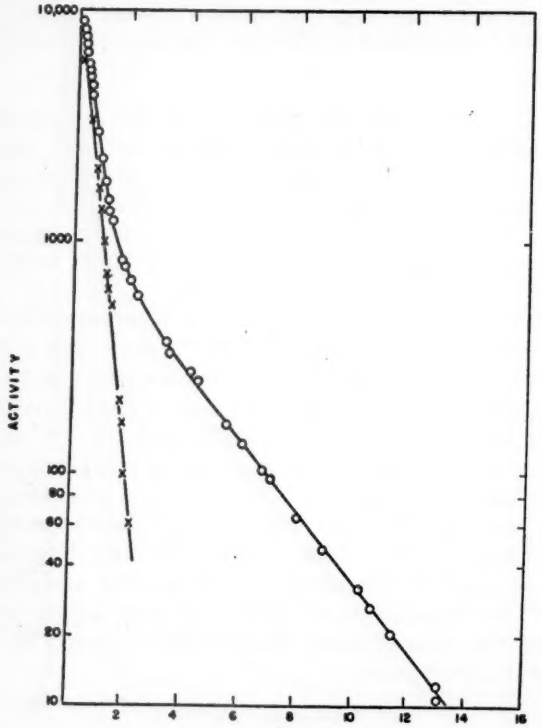

FIG. 10. γ-ray decay of 4.0-hour Au^{192} and 39.5-hour Au^{194} from Ir+α bombardment. Measurements made through 10 g/cm^2 lead absorber.

The radiations of the isotope consist of soft electrons of range 14 ± 1 mg/cm^2 aluminum, corresponding to 0.1 Mev, and electromagnetic radiation of half-thicknesses 29 ± 1 mg/cm^2 aluminum, 196 ± 3 mg/cm^2 lead, $\sim$400 mg/cm^2 lead, and 14 ± 0.5 g/cm^2 lead, corresponding, respectively, to 9.3 kev, 69 kev, 190 kev, and 1.6 Mev. The two soft quantum radiations agree well with values for the L and K x-radiation of gold or platinum.

The gross decays of samples from both Pt+d and Ir+α-bombardments, and x-ray and hard γ-ray decays of the very active gold samples have been followed for two years. All the radiations decay with the same half-life, the best value for which at present is 185 ± 3 days.

The isotope has been further examined on a crude β-ray spectrometer; no positrons, but only a peak of conversion electrons $\sim$100 kev in energy were observed.

The ratios of the various radiations were obtained from aluminum absorption measurements (Fig. 7) on an "infinitely thin" gold sample, and from lead absorption measurements (Fig. 8). The following ratios corrected for counting efficiency, etc., were obtained.

Electrons: L x-rays: K x-rays: 190 kev γ: 1.6 Mev γ
$= 1.5:3:1:3\times10^{-2}:1\times10^{-2}$.

As was observed with the platinum isotopes, the ratio of electrons and L x-radiation to K x-radiation is very high; this, and also the high yield of electrons, might arise from L electron capture or conversion of a γ-ray in the L shell. Since the decay scheme is somewhat indeterminate, bombardment yields were estimated assuming that one K x-ray represents one disintegration.

C. 39.5-Hour Au^{194}

After decay of the shorter-lived gold activities, the decay curve (Fig. 7) of the gold fraction from the α-particle bombardment of iridium shows only two components of half-lives 39.5 hours and 185 days. No 5.5-day Au^{196}, which could be formed by α,n reaction, was observed; the yield of an α,n reaction in this region at 38 Mev would be expected to be very small.

The 39.5-hour isotope has been further observed in high yield consistent with $d,2n$ reactions in the gold fraction from deuteron bombardment of platinum; in this case, however, resolution of the

[10] J. L. Lawson, and J. M. Cork, Phys. Rev. **58**, 580 (1940).
[11] J. M. Cork and O. Halpern, Phys. Rev. **58**, 201A (1940).

radiation characteristics is complicated by presence of the 5.5-day Au^{196} and 2.7-day Au^{198}.

The radiation characteristics of the isotope were determined by resolution of decay and aluminum absorption curves of the 39.5-hour and 185-day mixture from Ir+α-bombardments, and also of the gold fraction from short deuteron bombardments of platinum. The aluminum absorption curve (Fig. 9c) shows electrons of ranges 75 ± 5 mg/cm² (0.3 Mev) and ~800 mg/cm² (~1.8 Mev) aluminum. Using a crude beta-ray spectrometer, the harder electron has been shown to be a positron with a maximum energy of 1.8 Mev.

The softer electron has negative sign and may be a beta-particle or a conversion electron, or a mixture of both. The electromagnetic radiation of half-thicknesses ~28 mg/cm² aluminum, and 15 ± 0.5 g/cm² lead; complex radiations of intermediate energy can be resolved by assuming them to be a mixture of platinum K x-rays (195 mg/cm² lead) and γ-rays of energy 0.4–0.5 Mev. From the measurements the following ratios for the various radiations were obtained:

0.3 Mev e^-:1.8 Mev β^+: L x-rays:K x-rays: ~0.5 Mev γ:~1.8 Mev γ
$=0.2:0.03:\sim1.5:1:\sim0.1:1.5.$

All the various radiations decay with the same half-life; the decay of electrons and positrons was followed through eight half-lives and electromagnetic radiation through six half-lives to give a value of 3.9 ± 0.5 hours.

Assuming that one K x-ray represents one disintegration by orbital electron capture, about 3 percent of the disintegrations of the 39.5-hour activity occurs by positron emission. The isotope is the heaviest positron emitter yet characterized.

D. 4.0±0.2-Hour Au^{192}

In the gold fraction from long bombardments of iridium with 38-Mev α-particles, an activity of 4–6 hours was observed (Fig. 7). The isotope has been produced in short α-particle bombardments of iridium foil and was studied without chemical separation. Essentially similar results for the half-life and radiation characteristics were obtained for the separated gold fraction from short deuteron bombardments of platinum. The aluminum absorption curves are somewhat difficult to resolve, even in short bombardments, as a result of the presence of other gold activities. Electrons of range ~100 mg/cm² and with the 4.0-hour half-life. The electromagnetic radiation consists of K x-rays, and some soft γ-rays, but comprise mainly a very hard γ-ray of half-thickness 16–17 g/cm², corresponding to 2–3 Mev energy. The gross decay was followed through six half-lives and the decay of the very hard γ-radiation (Fig. 10) through seven half-lives

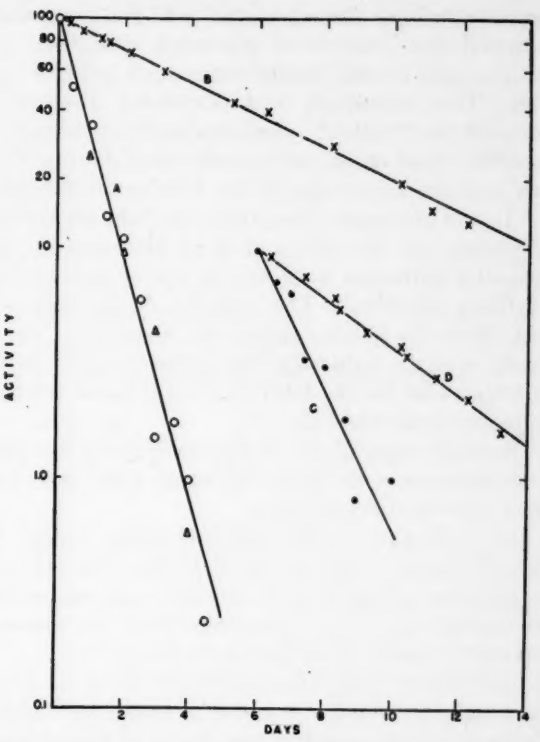

FIG. 11. Growth of Pt^{191} and Pt^{193} from Au^{191} and Au^{193}. (*A*) Decay of 15.8-hour Au^{193} as determined from "milked" activities of 4.33-day Pt^{193}. (*B*) Decay of "milked" 4.33-day Pt^{193}. (*C*) and (*D*) are similar curves for Au^{191} and Pt^{191}. △: data from Ir+α bombardments; ⊙: data from Pt+d bombardments.

to give a value of 4.0 ± 0.2 hours. The activity produced in short bombardments of iridium with 38 Mev α-particles was studied on a crude beta-ray spectrograph. The radiations were found to consist of positrons of maximum energy ~1.9 Mev. The negative electrons consisted of two distinct groups of maximum energies ~0.4 and ~1.5 Mev. The ratios of positron and negative electrons were obtained from the crude beta-ray spectrometer; comparing these values with those obtained from aluminum absorption measurements, and assuming that the gross electromagnetic radiation has a counting efficiency of 1 percent, the following ratios were obtained:

~0.4 Mev e^-:~1.5 Mev e^-:~1.9 Mev β^+:γ-radiation $=\sim0.07:\sim0.01:\sim0.01:1$

Assuming that one quantum of the gross electromagnetic radiation represents one disintegration by orbital electron capture, then about 1 percent of the disintegrations occur by positron emission.

E. 15.8-Hour Au^{193} and ~1-Day $Au^{191(?)}$

In both the deuteron bombardment of platinum and the α-particle bombardment of iridium, there should be produced Au^{193} which should be the parent of the 4.33-day Pt^{193}. Accordingly, in both

cases the bulk of the separated gold fractions were examined for growth of platinum daughter activities, and it was found that such growth did occur. The aluminum and beryllium absorption curves of the "milked" platinum activity, however, resembled that of the mixture of the 4.33-day Pt^{193} with a small percentage of the 3.0-day Pt^{191} activities. It was necessary, therefore, to follow separately the decays of the soft and hard electrons in the separated platinum fractions by use of appropriate beryllium absorbers. The energies of the soft and hard electrons in the aluminum absorption curve agreed with the values for the 4.33-day and 3.0-day activities, and the resolved decay curves for the two electrons confirmed this.

Chemical separations of platinum from the gold stock solution were made at equal time intervals under standard conditions.

The activities of the soft electrons, range 16 mg/cm² characteristic of the 4.33-day activity and the electron range 150 mg/cm² characteristic of the 3.0-day activity were determined from the absorption curve measured in standard geometry.

Corrections to the observed activities were made for chemical yield, i.e., the fraction of added platinum carrier counted, for decay of the activity between the time of separation and time of measurement and for self-weakening of the electrons in the various samples. In Fig. 11 activities of the platinum daughter activities, corrected to the time of extraction from the gold, are plotted as a function of time. The decay of these initial activities shows that the 4.33-day Pt^{193} grows from a parent with a half-life of 16 ± 1 hours. Separations were made over a period of seven days from the gold fraction produced in an 80-microampere hour bombardment of platinum with deuterons. The yields of the 3.0-day platinum and its parent, gold, were lower than those of the 4.33-day activity and its parent by a factor of ~15; measurements were consequently less decisive and the half-life of the gold parent can be placed only as about one day.

The 16-hour Au^{191} has been directly observed in the gross decay of the gold fraction from the 38-Mev α-particle bombardment of iridium (Fig. 8). The platinum daughter of this activity would be unobservable in the measured sample. Since the 5.5-day Au^{196} was not observed in the α-bombardment of iridium, it is then unlikely that the 15.8-hour activity observed was actually the 14-hour isomer of Au^{196}, formed by an α,n reaction. It has proved very difficult to determine the radiation characteristics of the 15.8-hour activity from absorption curves resulting from the presence of the other gold activities of not too dissimilar half-lives. The activity, has, however, x-radiation and soft electrons of range less than 50 mg/cm²; no hard γ-radiation was observed to decay with a 15.8-hour half-life.

V. DISCUSSION

The gold activities have been allocated as in the accompanying Table I. The 5.5-day and 14-hour activities can unequivocally be allocated to mass 196 on the basis of their formation in the $n,2n$ reaction on gold; the absence of the 5.5 day activity in the gold fraction from the 38-Mev α-particle bombardment of iridium is in agreement with this allocation since the α,n cross section at this energy is expected to be very low, i.e., less than $\sim10^{-4}$ barn.

Since the 4.33-day and 3.0-day platinum activities have been allocated to masses 193 and 191, respectively, the respective 15.8-hour and $\sim$1-day gold parents are allocated similarly.

Assuming that one quantum of the 2- to 3-Mev γ-ray of the 4.0-hour activity represents one disintegration and that the counting efficiency of such a ray is two percent, the cross section for formation of the isotope in the deuteron bombardment of platinum by Pt^{192}-d-$2n$ reaction is $\sim$0.1 barn, which agrees reasonably with order $d,2n$ yields estimated; with the same assumptions, the yield for the Ir^{191}-α-$3n$ reaction is 1.5 barns, again a reasonable value. Allocation to mass 192 agrees with the yields.

The 39.5-hour activity is allocated to mass 194 on the basis of reaction yields and absence of platinum daughter activity; in the α-particle bombardment of iridium, the yield, assuming Ir^{193}-α-$3n$ reaction and that one K x-ray represents one disintegration, is $\sim$1 barn; in the deuteron bombardment of platinum, Au^{194} could be formed both by $d,2n$ and $d,3n$ reactions, and the yields agree with the allocation.

The remaining unallocated isotope, the 185-day gold, is allocated to mass 195; the yield in the α-bombardment of iridium, for Ir^{193}-α-$2n$ reaction, and assuming one K x-ray represents one disintegration, is 0.1 barn, which agrees reasonably with values expected for $\alpha,2n$ reactions in this region. The present allocations agree reasonably with empirical rules for the stability of isotopes of odd atomic number and from comparison with half-lives of radioactive isotopes in similar positrons of other heavy elements. The short half-life of 15.8 hours for Au^{193}, however, seems anomalous; no longer-lived isomer has, however, been detected, and no activities of the 4.33-day platinum could be separated from the 0.4-millicurie source of the long-lived gold from deuteron-bombarded platinum.

Since the work on gold isotopes was terminated and a preliminary note published,[1] Steffen *et al.*[12] have reported that gold activities of half-lives 39 ± 1 hours and 180 ± 10 days are produced in the bombardment of platinum with 7-Mev protons. The mass allocation and radiation characteristics re-

[12] R. Steffen, O. Huber, F. Humbel, and W. Zünti, Helv. Phys. Acta 21, 195 (1948).

ported here were confirmed, but the latter, obtained from β-ray spectrometer and coincidence measurements, are given in greater detail than in the present paper.

ACKNOWLEDGMENTS

The author is much indebted to Dr. J. G. Hamilton and the crew of the 60-inch Crocker Laboratory cyclotron for their cooperation and assistance in bombardments, to Professor G. T. Seaborg and I. Perlman for their advice and encouragement, to Mr. H. G. Hicks and Mr. K. Street for assistance in part of the experimental work, and to the University of California for providing the facilities for this research.

PHYSICAL REVIEW VOLUME 75, NUMBER 7 APRIL 1, 1949

Boundary Conditions and Range of Force for *S* State of Two Protons

G. BREIT AND W. G. BOURICIUS
Yale University, New Haven, Connecticut*
(Received October 11, 1948)

The paper is divided into five sections the first of which is an introduction. In the second the possibilities of describing phase shifts by means of a boundary condition at a distance small compared with $e^2/mc^2=2.8\times10^{-13}$ cm is discussed. It is brought out that the irregular solution of the wave equation in a Coulomb field has a logarithmic infinity which masks the features of the wave function which have to do with phase shifts and therefore with observation. In Table I approximate values of essential quantities are listed. In Section III boundary conditions at moderate distances are studied. It is found that one can replace the "potential energy curve" description by the requirement that the logarithmic derivative of the wave function have an energy independent value at a distance of $\sim0.47\ e^2/mc^2$. Similarly the ^1S proton-neutron interaction can be approximately described by requiring the logarithmic derivative to have an energy independent value at $\sim0.49\ e^2/mc^2$. In the convention of dealing with distance times radial function the values of the logarithmic derivatives are ~0.08, 0.06 for the proton and neutron cases, respectively. It is also possible to require a linear variation of energy for the logarithmic derivative within limits and to retain agreement with experiment. It is pointed out in the introduction that theoretical arguments for considering a failure of the potential energy viewpoint exist and that the agreement of the boundary conditions of Section III with observation may be more than an accident. In Section IV the adjustment of the range of force is treated and evidence for a somewhat smaller value than 2.8×10^{-13} cm, perhaps 2.6×10^{-13} cm is discussed. Use is made of simple relationships between effective depth variation with energy and range. In Section V the function f of BCP is expanded in powers of energy E, the relations for potential energy curves of different shapes are taken up regarding equivalence of range, the deviations from linearity of f with E are discussed from the viewpoint of equivalent error in scattering, and a rapid procedure for finding the equivalent square well range by means of successive approximations is given.

I. INTRODUCTION

THE work reported on in this paper has two objects: (1) To investigate on an empirical basis the possibility of replacing the potential energy point of view for proton-proton scattering by boundary condition requirements; (2) to systematize the treatment of theoretically expected proton-proton scattering by bringing out the way in which different compact potential energy curves can give similar results and to make available convenient ways of adjusting the nuclear potential well parameters to experimental data.

The first of the two objects is related to the general desire of describing the collision process with a minimum of detailed hypothesis concerning the mechanism of the interaction. It has been brought out[1] that a description entirely by means of phase shifts is a possible one and that the isotropy of space implies certain restricting conditions on the possible set of phase shifts. This point of view is closely related to Heisenberg's S matrix.[2] While it is possible to describe the collision process in such a generalized manner, it is difficult to make such a theory quantitatively specific and to establish relations between different phenomena such as those of proton-proton scattering and of the meson field. For this reason it appears advisable not to neglect an approach of intermediate generality with the hope that the investigation might eventually be of help in the formation of a theory of nuclear forces. The question of representing the proton-neutron interaction by means of a suitable boundary condition at zero distance between nuclear particles has been thought about by Wigner about 15 years ago[3] but subsequent calculations on binding energies and other nuclear phenomena have pointed to the potential energy curve of finite width as the more promising temporary expedient. The possibility that the interaction between protons might be confined to distances of negligible amount on the

* Assisted by ONR, Project NR 024-055.

[1] G. Breit, nuclear physics volume of the *University of Pennsylvania Bicentennial Conference*, N-15-15 (University of Pennsylvania Press, Philadelphia, 1941).

[2] W. Heisenberg, Zeits. f. Physik. 120, 513, 673 (1943).

[3] E. P. Wigner, private communication.

scale of an electronic radius has been borne in mind in the early work on proton-proton scattering[4] and for this reason a formula [Eq. (7.9) of BCP] has been given by BCP[4] by means of which the phase shift expected for an interaction at any energy can be obtained from a preassigned phase shift at one energy. Figures 8, 9, 10, and 11 of BCP show the comparison of the variation of the phase shift according to this formula with variations to be expected for interactions of finite range and the then available experimental material. It was clear from this as well as the later work of BTE that on the hypothesis of zero range of force the phase shift increased much too fast with energy. The relation under discussion was obtained by going to the limit of an interaction potential of zero range which was made to fit the preassigned value of the phase shift at a preassigned energy during the limiting process. The interaction energy in the limit of zero range is infinite.

Although experiment speaks in favor of interaction potentials of finite rather than zero range, one cannot claim that the potential energy curves are more than convenient and temporary expedients. In particular the meson theory of nuclear forces[5] implies that when the protons are close together they exist part of the time as neutrons and positive mesons or as protons and neutral mesons. The meson theory,[5] while similar to quantum electrodynamics differs from the latter in two important respects: (a) the finite rest mass of the meson as contrasted with the zero mass of the photon, (b) the relatively large value of the parameter which corresponds to the fine structure constant $e^2/\hbar c$. Meson theory does not presuppose the existence of interactions between mesons other than the ordinary electromagnetic interaction. It is not known, however, that such interactions do not exist. Supposing for the moment that they are present, one would have a theory of nuclear forces somewhat analogous to that of molecular forces. The ratio of the meson mass to the proton mass being much larger than the corresponding electron-nucleus ratio for the molecular case one expects the picture of a static potential energy curve to be relatively much poorer. For the same kinetic energy the residual proton's or neutron's velocity is only about $(1836/330)^{\frac{1}{2}}=2.4$ times smaller than that of the meson. The conditions of the Born-Oppenheimer approximation are satisfied on this crude picture very poorly. It appears doubtful, therefore, that the usual type of wave mechanical treatment of nuclear particles inside the potential energy hole can be taken literally. This appears to be especially questionable in relation to the assignment of the same effective mass to the protons in the region where the interaction takes place as when they are free. The two-particle wave equation in this region is only a substitute for a many particle equation of a character which cannot be definitely stated until the meson theory is more fully developed. It would not be surprising, therefore, if the rather good agreement of calculations making use of potential energy curves were somewhat accidental. It was thought of interest, therefore, to look into the possibility of describing the ^1S interaction on a basis intermediate between that of a boundary condition at zero distance and a potential energy curve. It was found that if one assumes that the logarithmic derivative of the wave function has a value independent of the energy at a suitable distance then the agreement with experiment is about as good as for a potential energy well. The distance at which this is the case is about $0.47\ e^2/mc^2$ and the value of the homogeneous logarithmic derivative Y is about 0.08. The function of which the derivative is taken is the distance times the radial function so that the homogeneous logarithmic derivative of the radial function is -0.92. It is supposed in this consideration that the radial function is continued from large distances down to the point at which Y is calculated without any interaction potential except for the Coulomb energy. If such an explanation had a literal significance it would imply that the kinetic energy before collision has no influence on the wave function of the protons just inside the boundary distance. This cannot be true, of course, except as an approximation, and it is not desired to emphasize the rather good fit with experiment which one obtains except insofar as it shows that the extreme requirement of energy independence of Y is in no worse agreement with experiment than the requirement of an energy independent potential energy curve. If the boundary condition under discussion were to be taken literally, one would have to conclude that the kinetic energy before collision becomes subdivided among mesons and nucleons inside the sphere of interaction to such a degree

[4] G. Breit, E. U. Condon, and R. D. Present, Phys. Rev. **50**, 825 (1936), referred to as BCP. G. Breit, H. M. Thaxton, and L. Eisenbud, Phys. Rev. **55**, 1018 (1939), referred to as BTE. L. E. Hoisington, S. S. Share, and G. Breit, Phys. Rev. **56**, 884 (1939), referred to as HSB. E. Creutz, Phys. Rev. **56**, 893 (1939). Leslie L. Foldy, Phys. Rev. **72**, 125, 731 (1947). R. E. Peierls and M. A. Preston, Phys. Rev. **72**, 250 (1947). G. Breit, A. A. Broyles, and M. H. Hull, Phys. Rev. **73**, 869 (1948), referred to as BBH.

M. A. Tuve, N. P. Heydenburg, and L. R. Hafstad, Phys. Rev. **50**, 806 (1936). Herb, Kerst, Parkinson, and Plain, Phys. Rev. **55**, 247 (1939), referred to as HKPP. L. R. Hafstad, N. P. Heydenburg, and M. A. Tuve, Phys. Rev. **56**, 1078 (1939), referred to as HHT. G. L. Ragan, W. R. Kanne, and R. F. Tashek, Phys. Rev. **60**, 628 (1941), referred to as RKT. A. N. May and C. F. Powell, Proc. Roy. Soc. **A190**, 170 (1947). R. R. Wilson and E. C. Creutz, Phys. Rev. **71**, 339 (1947). Robert R. Wilson, Phys. Rev. **71**, 384 (1947). Wilson, Lofgren, Richardson, Wright, and Shankland, Phys. Rev. **72**, 1131 (1947). I. H. Dearnley, C. L. Oxley, and J. E. Perry, Jr., Phys. Rev. **73**, 1290 (1948). Blair, Freier, Lampi, Sleator, Jr., and Williams, Phys. Rev. **74**, 553 (1948), referred to as BFLSW.

[5] H. Yukawa, Proc. Phys. Math. Soc. Japan **17**, 48 (1935).

that the emerging protons, although possessing the original kinetic energy, have shared it with other particles almost up to the instant of emergence. The logarithmic derivative could conceivably be determined under such conditions mainly by other factors than the external kinetic energy. In this connection it is natural to consider the fact that for a single body problem with potential energy there is a connection between the logarithmic derivative and the probability of the particle being inside the boundary. This states that the rate of change of the logarithmic derivative with energy is proportional to the ratio of the probability of finding the particle inside the boundary to the square of the wave function at the boundary. This relation is the last of the three formulas under Eq. (10.3) of BCP and is in the notation of BCP as well as that of the present paper;

$$\frac{\partial}{\partial E'}\left(\frac{\partial \mathfrak{F}}{\mathfrak{F}\partial r}\right)=\frac{1}{\mathfrak{F}^2}\int_0^r \mathfrak{F}^2 dr.$$

If such a connection were to exist in the physical problem, the requirement of energy independence could not be maintained. It is seen, however, that if the lower limit in the above integral were to be a number close to the upper limit the value of the right side could be appreciably decreased. The change in the lower limit corresponds to applying the one-body wave equation to a part of the region inside the boundary and this fits in with the picture of the protons forming themselves in the physical state in which they emerge a short distance inside the boundary sphere. The evidence for the empirical validity of this boundary value description is discussed in Section III. It is pointed out there that a similar description of the proton-neutron interaction in the ^1S state is possible and that slow neutron scattering data point to approximate constancy of the logarithmic derivative at ~ 0.49 e^2/mc^2 and with a value of $Y \sim 0.06$, values not very different from those for proton-proton scattering. The data on scattering of neutrons of ortho- and parahydrogen are not discussed because the scattering in the triplet state is essential here and because it involves the "tensor force" which provides additional parameters. From the point of view of the boundary condition, calculations of nuclear binding energies by means of Hamiltonian functions with customary exchange forces would require formal changes. Since the evidence considered here is concerned only with the ^1S states, it is possible to avoid difficulties with the saturation of nuclear forces by imposing suitable requirements on states with other orbital and spin angular momenta. It would be possible to attempt to form a theory in which interactions of nuclear particles would be primarily in S states.[6] On such a view p scattering for nucleons would be expected to be present for nuclear particles in a subordinate way if at all. While there are claims of appearance of p waves for proton-proton scattering[7] the experiments used are subject to many sources of error and it is possibly premature to draw a definite conclusion. In closing the preliminary discussion of the energy independent logarithmic derivative, it appears appropriate to emphasize three negative points: (a) There is no evidence so far that the new description is better than the potential energy point of view. (b) It is not probable from the viewpoint of field theories that it can be more than an idealization of a more involved condition. (c) It is possible to fit experiment on the assumption of an energy independent $\partial Y/\partial E$ with a wide choice of values of $\partial Y/\partial E$ of which the value zero, especially emphasized here is a special case.

The last of the three negative points is connected with the fact that $\partial Y/\partial E$ is also nearly energy independent at the boundary of a compact potential well. Some of the consequences of the linear dependence of Y on E are looked into in Section V. The behavior of the energy dependent function f of BCP is considered and its deviation from linearity is worked out. There is a connection between the formulas worked out here and the claims of Landau and Smorodinsky.[8] These writers take a critical and condemning attitude towards the work on proton-proton scattering by one of the authors of the present paper and his former collaborators. In the interests of clarity of the relationship between supposedly different treatments of the same subject as well as a matter of justice to the people involved it becomes necessary to point out that:

(1) Landau and Smorodinsky set up the problem of calculating the dependence of the phase shift on energy on the assumption that the range of force is very small and discuss the limiting case when the range is zero. They find that agreement with experiment is not obtained but they also find that agreement can be secured if the "constant" which they call α_{pp} is made to vary linearly with E. They make a qualitative statement indicating that they believe it reasonable for α_{pp} to vary linearly. They fail to state, however, that the dependence of the phase shift K_0 on E for the case of zero range has been printed as Eq. (7.9) of BCP and that curves corresponding to this relation have been sketched in Figs. 8, 9, 10, 11 of BCP. They also do not state that the quantity with which they deal is within a constant the energy dependent but distance inde-

[6] This general point of view has been considered independently for some years by E. Fermi and E. P. Wigner (private considerations).

[7] R. E. Peierls and M. A. Preston, Phys. Rev. **72**, 250 (1947).

[8] L. Landau and J. Smorodinsky, J. Phys. Acad. Sci. U,S,S,R, **8**, 155 (1944).

pendent quantity f of BCP by means of which phase shifts have been calculated by BCP for the smaller ranges of force.

(2) The requirement of linearity of α_{pp} of Landau and Smorodinsky is identical in consequences with approximating the logarithmic derivative occurring on the left side of Eq. (7.5) of BCP by a linear function of the energy and retaining in the four power series which occur on the right side of this equation only terms of zero and first power in the energy. As has been stated by BCP this Eq. (7.5) is especially suitable for the discussion of conditions for short ranges of force. It is obvious from it that with the approximations just mentioned the quantity f should vary linearly with E, as was realized in the course of the calculations of BCP. The numerical conversion factors have been stated explicitly by BCP, and it was presumed that any interested reader would estimate the relative importance of the terms.

In view of the above it appears fair to say that the relation which Landau and Smorodinsky state to be an improvement on all previous work is in reality an old relation and that its limitations have been stated in the form of equations and numbers in the work to which Landau and Smorodinsky take exception.

(3) It is not true as Landau and Smorodinsky state that the series of papers which they criticize fails to bring out the fact that potential energy curves of different shapes can give the same phase shift in the energy region 0.6 to 2.4 Mev within or close to the accuracy of available data. This was verified by numerical calculation for the square well, Gauss Error, Exponential, and Meson Potentials. In the first column of p. 844 of BCP it was brought out how one can compare potential curves of different shapes making use of the connection between the logarithmic derivative Y and the phase shift and of the general connection between $\partial Y/\partial E$ and the "form factor" of the wave function which is shown by the last of the three formulas in Eq. (10.3) of BCP. The features which matter for the equivalence of potentials of different shapes have been studied in HSB where curves showing approximate sensitivity of phase shift to potential changes at different distances have been given. By means of these one can estimate to what degree potential energy curves of different shapes are equivalent. This work is also stated by L and S as being inadequate. In point of fact it goes farther than the conclusions of L and S because by means of it one can discuss the limitations of equivalence of potential wells.

(4) It is stated by L and S on p. 154 that in the series of papers to which they take exception: "The fundamental conclusion about the approximate identity of the specific forces acting between a proton and a neutron, on the one hand, and a proton and a proton, on the other, is based on the application of the rectangular wells." It is relevant to remark that: (*a*) On p. 845 of the paper by BCP the comparison is made for the Gauss Error potential and in a related paper Breit and Stehn have also used the Gauss Error potential. Similarly BTE made comparisons for the Gauss Error potential. (*b*) Comparisons of proton-proton and proton-neutron interactions have been made for the meson well by HSB.

(5) It is also not true as is implied on p. 224 in a sequel paper by Smorodinsky[9] that the importance of the assumption of equality of range of force for drawing conclusions about equality of depth of potentials has been overlooked in the work preceding the paper of Landau and Smorodinsky. Thus on p. 14 of reference 1 in the section on the "Comparison with the Proton-Neutron Potential" it is stated that the range of force for the proton-neutron interaction is not known directly and that "Assuming that in the $^1S_0$ states the proton-proton and proton-neutron interactions have the same range their magnitudes can be compared." The sentence starting on the second line of the next page brings out the dependence of the estimate on "the assumed range of the triplet interaction." It is hard to see how there could be doubt about the conditional and speculative attitude towards the hypothesis of approximate charge independence of non-Coulombian nuclear forces. In Table XIV, p. 842 of BCP the large sensitivity of the depth of the potential to assumed range is clearly seen and the purpose of this section of BCP's paper has been stated in the first column of p. 842: "It appears of interest to see whether it is possible to consider the proton-proton and proton-neutron interactions to be the same in the ^1S states." The strong sensitivity of depth to range was so well known to the majority of nuclear physicists that it appeared absurd to elaborate the point in the Physical Review. It was brought out more explicitly, however, in the University of Pennsylvania paper[1] which is quoted by L and S. It is also necessary to state that the important part of approximate resonance of the potentials to zero energy for the comparison of the two potentials which Landau and Smorodinsky bring out and apparently consider as meeting the situation is precisely the starting point of Section 5, p. 842 of BCP. In later papers of the ill spoken of series the closely related viewpoint of the virtual level has been used.

(6) It is not the desire to produce the impression that the series of papers under discussion is considered to be correct in all respects or to contain the best point of view. The papers were reports on

[9] J. Smorodinsky, J. Phys. Acad. Sci. U.S.S.R. 8, 219 (1944).

work done with the usual purpose of making it easier for others to further progress with the aid of information supplied. They were not written in the spirit of patent applications and well known or obvious facts were, therefore, left unemphasized. It is in this perhaps that the misunderstanding lies.

The discussion of the linearity of f is carried out in Section V of the present paper and the accuracy of linear and parabolic approximations is examined. It is found that the linear approximation is good to within ~ 0.13 percent of the scattering cross section at a scattering angle of 45° at 600 kev but that the accuracy decreases as the bombarding energy is increased. Equivalence of range of potential wells having different shapes is discussed more systematically than previously in connection with Eqs. (7.46), (7.47). The determination of range and depth of a square well by means of values of f and df/dE at $E=0$ is discussed in connection with Eqs. (8.6), (8.61), (8.63) by means of which the potential well parameters can be determined by a rapidly converging method of successive approximations. The equivalent parameters for scattering at low energies by other than square well potentials can then be found by means of Eqs. (7.46), (7.47). The expansions of Coulomb functions in powers of the energy involving Bessel functions which have been worked out by Yost, Wheeler, and Breit[10] can be used to work out terms of higher powers in E if desired.

In Section IV the adjustment of the range of force is discussed by the simple method of plotting the logarithmic derivative at the boundary of a square well with approximately the correct range and comparing the graph with the computed value for the square well. Formulas are given for making the final adjustment by means of the graph. This method is more directly related to the properties of the potential well than that of the f function. For potential curves of different shapes the equivalent parameters can be obtained by means of Eqs. (7.44), (7.47).

The possibility of describing the interaction by a boundary condition at $r=0$ is considered in Section II. Characteristic differences between the proton-proton and proton-neutron problem are taken up and reasons for the failure of appearance of simple boundary conditions at $r=0$ are brought out in connection with differences in asymptotic form of the irregular solution in the two cases. The considerations of this section do not exclude the possibility of describing the measured phase shifts by a statement concerning the asymptotic form of the solution of the Schroedinger equation in a Coulomb field extrapolated to $r=0$. This can obviously be done by simple continuation of the function. The discussion indicates, however, that a logarithmic infinity masks the features of the wave function which matter for scattering. The logarithmic term in Eq. (2.5) is the trouble maker and as one sees by means of Eq. (2.4) the logarithmic derivate $d\mathfrak{F}/\mathfrak{F}dr$ is directly related to the quantity f_1 rather than to f. The conclusions of Section II would have to be reversed if one could find a reason for requiring a simple behavior of the limit of $d\mathfrak{F}/\mathfrak{F}dr-(2/a)\times\ln(2r/a)$ rather than of $d\mathfrak{F}/\mathfrak{F}dr$. Equation (7.5) of BCP and the more detailed considerations of Section V of the present paper show to be sure that on the assumption of the potential well explanation the above quantity should vary approximately linearly with E. This restatement of conditions is, however, only another way of describing scattering by means of a potential energy curve and does not bring in a new physical picture. The evidence seems to point to the logarithmic derivative at distances of the order of 1.4×10^{-13} cm rather than zero as being the more relevant.

[10] F. L. Yost, J. A. Wheeler, and G. Breit, Phys. Rev. **49**, 174 (1936).

Notation

M = mass of proton.
$\mu=M/2$ = reduced mass in the collision of two protons.
v = relative velocity of the two protons before the collision.
$E=\frac{1}{2}Mv^2$.
E' = energy in frame of center of gravity $=E/2$.
$\Lambda=\hbar/\mu v$ = de Broglie wave-length.
$k=2\pi/\Lambda$.
$a=\hbar^2/\mu e^2$ = length analogous to Bohr radius.
$\eta=1/ka=(e^2/\hbar c)c/v$.
r = distance between protons.
$\rho=kr$.
$L\hbar$ = angular momentum.
F_L, G_L = regular and irregular solutions of differential equation for $r\times$radial function; the signs and normalization are as in YWB, BCP.
K_L = phase shift for angular momentum $L\hbar$ for proton-proton scattering.
$F=F_0$ when the specification of L is not needed.
$G=G_0$ when the specification of L is not needed.
$K=K_0$ when the specification of L is not needed.
$\gamma=0.5772\cdots$ = Euler's constant.
$\Gamma(x)$ = gamma-function of x.
$\mathfrak{F}$ = solution of wave equation for $r\times$radial function normalized in the same convention as F and G with a phase equal to phase of F plus K.
F_i = internal value of $\mathfrak{F}$.
b = value of r for boundary of proton-proton nuclear well; in some cases r is used for b.
$z=[(M/\hbar^2)(D+E/2)]^{\frac{1}{2}}r=0.4371(rmc^2/e^2)\times[D_{\text{Mev}}+(E/2)_{\text{Mev}}]^{\frac{1}{2}}$.
δ_0 = phase shift in ^1S state for proton-neutron scattering.

TABLE I. Contributions to logarithmic derivative at very small distances.

$\ln(2r/a)$	-3	-4	-5	-6	-7	-8
rmc^2/e^2	0.51	0.187	0.069	0.0254	0.0093	0.00343
Linear term of Eq. (2.4)	0.12	0.025	0.0024	−0.0016	−0.0015	−0.0009
$rd\mathfrak{F}/\mathfrak{F}dr$	0.09	0.021	0.002	−0.0017	−0.0015	−0.0009
Correction for kinetic energy	0.012	0.0017	0.00023	0.00003	0.00000	0.00000
Coulomb correction	−0.041	−0.015	−0.0055	−0.0020	−0.0007	−0.0003
$[rdF_i/F_i dr]_{E=0,\epsilon=0}$	0.06	0.007	−0.003	−0.004	−0.002	−0.001

r_0 = radius of square well for proton-neutron interaction.
$C_0=[2\pi\eta/(-1+\exp 2\pi\eta)]^{\frac{1}{2}}$.
$\Phi_0=F_0/C_0\rho$.
$\Phi_0^*==dF_0/C_0d\rho$.
$\Theta_0=C_0G_0$, $\Theta_0^*=C_0\rho dG_0/d\rho$.
$\Psi_0=\Theta_0-\rho(2\eta\ln 2\rho+q)\Phi_0$.
$\Psi_0^*=\Theta_0^*-\rho(2\eta\ln 2\rho+q)\Phi_0^*-2\rho\eta\Phi_0$.

Where no confusion can arise the six functions just defined will be written as Φ, Φ^*, Θ, Θ^*, Ψ, Ψ^*, respectively.

$Y=rd\mathfrak{F}/\mathfrak{F}dr$.
$y=d\mathfrak{F}/\mathfrak{F}dr$.
$r_e=rmc^2/e^2$.

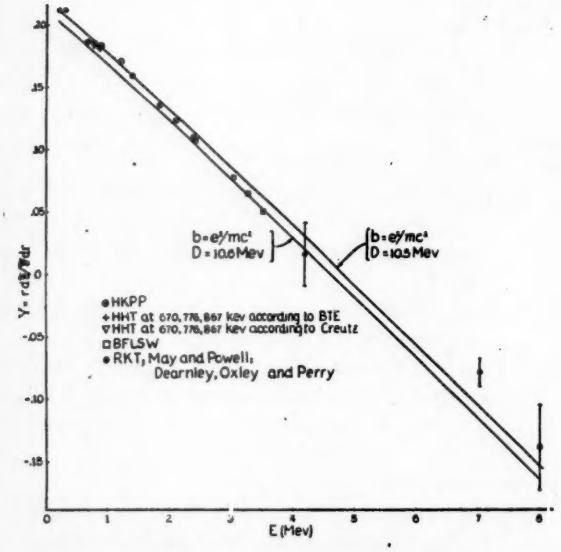

FIG. 1. Homogeneous logarithmic derivative Y at $r=e^2/mc^2$ plotted against energy. Circles, crosses, triangles, and squares correspond, respectively, to the experiments (see reference 4) of HKPP, HHT with values from BTE, HHT with values according to Creutz and BFLSW. The values at energies above 4 Mev and those of RKT are indicated by dots. The same notation is used in Figs. 2, 3, 4. The comparison curves correspond to assumed square well potentials of radius e^2/mc^2 and depths 10.5 and 10.6 Mev. These depths are in the convention of no Coulomb energy for $r<$radius of square well. Treatment of data is discussed in Appendix I.

II. BOUNDARY CONDITIONS AT VERY SMALL DISTANCES

For the analogous neutron-proton scattering problem it has proved useful to deal not only with the phase shift but also with the real and virtual levels in the singlet and triplet states as well as with Fermi's characteristic scattering length. The latter has the significance of an intercept on the axis of r formed by the tangent to the plot of $\mathfrak{F}$ against r. For thermal energy neutrons the characteristic lengths are constant and in this case the scattering can be described by a boundary condition at $r=0$. This boundary condition is simply a statement to the effect that the length $\mathfrak{F}dr/d\mathfrak{F}$ has a certain constant value. There is some evidence that for an energy range of several Mev the intercepts cannot perhaps be assumed to be constant because experimental data can be fitted by potential energy assumptions which imply a variation of the intercepts with energy. The variation in the values of the intercepts with energy is sufficiently mild to make it questionable whether the picture of an interaction potential has more significance than the description of scattering by means of the intercepts. Such a description amounts to the specification of a boundary condition having a mild energy dependence. In the present section the corresponding question is looked into for proton-proton scattering. Specifically the conditions on

$$[Y/r]_{r=0}=[d\mathfrak{F}/\mathfrak{F}dr]_{r=0}.$$

are dealt with.

The value of the logarithmic derivative of the function $\mathfrak{F}$ continued in towards small r from ∞ is conveniently obtainable from Eq. (7.5) of BCP[4] which is in the notation of the present paper.

$$Y=(r/a)\frac{X+[2\ln(2r/a)+f]\Phi^*}{\Psi+(r/a)[2\ln(2r/a)+f]\Phi}, \quad (2)$$

where

$$f=(C_0^2/\eta)\cot K_0+q/\eta-2\ln\eta;\quad C_0^2=2\pi\eta/(e^{2\pi\eta}-1), \quad (2.1)$$

$$X=[\Psi^*+2(r/a)\Phi]/(r/a), \quad (2.2)$$

$$q/2\eta=-1+2\gamma+\text{R.P.}[\Gamma'(i\eta)/\Gamma(i\eta)]. \quad (2.3)$$

In this formula the quantities X, Φ^*, Ψ, Φ are power series in r and in $1/\eta^2$ i.e., in the energy E the first few terms of which are found in Eq. (7.7) of BCP. Expanding the right side of Eq. (2) in powers of (r/a) one obtains

$$Y=(r/a)\{2+f_1+(-4-1/\eta^2-f_1^2)(r/a) +[2+1/\eta^2+(6+1/\eta^2)f_1-f_1^2+f_1^3] \times(r/a)^2+\cdots\}, \quad (2.4)$$

where

$$f_1=f+2\ln(2r/a). \quad (2.5)$$

If r is made to approach zero for a fixed energy, the quantity in the $\{\ \}$ in Eq. (2.4) approaches aymptotically the term $2+f_1$. One may also look at Eq. (2.4) without any reference to an interaction potential. It determines the value of the logarithmic derivative of the continuation of $\mathfrak{F}=F\cos K+G\sin K$ into the region of small r. The continuation is made by means of the radial equation for $\mathfrak{F}$ employing in that equation only the Coulomb energy and no specifically nuclear interaction energy. From this point of view Eq. (2.4) tells one how one should start the radial function $\mathfrak{F}/r$ at small values of r so as to reproduce a preassigned value of the phase shift K_0.

If r goes to zero, Y goes to zero also. On the other hand

$$Y/r\sim(2+f_1)/a \quad (2.6)$$

and this quantity approaches $-\infty$ for small r. If one wishes to account for Y/r by means of an interaction potential between zero and b then one has to use an interaction potential which makes

$$\lim(dF_i/F_i dr)_{r=b,\ b=0}=-\infty, \quad (2.7)$$

where F_i is the wave function in the region between zero and b. This condition as well as Eq. (2.6) imply that the intercept a_1 is such that

$$\lim 1/(b+a_1)=-\infty \quad (2.8)$$

and this means that $b+a_1$ approaches zero from the direction of negative values. A straight line drawn tangentially to the curve representing F_i as a function of r must cut the axis of r at a point for which

$$r=-a_1\sim b+\frac{a}{2|\ln(2b/a)|}. \quad (3)$$

As b approaches zero this point approaches the point $r=b$. This does not mean, however, that $\mathfrak{F}$ has a node at a point approximately located at $r=b$. In fact

$$-a_1/b\sim 1+[(2b/a)\ln(2b/a)]^{-1}. \quad (3.1)$$

The right side of the last equation approaches infinity as b/a approaches zero. With b at a *unit of length* the intercept assumes a position infinitely far to the right of the joining point b. The curve of $\mathfrak{F}$ against r/b when drawn on a scale of b as unit length is thus practically horizontal at the point $r=b$ and is only slightly inclined toward the axis of r/b. This behavior of $\mathfrak{F}$ is readily understood if it is remembered that

$$\mathfrak{F}=F\cos K+G\sin K,$$

and that $G\gg F$ for small r. The dominant term in G is

$$G\sim[1+(2r/a)\ln(2r/a)]/C_0, \quad (3.2)$$

and this means that

$$dG/Gdr\sim(2/a)\ln(2r/a), \quad (3.3)$$

which is just the behavior of $d\mathfrak{F}/\mathfrak{F}dr$ which follows from Eqs. (2.5), (2.6). The nearly horizontal direction of $\mathfrak{F}$ and the slightness of its inclination towards the r axis are obvious from Eq. (3.2). The properties of the boundary condition are thus direct consequences of properties of the irregular solution G.

The logarithmic derivative is seen in Eq. (3.3) to be dominated by a logarithmically infinite negative term. The interaction potential needed to reproduce this value by means of $dF_i/F_i dr$ is such, therefore, that it would correspond in the absence of the Coulombian potential to a real level at an energy E_1 given by

$$E_1\cong-(\hbar^2/M)(4/a^2)[\ln(2b/a)]^2 =-Mc^2(e^2/\hbar c)^2]\ln(2b/a)]^2. \quad (3.4)$$

The coefficient multiplying the square of the logarithm is of the order $mc^2/10.2=50$ kev. The quantity a is approximately 20.5 e^2/mc^2, the value of $\ln(2b/a)$ is roughly -5 when $2b$ is $e^{-2}=1/7.4$ of e^2/mc^2 and the level is then at ~-1.2 Mev. It would be preposterous to attach a literal significance to these numbers but it is true that the level under discussion is reasonably close to zero except for small distances b. For small b a non-relativistic approach is doubtful and the "level" has only a formal significance. This is so also for another reason. The logarithmic derivative has the value $-[M(-E_1)/\hbar^2]^{\frac{1}{2}}$ only if one neglects Coulomb repulsion in the stable state. The quantity referred to in Eq. (3.4) is the value which the energy of the

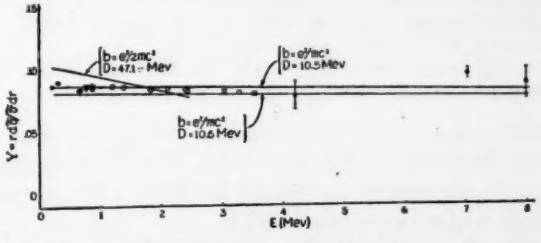

FIG. 2. Values of Y at $r=e^2/2mc^2$ obtained by continuation of Coulomb function with phase shift i.e., by means of $\mathfrak{F}=F\cos K+G\sin K$. The two nearly horizontal lines correspond to phase shifts computed for the square wells used in Fig. 1. The oblique line corresponds to square well with $b=e^2/2mc^2$, $D=47.14$ Mev. The notation of Fig. 1 is used.

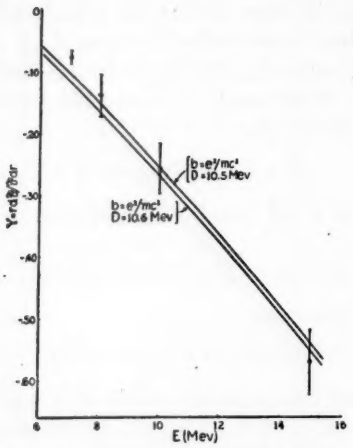

FIG. 3. Values of Y at $r=e^2/mc^2$ plotted against energy. The notation of Fig. 1 is used. This figure is an extension of Fig. 1 to higher energies.

stable level would have if the Coulomb interaction were removed in the region $r>b$. On account of the Coulomb interaction $|y|$ has to be larger than $[M(-E_1)/\hbar^2]^{\frac{1}{2}}$ and the above estimates have no direct relation to the existence of a stable level of two protons in each other's field. It is nevertheless convenient to deal with the concept of a level as employed here because by means of it one can describe by a single quantity some of the properties of the potential well, and because by defining the level in terms of y one can compare the proton-proton interaction directly with corresponding proton-neutron and neutron-neutron interactions. It may be pertinent to recall that in discussions of nuclear binding energies it is customary to characterize the interactions by means of an equivalent potential energy with the convention of considering it as acting in addition to the Coulomb effect and it is convenient for this reason to make the comparison in terms of a characteristic property of the potential well which is not affected by interactions outside the well radius b.

The considerations presented so far as too crude in the following respects:

(a) Only the terms which are dominant in Eq. (2.4) at small distances have been considered.
(b) Corrections for the effect of the kinetic energy of relative motion on y have not been made.
(c) Corrections for the effect of the Coulomb interaction inside the potential well also have to be taken into account.

The corrections mentioned as (b) and (c) will be made here only to the first order. The technique for making them can be found in BCP and in more detail and refinement in BTE.

The effect of these corrections can be put the form

$$[rdF_i/F_i dr]_{E=0,\,e=0,\,r=b} = \{Y+0.0489(E'/mc^2)(rmc^2/e^2)^2\xi - 0.0804(rmc^2/e^2)\xi'\}_{r=b}. \quad (4)$$

Here Y is obtainable accurately as the right side of Eq. (2) or as a series expansion in the form of Eq. (2.4). The logarithmic derivative on the left side is the value which follows from the radial wave equation if one starts its solution at $r=0$ subject to usual requirements of regularity and continues the solution to $r=b$. It is supposed that in this process the shape of the potential well has been fixed and that the depth has been adjusted to reproduce the value of Y required by experiment. In this adjustment the kinetic energy of relative motion inside the well and the term e^2/r are not neglected. After the depth of the well has been determined the radial equation is supposed to be solved once more and this time E and e are set equal to zero while the potential well is left unchanged. The function F_i so obtained is used in Eq. (4). If the same potential well acounts for experimental results at all energies then the left side of Eq. (4) is independent of energy. But for an arbitrary shape of the well and an arbitrary range the potential well depth depends on the energy and the left side of Eq. (4) is also in general dependent on the energy.

The first of the two correction terms in Eq. (4) corresponds to the removal of the kinetic energy term in the radial equation. The first three factors in it correspond to a "square well" and to a vanishing slope of F_i at $r=b$. The factor ξ takes into account geometrical differences produced by varying the well shape and also the effect of the slight angle between the direction of the curve representing F as a function of r/b and the horizontal. This correction depends only on

$$F_i^{-2}\int_0^b F_i^2 dr \quad (4.1)$$

and is insensitive to the shape of the well because the function F_i is approximated rather closely by an arc of a sine curve. For small b the value of F_i at $r=b$ is close to the maximum and the effect of deviation from the horizontal direction is slight.

The second correction term in Eq. (4) consists of three factors. The first two factors correspond to the correction under the same conditions as the first three factors of the kinetic energy correction. The last factor ξ' brings in the effects of differences in shape of the potential well and of the deviation of the direction of the plot of F_i against r/b from a horizontal direction. In this case the correction depends on

$$F_i^{-2}\int_0^b (F_i^2/r)dr \quad (4.2)$$

and is again not sensitive to the effects incorporated in ξ'. Both ξ and ξ' are nearly unity.

A numerical example will be helpful in showing

the relative importance of terms contributing to the right side of Eq. (4). For $E=1$ Mev the experimental interpolated value of K_0 is close to 32.4° and $\tan K_0=0.6346$. The other pertinent quantities are $\eta=0.1581$, $C_0^2=0.5842$, $q/\eta=-0.7868$, $f=8.725$. Neglecting terms beyond the one in $(r/a)^3$ of Eq. (2.4) one has values as in Table I. It is seen that the linear term $(r/a)(2+f_1)$ of Eq. (2.4) accounts for the trend of the logarithmic derivative in a qualitatively correct manner. For the smaller r in the table only the linear term and the Coulomb correction matter. At still smaller r the Coulomb correction becomes much smaller than $(r/a)(2+f_1)$ on account of the dominance of the logarithmic term in f_1. Taking into account the difference between the $2+f_1$ and the logarithmic term, one obtains as an improved approximation to the energy value of the quasi-stable level defined in the same way as for Eq. (3.4),

$$-E_1\cong Mc^2(e^2/\hbar c)^2 \times[1+(f/2)+\ln(2r/a)-0.82\xi]^2. \quad (4.3)$$

For the numbers considered in Table I the quantity $1+(f/2)\cong 5.4$ and contributes more to the position of the level than the Coulomb correction. The level lies higher than according to Eq. (3.4) by an amount which increases with $|\ln(2r/a)|$. Experimental values enter only through f and are masked for small r by the logarithmic term. The level moves to $-\infty$ as r approaches zero and the phase shift enters by raising the level by an amount which is infinite but negligible in comparison with the value of $|E_1|$. This differs from the simple conditions for the proton-neutron case. If one is to characterize the function in terms of its behavior at very small distances, then the logarithmic derivative itself would offer a simpler criterion. But either $dF_i/F_i dr$ or $rdF_i/F_i dr$ still contains as a dominant part the term in $\ln r$ which swamps all other effects. The considerations made above appear to indicate that it is improbable that the value of $dF_i/F_i dr$ at $r=0$ can be useful because the reason for its being infinite follows from properties of the irregular Coulomb function at short distances.

III. THE LOGARITHMIC DERIVATIVE AT MODERATE DISTANCE

It is expected from Eqs. (10.3) of BCP that the logarithmic derivative Y of the internal wave function varies linearly with the energy. This fact does not depend on the shape of the potential well as long as the well is "compact" *i.e.*, as long as it does not have a shallow and wide part extending to a large distance. Equations (10.3) of BCP give the rate of change of Y/r with energy in terms of the form factor listed in Eq. (4.1) of the present paper. This quantity is nearly independent of the incident kinetic energy at the boundary of a deep and narrow potential well because of the shape of the function F_i is nearly independent of the incident energy. The slope of the plot of $dF_i/F_i dr$ plotted against E is, therefore, nearly constant and this plot can be represented by a straight line to a good approximation. Two simple circumstances contribute to its goodness. In the first place the incident energy matters in determining the local wave-length by combining itself with the depth of the well under a square root. Secondly, only half of the incident energy counts because half goes into the kinetic energy of the center of mass.

Since the experimentally determined phase shift can be represented approximately by means of a potential well model, one expects that a plot of Y/r against E to be approximately a straight line provided r is made equal to the radius of a "well" that fits experiment. It turns out to be also true that Y/r varies linearly with the energy for other values of r and that the slope of the line can be made nearly zero through a wide range of energies by taking $r\cong e^2/2mc^2$.

The logarithmic derivative cannot be an exactly linear function of the energy through a range of distances r. In fact in terms of

$$y=Y/r, \quad (5)$$

then

$$dy/dr+y^2+(M/\hbar^2)[(E/2)-e^2/r]=0,$$

and if

$$y=a+bE+cE^2+\cdots, \quad (5.1)$$

then

$$\begin{aligned} da/dr+a^2-(M/\hbar^2)e^2/r&=0,\\ db/dr+2ab+M/2\hbar^2&=0,\\ dc/dr+b^2+2ac&=0. \end{aligned} \quad (5.2)$$

The first two of these equations give functions of r for a and b which do not vanish identically. The third equation cannot be satisfied unless c also does not vanish identically. It is thus impossible to have a strictly linear dependence of y on E at different distances. This does not mean however that this condition cannot be a good approximation. In particular, if by a suitable choice of r one makes $b=0$, then for this r a necessary condition for both $c=0$ and $dc/dr=0$ is satisfied.

In Fig. 1 is shown a plot of Y against E in the energy range 0 to 8 Mev for $r=e^2/mc^2$. The two

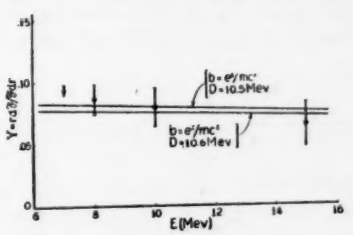

FIG. 4. Values of Y at $r=e^2/2mc^2$ plotted against energy. The notation of Fig. 1 is used. This figure is an extension of Fig. 2 to higher energies.

TABLE II. Values of denominator of Eq. (6.1) for use in finding width of well.

E (Mev)	0.2	0.8	1.4	2.4	3.4	6.0	8.0
z	1.424	1.445	1.464	1.496	1.528	1.606	1.665
$(-$ denominator$)$	0.41	0.42	0.43	0.45	0.47	0.52	0.56

lines which are nearly straight correspond to the calculated values for square wells with an assumed radius e^2/mc^2 and depths 10.5, 10.6 Mev, respectively, for the upper and lower lines. The experimental values of the phase shifts were used to compute the values of Y indicated by circles, squares, triangles, etc. as explained in the legend. No Coulomb energy was assumed to be acting inside the wells.

In Fig. 2 the values of Y computed for $r=e^2/2mc^2$ are plotted against E. There are in the figure two nearly straight lines between which most of the experimental points lie. These have been obtained by taking $\mathfrak{F}=F\cos K_0+G\sin K_0$ where K_0 corresponds to square wells with radius e^2/mc^2 and depths 10.5, 10.6 Mev, respectively, for the upper and lower lines. The value of Y corresponding to the $\mathfrak{F}$ obtained in the manner described was taken at $r=e^2/2mc^2$. There is besides in Fig. 2 a nearly straight line which cuts obliquely across the other lines. This corresponds to the value of Y at $r=e^2/2mc^2$ which is obtained for a "square well" with radius $e^2/2mc^2$ and depth 47.143 Mev. It is shown for comparison with the approximate fit of the 10.5, 10.6 Mev wells to experiment. The comparison shows the superiority of the larger radius in fitting experiment. The experimental points fall on a practically horizontal straight line. From an empirical point of view one can describe the observations about as well by requiring the logarithmic derivative to be constant at this distance as by dealing with a potential energy curve.

The experimental values of the phase shift which have been derived from the Wisconsin and Minnesota experiments fall approximately on a straight line which in Fig. 2 drops by approximately 0.004 in the value of Y as the energy changes from 0.2 to 3 Mev. The change in r which must be made in order to make the line horizontal will now be estimated. The equation satisfied by $\mathfrak{F}$ is

$$d^2\mathfrak{F}/dr^2+(M/\hbar^2)(E/2-e^2/r)\mathfrak{F}=0.$$

It follows from this equation that

$$rdY/dr=Y-Y^2-(Mr^2/\hbar^2)(E/2-e^2/r), \quad (5.3)$$

where the notation

$$Y=rd\mathfrak{F}/\mathfrak{F}dr \quad (5.4)$$

is used also with the modified meaning of $\mathfrak{F}$. Expressing E in Mev and r in e^2/mc^2 this relation becomes

$$rdY/dr=Y-Y^2-0.0955(r^2E-1.023r). \quad (5.5)$$

It can be verified that the values of dY/dr for the lines marked (10.5, 1) in Figs. 1 and 2 at 0.2 and 3 Mev give to a good approximation the mean rate of change of Y between $r=e^2/2mc^2$ and $r=e^2/mc^2$. This fact indicates that Y varies approximately linearly between these values of r and gives one confidence in Eq. (5.5) as a way of estimating changes in Y caused by changes in r. Interpreting Fig. 2 in the sense that experiment indicates $Y=0.089$ at $E=0.2$ Mev and $Y=0.085$ at $E=3$ Mev for $r=\frac{1}{2}$ one finds by means of Eq. (5.5) that

$$(dY/dr)_{E=0.2}=0.250, \quad (dY/dr)_{E=3}=0.110. \quad (5.6)$$

The line of Y will be made horizontal if the drop of $0.089-0.085=0.004$ is removed by a change from $r=0.5$ to $r=0.5+\delta r$. The value of δr is then such that

$$(0.110-0.250)\delta r=0.004,$$

which gives

$$\delta r=-0.02(9)$$

or

$$r=0.47.$$

The change in Y produced by this change in r is of the order -0.003 at $E=3$ Mev and -0.007 at $E=0.2$ Mev. This is an effect of roughly 10 percent in Y at 0.2 Mev. The slightly oblique line of experimental points can be made horizontal by decreasing the radius ~ 6 percent and lowering the line by ~ 10 percent at the left.

Figures 3 and 4 correspond to Figs 1 and 2 for the region 6 to 16 Mev, respectively. The experimental material is less certain in this region. It appears not to contradict either the potential well or the "boundary condition" at $r=0.47\,e^2/mc^2=1.32\times 10^{-13}$ cm type of fit. The limits of experimental error indicated in the figures are approximate only.[11]

For proton-neutron scattering a similar boundary condition for the ^1S interaction can be used. This case differs from proton-proton scattering through the absence of the Coulomb field, but it may be expected that there will be no great change because the effect of the Coulomb field is relatively small. If, for example, one assumes that the scattering is represented by a square well of depth D of radius r_0,

[11] The abbreviations HHT, HKPP, etc. of footnote 2 are used in the legends to and in Figs. 1, 2, 3, 4. These refer to the origin of experimental data. The points of BFLSW have been obtained by a somewhat crude analysis by the present authors. Since making the analysis and while the present paper was typed the authors received the results of a more careful study of the Minnesota material by Professor C. L. Critchfield which agrees closely with that used here. The authors should like to acknowledge their indebtedness to Professor Critchfield and to Messrs. Blair, Freier, Lamp, Sleator, and Williams for the communication of their results before publication. An account of the treatment of other experimental data is given in Appendix I.

then an extrapolation of the field free wave function to smaller distances gives the following expansion in E for the homogeneous logarithmic derivate Y^N

$$Y^N(r)=Y_0{}^N(r)+Y_1{}^N(r)E+Y_2{}^N(r)E^2+\cdots. \quad (5.7)$$

Here the coefficients of E are determined by their values at r_0 by the following relations:

$$Y_0{}^N(r)=r/(r+r_0\beta), \qquad \beta=[1-Y_0{}^N(r_0)]/Y_0{}^N(r_0), \quad (5.71)$$

$$Y_1{}^N(r)=-(Ar_0{}^2/3)(1+\beta)+C/[r_0(1+\beta)^2], \quad (5.72)$$

$$Y_2{}^N(r)=-(A^2/45)r(r+r_0\beta)^2 +ACr/3+C^2r/(r+r_0\beta)^3+C_1r(r+r_0\beta)^2, \quad (5.73)$$

where the constant A has the value

$$A=(M/2m)(e^2/\hbar c)^2(1\text{ Mev}/mc^2)=0.0955(3) \quad (5.74)$$

for r and r_0 in e^2/mc^2 and E in Mev. The constants C, C_1 are determined by the known values of $Y_1{}^N(r_0)$ and $Y_2{}^N(r_0)$ for which explicit formulas are listed as Eqs. (8.2), (8.3) later in this paper. It is also possible to compute $Y^N(r)$ directly since

$$Y^N(r)=\rho\cot(\rho+\delta_0), \quad (5.75)$$

where δ_0 is the phase shift for proton-neutron ^1S scattering. This can be determined by means of

$$Y^N(r_0)=z_0\cot z_0, \quad (5.76)$$

where z_0 is as defined in the list of notation. If one assumes that scattering is approximately represented by the square well parameters $D=11.75$ Mev, $r_0=e^2/mc^2$, then one obtains

$$Y^N(e^2/2mc^2)=0.05754-0.00027E -0.00004E^2+\cdots, \quad (5.8)$$

where E is in Mev. The linear term in E can be made to disappear by changing r to $\sim 0.490\ e^2/mc^2$ which gives $Y^N=0.0566$ at $E=0$. The value of r which makes the average slope zero between 1 and 10 Mev is $\sim 0.488\ e^2/mc^2$ which is practically the same as $0.490\ e^2/mc^2$ which makes the slope zero at $E=0$. If one wishes to reproduce the scattering expected for the square well parameter $D=11.33$ Mev, $r_0=e^2/mc^2$, then one obtains

$$Y^N(e^2/2mc^2)=0.07927-0.00038E -0.00004E^2, \quad (5.81)$$

and the linear term in E vanishes in this case for $r=0.492\ e^2/mc^2$. The reason for choosing the values 11.75 Mev, 11.33 Mev in the above examples is that the smaller value corresponds to the depth of the proton-proton well when corrected for Coulomb repulsion inside the well while the larger corresponds to the rather large value of 80×10^{-24} cm^2 for the scattering of thermal neutrons by bound protons. The two values are intended to cover approximately the range of possibilities.

The calculations of coefficients of powers of E for Eqs. (5.8), (5.81) have been checked by comparison with values of $Y^N(r)$ obtained by means of Eq. (5.75). The expansions in powers of E were found to reproduce the directly calculated values with errors not exceeding -0.00002 up to $E=3$ Mev, -0.00006 up to 10 Mev, -0.0015 up to 14 Mev. Powers of E higher than the second are seen not to be important in the energy range considered here. No direct significance is attached to the precise values of the coefficients in Eqs. (5.8), (5.81) or to the values of r for which $Y_1{}^N=0$. They are reproduced here as an illustration of the relative stability of conclusions to adjustments in the interpretation of experimental material. No attempt is being made here to cover the question of variation of the observed proton-neutron scattering cross section with energy since this is concerned also with the triplet state of the two particles. It is only intended to bring out that the contributions to the total cross section which arise from the singlet state can be considered as having closely equal values on the boundary condition and the potential energy points of view. The scattering of neutrons by ortho- and parahydrogen or the coherent scattering by crystals is not considered here because the spin-orbit-spin tensor interaction and the unknown range of the triplet force complicate the situation by introducing additional parameters. As in the case of proton-proton scattering the most that can be claimed for the boundary condition point of view is that it might deserve consideration alongside with the potential energy curve explanation.

It may also be of interest to mention that the constant value of $Y\sim0.08$ for proton-proton scattering is approximately the same as the absolute value of the correction to Y for internal Coulomb effect for $r=e^2/mc^2$. If one were to make this correction simply as in Eq. (4) one would obtain a much smaller Y which would correspond to $d\mathfrak{F}/dr\cong0$ at $r=0.47\ e^2/mc^2$. One could hardly justify the inclusion of the whole last term of Eq. (4) for $r=e^2/mc^2$ and the above coincidence of numbers appears to have no direct significance. The fact that the value of Y can be expected to become somewhat smaller when corrected for the internal Coulomb effect appears to be less open to criticism and seems to be connected with the fact that $Y_{E=0}{}^N\sim0.06$ of the proton-neutron interaction is a smaller number than $Y_{E=0}\sim0.09$ for protons interacting with protons. On this view there is a possibility of regarding the proton-proton and proton-neutron interactions as basically the same.

In concluding this section it is desired to emphasize the speculative character of the boundary condition, the fact that it is closely related to the velocity dependent potentials of BTE and also that no special significance is attached to exact

constancy rather than slow variability with energy of the logarithmic derivative.

IV. ADJUSTMENTS OF RANGE OF FORCE FOR SQUARE WELLS

The figures described in the preceding section have been prepared without making a correction for the effect of Coulomb energy acting between 0 and e^2/mc^2 on y. The lines marked as 10.5 Mev and 10.6 Mev correspond to interaction potentials which are constant between $r=0$ and $r=e^2/mc^2$. The practical considerations for preferring these lines to other possible lines is the simplicity of calculation for square wells without internal Coulomb energy and the fact that most of the more accurate experimental points fall between them. The estimate of the distance r at which y is energy independent is not affected by whether one takes the internal Coulomb energy into account or not. This estimate makes use of the 10.5 Mev, 10.6 Mev lines only as convenient computational devices. The estimates of range of equivalent potentials depend slightly on whether one assumes an internal Coulomb potential or not. This fact has been recognized in the work of BCP and BTE. Table XVI and Eqs. (11.2), (11.3) of the latter reference make it easy to compute the effect. The internal phase z used in Table XVI of BTE has the values 1.416, 1.482, 1.545, 1.635 at $E=0$, 2, 4, 7 Mev, respectively. It varies nearly linearly with energy. Table XVI of BTE and the numerical example preceding it show that only the first-order correction is important. The second line of the table shows that as z changes from 1.4 to 1.6 the internal Coulomb effect correction to the equivalent depth of the square well increases fractionally in the ratio $1.655/1.613=1.026$. The whole correction is of the order of 0.83 Mev, and the effect of taking into account the internal Coulomb energy is, therefore, to increase the effective depth by $0.83\times0.026=0.021$ Mev for a change of internal phase z of 0.2. The change in z from $E=0$ to $E=4$ Mev is $1.545-1.416=0.129$. The equivalent square well depth with internal Coulomb potential required to reproduce the phase shifts for a square well without Coulomb potential increases, therefore, approximately linearly by $(0.129/0.2)0.021=0.013$ Mev from $E=0$ to $E=4$ Mev. This change is about 1/8 of the difference in equivalent square well depth between the two lines marked (10.5, 1), (10.6, 1) in the figures. The experimental points form a line which appears to cut across the (10.5, 1), (10.6, 1) reference lines between $E=0$ and $E=4$ Mev. If the change in the range of force from e^2/mc^2 is as large as this cross over would call for, then it is about 8 times larger than the change from a nominal range of e^2/mc^2 which results from bringing in the internal Coulomb energy. The same experimental material calls for a slightly shorter range of force with internal Coulomb potential than without. The numerical value of this correction can be given more conveniently after the discussion of changes produced by newer trends in experimental values.

The approximate equivalence between a progressive depth change between two energies and a change in the range of force can be represented by a simple formula which can be derived by means of Eq. (10.3) of BCP. The derivation is straightforward and is omitted. The formula is:

$$\delta b/b=(\Delta D/2D)/\{[zs^2/(z-sc)]_2 - [zs^2/(z-sc)]_1\}, \quad (6)$$

where

$$s=\sin z, \quad c=\cos z.$$

Here it is supposed that for an assumed value of the range b experiment requires a potential depth D at $E=E_1$ and a depth $D+\Delta D$ at $E=E_2$. The range is supposed to be changed to $b+\delta b$ and the depth to $D+\delta D$ in such a way that the same range and depth account for experiment at both E_1 and E_2. All changes are supposed small enough to justify first-order calculations. The change in depth δD is eliminated and Eq. (6) results. The subscripts 1, 2 in this equation indicate that quantities are evaluated for $E=E_1$, E_2, respectively. The denominator consists of a difference of two such quantities and can be approximated by the result of differentiating the quantity in brackets with respect to E. It is found in this way that

$$\frac{\delta b}{b}\cong\frac{(\Delta D/D)\dot{[}D+(E/2)]/(E_2-E_1)}{[zs^2/(z-sc)][\frac{1}{2}+zc/s-zs^2/(z-sc)]}, \quad (6.1)$$

where z, s, c are to be evaluated at a suitably chosen mean energy. The denominator in the above Eq. (6.1) has the values listed in Table II as a function of energy. The table gives also the corresponding values of z. If the experimental curve is intrepreted as crossing over from the (10.5, 1) line at $E=1.4$ Mev to the (10.6, 1) line at $E=3.4$ Mev then Eq. (6.1) and Table II give

$$\delta b/b=(1/10.5)[(10.5+1.2)/2]/(-0.45)=-0.12$$

indicating $b\cong0.88e^2/mc^2=2.47\times10^{-13}$ cm. If the cross over takes place from $E=0.2$ Mev to $E=3.4$ Mev a similar estimate gives $\delta b/b=-0.07(7)$ indicating $b=2.59\times10^{-13}$ cm. If the cross over takes place from $E=0.2$ Mev to $E=8$ Mev then $\delta b/b=-0.032$ and $b=2.72\times10^{-13}$ cm. It is difficult to decide which of these values is the better.

The discussion of the effect of the thermal Coulomb potential indicated that it is approximately equivalent to an increase in well depth by 0.013 Mev from $E=0$ to $E=4$ Mev. Equation (6.1) and Table II indicate a corresponding $\delta b/b=-0.008$ which corresponds to an additional 0.8 percent

shortening of the range. This effect is smaller than the apparent uncertainties of available experimental material.

Changes in equivalent square well range obtained above can be translated into changes of the range parameter of other potential energy wells by means of Eq. (7.47) in a later section of this paper. It should be pointed out, however, that according to the work of HSB and of BBH the equivalence between potential wells is only approximate and that the equivalence in the sense of Eq. (7.47) has the meaning of giving the same results for scattering under a somewhat idealized condition of zero scattering energy. The adjustment of range outlined above is independent of questions of degree of linearity of the logarithmic derivative with energy and can be made as an over-all adjustment between any two energies.

V. EXPANSIONS IN TERMS OF ENERGY; NATURE OF APPROXIMATIONS

Solving Eq. (2) for f one has

$$f+2\ln(2r/a)=\frac{X-(a/r)Y\Psi}{Y\Phi-\Phi^*}, \tag{7}$$

where the quantities X, Φ, Φ^*, Ψ, f are as defined in Eqs. (2.1), (2.2), (2.3) and corresponding formulas of BCP. The quantity Y is the homogeneous logarithmic derivative of Eq. (5.4). Whether the potential energy is assumed to be a square well or some other potential curve which does not extend to large distances, Y varies nearly linearly with energy as discussed in Section III with reference to Eq. (10.3) of BCP. The quantities[12] X, Ψ, Φ, Φ^* also vary approximately linearly with E. One expects,[13] therefore, that the left side of Eq. (7) will be an approximately linear function of E.

If the potential acting inside the well is assumed to have the form

$$V=-A\mathfrak{v}(r/\beta), \tag{7.1}$$

where $\mathfrak{v}$ is an otherwise unspecified but regular function one has the depth parameter A and the range parameter β available for adjustment to observation. For an assumed β one can fit experiment at one energy say $E=E_1$ by adjusting the depth parameter A. The pair of values A, β will not fit in general the experimental values at another energy $E=E_2$. Whether it does or not depends only on how Y varies with E because V matters only through Y. If all quantities are approximated by linear functions of E then $\partial Y/\partial E$ depends only on the expression in Eq. (4.1). This expression will be called the range-energy form factor. The range parameter β enters the form factor implicitly through the internal function F_i. For different forms of the shape function $\mathfrak{v}$ the form factors can be made to have the same value by suitably adjusting β. Values of β obtained in this manner can be said to be equivalent for range adjustment. In making the comparison of form factors for potential energy curves having different shapes the larger of the two nuclear well radii b has to be used so as to be able to have X, Ψ, Φ, Φ^* the same. It is clear that it is possible to introduce an equivalent square well range for a potential of any shape and that the equality of the range energy form factor for equivalent ranges is a convenient criterion. Potentials with different shapes can have the same equivalent range at one energy but different equivalent ranges at other energies on account of the presence of terms in E^2 and E^3 in Y. This situation will now be described quantitatively.

Expansions convenient for Φ, Φ^* can be obtained through the work of YWB.[10] A power series for the irregular function has been set up in that paper also. This has been more firmly established in connection with the present work and its accuracy has been tested by comparison with other methods of calculation. The series does not show rapid convergence for the irregular Coulomb function for energies of 10 Mev or higher. Nevertheless it gives a convenient representation of X and Ψ with satisfactory accuracy for $r=e^2/mc^2$ without terms in E of higher degree than the second. In the notation of YWB the expansions and other relevant relations are:

$$x=(8\rho\eta)^{\frac{1}{2}}=(8r/a)^{\frac{1}{2}};\qquad \rho=kr=Mv/2\hbar;\quad \eta=e^2/\hbar v', \tag{7.2}$$

$$v=\text{relative velocity}, \tag{7.21}$$

$$F_0=C_0\rho\Phi_0, \tag{7.22}$$

$$G_0=\Theta_0/C_0, \tag{7.23}$$

$$\Phi_0=\varphi_0+\varphi_1/\eta^2+\varphi_2/\eta^4+\cdots, \tag{7.24}$$

$$\Phi_0^*=\varphi_0^*+\varphi_1^*/\eta^2+\varphi_2^*/\eta^4+\cdots, \tag{7.25}$$

$$-2\Theta_0/x^2=\theta_0+\theta_1/\eta^2+\theta_2/\eta^4+\cdots, \tag{7.26}$$

$$-\partial\Theta_0/x\partial x=\theta_0^*+\theta_1^*/\eta^2+\theta_2^*/\eta^4+\cdots, \tag{7.27}$$

$J_\nu(ix)=$ Bessel function of order ν of argument ix.

$$I_\nu=I_\nu(x)=i^{-\nu}J_\nu(ix), \tag{7.28}$$

$$\mathrm{K}_\nu=\mathrm{K}_\nu(x)=\lim(\pi/2)[I_{-\nu}(x)-I_\nu(x)]\cot(\pi\nu)$$
$$=\lim\cos(\pi\nu)[\text{Basset's } K_\nu]. \tag{7.29}$$

For integral ν the quantity of which the limit is

[12] BCP, footnote 2. Additional terms of the series are given in Eqs. (7.5) to (7.94) of the present paper.

[13] This is an obvious consequence of Eqs. (7.5), (7.6), (7.7) of BCP and has been known since that paper. The reason for introducing the quantity X and f was that of isolating the exponential dependence of η contained in C_0^2 from the quantities varying slowly with energy such as X, Ψ, Φ, Φ^*. The same step has been made by Landau and Smorodinsky (see reference 8) afterwards in a less complete form.

TABLE III. Values of $\Phi_0^* - Y\Phi_0$ and its approximation by quadratic in energy.

E (Mev)	Exact value	Quadratic approximation
1	0.8684	0.8685
2.8	0.8683	0.8683
6	0.8689	0.8692
9	0.8710	0.8719

taken becomes indeterminate. The notation is the same as that of Whittaker and Watson, *Modern Analysis*. Watson's Bessel functions denotes by K_ν a function which for integral ν is $(-)^\nu$ times the K_ν used here and by YWB. This choice of K_ν makes the recurrence relations for the K_ν have the same form as for the I_ν.

$$\varphi_0=(2/x)I_1, \quad \varphi_1=(x/2)^3(I_3-I_1)/24; \tag{7.3}$$

$$\varphi_2=[(x/2)^5+(x/2)^3]I_3/240-(x/2)^5I_1/1440. \tag{7.31}$$

$$\varphi_0^*\equiv I_0, \quad \varphi_1^*=(x/2)^3(I_3-3I_1)/24. \tag{7.32}$$

$$\varphi_2^*=\{(5/2)(x/2)^7(I_1-I_3) +[9(x/2)^5+6(x/2)^3]I_3 -(x/2)^5I_1\}/1440. \tag{7.33}$$

If

$$\varphi_j=\textstyle\sum_{i,\nu} a_{ji}{}^\nu x^i I_\nu, \quad \varphi_j^*=\sum_{i,\nu} b_{ji}{}^\nu x^i I_\nu, \tag{7.34}$$

then

$$\theta_j=\textstyle\sum_{i,\nu} a_{ji}{}^\nu x^i \mathrm{K}_\nu, \quad \theta_j^*=\sum_{i,\nu} b_{ji}{}^\nu x^i \mathrm{K}_\nu, \tag{7.35}$$

Replacement of letter I by K in formulas changes φ_j into θ_j, φ_j^* into θ_j^*. The remaining relations needed here are:

$$\Psi=-(x^2/2)\{\theta_0+\theta_1/\eta^2+\theta_2/\eta^4+\cdots +[\ln(x/2)+\tfrac{1}{2}S(\eta)] \times(\varphi_0+\varphi_1/\eta^2+\varphi_2/\eta^4+\cdots)\}, \tag{7.36}$$

$$S(\eta)=-1+2\gamma+1/12\eta^2+1/120\eta^4+\cdots =-1+2\gamma-\ln\eta+\text{R.P. }\Gamma'(i\eta)/\Gamma(i\eta), \tag{7.37}$$

where $\gamma=0.5772\cdots=$Euler constant.

$$X=-4\{\theta_0^*+\theta_1^*/\eta^2+\theta_2^*/\eta^4+\cdots +[\ln(x/2)+\tfrac{1}{2}S(\eta)] \times(\varphi_0^*+\varphi_1^*/\eta^2+\varphi_2^*/\eta^4+\cdots)\}. \tag{7.38}$$

These expansions can be used, of course, not only for the proton-proton scattering problem. For the latter one has the special relation

$$1/\eta^2=40.00(5)E/\text{Mev}. \tag{7.39}$$

The expansions in terms of the I_ν, K_ν will be discussed in more detail in another publication. Detailed understanding of reasons for similarity of form of different expressions is not essential for the present discussion. It suffices to know that X, Ψ, Φ, Φ^* are power series both in the energy and in the radius. The expansions in Bessel functions simply give a way of writing down the coefficient of any power of r which occurs with the first or the second power of the energy. Otherwise Eqs. (7.2) . . . (7.38) do not contain more information than Eqs. (7.7) of BCP. In the latter the expansion is arranged in powers of r/a with coefficients which are polynomials in the quantity $1/\eta^2$ which is proportional to the energy E. In the present paper the same series are rearranged in powers of $1/\eta^2$ with coefficients which are functions of the quantity x and are power series in r/a as a consequence of the definition of x given in Eq. (7.2).

In order to use Eq. (7) one has to know the value of Y for different energies. This quantity depends on the shape of the potential well, i.e., on the nature of the function $\mathfrak{v}$ of Eq. (7.1). For small energy changes and for compact potential wells, however, one can speak of the equivalence of potential wells of different shapes. It follows, for instance, from the work of BCP, BTE, and HSB that the square well, the Gauss error well, the exponential well, and the meson well give very similar variations of the phase shift K_0 with E. The reason can be explained in terms of the three relations listed under Eq. (10.3) in BCP where the usefulness of the relations for the present purpose has been indicated but not elaborated. By means of these relations the quantity Y can be expressed by a first-order perturbation calculation making use of the wave function for a condition in which the depth A and range β have been adjusted to give $Y=0$, for $E=0$ at the boundary and, therefore, also outside the potential well. Let it be supposed that there are two potentials to be compared with each other and that they are represented by Eq. (7.1) and by

$$V'=-A'\mathfrak{v}'(r/\beta'). \tag{7.4}$$

Here $\mathfrak{v}'$ is not the derivative of $\mathfrak{v}$ but a different function. Thus, for example, $\mathfrak{v}$ can be the function appropriate to the square well while $\mathfrak{v}'$ can apply to the Gauss error potential. The values of A and A' which correspond to the resonance depth for zero external kinetic energy will be denoted by A_0 and A_0'. They are connected with the range parameters β, β' by the relations

$$A_0\beta_0{}^2=\lambda_0\hbar^2/M, \quad A_0'\beta_0'{}^2=\lambda_0'\hbar^2/M, \tag{7.41}$$

where λ_0 is defined as the eigenvalue of the problem

$$d^2\mathfrak{F}/d\xi^2+\lambda_0\mathfrak{v}(\xi)\mathfrak{F}=0, \quad \xi=r/\beta \tag{7.42}$$

subject to usual conditions of regularity at $r=0$ and of $dF/d\xi=0$ at $\xi=\infty$. The definition of λ_0' is similar to that of λ_0 with a change from $\mathfrak{v}_0$ to $\mathfrak{v}_0'$. In comparing two potentials in their effects on

scattering, it will be convenient to choose a distance $r=R$, such that both potentials are negligible for $r>R$. One has then from the relations in BCP, on expanding Y in powers of E and $A-A_0$ and keeping only the first-order terms, the following conditions for the equivalence of the potentials:

$$[(A-A_0)/\mathfrak{F}^2]\int_0^\infty \mathfrak{F}^2\mathfrak{v}(r/\beta)dr$$

$$=[(A'-A_0')/\mathfrak{F}'^2]\int_0^\infty \mathfrak{F}'^2\mathfrak{v}'(r/\beta')dr, \quad (7.43)$$

$$(1/\mathfrak{F}^2)\int_0^R \mathfrak{F}^2dr=(1/\mathfrak{F}'^2)\int_0^R \mathfrak{F}'^2dr. \quad (7.44)$$

The first of these relations makes the two potentials give the same value of Y for $E=0$. The second makes the variation of Y with E the same at the two energies. In Eqs. (7.43), (7.44) the functions $\mathfrak{F}$, $\mathfrak{F}'$ are, respectively, the solutions of Eq. (7.42) and the equation obtained from the latter by changing $\mathfrak{v}$ into $\mathfrak{v}'$ and β into β'. In other words $\mathfrak{F}$, $\mathfrak{F}'$ are solutions of the radial equation for the reference states of zero energy having zero slope at $r=\infty$. The second of the two equivalence relations just considered does not involve the depth of the wells and gives, therefore, a convenient criterion for the equivalence of range. According to this Eq. (7.44) if one were to normalize the functions in such a way as to have the same amplitude in the region

$$R<r<\infty, \quad (7.45)$$

then

$$\int_0^R \mathfrak{F}^2dr=\int_0^R \mathfrak{F}'^2dr. \quad (7.46)$$

This condition means qualitatively that two potential wells have equivalent ranges for the resonant states at $E=0$ if their respective wave functions come up to their asymptotic values equally rapidly. It is perhaps useful to state the condition in another form *viz.*

$$\int_0^\infty [-\mathfrak{F}^2+\mathfrak{F}^2(\infty)]dr=\int_0^\infty [-\mathfrak{F}'^2+\mathfrak{F}'^2(\infty)]dr,$$
$$\mathfrak{F}^2(\infty)=\mathfrak{F}'^2(\infty), \quad (7.47)$$

which expresses equivalence of range in terms of equality of areas between the curves for $\mathfrak{F}^2$, $\mathfrak{F}'^2$ and their constant asymptotes at $r=\infty$.

While the existence of relations given here as Eqs. (7.46), (7.47) was realized at the time of writing the paper referred to here as BCP, it was also realized that there are some limitations as well as practical disadvantages to this method of comparing ranges. The comparison was, therefore, usually stated in terms of direct calculation. The reasons were as follows:

TABLE IV. Effect on scattering at 45° and phase shift of quadratic terms in E.

E (Mev)	δf	$-\delta K_0$ (degrees)	—change in scattering (percent)	Power series value for preceding column
0.2	0.00023	0.00024	−0.003	
0.6	0.0020	0.0069	+0.13	
0.8	0.0035	0.014	0.16	
1.0	0.0056	0.025	0.21	0.21
2.2	0.0265	0.12	0.50	
3	0.049	0.21	0.72	0.79
6	0.19	0.56	1.6	1.8
9	0.42	0.96	2.7	
10	0.49	1.04	2.9	3.1

(a) Range adjustment by means Eqs. (7.46), (7.47), and (7.48) is subject to errors caused by neglect of quadratic terms in E and in $A-A_0$. These increase with energy and it is somewhat better, therefore, to make the fit by direct calculation at energies equal or close to those for which measurements are available. (b) In order to make a comparison of ranges by any method one needs reasonably exact wave function for energy. There is little difference in the work required to obtain a solution of Eq. (7.42) or at an energy which is not zero. Also the amount of work per numerical integration of a differential equation is smaller if a number of them are performed for neighboring values of parameters. (c) Potentials such as the Exponential and the Meson are not definitely compact. (d) At the time of the work of BCP the effective range of nuclear force was not known. It was necessary, therefore, to include calculations for longer ranges of force such as $2e^2/mc^2$ for which the linearity of Y as a function of E is poorer than for the shorter ranges.

The expansions of Φ_0, Φ_0^*, Ψ, X in terms of Bessel functions of imaginary argument which are described by Eqs. (7.25)–(7.39) can be arranged as power series in x or in r. They appear then as follows:

$$\varphi_0=\sum_0^\infty \frac{(x/2)^{2s}}{s!(s+1)!}=\sum_0^\infty \frac{(2r/a)^s}{s!(s+1)!}, \quad (7.5)$$

$$\varphi_1=\frac{(x/2)^4}{24}\left[-1-2\sum_0^\infty \frac{(x/2)^{2(s+1)}}{(s+1)!(s+3!)}\right]$$

$$=\frac{1}{6}\left(\frac{r}{a}\right)^2\left[-1-2\sum_0^\infty \frac{(2r/a)^{s+1}}{(s+1)!(s+3)!}\right]$$

$$=-\frac{1}{6}\left(\frac{r}{a}\right)^2\left[1+\frac{2}{3}\frac{r}{a}+\frac{1}{6}\left(\frac{r}{a}\right)^2+\frac{1}{45}\left(\frac{r}{a}\right)^3+\cdots\right].$$

$$\varphi_2=\frac{(x/2)^3}{1440}\sum_0^\infty\frac{(5s+18)(x/2)^{2s}}{s!(s+4)!}$$
$$=\frac{1}{90}\left(\frac{r}{a}\right)^4\sum_0^\infty\frac{(5s+18)}{s!(s+4)!}\left(\frac{2r}{a}\right)^s$$
$$=\left(\frac{r}{a}\right)^4\left(\frac{1}{120}+\frac{23}{5400}\frac{r}{a}+\cdots\right). \quad (7.52)$$

$$\varphi_3=\left(\frac{r}{a}\right)^6\left(-\frac{1}{5040}+\cdots\right). \quad (7.52')$$

$$\varphi_0^*=\sum_0^\infty\frac{(2r/a)^s}{(s!)^2}. \quad (7.53)$$

$$\varphi_1^*=-\left(\frac{r}{a}\right)^2\left[\frac{1}{2}+\frac{1}{3}\sum_0^\infty\frac{(s+4)(2r/a)^{s+1}}{(s+1)!(s+3)!}\right]$$
$$=-\left(\frac{r}{a}\right)^2\left[\frac{1}{2}+\frac{4}{9}\left(\frac{r}{a}\right)+\frac{5}{36}\left(\frac{r}{a}\right)^2\right.$$
$$\left.+\frac{1}{45}\left(\frac{r}{a}\right)^3+\cdots\right]. \quad (7.54)$$

$$\varphi_2^*=\frac{1}{90}\left(\frac{r}{a}\right)^4\sum_0^\infty\frac{(s+5)(5s+18)}{s!(s+4)!}\left(\frac{2r}{a}\right)^s$$
$$=\left(\frac{r}{a}\right)^4\left[\frac{1}{24}+\frac{23}{900}\frac{r}{a}+\cdots\right]. \quad (7.55)$$

$$\varphi_3^*=\left(\frac{r}{a}\right)^6\left(-\frac{1}{720}+\cdots\right). \quad (7.55')$$

It is useful to remember that in order to obtain the coefficient of r^s in a φ_j^* one has to multiply the coefficient of r^s in φ_j by $s+1$. While the occurrence of the K_ν in $\theta_j\theta_j^*$ is simply expressed by means of Eqs. (7.34), (7.35) in terms of the corresponding relations involving I_ν, φ_j, φ_j^*, an arithmetical calculation of Ψ or X takes place through Eqs. (7.36), (7.38). In these the functions K_ν occur in the combinations

$$\mathfrak{K}=K_\nu+[\ln(x/2)+\gamma-(1/2)]I_\nu. \quad (7.6)$$

These functions are the following power series in x:

$$\mathfrak{K}_1=-\frac{1}{x}+\frac{1}{2}\sum_0^\infty\frac{(x/2)^{2s+1}}{s!(s+1)!}$$
$$\times\left[-1+\left(1+\frac{1}{2}+\cdots+\frac{1}{s}\right)\right.$$
$$\left.+\left(1+\frac{1}{2}+\cdots+\frac{1}{s+1}\right)\right]; \quad (7.7)$$

$$\mathfrak{K}_3=-\frac{1}{2}\left[2\left(\frac{2}{x}\right)^3-\frac{2}{x}+\frac{1}{2}\frac{x}{2}\right]$$
$$+\frac{1}{2}\sum_0^\infty\left[-1+\left(1+\frac{1}{2}+\cdots+\frac{1}{s}\right)\right.$$
$$\left.+\left(1+\frac{1}{2}+\cdots+\frac{1}{s+3}\right)\right]\frac{(x/2)^{2s+3}}{s!(s+3)!}. \quad (7.8)$$

It will be noticed that these functions do not contain the $\ln x$ term and that the dependence of Ψ and X on $\ln x$ which might be surmised from Eqs. (7.36), (7.38) is only apparent. It is useful to have on hand the formula

$$\Psi=-x\mathfrak{K}_1-\frac{1}{12\eta^2}\left[\left(\frac{x}{2}\right)^5(\mathfrak{K}_3-\mathfrak{K}_1)+\left(\frac{x}{2}\right)\varphi_0\right]$$
$$-\frac{(x/2)^2}{\eta^4}\left[\frac{(x/2)^5+(x/2)^3}{120}\mathfrak{K}_3\right.$$
$$\left.-\frac{(x/2)^5}{720}\mathfrak{K}_1+\frac{\varphi_0}{120}+\frac{\varphi_1}{12}\right]+\cdots \quad (7.9)$$

which gives the coefficient of any power of x in the linear and quadratic terms in the energy E. From Ψ one readily finds Ψ^* by means of Eqs. (19), (25) of YWB. These equations are needed here only to show that the series for Ψ^* when arranged in powers of r has coefficients of r^j which are equal to j times the coefficient of r^j in Ψ. By means of Eq. (2.2) of the present paper and the series for Φ one has available terms of any power in r in the coefficients of $1/\eta^2$ and $1/\eta^4$ in the quantity X. The recurrence formulae for the coefficients of which are dealt with by YWB are not needed if use is made of the formulae just described. The accuracy required for proton-proton scattering problems is sufficiently moderate to make it possible to neglect terms in E^3 in most of the applications in the present paper. The following series often suffice:

$$X=2-4(r/a)-4(r/a)^2$$
$$-(32/27)(r/a)^3-(19/108)(r/a)^4$$
$$-(107/6750)(r/a)^5-\cdots$$
$$+\frac{(r/a)}{\eta^2}\left[-1+\frac{37}{27}\left(\frac{r}{a}\right)^2+\frac{71}{108}\left(\frac{r}{a}\right)^3\right.$$
$$\left.+\frac{353}{2700}\left(\frac{r}{a}\right)^4+\cdots\right]$$
$$+\frac{(r/a)^3}{\eta^4}\left[\frac{1}{6}-\frac{r/a}{36}-\frac{1261}{13500}\left(\frac{r}{a}\right)^2+\cdots\right]$$
$$+\frac{(r/a)^5}{\eta^6}\left[-\frac{1}{120}+\cdots\right]+\cdots. \quad (7.91)$$

$$X_{E=0}=-4\mathfrak{R}_0(x)=-4\Big[-\frac{1}{2}+\frac{2r/a}{(1!)^2}(1-\tfrac{1}{2})+\frac{(2r/a)^2}{(2!)^2}(1+\tfrac{1}{2}-\tfrac{1}{2})+\frac{(2r/a)^3}{(3!)^2}\times(1+\tfrac{1}{2}+\tfrac{1}{3}-\tfrac{1}{2})+\cdots\Big]. \quad (7.92)$$

$$\Psi=1-3(r/a)^2-(14/9)(r/a)^3-(35/108)(r/a)^4-(101/2700)(r/a)^5-\cdots+\frac{1}{\eta^2}\Big[-\frac{(r/a)^2}{2}+\frac{(r/a)^3}{9}+\frac{43}{108}(r/a)^4+\frac{77}{540}(r/a)^5+\cdots\Big]+\frac{1}{\eta^4}\Big[\frac{(r/a)^4}{24}-\frac{2(r/a)^5}{225}-\frac{172(r/a)^6}{10125}+\cdots\Big]+\frac{1}{\eta^6}\Big[-\frac{(r/a)^6}{720}+\cdots\Big]+\cdots. \quad (7.93)$$

$$\Psi_{E=0}=-x\mathfrak{R}_1(x)=1+\frac{(2r/a)^2}{1!2!}[1-1-(1+\tfrac{1}{2})]+\frac{(2r/a)^3}{2!3!}[1-(1+\tfrac{1}{2})-(1+\tfrac{1}{2}+\tfrac{1}{3})]+\cdots. \quad (7.94)$$

The relative importance of successive powers of E will now be illustrated. For a square well potential the expansion of Y as a power series in the energy is

$$Y=Y_0+Y_1E+Y_2E^2+\cdots, \quad (8)$$

where

$$Y_0=z_0\cot z_0, \quad z_0=z_{E=0}, \quad (8.1)$$

$$Y_1=(1/4D)[Y_0-(z_0/\sin z_0)^2], \quad (8.2)$$

$$Y_2=(1/32D^2)\{2[(z_0/\sin z_0)^2-1]Y_0-(z_0/\sin z_0)^2\}. \quad (8.3)$$

Experiment is fitted reasonably well by $D=10.5$ Mev, $r=b=e^2/mc^2$. These values give

$$Y=0.2205-0.04367E-0.0003881E^2+\cdots, \quad (8.4)$$

where E is in Mev.

The conversion factors in this illustration are as follows:

$$\rho\eta=r/a=0.04886(rmc^2/e^2), \quad \eta=0.1581/E_{\text{Mev}}{}^{\frac{1}{2}}.$$

The numbers in Eq. (8.4) and in the following Eqs. (8.41), (8.42) are carried out to a larger number of digits than is warranted by the accuracy with which the conversion factors are known. The object in listing the extra digits is that of showing how the terms combine and how some of them nearly cancel. This will enable the reader to form his own judgment about the applicability of some of the approximations.

The Coulomb function expansions yield

$$\begin{aligned}\Phi_0&=1.049662-0.016443E+0.00007793E^2+\cdots,\\ \Phi_0{}^*&=1.100133-0.049860E+0.00039160E^2+\cdots,\\ \Psi&=0.992655-0.047144E+0.00037574E^2+\cdots,\\ X&=1.794872-1.94820E+0.030810E^2+\cdots.\end{aligned} \quad (8.41)$$

Calculation of f_1 by means of Eq. (7) gives

$$f_1=3.090\frac{1+0.3160E+0.00191E^2+\cdots}{1-0.00045E+0.0000733E^2+\cdots}=3.090[1+0.3164E+0.00198E^2+\cdots]. \quad (8.42)$$

Here E is again in Mev. It will be noted that:

(a) Most of the dependence on E is contained in the numerator of Eq. (8.42). It arises as a result of the dependence on E of the quantity $X-(a/r)Y\Psi$ of Eq. (7). The denominator of Eq. (7) is on the other hand nearly constant being equal in the present case to

$$-0.8687+0.00039E-0.0000637E^2+\cdots.$$

Comparing this expression with $\Phi_0{}^*$ in the form of Eq. (8.41) it is clear that $\Phi_0{}^*-Y\Phi_0$ depends on the energy relatively much less than $\Phi_0{}^*$.

(b) The energy dependence of $\Phi_0{}^*$ is appreciably reduced by the subtraction of $Y\Phi_0$ not only in the linear but also in the quadratic terms in E.

(c) The cancellation of terms is more pronounced for $\Phi_0{}^*-Y\Phi_0$ than for $\Phi_0{}^*/\Phi_0-Y$. The latter quantity can be expected to be approximately energy independent because Φ^*/Φ is the homogeneous logarithmic derivative of the regular Coulomb function while Y is the homogeneous logarithmic derivative of the internal function and because neither of these varies with energy especially rapidly and also because the two quantities vary in the same direction. The cancellation under discussion is a more precise one, however.

In view of the fact that this cancellation makes it possible to approximate the relation of the phase shift to the energy in a simple way it appears appropriate to explain why it occurs. In terms of the regular Coulomb function F_0 denoted here by F and the energy-dependent but distance-independent parameter C_0 one has

$$\Phi_0{}^*-\Phi_0Y=[dF/d\rho-Fd\mathfrak{F}/\mathfrak{F}d\rho]/C_0=(\sin K_0)/\mathfrak{F}C_0, \quad (8.5)$$

TABLE V. Values of quantities for range determination by means of Eqs. (8.6), (8.61).

r_0	$K_0(x)/I_0(x)$	$I_0(x)$	$(2/x)I_1(x)$
0.75	0.79 95	1.07 46	1.03 71
0.80	0.77 17	1.07 97	1.03 96
0.85	0.74 58	1.08 48	1.04 21
0.90	0.72 17	1.08 99	1.04 46
0.95	0.69 90	1.09 50	1.04 71
1.00	0.67 77	1.10 01	1.04 97
1.05	0.65 77	1.10 53	1.05 22
1.10	0.63 87	1.11 04	1.05 47

use having been made in the last step of the constancy of the Wronskian and of the asymptotic forms of $\mathfrak{F}$, F for the last step. It follows, on the other hand from the differential equations satisfied by F, $\mathfrak{F}$ that

$$\sin K_0 = -(M/k^2\hbar^2)\int_0^b VF\mathfrak{F}d\rho, \qquad (8.51)$$

as has been pointed out by Ramsey.[14] Combining Eqs. (8.5), (8.51) one has

$$\Phi_0^* - \Phi_0 Y = -(M/\hbar^2\mathfrak{F}_b)\int_0^b V(r\Phi_0)\mathfrak{F}dr. \qquad (8.52)$$

Here V is the potential energy in excess of the Coulombian and $\mathfrak{F}_b$ is the value of $\mathfrak{F}$ at the nuclear boundary. The energy dependent quantities on the right side are seen to be $r\Phi_0$ and $\mathfrak{F}/\mathfrak{F}_b$. The energy dependent part of $r\Phi_0$ is to a first approximation the same as though there were no Coulomb interaction as may be seen from the expansions given above. For example, the approximation

$$\Phi_0 \cong \sin\rho/\rho = 1 - 0.0159E(r/mc^2/e^2)^2 + \cdots$$

agrees with the first two terms for Φ_0 in the first of the four Eqs. (8.41) at $rmc^2/e^2 = 1$ which give $1.04966[1 - 0.0157E + \cdots]$ for the same quantity. The good agreement of the variation of Φ_0 with energy and distance in the Coulombian and field free cases suggests that the high degree of energy independence of the quantity $\Phi_0^* - \Phi_0 Y$ can be explained making use of the field free approximation. This can be done by means of Eq. (8.52) the right side of which contains the energy only in the quantity Φ_0 and the ratio $\mathfrak{F}/\mathfrak{F}_b$. The former has been discussed. The latter has the same energy dependence for a compact shape of V as in the absence of a Coulomb field even to a higher degree than $r\Phi_0$ because the effective wave-length for $\mathfrak{F}$ is largely determined by V rather than e^2/r. Equation (8.52) shows, therefore, that the variability of $\Phi_0^* - \Phi_0 Y$ with energy can be discussed to a good approximation by calculating this quantity in the absence of the Coulomb field. One finds by a straightforward calculation for this case that

$$\Phi_0^* - \Phi_0 Y \cong 1 - z_0 \cot z_0 + \frac{E}{2D}\left[\left(\frac{z_0^3}{6} - \frac{z_0}{2}\right)\cot z_0 + \frac{z_0^2}{2}\cot^2 z_0\right] \qquad (8.53)$$

with

$$z_0 = [MD/\hbar^2]^{\frac{1}{2}}\cdots, \qquad (8.54)$$

where a specialization to the case of a square well has been made. The correction term of first order in E vanishes for $z_0 = \pi/2$ which is approximately the case. Setting

$$z_0 = \pi/2 - \epsilon \qquad (8.55)$$

and keeping only terms of first order in ϵ there results

$$[\Phi_0^* - \Phi_0 Y]/[\Phi_0^* - \Phi_0 Y]_{E=0} \cong 1 - 0.07\epsilon E/D, \qquad (8.56)$$

where 0.07 arose as the digital equivalent of $\pi/8 - \pi^3/96$. In making a numerical estimate it is proper to employ for D the value which corresponds to an assumed action of the Coulomb field inside the potential well because in Eq. (8.52) the potential energy V is that acting in addition to the Coulombian. A fair value of this D, which has been designated as D^c in BCP, for an assumed range e^2/mc^2 is 11.3 Mev and the value of ϵ which corresponds to this well depth is 0.10. Substitution of these numbers into Eq. (8.56) gives

$$1 - 0.0006E \qquad (8.57)$$

for the right side of Eq. (8.56). This estimate agrees approximately with the denominator of Eq. (8.42). A precise agreement cannot be expected on account of the relative crudeness of the approximations made in arriving at Eq. (8.56). The existence of the agreement shows that the compensation of effects does not have anything special to do with the Coulomb field and that the approximate resonance at $E = 0$ is a strong contributing factor. It is also seen from the form of the right side of Eq. (8.52) that this quantity will behave similarly for potential wells of different shapes because $\mathfrak{F}/\mathfrak{F}_b$ behaves similarly. This is also expected on the grounds of equivalence of different shapes of potential wells for effects on Y which are linear in the energy E.

The constancy of $\Phi_0^* - \Phi_0 Y$ with E is not only a property of the approximation which neglects higher powers of E than E^2 but is practically as good including all powers of E. The condition is shown in Table III. The error in f caused by neglecting the quadratic terms in E in the numerator and denominator of Eq. (8.42) is small at small energies but not negligible at several Mev. This situation and the effect on scattering at a scattering angle of 45° in the laboratory system is illustrated in Table IV. In this table an alternative convention for recording the error of quadratic terms based on the form of f_1 obtained by expanding

[14] W. H. Ramsey, Proc. Camb. Phil. Soc. **44**, 87 (1948); *cf.* also L. Hulthén, K. Fysiogr, Sällsk. Lund Forhandl. **14**, Nrs. 8, 21 (1944).

it into a power series in E is given as well. The values of the phase shift corresponding to a square well with a range e^2/mc^2 and a depth $D=10.5$ Mev were used as an approximation to the experimental values of the phase shifts in preparing the table. In the first column of Table IV are listed the values of the energy. In the second column the corresponding values of the quantity δf are given. This quantity is the value of the fraction representing f_1 in Eq. (8.42) minus the value of the fraction obtained on neglecting the terms in E^2 in the numerator and denominator. In the third column are listed the negatives of corresponding differences of the phase shift K_0 expressed in degrees. In the fourth column are the negatives of corresponding differences in theoretically expected scattering for a scattering angle of 45° in the laboratory system. By "theoretically expected" scattering in the preceding sentence is meant the scattering which one would compute if one were to use either the quadratic or the linear approximation to the numerator and denominator of the fraction representing f_1. The fifth column of Table IV differs from the fourth only in that the effect of the quadratic term in the power series obtained by dividing the numerator by the denominator is dealt with. It will be noted from Table IV that: (a) there is no marked difference between the values in the last two columns of the table. (b) At energies below 0.6 Mev the effect of quadratic terms is smaller than the accuracy of most experiments. (c) At 2.2 Mev it is preferable to include the effect of quadratic terms because the experimental error is not many times greater than 0.5 percent. From 3 Mev on the approximation of neglecting quadratic terms in E appears to be definitely undesirable because systematic errors between 1 and 3 percent in scattering result. If one adopted a policy, common in some fields, of having the theoretical calculation ten times better than the experimental error and if the experimental error were one percent, one would hesitate to apply the linear approximation at bombarding energies above 0.5 Mev. (d) The importance of quadratic terms decreases as the range of force b is decreased. If one were sure of the range being shorter than e^2/mc^2, in square well equivalents, then it would be possible to apply the linear approximation at higher energies with the same utilization of experimental accuracy. The effect of a possible change in range while appreciable is not a very pronounced one as may be seen from the following estimate. An appreciable part of the quadratic term in X is canceled by terms in $(a/r)Y\Psi$ when one substitutes into Eq. (7) to obtain Eq. (8.42). The term in X which is quadratic in E is approximately proportional to r^3. It appears fair to estimate the dependence of quadratic terms on b as being not more critical than b^4, therefore. A change in the radius b from 2.81×10^{-13} cm to 2.47×10^{-13} cm which was discussed in connection with Table II corresponds to a factor 0.88 in b and 0.6 in b^4. Such a factor would indeed extend appreciably the range of applicability of the linear approximation. If one were to be satisfied with 0.5 percent accuracy in theoretical prediction the region below $E=3.5$ Mev rather than the 2.2 Mev of Table IV would be satisfactory. But if b were 2.65×10^{-13} cm which is the mean of the other two values considered after Table II, the error would decrease in comparison with that for $b=e^2/mc^2$ by the factor 0.8 which makes little difference in comparison with Table IV.

TABLE VI. Values of quantities determining linear and quadratic dependence on E.

r_0	X_0	$r_0^{-1}X_1$	$r_0^{-2}X_2$	$(\Psi_0)_0$	$r_0^{-2}(\Psi_0)_1$	$r_0^{-4}(\Psi_0)_2$
0.75	1.8480	−1.9511	0.03090	0.99589	−0.047313	0.000377
0.80	1.8375	−1.9506	0.03089	0.99532	−0.047281	0.000377
0.85	1.8269	−1.9500	0.03087	0.99472	−0.047247	0.000376
0.90	1.8163	−1.9495	0.03085	0.99407	−0.047213	0.000376
0.95	1.8056	−1.9488	0.03084	0.99338	−0.047179	0.000376
1.00	1.7949	−1.9482	0.03082	0.99265	−0.047144	0.000376
1.05	1.7841	−1.9475	0.03080	0.99189	−0.047108	0.000376
1.10	1.7733	−1.9468	0.03079	0.99109	−0.047071	0.000375
r_0	$(\Phi_0)_0$	$r_0^{-2}(\Phi_0)_1$	$r_0^{-4}(\Phi_0)_2$	$(\Phi_0^*)_0$	$r_0^{-2}(\Phi_0^*)_1$	$r_0^{-4}(\Phi_0^*)_2$
0.75	1.0371	−0.01631	0.0000774	1.0746	−0.04933	0.000389
0.80	1.0396	−0.01634	0.0000775	1.0797	−0.04943	0.000389
0.85	1.0421	−0.01636	0.0000776	1.0848	−0.04954	0.000390
0.90	1.0446	−0.01639	0.0000777	1.0899	−0.04965	0.000390
0.95	1.0471	−0.01642	0.0000778	1.0950	−0.04975	0.000391
1.00	1.0497	−0.01644	0.0000779	1.1001	−0.04986	0.000392
1.05	1.0522	−0.01647	0.0000780	1.1053	−0.04997	0.000392
1.10	1.0547	−0.01650	0.0000781	1.1104	−0.05007	0.000393

It is useful to consider the relative magnitudes of contributions to f by its component parts. At 1 Mev the total of 8.7 is made up of 5.82 for $(C_0^2/\eta)\cot K_0$, −0.79 for q/η and 3.69 for $-2\ln\eta$. At 6 Mev the total of 13.7 is made up of contributions 9.1, −0.84, 5.48 in the same order. At 9 Mev the contributions are $11.9-0.84+5.9=16.9$. The numbers just given show that only part of f contains the phase shift in the form of $\cot K_0$ and that at 1 Mev a contribution of 2.9 out of a total of 8.7 comes from $(q/\eta)-2\ln\eta$ which does not contain the phase shift. The way in which f varies with E is conditioned by several factors and the increase of $(C_0^2/\eta)\cot K_0$ with E is not directly related to the increase of K_0 with E but rather to the behavior of C_0^2/η which more than compensates the decrease in $\cot K_0$. The term $-2\ln\eta$ is zero at $0.1581^2=0.025$ Mev. For smaller E it becomes negative and approaches $-\infty$ at $E=0$. The combination $q/\eta-2\ln\eta$ is finite, however, at $E=0$ and so is $(C_0^2/\eta)\cot K_0$, therefore. For small values of E one can approximate

$$q/\eta-2\ln\eta\cong 2(2\gamma-1)+1/6\eta^2 \cong 0.309+20E/3, \quad (8.58)$$

where E is in Mev. This approximation is fair at $E=0.2$ and lower energies but very crude at higher energies. It is seen that from the point of view of seeing simply how errors in the experi-

mental values affect conclusions regarding the interaction potential, the quantity f is not the easiest to deal with. Also, while it owes its linearity in E to the linearity of the logarithmic derivative Y, it is related to the latter through the quantities X, Ψ, Φ, Φ^*. It may also be mentioned that if the quantity f is considered as a function of K_0 and η, then its values for the Gauss error and meson potentials show deviations from linearity and from each other which are of the same order as those for a square well. This matter will be discussed in more detail in another publication. For the limited energy region considered by BTE the form of f suggested plotting $(\eta/C_0^2)\tan K_0$ which is approximately constant in that energy region.

The plot of f against E has advantages at low energies because here the linearity is good. The slope of f as a function of E is related to the range of force of the equivalent square well. By means of Eq. (7.47) this range determines also the range parameter for other compact potentials. It is, therefore, of interest to examine df/dE and f for $E=0$. The value of f at $E=0$ will be referred to as the intercept of f. It can be found by extrapolating the experimentally determined line for f to the axis $E=0$ and taking the intercept on that axis. The value of the intercept will be seen to be sensitive to Y_0 and hence to the depth of the potential well for an assumed range.

The value of the intercept is obtained from Eqs. (7), (7.3), (7.32), (7.92), (7.94) as

$$f_{E=0}=4\frac{\mathfrak{K}_0-(2/x)\mathfrak{K}_1Y_0}{I_0-(2/x)I_1Y_0}-2\ln(2r/a).$$

The relation

$$-I_0\mathrm{K}_1+I_1\mathrm{K}_0=1/x$$

has as a consequence

$$-I_0\mathfrak{K}_1+I_1\mathfrak{K}_0=1/x,$$

and hence, making use of the definition of $\mathfrak{K}$ in Eq. (7.6)

$$f_{E=0}=4\left[\frac{\mathrm{K}_0}{I_0}+\frac{2Y_0/(x^2I_0)}{I_0-(2/x)I_1Y_0}\right]+4\gamma-2. \quad (8.6)$$

In the determination of the slope df/dE the approximate constancy of the denominator in Eq. (7) will be made use of. By neglecting the energy dependence of the denominator the theoretically expected slope will be only ~ 0.15 percent too low for a range of e^2/mc^2 as is apparent from Eq. (8.42). For a square well one obtains by means of Eqs. (7.91), (7.93), (8), (8.1), (8.2)

$$(df/dE)_{E=0}\cong\{(r/a)(1-Y_0)(1+Y_0/z_0^2)/2 +(r/a)^2Y_0/9+\cdots\} \times(d\eta^{-2}/dE)/[I_0-(2/x)I_1Y_0], \quad (8.61)$$

where the result has been ordered in powers of r/a. Here Y_1 has been expressed in terms of Y_0 and for E in Mev

$$d\eta^{-2}/dE=40.0. \quad (8.62)$$

The phase z_0 is the value of the phase z for $E=0$. A convenient approximation is obtained by using Eq. (8.55) and neglecting powers of ϵ higher than the first.

In this approximation

$$[I_0-(2/x)I_1Y_0](df/dE)_{E=0} \cong 40.0\{(\tfrac{1}{2}-0.467\epsilon)(r/a)+0.174\epsilon(r/a)^2\}, \quad (8.63)$$

where the numbers 0.467, 0.174 arose as $(\pi/4)-1/\pi$, $\pi/18$, respectively. For $r=e^2/mc^2$ the above formula contains a quadratic term in r which is ~ 0.3 percent of the linear term. The slope of a plot of f against E is, therefore, nearly proportional to the square well range b which in the remainder of the paper will be also called r. For $b=e^2/mc^2$, $D=10.5$ Mev the right side of Eq. (8.63) is ~ 0.838 while the value of the left side is ~ 0.848. The error made in introducing the approximations between Eq. (8.61) and Eq. (8.63) amounts to ~ 1.2 percent and is in the direction of overestimating the range.

Equations (8.6), (8.61) are suitable for the determination of the range b and Y_0 by successive approximations. The essential reason for the rapid convergence of the process is that Eq. (8.6) is equivalent to Eq. (2) for the determination of Y_0. According to Eq. (2)

$$Y_0\cong(2+f_1^0)(r/a), \quad (8.7)$$

where f_1^0 is the value of f_1 of Eq. (2.5) for $E=0$. Since f_1^0 is approximately 3, the above equation determines Y_0 as $\sim 5r/a$ which is $\sim 1/4$ for the value of r/a indicated by experiment. On the other hand $Y_0\cong\pi\epsilon/2$ and hence ϵ is so small that its precise value matters little in the determination of r/a by means of Eq. (8.63). The value of r/a so determined is nearly independent of the initial guess. For a small error $\delta\zeta$ in $\zeta=r/a$ the solution of Eq. (2) for Y_0 gives an error δY_0 in Y_0 which to within the first two powers of ζ is

$$\delta Y_0=\{(f_1^0+4)/[\zeta(f_1^0+2)] -4(f_1^0-2)/(f_1^0+2)^2 +2f_1^0/(f_1^0+2)-(f_1^0+2)\}Y_0\delta\zeta. \quad (8.8)$$

To a good approximation the employment of $\zeta+\delta\zeta$ in $I_0-(2/x)I_1Y_0=B$ together with the use of $Y_0+\delta Y_0$ instead of Y_0 in that expression produces an error

$$\delta B\cong[2(1+\zeta)-(1+2\zeta/3)Y_0]\delta\zeta-(1+\zeta)\delta Y_0. \quad (8.81)$$

The quantity which multiplies r/a in Eq. (8.61) is

$$A=(1-Y_0)(1+Y_0/z_0^2)/2. \quad (8.82)$$

The error in it caused by the error δY_0 is

$$\delta A = -(1/2)\{1-z_0^{-2}+2Y_0z_0^{-2}[1-(1-Y_0^2)z_0^{-2}] \times[1-Y_0(1-Y_0)z_0^{-2}]^{-1}\}\delta Y_0. \quad (8.83)$$

The coefficient of $40.0E/B$ in the right side of Eq. (8.61) is a quadratic expression in (r/a). The error in its value caused by δB, and the errors in its coefficients caused by δY_0 result in an error

$$\frac{\delta(r/a)}{(r/a)} = \frac{\delta B}{B} - \frac{\delta A}{A} - \frac{\zeta}{9A}\left[\delta Y_0 + Y_0\left(\frac{\delta B}{B} - 2\frac{\delta B}{A}\right)\right]. \quad (8.84)$$

In addition to the approximation of neglecting terms in $(\delta r)^2$ this formula takes into account the term in $Y_0(r/a)^2/9$ on the right side of Eq. (8.61) to the first order also. The latter approximation is a good one. The first two terms in Eq. (8.84) give the error which would exist if the term in $(r/a)^2/9$ were absent. Assuming, for purposes of illustration, that f, df/dE have values corresponding to $b=e^2/mc^2$, $D=10.5$ Mev and that b, D are to be determined by successive approximations Eq. (8.84) indicates a value of $\delta(r/a)/(r/a)$ about 1/40 of the initial error $\delta\zeta/\zeta$. The first two terms account for ~80 percent of the right side of Eq. (8.84). Calculations carried out in detail for an assumed initial error of 10 percent in ζ indicate that the ratio of improvement is more nearly 1/35 than 1/40 and that Eq. (8.8) underestimates δY_0 by about 2 percent. The method of successive approximations is seen to converge very rapidly and to be very practical for range determination. Values of quantities involving Bessel functions occurring in Eqs. (8.6), (8.61) are listed in Table V so as to facilitate range determination by means of these formulas.

In Table V the quantities are listed so as to agree with conversion factors in the following relations:

$$\zeta = r/a = \rho\eta = 0.04886 r_e, \quad x^2 = 8\zeta = 0.39088 rmc^2/e^2, \quad r_e = rmc^2/e^2.$$

The number of significant figures in the table and in the conversion factors is greater than that corresponding to the accuracy with which fundamental constants are known. The object in including the extra digits is to make it possible to carry out self-consistent calculations for assumed values of fundamental constants which matter here only in the conversion factor 0.04886. To change to another choice of the constants it suffices to change the numbers in the first column of the table.

In Table VI are listed values of quantities which are needed in order to express X, Ψ_0, Φ_0, Φ_0^* as power series in E. The unit of energy is 1 Mev. The columns are labeled in terms of X_0, X_1, $\cdots$, $(\Phi_0^*)_2$ defined by:

$$\Psi_0 = (\Psi_0) + (\Psi_0)_1 E + (\Psi_0)_2 E^2 \quad (8.86)$$

and similarly for the other quantities. In order to facilitate interpolation the quantities tabulated are the coefficients of E divided by a suitable power of r_e. The object of including the extra digits is the same as for Table V. The relation $\eta^{-2}=40.00(7)E$ was used. If it is desired to change the choice of fundamental constants so that η^{-2}/E is changed then one has to multiply the columns for linear effects in E by $(\eta^{-2}/E)/40.007$ and the columns for quadratic effects by the square of that quantity. Changes in fundamental constants resulting in a change of ζ/r_e result in a change in the first column as for Table V.

The entrance of the range of force for the important quantities X, Ψ for coefficients of different powers of E can be seen in Eqs. (7.91), (7.93). The principal dependence of Y_0 on the assumed range of force is given by Eq. (8.7) and Y_1 is approximately proportional to the square of the range. The main contributions to the coefficient of E in f come from X and Y_1. While the above discussion refers mainly to properties of square wells, Eq. (7.47) makes it possible to transfer conclusions to wells of other shapes for terms in f varying linearly with E. Calculations made in collaboration with Messrs. Hatcher and Arfken indicate that quadratic terms in E depend on the shape of the potential well.

The writers wish to express their indebtedness to Professors Critchfield and Williams and other workers at the University of Minnesota,[11] to Professor Feshbach of M.I.T. for critical remarks concerning the boundary condition view, and to Messrs. Arfken and Hatcher for permission to quote their work before publication.

APPENDIX I

Experimental errors are not indicated for the points of HHT, HKPP, BFLSW, and RKT because the statistical counting errors are not significant in these cases and the internal consistency at one energy is not a completely satisfactory criterion. In most measurements of this group the estimated errors lead to uncertainties small compared with the distance between the $D=10.5$, 10.6 Mev lines. Comparison of points obtained by different experimental groups with each other is probably the best criterion of accuracy and allows some judgment of the certainty of conclusions from this group of observations. The phase shifts corresponding to the work of RKT were obtained by observing that their higher scattering angle data form a self consistent picture at 250 and 300 kev according to their Figs. 10, 11 and that the possibility of multiple scattering might be responsible for the apparent inconsistencies at the smaller angles. The relative position of the experimental values with respect to the theoretical curves in their Figs. 10, 11 indicated $K_0=9.0°$ for $E=250$ kev and $K_0=10.9°$ at $E=300$ kev. The points on the graphs were also located by comparison of the theoretical values of the logarithmic derivative y expected for $b=e^2/mc^2$, $D=10.5$, 10.6 Mev and $b=0.75\ e^2/mc^2$, $D=19.6905$ Mev. The data of Heydenburg, Hafstad and Tuve in the region 220-640

kev were not used in the present analysis partly because, as remarked by J. K. Lubansky and C. De Jager,[15] these observations do not agree very well with other measurements and primarily because these data were taken mainly in order to confirm the smallness of scattering at 90° in the center of mass system rather than for quantitative purposes.

The values and experimental uncertainties for $E=4.2$, 7.03 Mev have been used in accordance with published statements of May and Powell and of Dearnley, Oxley, and Perry. The data of R. R. Wilson and E. C. Creutz[4] at 8 Mev, R. R. Wilson[4] at 10 Mev and of Wilson, Lofgren, Richardson, Wright, and Shankland were treated in the following manner. The values of the phase shift and of y, Y at 8 Mev were determined from the value $\sigma=1.7\pm0.1\times10^{-25}$ cm² for the scattering cross section in the laboratory system of Wilson and Creutz. This was compared with a theoretical value of 1.75×10^{-25} cm² which corresponds to $K_0=53.6°$, which is the value of Hoisington and Thaxton[4] at $E=8$ Mev for $b=e^2/mc^2$, $D=10.5$ Mev. By means of the relation

$$\delta Y=-\rho\mathfrak{F}^{-2}\delta K_0, \qquad \text{(I, 1)}$$

which applies to small changes in the logarithmic derivative and phase shift and the approximate first-order relation:

$$\delta K_0\cong\tan K_0(\delta\sigma/2\sigma) \qquad \text{(I, 2)}$$

gave $\delta Y=0.017$. This is the estimated difference between Y for the experimental cross section and the Y corresponding to $b=e^2/mc^2$, $D=10.5$ Mev. The limits of experimental uncertainty were drawn in so as to correspond to the uncertainty $\pm0.1\times10^{-25}$ cm² in σ.

At $E=14.5$ Mev it was assumed that the value of σ for a scattering angle of 45° in the laboratory system is about 0.0125×10^{-25} cm² higher than that expected for a square well with $b=e^2/mc^2$, $D=10.5$ Mev. The reason for this assumption is that the experimental point for the above mentioned scattering angle is about 0.025×10^{-25} cm² higher than the S wave curve in Fig. 3 of Wilson *et al.* It appears that a shift of the S wave curve up by about the assumed amount would fit experiment reasonably well. On this admittedly rough and somewhat arbitrary interpretation it was calculated that, $\delta K_0=1.2(8)°$ and by means of (I, 1) it followed that $\delta Y=-0.031$. The approximation (I, 2) agrees with this estimate within about 10 percent. Since δY is used as an addition to the Y of the square well the accuracy required is moderate. The experimental uncertainty was made to correspond to an uncertainty of $\pm0.2\times10^{-26}$ cm² in σ_{cm} the cross section in center of mass system. Rough checks were made on the curve marked S in Wilson *et al.*

Since for 10 Mev absolute values of the cross section are not available the experimental error was taken to be about the same as for 8 Mev and 14.5 Mev. The relative values of the cross section at different angles do not determine K_0 with good accuracy even on the assumption that other phase shifts are absent. It is difficult to do much with the value at 10 Mev. The value of Y for this energy was somewhat arbitrarily taken to be on the $D=10.5$ Mev line. This position fits in which the points at $E=8$, 14.5 Mev but the point at $E=10$ Mev has very little weight in comparison with the others.

The experimental uncertainties in the 8 Mev–14.5 Mev region are so large that accurate calculations appeared out of place. It was assumed throughout that only S wave scattering enters close to $\Theta=45°$. This assumption can be doubted. It was made only because it is impossible to evaluate the complicated effect of higher phase shifts and because there is no decisive experimental evidence indicating their presence.

[15] J. K. Lubansky and C. De Jager, Physica **XIV**, 8 (1948).

PHYSICAL REVIEW VOLUME 75, NUMBER 7 APRIL 1, 1949

Separation of a Gas Mixture Flowing through a Long Tube at Low Pressure*

R. D. PRESENT
University of Tennessee, Knoxville, Tennessee
AND
A. J. DEBETHUNE
Boston College, Chestnut Hill, Massachusetts

(Received December 20, 1948)

The separation of a binary gas mixture by diffusion through a capillary of radius r depends on the fact that the molecules have different masses m_i and mean speeds v_i. When the inlet pressure is so low that the mean free path λ is much greater than r, the flow is diffusive and the separation factor (at zero outlet pressure) has its maximum value $(m_2/m_1)^{\frac{1}{2}}$. At high pressures ($\lambda\ll r$) no separation occurs. This paper treats the intermediate case ($\lambda\approx r$) where the transfer of forward momentum from light to heavy molecules in unlike collisions equalizes the transport velocities and decreases the separation factor. As the inlet pressure rises, this effect makes the flow non-separative before it becomes viscous. Flow equations are derived by equating the momentum acquired by the light component from the pressure gradient to the momentum lost to the wall plus that transferred to the other component. The viscous effects are treated as a small additive perturbation on the flow. The integrated flow equations express the separation factor as a function of the inlet and outlet pressures.

INTRODUCTION

FOR purposes of orientation, we consider first the effusion of a gas mixture through a circular orifice. The nature of the flow depends on the comparative magnitude of the mean free path λ and the radius r of the opening. When the opening is large ($r\gg\lambda$), many collisions occur in the vicinity of the orifice and, if two kinds of molecules are present, there is a continual transfer of momentum from the lighter, faster molecules to the heavier, slower molecules with the result that both kinds of

* This article is based on work performed by the authors while members of the staff of the Columbia University Division of War Research, SAM Laboratories. The main reference is to Manhattan Project Reports A-1289, Part I, June 8, 1944, and Part II, September 5, 1944. A preliminary abstract was published in Phys. Rev. 69, 259 (1946).

molecules pass through the opening together with a common mass motion. Such a flow may be treated by the methods of hydrodynamics and the results are well known. Since both components travel with the common drift velocity, the flow is non-separative. In the other limiting case ($r \ll \lambda$), a molecule traveling through the hole has very little chance of colliding with another molecule in the vicinity of the hole, i.e., the molecules effuse through the orifice independently with a velocity component proportional to the mean speed $\bar{v}$ of thermal agitation and inversely proportional to $m^{\frac{1}{2}}$, where m denotes the molecular mass. Hence the flow in this limit is separative. If the molecular particle density in front of the orifice be denoted by n_F and behind the orifice by n_B, the net molecular flow per unit time per unit area of the opening is $(1/4)\bar{v}(n_F - n_B)$ according to elementary kinetic theory. The intermediate or transition region where λ and r are comparable is very difficult to treat. However, it is qualitatively clear that the nature of the flow and the amount of separation will depend essentially on the parameter r/λ. For a given hole size the separation can be improved by decreasing the pressures and thus increasing the mean free path or, conversely, if the pressures are fixed, the separation is improved by decreasing the size of the orifice. We are primarily interested in the transition region where r and λ are comparable. The practical separation of gas mixtures by low pressure diffusion is accomplished through the use of some kind of a porous medium or "barrier."[1] It has been shown experimentally that the flow through a porous medium is in essential respects similar to the flow through a long capillary tube and quite unlike the flow through the orifices of a thin perforated membrane.[2] Thus, at high pressure the pressure dependence of the flow through a porous medium is that of capillary viscous laminar flow and not that expected for orifice flow. At very low pressures the order of magnitude of the permeability or inverse flow resistance is compatible with the capillary flow value but not with the orifice flow model. Therefore, the case of capillary flow at pressures in the transition region is of greater practical interest and, in addition, is more amenable to theoretical treatment than the analogous problem for orifice flow.

The nature of the flow of a gas through a long circular capillary of radius r depends again on the comparative size of r and λ. If $\lambda \ll r$, the flow is given by the Poiseuille formula; in the case of a gas mixture both components are transported with the drift velocity and no separation takes place. In the other limit ($\lambda \gg r$) the flow obeys the well-known Knudsen formula,[3]

$$\bar{\Gamma} = -(16r/3\pi m\bar{v})dp/dx = -(2\bar{v}r/3)dn/dx, \quad (1)$$

where $\bar{\Gamma}$ denotes the mean flow in molecules per unit area per unit time in the x direction (axis of the capillary). The flow per unit area Γ varies with the distance from the axis[4] and $\bar{\Gamma}$ represents the total flow divided by the area of cross section πr^2. Formula (1) has been confirmed by both Knudsen[3] and Adzumi[5] in experiments with bundles of capillary tubes at very low pressures. Equation (1) will be referred to as the Knudsen or free-molecule flow formula and it is valid only when $\lambda \gg r$. It clearly represents a diffusive flow and the diffusion coefficient is $2\bar{v}r/3$. This corresponds to a mean random-walk step-size of $2r$; i.e., the mean free path for intermolecular collisions (ordinary gaseous diffusion) is replaced by the mean free path for wall collisions (Knudsen diffusion). Since the molecules diffuse independently of each other, Eq. (1) can be applied to both components of a gas mixture if the partial density gradients are used. We denote the concentration or mole fraction of the lighter gas at the inlet of the capillary by N and at the outlet by ν. The separation factor f is customarily defined by

$$f = (\nu/1-\nu)/(N/1-N). \quad (2)$$

When $\lambda \gg r$ and the outlet pressure is zero, the separation factor has its maximum or "ideal" value f^+. It follows immediately from (1) that $f^+ = (m_2/m_1)^{\frac{1}{2}}$, where m_2 is the molecular mass of the heavier and m_1 of the lighter gas. According to Eq. (1), when the outlet or back pressure is zero the composition of the flowing gas is constant down the length of the tube and changes discontinuously at the exit to the composition of the enriched outlet mixture. This may be understood as follows: the concentration ratio of the two components in the outlet mixture is the same as the flow ratio of the two components in the tube; however, the flow ratio is equal to the concentration ratio times the ratio of transport velocities and the latter is constant and equal to $(m_2/m_1)^{\frac{1}{2}}$. When the back pressure is not zero the outlet mixture diffuses back into the tube and, according to Eq. (1), the concentration of light gas increases monotonically from the inlet to the outlet. In this case f obviously decreases as p_B/p_F, the back- to fore-pressure ratio, increases.

[1] H. de W. Smyth, *Atomic Energy for Military Purposes* (Princeton University Press, Princeton, New Jersey, 1945).

[2] R. R. Sullivan and K. L. Hertel, *Advances in Colloid Science* (Interscience Publishers, Inc., New York, 1942), Vol. I, pp. 37–80; W. G. Pollard, A-2136, September 25, 1944. References to non-project work may be found in the former, to project work in the latter.

[3] M. Knudsen, Ann. d. Physik **28**, 705 (1909).

[4] As shown in reference 7, appendix II, Γ is equal to $-\frac{1}{3}\sqrt{a}E(r/a)dn/dx$ where r is the distance from the axis, a the tube radius, and E denotes the complete elliptic integral of the second kind.

[5] H. Adzumi, Bull. Chem. Soc. Japan **12**, 285, 291, 295, 304 (1937); **14**, 343 (1939).

Knudsen,[3] Gaede,[6] and Adzumi[5] measured the flow of pure gases through capillaries over the entire pressure range from $\lambda \gg r$ to $\lambda \ll r$, and Gaede also made similar measurements of the flow between parallel plates. At high pressures their results can be represented in the usual way by the Poiseuille formula for viscous laminar flow plus a small correction term proportional to the pressure gradient. This correction term, which was originally attributed by Maxwell to "slip," has the same form as, but is smaller than, the free-molecule flow. When the specific flow (total flow/pressure drop) was plotted against the mean pressure, all three investigators found evidence of a slight minimum at low pressures when the mean free path was nearly equal to the tube diameter. Thus the specific flow initially decreases slightly (10 to 20 percent) below the free-molecule value and then increases linearly with the pressure according to the Poiseuille law. A theoretical treatment of self-diffusion through a long capillary tube valid over the entire pressure range from $\lambda \gg r$ to $\lambda \ll r$ has been given by Pollard and Present.[7] Their work explains the existence of the minima observed by Knudsen, Gaede, and Adzumi; furthermore, it predicts the absence of such minima in the case of flow through porous media. Observations[8] on the flow of pure gases through many types of porous media have shown the relation between specific flow and average pressure to be accurately linear down to pressures for which the mean free path λ is of the order of several hundred times the mean pore radius $\bar{r}$. These results imply that the flow through a porous medium can be accurately represented over the entire pressure range from $\lambda \gg \bar{r}$ to $\lambda \ll \bar{r}$ by an expression of the form

$$(c_1/m^{\frac{1}{2}})dp/dx + (c_2/\eta)pdp/dx, \qquad (3)$$

i.e., by simply adding a laminar flow (viscosity η) to a free-molecule diffusive flow. Therefore, both theory and experiment have shown that the two types of flow, while not strictly additive in long capillary tubes, appear to be so in many porous media.

Further experiments performed at the SAM laboratories[9] indicated that, in the case of a binary gas mixture flowing through a porous medium, the separation factor at intermediate pressures ($\lambda \sim \bar{r}$) could not be accounted for by assuming an equation of the form of (3) to hold for each component. At fore-pressures for which f (measured at zero back-pressure) was well below its ideal value f^+, flow measurements showed that the non-separative viscous flow could be altogether negligible; i.e., the flow of the mixed gas was simply proportional to the pressure gradient. The experiments thus indicated the existence at intermediate pressures of a non-separative non-viscous component of the flow which, when added to the separative free-molecule flow, gives rise to a total flow proportional to the pressure gradient as observed. Epstein[10] came to the same conclusion from a theoretical argument and Badger[11] made this the basis of a semi-empirical flow equation. Badger assumed that in a mixed flow the separative Knudsen diffusion should be weighted by a factor $1/1+cp$ and he added to this a non-separative diffusion term weighted by the factor $cp/1+cp$. Apart from the effects of viscosity, which were neglected by Badger, his equations are very similar to, though not identical with, those to be derived in the following section.

MOMENTUM TRANSFER THEORY

Let us consider first the changes that take place in the character of the flow as λ decreases from an initially large value. In a long tube of length $L \gg r$ there will be no intermolecular collisions so long as $\lambda \gg L$. If $L \gg \lambda \gg r$, a molecule will make many intermolecular collisions before reaching the outlet, but for every collision that a molecule makes with another molecule, it will make many collisions with the wall. Now the flow is ideally separative as long as intermolecular collisions can be neglected; when these occur momentum is transferred on the average from the lighter to the heavier gas so that the flow rates tend to equalize. If $\lambda \gg r$, the effect of a momentum transfer in an intermolecular collision is effaced during the many subsequent collisions with the wall which precede another intermolecular collision, and in which the molecule comes into equilibrium with the molecules of the wall. Thus the flow remains ideally separative Knudsen flow until the mean free path λ becomes comparable to the diameter of the tube. When $\lambda \sim r$ the effect of an intermolecular collision persists until the next intermolecular collision, and the cumulative effect of collisions between unlike molecules is to equalize the flow rates and diminish the separation efficiency. The transfer of forward momentum from the lighter to the heavier gas can take place in the absence of an appreciable gradient of the drift velocity normal to the tube axis, whereas the viscous transfer of momentum sets in only after the transverse velocity gradient has been established. We calculate first the non-separative effect of collisions between unlike molecules on the free-molecule flow, neglecting viscous effects.

[6] W. Gaede, Ann. d. Physik **41**, 289 (1913).
[7] W. G. Pollard and R. D. Present, Phys. Rev. **73**, 762 (1948).
[8] H. Kuhn, letter from N. Kurti to F. G. Slack, March 8, 1944; A. D. Callihan, M-1157, September 4, 1944; K. Schleicher, M-1472, January 5, 1945.
[9] This work was performed mainly by Lagemann, Weil, Schleicher, Slack, Callihan, and Roberts, of the SAM Laboratories.
[10] P. Epstein, A-1707, December 3, 1943.
[11] R. Badger, A-1751, March 30, 1944.

Consider the steady-state flow of a mixed gas through a long capillary of radius r extending in the x direction. Regarding a cylindrical element of gas of length dx, it is clear that the molecules of component 1 will receive a net forward momentum per unit time equal to $-\pi r^2(dp_1/dx)dx$, where p_1 is the partial pressure of gas 1. If component 1 is the lighter gas, this momentum is transferred partly to the wall and partly to gas 2; on the other hand, gas 2 receives momentum from the pressure gradient and from collisions with gas 1 and transmits it to the wall of the tube. Consider first the momentum transfer to the wall and let us denote by u_1 the transport or mean x-component of velocity of gas 1. If the molecules leave the wall in completely random directions after a collision with the surface (an assumption well confirmed by experiment[12]), they must—on the average—communicate their whole forward or x component of momentum to the wall. The momentum transferred each second would then be expected to be $mu\cdot(n\bar{v}/4)\cdot 2\pi r dx$ for a pure gas. This is confirmed by a direct calculation using an approximate distribution function for a drifting gas (see reference 7, Appendix I). However, this result implies no variation of n, u, and $\Gamma=nu$ over the cross section of the tube and, as previously mentioned,[4] Γ varies with distance from the axis in free-molecule flow. From Eq. (1) we obtain

$$dp/dx=-(3\pi m\bar{v}/16r)\overline{\Gamma}=-(3\pi m\bar{v}nu/16r), \quad (4)$$

where u represents the drift velocity averaged over the cross section. Multiplying both sides of (4) by $\pi r^2 dx$, the left-hand side becomes the resultant force on a cylindrical element as a result of the pressure gradient and the right side then represents the mean transfer of momentum from the gas to the wall per unit time: $(3\pi/8)\cdot mu\cdot(n\bar{v}/4)\cdot 2\pi r dx$. This result, which differs by a factor of $3\pi/8$ from that first given, will be used in the following.

We come next to the calculation of the momentum exchange between the two components of the gas mixture in the cylindrical element. Assume $u_1>u_2$ so that the molecules of gas 1 give up forward momentum on the average when colliding with molecules of gas 2. For purposes of orientation let us first assume, as in the hard elastic sphere model, that the scattering is isotropic in the center of mass system. Then the average momentum of molecule 1 in the x direction after collision will be $m_1\bar{u}_c$ where $\bar{u}_c$ is the x component of the mean velocity of the center of mass and is given by

$$\bar{u}_c=(m_1u_1+m_2u_2)/(m_1+m_2).$$

The average momentum of molecule 1 before collision is m_1u_1; therefore, the average amount of forward momentum lost in one collision is $m_1(u_1-\bar{u}_c)$ or $m^+(u_1-u_2)$ in terms of the reduced mass. The number of collisions per second per unit volume between unlike molecules is

$$n_1n_2\pi d_{12}^2(\bar{v}_1^2+\bar{v}_2^2)^{\frac{1}{2}},$$

where d_{12} is the collision diameter for unlike molecule encounters. Hence the momentum transferred per second from gas 1 to gas 2 per unit volume (M_{12}) would appear to be

$$m^+(u_1-u_2)\cdot n_1n_2\pi d_{12}^2\cdot(\bar{v}_1^2+\bar{v}_2^2)^{\frac{1}{2}}$$

on the average; however, the average momentum transferred is not quite the same as the average momentum loss per collision multiplied by the average number of collisions. Furthermore, the assumption of "hard elastic sphere" molecules is unnecessarily restrictive. It is readily seen that the momentum exchange M_{12} can be expressed directly in terms of the coefficient for ordinary mutual diffusion D_{12} without special assumptions about the law of force or the distribution-in-angle of the scattering. Provided only that the drift velocities u_1 and u_2 are small in comparison with the thermal velocities $\bar{v}_1$ and $\bar{v}_2$, the momentum transfer M_{12} will be simply proportional to u_1-u_2 and will not otherwise depend on the drift velocities (see Appendix I). Consider now a mutual diffusion of the same gas mixture at uniform total pressure with no total flow of molecules. Denoting the momentum transfer per unit volume per unit time from species 1 to species 2 by $M_{12}^{(D)}$ under the special conditions of mutual diffusion, we have

$$M_{12}/M_{12}^{(D)}=(u_1-u_2)/(u_1^{(D)}-u_2^{(D)})=(u_1-u_2)n_1n_2/n\Gamma_1^{(D)}, \quad (5)$$

since $\Gamma_1^{(D)}+\Gamma_2^{(D)}=n_1u_1^{(D)}+n_2u_2^{(D)}=0$. Considering now a steady mutual diffusion in the x direction through an element of gas of unit area and thickness dx, it is evident that the momentum received by component 1 from its partial pressure gradient is transferred to component 2 giving

$$(dp_1/dx)dx+M_{12}^{(D)}dx=0,$$

whence

$$\Gamma_1^{(D)}=-D_{12}(dn_1/dx)=D_{12}M_{12}^{(D)}/kT,$$

and therefore

$$M_{12}=(u_1-u_2)(n_1n_2kT/nD_{12}). \quad (6)$$

Equation (6) is independent of the law of force acting between the molecules and for small drift velocities is practically independent of the distribution function. In the special case of "hard elastic sphere" molecules, the value obtained for D_{12} either by Stefan's momentum transfer method[13] or

[12] Blankenstein, Phys. Rev. 22, 582 (1923). See also L. B. Loeb, *Kinetic Theory of Gases* (McGraw-Hill Book Company, Inc., New York, New York, 1927).

[13] See the review article by W. H. Furry, Am. J. Phys. 16, 63 (1948).

in the first approximation of the Enskog-Chapman theory[14] is

$$D_{12}=\tfrac{3}{8}(\pi kT/2m^{+})^{\frac{1}{2}}\cdot(1/n\pi d_{12}^{2}). \quad (7)$$

Introducing (7) into (6) and replacing $8kT/\pi m^{+}$ by $\bar{v}_1^2+\bar{v}_2^2$ we obtain

$$M_{12}=(4/3)m^{+}(u_1-u_2)\cdot n_1n_2\pi d_{12}^{2}\cdot(\bar{v}_1^2+\bar{v}_2^2)^{\frac{1}{2}}, \quad (6')$$

which differs by a factor of 4/3 from our preliminary result. Formulas (6) and (6′) apply to any volume element in the flowing gas. The momentum transfer from gas 1 to gas 2 in the cylindrical element bounded by the wall of the capillary is then $M_{12}\pi r^2dx$ provided that u_1 and u_2 are interpreted as the drift velocities averaged over the cross section. The following equations express the momentum balance in the cylindrical element:[15]

$$\begin{aligned}-\pi r^2\cdot(dp_1/dx)&=(3\pi/8)\cdot m_1u_1\cdot(n_1\bar{v}_1/4)\cdot 2\pi r\\&\quad+(u_1-u_2)\cdot(n_1n_2kT/nD_{12})\cdot\pi r^2\\-\pi r^2\cdot(dp_2/dx)&=(3\pi/8)\cdot m_2u_2\cdot(n_2\bar{v}_2/4)\cdot 2\pi r\\&\quad-(u_1-u_2)\cdot(n_1n_2kT/nD_{12})\cdot\pi r^2. \quad (8)\end{aligned}$$

Adding and introducing the molecular flows per unit area G_1 and G_2 averaged over the cross section, i.e., $G_i=n_iu_i$, we find

$$-r(dp/dx)=(3\pi/16)(m_1\bar{v}_1G_1+m_2\bar{v}_2G_2). \quad (9)$$

Since the right-hand side of (9) is a constant, the total pressure decreases linearly along the tube. Introducing the abbreviations

$$b(N)=\frac{8r}{3\pi}\cdot\left(\frac{\pi kT}{2m^{+}}\right)^{\frac{1}{2}}\cdot\frac{\langle m^{\frac{1}{2}}\rangle_N}{(m_1+m_2)^{\frac{1}{2}}}\cdot\frac{1}{pD_{12}}, \quad (10)$$

$$\langle m^{\frac{1}{2}}\rangle_N=Nm_1^{\frac{1}{2}}+(1-N)m_2^{\frac{1}{2}},$$

where $N(x)$ denotes the mole fraction of gas 1 and using the Maxwellian value of $\bar{v}$, one finds from Eq. (8) that

$$-G_1=\frac{8}{3\pi}\left(\frac{\pi}{2kT}\right)^{\frac{1}{2}}r\left\{\frac{1}{m_1^{\frac{1}{2}}}\cdot\frac{1}{1+b(N)p}\cdot\frac{d(Np)}{dx}+\frac{N}{\langle m^{\frac{1}{2}}\rangle_N}\cdot\frac{b(N)p}{1+b(N)p}\cdot\frac{dp}{dx}\right\}. \quad (11)$$

The first term, which is inversely proportional to $m^{\frac{1}{2}}$, is ideally separative. The second term is non-separative, it vanishes as the pressure goes to zero ($\lambda\gg r$), and for large pressures ($\lambda\ll r$) it is negligible compared with viscous flow. In the case of a pure gas ($N=1$) the two terms coalesce to give the free-molecule flow formula (1). It is readily seen that if the capillary has a uniform non-circular cross section, the same expressions for b and G_1 are valid if r is interpreted as twice the cross-sectional area divided by the perimeter. Badger's[11] semi-empirical equation is similar to (11); however, in his formulation $b(N)/\langle m^{\frac{1}{2}}\rangle_N$ was not independent of concentration. The second term of (11) representing a non-separative diffusion becomes important when $b(N)p\sim 1$. In the case of an isotopic mixture it is evident that

$$\begin{aligned}bp&=[2r/3]\cdot(8kT/\pi m)^{\frac{1}{2}}\cdot[1/D_{11}]\\&=D_K/D_{11}=K(r/\lambda), \quad (12)\end{aligned}$$

where D_{11} is the self-diffusion coefficient and D_K the Knudsen coefficient $2\bar{v}r/3$ for free molecule diffusion. The mean free path λ has been introduced in connection with the isotopic mixture and K denotes a numerical factor in the neighborhood of unity whose precise value depends on the relationship assumed between D_{11} and λ. It follows from (11) and (12) that the separation ceases to be ideal when λ becomes comparable to r.

CAPILLARY THEORY OF SEPARATION

In the preceding section it has been assumed that the effects of viscosity could be neglected in first approximation because of the small transverse gradient of the transport velocity. However, the transition to viscous flow takes place in the same range of pressures ($\lambda\sim r$) in which the non-separative diffusion becomes important. Consequently, although the effects of viscosity on separation are small in this range of pressure, they cannot be neglected. At higher pressures the entire diffusive flow (11) becomes negligible compared to the viscous flow. We now assume that the flow of a mixture of two gases at intermediate pressures can be represented by adding the viscous laminar flow to the diffusive flow of Eq. (11). In the case of pure gas flow through capillaries the transition region can be represented only approximately by adding the free-molecule and laminar flows. The minima found by Knudsen, Gaede, and Adzumi in the curve of specific flow *versus* mean pressure indicate that the flows are not strictly additive. Except at high pressures and low separation efficiencies, however, the effect of the viscous term is small and the error made by assuming exact additivity is of second order. The Poiseuille term in the following formulas may be regarded as an additive perturbation on the main diffusive flow. As previously noted, the assumption of additivity is a better approximation for porous media than for capillary tubes.

Equation (11) is now rewritten for each compo-

[14] S. Chapman and T. Cowling, *Mathematical Theory of Non-Uniform Gases* (MacMillan Company, Inc., New York, New York, 1939).

[15] It is readily seen that under the specified conditions of low pressure flow through long tubes the dynamical inertia term proportional to $u\partial u/\partial x$ can be neglected.

nent to include the viscous flow:

$$\frac{G_1}{g}=\frac{f^+}{1+b(N)p}\cdot\frac{d(Np)}{dx}+\frac{\bar{f}(N)b(N)p}{1+b(N)p}\cdot N\frac{dp}{dx}+Na(N)p\frac{dp}{dx},$$
$$\frac{G_2}{g}=\frac{1}{1+b(N)p}\cdot\frac{d(1-N)p}{dx}+\frac{f(N)b(N)p}{1+b(N)p}\cdot(1-N)\frac{dp}{dx}+(1-N)a(N)p\frac{dp}{dx}, \quad (13)$$

where

$$g=(8/3\pi)(\pi/2kTm_2)^{\frac{1}{2}}r,$$
$$\bar{f}(N)=m_2^{\frac{1}{2}}/\langle m^{\frac{1}{2}}\rangle_N, \quad (14)$$
$$a(N)=3r/16\eta(N)\bar{v}_2.$$

The value of a is obtained from the Poiseuille flow through a circular capillary divided by the area of cross section: $(r^2p/8\eta)dn/dx$. All three terms in (13) represent averages over the cross section of the tube. The relative importance of the non-separative diffusion and the viscous flow term is measured by the ratio $X(N)=b(N)/a(N)$. It follows from Eqs. (10) and (14) that

$$X(N)=\frac{256}{9\pi}\cdot\frac{\langle m^{\frac{1}{2}}\rangle_N\langle m\rangle_N}{m_2m_1^{\frac{1}{2}}}\cdot\frac{\eta(N)}{\rho(N)D_{12}}, \quad (15)$$

where $\rho(N)$ is the mass density and $\langle m\rangle_N=Nm_1+(1-N)m_2$. In the case of an isotopic mixture D_{12} reduces to the self-diffusion coefficient D_{11}. The dimensionless constant $\rho D_{11}/\eta$ may range in value from 1.20, corresponding to "rigid elastic sphere" molecules, up to about 1.5 for molecules repelling nearly as the inverse fifth power of the distance. In practice, $\rho D_{11}/\eta$ lies usually between 1.30 and 1.40; hence, the value of X for an isotopic mixture is roughly independent of the gas. Experiments[16] indicate that the best value of $\rho D_{11}/\eta$ for the UF_6 isotopic mixture is in the neighborhood of 4/3, corresponding to $X=64/3\pi$.

The differential equation of separation will now be obtained. Let ν denote the molar fraction of the first gas at the outlet; then $G_1/G_2=\nu/1-\nu$, expressing the condition that the composition of the gas at the exit is determined entirely by the flow rates through the tube. By substituting Eqs. (13) in this relation and writing $dN/dx=(dN/dp)(dp/dx)$ one obtains

$$p(dN/dp)\{f^+(1-\nu)+\nu\}+(N-\nu)\{(\bar{f}b+a)p+abp^2\}+f^+N(1-\nu)-\nu(1-N)=0. \quad (16)$$

Let $y=N-\nu$ and $h(\nu)=1+(f^+-1)(1-\nu)$. Then (16) becomes

$$hp(dy/dp)+[h+\{\bar{f}b+a(y)\}p+a(y)b(y)p^2]y+(f^+-1)\nu(1-\nu)=0. \quad (17)$$

Evidently ν and $\bar{f}b$ are constants but the parameters a and b depend on the composition at every point through $\eta(N)$ and $\langle m^{\frac{1}{2}}\rangle_N$, respectively. Since $\langle m^{\frac{1}{2}}\rangle_N$ is a linear function of N and since $1/\eta(N)$ can be approximately represented by a linear function over not too large a range, we may rewrite Eq. (17) in the form (neglecting the small terms py^2 and p^2y^3)

$$p(dy/dp)+\{1+cp+lp^2\}y+mp^2y^2+s=0. \quad (18)$$

The solution of Eq. (18) can be obtained analytically in terms of confluent hypergeometric functions (see appendix II) or more simply by numerical integration. However, even in the case of a gas mixture in which the molecular mass ratio and the change of composition are large and the coefficient of p^2 in (17) varies considerably, e.g., H_2-CO_2, the solution of (17) is found to differ by only a few percent at low and negligibly at high separation efficiencies from the solution in which a and b are treated as constants and given their values at the inlet. Since the composition of the gas in ideal Knudsen flow is constant at the inlet value throughout the length of the tube, it is obviously preferable to use the inlet rather than the outlet values of a and b. Hence for all mixtures in which the molecular mass ratio of the components is not too large, we may replace (17) by

$$h(\nu)p(dy/dp)+\{h(\nu)+c_1p+c_2p^2\}y+(f^+-1)\nu(1-\nu)=0, \quad (19)$$

where $c_1=\bar{f}b+a$ and $c_2=ab$. On integrating from the outlet to the inlet we obtain

$$y(p_F)=N_0-\nu=-\frac{(f^+-1)\nu(1-\nu)}{h(\nu)p_F}\cdot\frac{\int_{p_B}^{p_F}\exp\{(c_1p+(c_2/2)p^2)/h(\nu)\}dp}{\exp\{(c_1p_F+(c_2/2)p_F^2)/h(\nu)\}}, \quad (20)$$

where p_F and p_B denote fore- and back-pressures and N_0 the inlet concentration. We define the separation efficiency Z as the ratio of the actual enrichment to the ideal enrichment at constant back-composition. It is readily seen that

$$Z=\frac{(\nu-N_0)h(\nu)}{(f^+-1)\nu(1-\nu)}=\frac{\int_{\phi_B}^{\phi_F}\exp\{[(1+X\bar{f})\phi+(X/2)\phi^2]/h(\nu)\}d\phi}{\phi_F\exp\{[(1+X\bar{f})\phi_F+(X/2)\phi_F^2]/h(\nu)\}}, \quad (21)$$

[16] E. P. Ney and F. C. Armistead, Phys. Rev. 71, 14 (1947).

where the "reduced pressure" $\phi=ap=3rp/16\eta\bar{v}_2$ has been introduced. A curve of Z *versus* ϕ_F for fixed ϕ_B/ϕ_F will be referred to as a "fore-pressure curve." It is apparent from Eq. (21) that there is no universal fore-pressure curve which would be independent of the gas mixture. However, since the X of an isotopic mixture is approximately independent of the gas, one may, to good approximation, use a universal fore-pressure curve for isotopic mixtures. In this case ($\bar{f}\approx 1$, $h(\nu)\approx 1$) Eq. (21) reduces to

$$Z=\frac{\int_{\phi_B}^{\phi_F}\exp\{(1+X)\phi+(X/2)\phi^2\}d\phi}{\phi_F\exp\{(1+X)\phi_F+(X/2)\phi_F^2\}}. \quad (21\text{i})$$

It is convenient for purposes of comparison with experiment to have the pressures expressed in terms of p_{50}, the fore-pressure at which $Z=0.50$ when the back-pressure is zero. Using $X=64/3\pi$, one finds that $Z=0.50$ when $\phi_F=0.1834$ and $\phi_B=0$. Introducing the "relative pressure" $\pi=p/p_{50}=\phi/\phi_{50}$, Eq. (21i) becomes[17]

$$Z(\pi_F,\pi_B)=\frac{\int_{\pi_B}^{\pi_F}\exp\{1.430\pi+0.1142\pi^2\}d\pi}{\pi_F\exp\{1.430\pi_F+0.1142\pi_F^2\}}. \quad (21\text{i}')$$

Numerical results from Eq. (21i) are insensitive to variations in X arising from the slightly different values of $\rho D_{11}/\eta$ appropriate to different gases. When $\pi_B=0$ a good approximation to Eq. (21i') is given by

$$Z^{-1}=1+0.662\pi_F+0.338\pi_F^2, \quad 0\leq\pi_F\leq 2. \quad (21\text{i}'')$$

In the stated range of fore-pressures this formula is nowhere in error by more than one percent.

In the case of a general binary gas mixture it is convenient to introduce the variable

$$t=(X/2h)^{\frac{1}{2}}\phi+t_0, \quad t_0=(1+X\bar{f})/(2hX)^{\frac{1}{2}}.$$

Equation (21) can then be written in a general form for all gas mixtures as the simple three-parameter function

$$Z(t_F,t_B,t_0)=\int_{t_B}^{t_F}\exp[t^2]dt/(t_F-t_0)\exp[t_F^2]. \quad (22)$$

The integrals are conveniently evaluated from the following formula[18] based on an approximation by Tschebyscheff polynomials and having in the range $2\leq x<\infty$ an error nowhere exceeding 1 part in 2000:

$$\int_0^x\exp[t^2]dt=(\exp[x^2]/2x)\times\{0.9995+0.1489(2/x)^2-0.1361(2/x)^4+0.4525(2/x)^6-0.2184(2/x)^8\}-0.56. \quad (23)$$

Graphs of Z *vs.* t_F for selected values of t_B and t_0 can be simply prepared and applied to the separation of various binary gas mixtures for the two cases of constant fore-composition and constant back-composition.

The integration of Eq. (19) from the outlet of the capillary (at given back-pressure and back-composition) to a variable pressure p enables one to plot N as a function of p. Starting from the inlet value N_0, N is found to decrease monotonically along the tube when $p_B=0$ and then jump discontinously to the value ν at the exit; when p_B is small but finite the concentration of light component first decreases and then rises steeply but continuously near the exit. The explanation of the initial decrease in N is as follows. The ratio of the light component transport velocity to that of the heavy component is not constant as in free-molecule flow but increases as the lower pressure region of the tube is reached because of the decreasing frequency of collisions between unlike molecules. Since the ratio of concentrations is inversely proportional to the ratio of transport velocities, the light component concentration must decrease down the tube rising near the outlet because of back-diffusion.

This article will be concluded with a brief consideration of the total flow of a mixed gas through the capillary tube. The total flow of the mixture is obtained by adding together the two Eqs. (13) and eliminating the term in dN/dp by the use of Eq. (16). The result for $G=G_1+G_2$ is simply

$$-G/g=\bar{f}(\nu)dp/dx+\{\bar{f}(\nu)/\bar{f}(N)\}a(N)pdp/dx, \quad (24)$$

where $\bar{f}$ and a are defined by Eqs. (14). Introducing $g'=gm_2^{\frac{1}{2}}$ and $a'=a(N)\eta(N)m_2^{-\frac{1}{2}}=3r/16\bar{v}_2m_2^{\frac{1}{2}}$ into (24), one obtains

$$-G/g'=\frac{1}{\langle m^{\frac{1}{2}}\rangle_\nu}\cdot\left\{1+\frac{a'\langle m^{\frac{1}{2}}\rangle_N p}{\eta(N)}\right\}\cdot\frac{dp}{dx}, \quad (24')$$

which may be compared with the corresponding formula for a pure gas:

$$-G/g'=\frac{1}{m^{\frac{1}{2}}}\cdot\left\{1+\frac{a'm^{\frac{1}{2}}p}{\eta}\right\}\cdot\frac{dp}{dx}. \quad (24'')$$

[17] Equation (21i') was derived independently by C. H. Bosanquet from a quite different point of view. Bosanquet's results, which were communicated to R. Peierls in letters dated May 8 and 19, 1944, were obtained slightly earlier than those of the present authors. The considerations of Bosanquet were restricted to isotopic mixtures; however, it has been shown by Pollard (A-3813, November 23, 1945) that the method of Bosanquet can be generalized to an arbitrary gas mixture.

[18] This formula was calculated for us by Dr. C. Lanczos.

The first term of Eq. (24′), which represents the free-molecule flow of a mixed gas, is seen to be inversely proportional to the average value of the square root of the molecular mass, the average being taken with respect to the outlet composition. The integration of Eqs. (24) or (24′) is complicated by the fact that the coefficient of pdp/dx is a function of composition and the composition varies with the pressure as the gas flows from the inlet to the outlet. Details will not be given here.[19]

APPENDIX I

Momentum transfer in the gas. It will be shown here that for simple approximate distribution functions the momentum transfer is proportional to the difference in transport velocities u_1-u_2. Since very similar derivations are to be found in the literature [see reference 13 or E. H. Kennard, *Kinetic Theory of Gases* (McGraw-Hill Book Company, Inc., New York, 1938), p. 190], the discussion is abbreviated.

Let $\mathbf{V}=\mathbf{v}_1-\mathbf{v}_2$ be the relative velocity of two unlike molecules before an encounter and let ψ denote the angle between $\mathbf{V}$ and the relative velocity after collision; i.e., ψ is the angle of deflection in the center of mass system. Assuming a spherically symmetrical interaction, the angle ψ evidently depends only on the relative speed $V=|\mathbf{V}|$ and the impact parameter b. The number of unlike molecule collisions per unit volume per unit time between molecules with velocities in the range $\mathbf{v}_1$ to $\mathbf{v}_1+d\mathbf{v}_1$ and molecules of the other type with velocities between $\mathbf{v}_2$ and $\mathbf{v}_2+d\mathbf{v}_2$ is $dn_1dn_2V\cdot 2\pi bdb$ for impact parameters between b and $b+db$. It is readily seen that the momentum transferred to molecule 2 in a single collision has a component $m^+\mathbf{V}(1-\cos\psi)$ in the direction of $\mathbf{V}$ and that the perpendicular component averages to zero. Hence the momentum transfer per unit volume per unit time from the group dn_1 to the group dn_2 is $dn_1dn_2m^+\mathbf{V}V\sigma(V)$ where

$$\sigma(V)=\int_0^\infty 2\pi bdb(1-\cos\psi)$$

is the cross section for momentum transfer (in the case of hard elastic spheres $\sigma=\pi d_{12}^2$ where d_{12} is the mean diameter). Evidently $dn_i=n_if_id\mathbf{v}_i$, where f_i is the velocity distribution function for gas i drifting in the x direction with velocity u_i. Provided that $u_i\ll v_i$, a good approximation is obtained by taking

$$\begin{aligned}f_id\mathbf{v}_i&=(\beta_i/\pi)^{\frac{3}{2}}\exp[-\beta_i(v_{ix}-u_i)^2]dv_{ix}\\&\quad\times\exp[-\beta_iv_{iy}^2]dv_{iy}\exp[-\beta_iv_{iz}^2]dv_{iz}\\&\cong(\beta_i/\pi)^{\frac{3}{2}}\exp[-\beta_iv_i^2](1+2\beta_iu_iv_{ix})d\mathbf{v}_i,\end{aligned}$$

where $\beta_i=m_i/2kT$. The total transfer of momentum per unit volume per unit time in the x direction is then

$$\begin{aligned}M_x&=m^+n_1n_2\int d\mathbf{v}_1\int d\mathbf{v}_2f_1^{(0)}f_2^{(0)}\\&\quad\times(1+2\beta_1u_1v_{1x})(1+2\beta_2u_2v_{2x})V_xV\sigma(V)\\&=2m^+n_1n_2\int d\mathbf{v}_1\int d\mathbf{v}_2f_1^{(0)}f_2^{(0)}(\beta_1u_1v_{1x}+\beta_2u_2v_{2x})V_xV\sigma(V)\end{aligned}$$

using the abbreviation $f_i^{(0)}=(\beta_i/\pi)^{\frac{3}{2}}\exp[-\beta_iv_i^2]$. The simplification of the above equation follows from considerations of parity. We transform coordinates from $\mathbf{v}_1$, $\mathbf{v}_2$ to $\mathbf{C}$, $\mathbf{V}$, where $\mathbf{C}$ is the velocity of the center of mass. It is readily found that

$$\begin{aligned}M_x=\frac{m^+n_1n_2}{kT}&\int d\mathbf{C}\int d\mathbf{V}f_C^{(0)}f_V^{(0)}V_xV\sigma(V)\\&\times\{(m_1u_1+m_2u_2)C_x+m^+(u_1-u_2)V_x\},\end{aligned}$$

where

$$f_C^{(0)}=(m_1+m_2/2\pi kT)^{\frac{3}{2}}\exp[-(m_1+m_2/2kT)C^2]$$

and

$$f_V^{(0)}=(m^+/2\pi kT)^{\frac{3}{2}}\exp[-(m^+/2kT)V^2].$$

The term in C_x vanishes since the integrand is odd. M_x is therefore proportional to u_1-u_2.

APPENDIX II

Equation (18) is rewritten

$$pdy/dp+\{1+cp+lp^2\}y+mp^2y^2+s=0, \tag{A}$$

where c, l, m, and s are constants characteristic of the gas mixture. The solution is subject to the condition that $y=0$ when $p=p_B$. Let $u=py$, then Eq. (A) becomes

$$du/dp+(c+lp)u+mu^2+s=0.$$

This is Riccati's equation. It can be transformed into a second-order linear equation by the substitution $u=(mw)^{-1}dw/dp$ and the resulting equation is

$$d^2w/dp^2+(c+lp)dw/dp+msw=0.$$

Let $z=l^{-\frac{1}{2}}(c+lp)$ and $\alpha=ms/2l$. Then

$$d^2w/dz^2+zdw/dz+2\alpha w=0. \tag{B}$$

The general solution of Eq. (B) can be written in terms of the confluent hypergeometric functions. In the notation of Jahnke-Emde and Webb-Airey the solution is

$$w=AM\left(\alpha,\frac{1}{2},-\frac{z^2}{2}\right)+Bz^{\frac{1}{2}}M\left(\alpha+\frac{1}{2},\frac{3}{2},-\frac{z^2}{2}\right), \tag{C}$$

$$\begin{aligned}dw/dz=&-2\alpha zAM\left(\alpha+1,\frac{3}{2},-\frac{z^2}{2}\right)\\&+(B/2)z^{-\frac{1}{2}}M\left(\alpha+\frac{1}{2},\frac{3}{2},-\frac{z^2}{2}\right)\\&-Bz^{\frac{1}{2}}((2\alpha+1)/3)M\left(\alpha+\frac{3}{2},\frac{5}{2},-\frac{z^2}{2}\right),\end{aligned}$$

where A and B are arbitrary constants, the ratio of which is fixed by the boundary condition: $y=0$ at $p=p_B$. Hence $dw/dz=0$ when $z=z_B=l^{\frac{1}{2}}p_B+cl^{-\frac{1}{2}}$.

$$\therefore\frac{B}{A}=\frac{12\alpha z_B^{\frac{1}{2}}M\left(\alpha+1,\frac{3}{2},-\frac{z_B^2}{2}\right)}{3M\left(\alpha+\frac{1}{2},\frac{3}{2},-\frac{z_B^2}{2}\right)-(4\alpha+2)z_B^2M\left(\alpha+\frac{3}{2},\frac{5}{2},-\frac{z_B^2}{2}\right)}.$$

By using the asymptotic value of $M(\alpha,\gamma,x)$ for large x, the asymptotic solution for large fore-pressures is found to be

$$\begin{aligned}w^{-1}dw/dz&\to-2\alpha/z,\quad z\to\infty,\\y&\to-s/lp^2,\quad p\to\infty.\end{aligned}$$

The asymptotic form of the solution for large fore-pressures indicates that the separation efficiency falls off as the inverse square of the pressure. This is in agreement with the result for high pressure differential diffusion based on the Chapman-Enskog diffusion formula [G. J. Kynch, MS-103 (Declassified British report)].

The formal solution (C) is inconvenient for numerical work. Actual calculations were carried out by two methods. In method I we made use of the fact that the solution of (A) was known for the case $m=0$ from previous work in which the variation of C_2 with y was neglected. Since the term in p^2y^2 is initially small, the previous solution in terms of the tabulated integral $\int_0^z\exp[t^2]dt$ was used for the first part of the interval and the Runge-Kutta method of numerical integration the rest of the way. In method II, Eq. (B) was solved by power series after first changing the independent variable to $z-z_B$. This method cannot be used when $p_B=0$.

[19] The calculations of this final paragraph were made by deBethune and Pollard, A-2145, October 18, 1944.

The Density Spectrum of Extensive Air Showers of Cosmic Rays

G. COCCONI* AND V. COCCONI TONGIORGI
Laboratory of Nuclear Studies, Cornell University, Ithaca, New York
(Received December 6, 1948)

The density spectrum of extensive showers has been measured both at 260 and at 3260 m above sea level. It has been found that the spectrum in both places is not a pure exponential.

I. METHODS FOR THE EVALUATION OF γ

IT has been established that the frequency $H(\Delta)$ of the extensive air showers in which the particle density (particles per unit surface) is greater than Δ can be satisfactorily expressed by the law:

$$H(\Delta)=K\Delta^{-\gamma}, \tag{1}$$

where K and γ are in first approximation constant in a large density range and vary with the altitude above sea level.

The determination of the value of the exponent γ can be achieved through different methods:

(a) n G-M counters, all with the same effective surface S, are placed at proper distances on a horizontal plane, and coincidences $N_{n-1}(S)$ and $N_n(S)$ are recorded.

From the ratio $N_n(S)/N_{n-1}(S)$ it is possible to deduce γ by using the expression:

$$\frac{N_n(S)}{N_{n-1}(S)}=\frac{\left[\binom{n}{1}-\binom{n}{2}2^{\gamma}+\binom{n}{3}3^{\gamma}-\cdots\right]}{\left[\binom{n-1}{1}-\binom{n-1}{2}2^{\gamma}+\binom{n-1}{3}3^{\gamma}-\cdots\right]}. \tag{2}$$

TABLE I. Experimental evaluations of γ and K.

Author	Method	Elevation (m.a.s.l.)	Density range (m^{-2})	γ	K (Δ in m^{-2}, time in sec.)
Cocconi, etc.[a]	*b*	110	10–1000	1.46	0.124
	b	2200	10–1000	1.55	1.0
Auger, Daudin[b]	*a*	50	~70	1.66	
	a	2060	~70	1.50	
	a	2860	~70	1.46	
Maze, etc.[c]	*a*	0	~100	1.67	
	a	6700	~100	1.41	
Treat, Greisen[d]	*a*	3260–4300	30–200	1.55	
	b	3260–4300	30–200	1.40	
Loverdo, Daudin[e]	*a*	2900	4–800	1.52–1.65	
	b	2900	4–800	1.30	
Williams[f]	*c*	3050	300–2000	1.50–1.90	2.70

[a] G. Cocconi, A. Loverdo, and V. Tongiorgi, Nuovo Cimento 2, 14 (1944); Phys. Rev. 70, 841 (1946).
[b] P. Auger and J. Daudin, J. de phys. et rad. 6, 233 (1945).
[c] R. Maze, A. Fréon, and P. Auger, Phys. Rev. 73, 418 (1948).
[d] J. E. Treat and K. I. Greisen, Phys. Rev. 74, 414 (1948).
[e] A. Loverdo and J. Daudin, J. de phys. et rad. 9, 134 (1948).
[f] R. W. Williams, Phys. Rev. 74, 1689 (1948).

* On leave from the University of Catania, Italy.

In this case it is tacitly assumed that the density of showers is the same at each of the n counters.

By varying the surfaces S, γ can be evaluated for showers of different densities, because the showers recorded by counters of surface S have a mean density $\sim 1/S$. When γ is known, the value of the constant K in the integral density spectrum (1) can be immediately deduced from the expression:

$$K=\frac{N_n(S)}{I_{(n,\gamma)}S^{\gamma\cdot\gamma}}, \tag{3}$$

where

$$I_{(n,\gamma)}=\int_0^{\infty}x^{-(\gamma+1)}(1-e^{-x})^n dx,$$

which can be written

$$I_{(n,\gamma)}=\frac{\Gamma(2-\gamma)}{\gamma(\gamma-1)}\left[\binom{n}{1}-\binom{n}{2}2^{\gamma}+\binom{n}{3}3^{\gamma}-\cdots\right]^{**}.$$

(b) When $N_n(S)$ is measured for different values of the surface S of the counters, γ may be deduced from the formula:

$$\gamma=\frac{d\log N_n(S)}{d\log S}. \tag{4}$$

If this is done for different values of S, here too γ may be evaluated for different densities.

Because of the fact that the space distribution function in the showers is very likely the same for all showers, it can easily be shown that this method does not require the assumption of uniform density over all the counters.

(c) With either ionization chambers or cloud chambers the extensive showers can be studied. From the graph of the frequency of the showers, *versus* the number of particles crossing the apparatus, γ can be deduced.

(d) Finally γ can be deduced theoretically; this requires, of course, hypotheses about the origin of the showers and the processes taking place in their

** This expression of the integral $I(n,\gamma)$ was pointed out to us by Mr. Aadne Ore, whom we want to thank. Other authors have used similar expressions, e.g., J. Daudin, J. de phys. et rad. 8, 301 (1947).

development as well as about the spectrum of the shower-producing radiation.

II. RESULTS OF PREVIOUS EVALUATIONS

The experimental evaluations of γ and K obtained thus far are collected in Table I.

As for theoretical evaluations of the density spectrum, it is well known that the behavior of the extensive showers cannot be satisfactorily described in terms of pure cascade theory, since besides electrons and photons, penetrating particles and neutrons are produced in such showers. Nevertheless, calculations have been carried out by several authors on the basis of the cascade theory, with the assumption of single electrons as primary particles.

Assuming an exponent 1.8 for the exponential spectrum of primary electrons, Cocconi[1] found for showers with densities between 10 and 1000 particles m^{-2},

$$\gamma=1.36 \quad \text{at sea level,}$$
$$\gamma=1.50 \quad \text{at 2300 m,}$$
$$\gamma=1.64 \quad \text{at 4100 m.}$$

We have now extended these calculations in order to evaluate γ over a larger range of densities, and we have found that for densities between 0.3 and 2.10^4 the best values for γ are, expressing Δ in m^{-2} and using natural logarithms,

$$\gamma=1.29+0.025\log\Delta \quad \text{at sea level,}$$
$$\gamma=1.41+0.028\log\Delta \quad \text{at 2300 m,}$$
$$\gamma=1.50+0.034\log\Delta \quad \text{at 4100 m.} \qquad (5)$$

The experimental results of Table I are not in good agreement among each other as well as with the theory, hence they do not give information on the question of the small variations of γ with the density of the showers and the altitude above sea level.

In our opinion the discrepancies arise from inaccuracy in the experimental procedures, from uncertainty in the corrections applied to the observed data, and from unreliability of the comparison of results obtained with different apparatus.

Therefore we thought it worth while to set up experiments in order to evaluate γ as accurately as possible at different altitudes and in a large density range. For the same reason we shall discuss here extensively the experimental details and the corrections to the measurements.

III. EXPERIMENTAL ARRANGEMENT

The experiments were performed both at Ithaca (260 m above sea level) and at Echo Lake (3260 m), and the arrangement was chosen in such a way as to allow evaluation of γ with both methods *a* and *b*.

[1] G. Cocconi, Phys. Rev. **72**, 974 (1947).

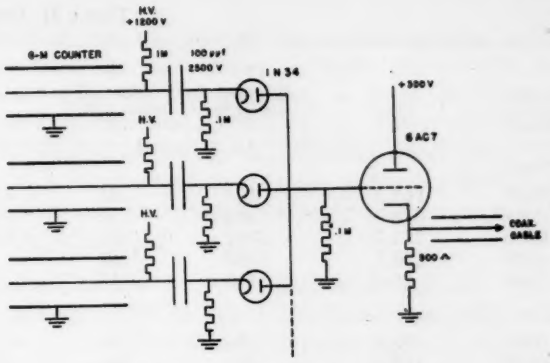

FIG. 1. Diagram of the mixing circuit.

The extensive showers were detected by four groups of counters, A, B, C, and D, placed in a horizontal plane, ABC being at the vertices of an equilateral triangle and D at the center. Threefold coincidences $A+B+C$ and fourfold $A+B+C+D$ were simultaneously recorded.

At both stations the counters were placed in light homosote boxes kept at constant temperature, which constituted the only shield from the open air.

In order to explore a density range as large as possible the following effective surfaces were used:

9 cm^2 (a single counter $\frac{1}{2}''\times 3''$)
29 cm^2 (a single counter $\frac{1}{2}''\times 10''$)
98 cm^2 (a single counter $1''\times 16''$)
500 cm^2 (a single counter $2''\times 40''$)
1500 cm^2 (three counters $2''\times 40''$)
5000 cm^2 (ten counters $2''\times 40''$)

The counters, all-metal type, were filled with an alcohol-argon mixture. The effective length of the central wire was measured and the sensitive surface of the counters was calculated as the product of such a length, times the internal diameter of the brass cylinder.

Inaccuracy in the determination of the effective surfaces may arise from the fact that some showers may fall on the counter trays with large zenith angles. Tests were made in order to evaluate the order of magnitude of such an effect. At Ithaca the frequencies of the extensive showers were recorded, once with the counter trays $ABCD$ consisting each of three counters (each $2''\times 40''$) close together, once with the same counters 2″ apart. If the number of showers in very slanting directions is significant, one has to expect lower frequencies with the counters arranged in the packed trays. No difference in the counting rates has been found, within the statistical errors (2 percent), therefore the conclusion was reached that the number of extensive showers in very slanting directions recorded by our apparatus was negligible.*** Yet, in order to

*** The same conclusion has been reached by Loverdo and Daudin (see reference e of Table I) and may be independently

TABLE II. Results of measurements.

1 Counter surface S (m²)	2 Time (hr.)	3 Observed coinc. ABC T	4 Observed coinc. $ABCD$ Q	5 Corrected values T/h	6 T/Q	7 S	8 Deduced γ Method a	9 Method b
Ithaca								
0.0029	761.2	102	63	0.134±0.013	1.62±0.12	0.0029	1.58±0.14	1.45±0.10
0.0098	336.2	260	172	0.780±0.05	1.51±0.07	0.0098	1.44±0.10	1.53±0.04
0.0500	271.7	2702	1751	9.350±0.2	1.525±0.02	0.0500	1.46±0.03	1.34±0.02
0.1500	133.2	5388	3584	40±0.6	1.49±0.014	0.1480	1.41±0.03	1.36±0.015
0.5000	24.3	5115	3313	206±3.0	1.47±0.015	0.4940	1.38±0.03	
Echo Lake								
0.0009	372.4	70	44	0.188±0.023	1.59±0.15	0.0009	1.55±0.19	1.55±0.12
0.0029	190.0	215	140	1.150±0.08	1.53±0.075	0.0029	1.47±0.12	1.50±0.06
0.0098	169.2	1187	799	7.120±0.21	1.48±0.03	0.0098	1.40±0.05	1.51±0.021
0.0500	41.65	3109	2019	83±1.4	1.50±0.02	0.0500	1.425±0.03	1.36±0.016
0.1560	30.6	11646	7881	378±3.7	1.46±0.01	0.1520	1.365±0.02	1.33±0.016
0.5000	2.35	4425	3011	1790±30.0	1.40±0.013	0.4880	1.27±0.03	

minimize the effect, if it exists, both at Ithaca and at Echo Lake, all the counter trays of large area were set up with the counters 2″ apart.

The negative pulses of the counters were fed into cathode followers in order to drive the coax cables with low impedance.

Particular precaution was taken when several counters were connected in parallel in order to obtain trays of large area. It is well known that the simple connection in parallel of the anodes of several counters causes an increase in the capacity of each counter and consequently decreases the size of its pulses; furthermore it introduces fluctuations of the voltage applied on each counter, owing to the pulses of the other counters of the tray. In order to avoid these troubles, the "mixing circuit" with crystal diodes drawn in Fig. 1 has always been used between the counters and the cathode followers. Mixing circuits and cathode followers were placed very close to the counters in the same boxes that contained the counters. The recording circuit consisted of channels of amplifiers and blocking oscillators, the outputs of which were put in coincidence through crystal diodes. The resolving time, measured by chance coincidences between two counters with very high rates, was 4.1 μsec. The outputs of the counters, as well as the circuits, were carefully shielded from electrical noise.

The side of the equilateral triangle at the vertices of which counters ABC were placed, was chosen as 4 m at Ithaca and 6 m at Echo Lake, in order to take into account the increase of the average spread of the showers, due to the lower atmospheric pressure at Echo Lake. In recording extensive showers, the choice of a proper distance between the counters is important because if it is too small, either showers very poor in particles, generated by knocks-on electrons of the mesons, or locally generated penetrating showers can be recorded in large percentage besides extensive showers; while if it is too large, on the other hand, some of the smaller extensive showers can be missed. Test measurements have been performed at Ithaca with the counters ($S=1500$ cm²) arranged in a triangle once of 4-m side, once of 8-m side. While the absolute rate of the coincidences shows a decrease in the second arrangement of ~10 percent, the ratios $A+B+C+D/A+B+C$ remains practically constant within the statistical errors (2 percent), which proves that in our arrangement the ratios of recorded rates do not depend critically on the distance among the counters. Of course, if the distance between the counters is increased to many meters, one has to expect a variation not only of the rate of the showers but also of the density spectrum, the smaller showers not being recorded: this has been observed by Loverdo and Daudin.†

IV. RESULTS AND CORRECTIONS

The results of the experiments at Ithaca and at Echo Lake are collected in columns 1, 2, 3, and 4 of Table II. The following corrections were then taken into account:

(*1*) *Chance coincidences:* Threefold and fourfold chance coincidences have been calculated in the usual way, the higher contribution to them arising from chance coincidence between a shower striking $n-1$ counters (and not n), and an incoherent particle striking the remaining counter.

(*2*) *Barometric effect:* All the data have been normalized to the mean barometric pressure at Ithaca and at Echo Lake by assuming a barometric coefficient of 10 percent per cm Hg, as deduced from the cascade theory of the extensive showers.[1]

reached from the measurement of the zenith angle distribution of extensive showers (see e.g., M. Deutschmann, Zeits. f. Natfor. 2, 61 (1947)) which shows a very pronounced maximum in the vertical direction.

† See reference e of Table I.

The experimental determinations of such a coefficient, though rather uncertain, are in agreement with the theoretical value.

(3) *Inefficiency of the counters:* It is known that the inefficiency ϵ of G-M counters is mainly due to the dead time following a discharge. We measured the dead time of our counters and calculated their efficiencies. The efficiency $(1-\epsilon)$ of the four kinds of counters we used ($\frac{1}{2}''\times 3''$, $\frac{1}{2}''\times 10''$, $1''\times 16''$, $2''\times 40''$) were, respectively:

at Ithaca 99.9%; 99.9%; 99.7%; 98.8%
at Echo Lake 99.9%; 99.8%; 99.5%; 97.5%.

The correction for inefficiency, if applied to the coincidences registered with trays of counters in parallel, requires the knowledge of the degree of coherence of the particles striking the trays; in fact if a tray is struck by two coherent particles, very likely the two particles hit two different counters, so that the efficiency of the tray is $(1-\epsilon^2)$ rather than $(1-\epsilon)$. Such considerations can be avoided by correcting, instead of the recorded coincidences, the effective surface of the counters' tray, i.e., by assuming as effective surface the real one, multiplied by the efficiency $(1-\epsilon)$.

(4) *Counter walls:* Another correction, at least in principle, must be introduced in order to take into account the effect of the walls of the counters on the particles in the showers. All our counters had brass walls 0.5–0.6 mm thick and were protected from the open air by a wall of homosote $\frac{1}{2}''$ thick, in total about 1.5 g cm^{-2}. Yet unpublished results obtained by E. Palmatier**** this summer at Echo Lake show that the rate of the extensive showers remains practically constant when the thickness of the walls of the counters varies from 0.4 mm Al to 0.4 mm Al plus 1.6 mm brass. Probably this result is due to multiplication of photons which compensates the absorption of the electrons. In any case we think that no correction must be introduced in our data for the walls of the counters.

Corrections 1, 2, 3 have been applied to the numbers of columns 3 and 4 of Table II, and the corrected rates and areas are listed in columns 5, 6, and 7. The rates of column 5, *versus* surface of the counters (column 7), are plotted on a log-log scale in Fig. 2. The values of γ deduced from the ratios fourfold/threefold (column 6) with formula (2) are written in column 8 of the table. In column 9 are reported instead the values of γ deduced with formula (4) from the slope of the curve of Fig. 2 taken at various S. All the values of γ deduced with the two methods are plotted in Fig. 3 as a function of the logarithm of $1/S$, which is proportional to the mean density of the showers. A check of the validity of the measurements is the fact that the agreement between the results deduced with the two methods is quite satisfactory both at Ithaca and at Echo Lake. From the results it is possible to reach the following conclusions:

(1) γ is observed to increase with the density of the showers. The lines drawn in Fig. 3 are expressed by the equations:

$$\begin{aligned} &\text{Ithaca (260 m)} && \gamma = 1.31 + 0.038 \log 1/S \\ &\text{Echo Lake (3260 m)} && \gamma = 1.26 + 0.043 \log 1/S \end{aligned} \qquad (6)$$

(S in m^2 and natural logarithms).

Remembering what has been said at the beginning, in first approximation it is legitimate to substitute $\bar{\Delta}$ for $1/S$ in expressions (6).

(2) The variation of γ with Δ implies a dependence of the constant K in formula (1) on Δ. This means that the law (1) cannot be considered true for ranges of densities in which $\Delta\text{max}/\Delta\text{min} > 10^2$.

(3) If we confine ourselves within the densities between 10 and 1000 particles per square meter, the value of K and γ which best fit our experimental points are (with Δ measured in m^{-2} and time in sec.):

at Ithaca $K=0.200$ $\gamma=1.48$,
at Echo Lake $K=1.68$ $\gamma=1.46$. (7)

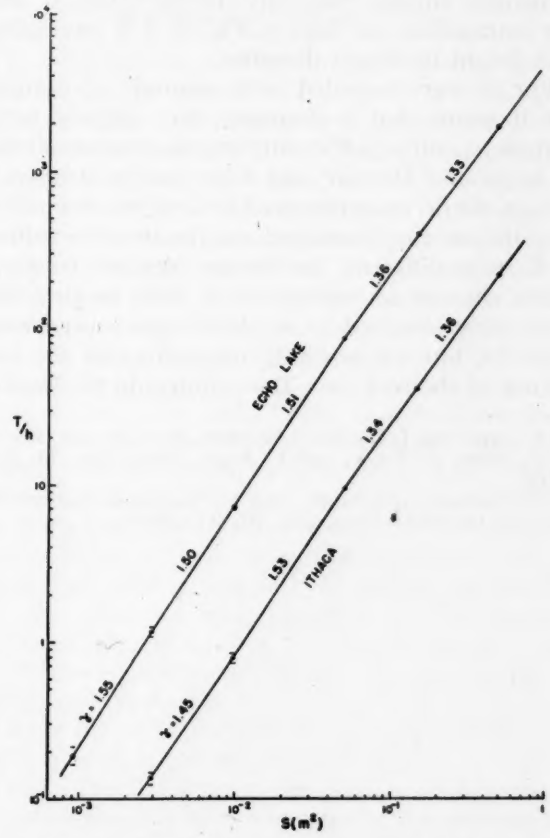

FIG. 2. Rate of threefold coincidences *versus* surface of the counters at Ithaca and Echo Lake.

**** We are very grateful to Mr. E. Palmatier for making his results available to us.

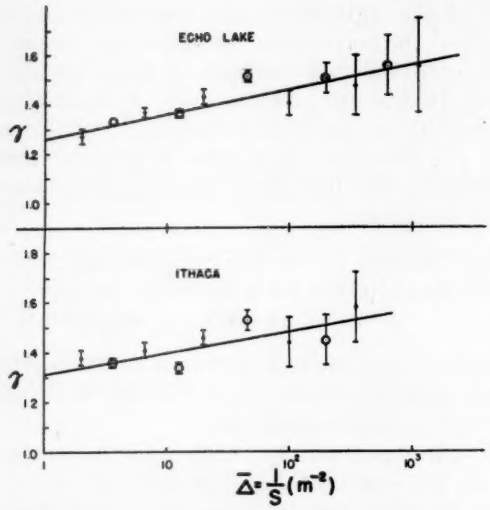

FIG. 3. γ *versus* mean density of the showers at Ithaca and Echo Lake.

Outside these limits, (7) are not applicable. For other ranges of densities, K varies, slightly increasing with Δ.

(4) The controversial point of the variation of γ with altitude is more complex than was thought before; while γ decreases with altitude for showers of density smaller than 10^3-10^4 m^{-2}, yet, if one can extrapolate our lines in Fig. 3, γ is increasing with height for bigger densities.

For showers recorded with counters of normal size it seems that γ decreases very slightly with altitude, qualitatively confirming the measurements of Auger and Daudin[2] and Maze and co-workers,[3] though the decrease observed by us is much smaller than the one they measured and the absolute values of K quite different. As for our previous results,[4] which showed an increase of γ with height, the value of γ obtained at sea level agrees very well with (7), but we probably overestimated the influence of the roof over the counters in the higher station; in fact the value of γ deduced there from the uncorrected measurements (1.45) is in excellent agreement with the present one. Our old values of K are instead not well in agreement with the present ones, even correcting them for the altitude differences. We consider the present figures more reliable. As for the showers observed by Williams[5] with ionization chambers, one has to expect γ's larger than ours, because the densities of the showers he recorded are generally bigger than ours, but even in the range of density where our measurements and his measurements overlap ($300<\Delta<1000$ m^{-2}), and the geometrical disposition of the chambers and of the counters is the same, his γ is larger. This may be in part due to the statistical errors, which are rather large in both measurements, but we think that something else contributes to the discrepancies. One has to remember that all data on the extensive showers taken in the past with ionization chambers were meaningless, because other phenomena (stars, local showers) strongly affected the measurements; all these data led to γ much bigger than the present ones. Maybe Williams did not eliminate completely the spurious phenomena which affected the previous measurements. Even the value of K found by Williams is bigger than ours, but this may be due, at least in part, to the increase of K with γ, as pointed out before.

(5) The comparison with the theoretical evaluations confirms what has been said before: the agreement is only qualitative, and we think this is due more than to defects in the cascade theory, to the inapplicability of such a scheme to the extensive showers, in which other processes, beside the multiplication of electrons and photons, take place.

The authors wish to thank Prof. K. Greisen for many helpful suggestions and discussions. They are grateful to the Research Corporation for a grant which covered part of the expenses of performing the experiments described above. The facilities of the Inter-University High Altitude Laboratory Association, and the help of Professors Cohn and Iona of Denver University were an invaluable aid in performing the experiment.

[2] P. Auger and J. Daudin, J. de phys. et rad. **6**, 233 (1945).
[3] R. Maze, A. Fréon, and P. Auger, Phys. Rev. **73**, 418 (1948).
[4] G. Cocconi, A. Loverdo, and V. Tongiorgi, Nuovo Cimento **2**, 14 (1944); Phys. Rev. **70**, 841 (1946).
[5] R. W. Williams, Phys. Rev. **74**, 1689 (1948).

Penetrating Particles in Extensive Cosmic-Ray Air Showers

G. Cocconi,* V. Cocconi Tongiorgi, and K. Greisen
Cornell University, Ithaca, New York

(Received December 6, 1948)

The number of penetrating particles in extensive air showers has been determined as a function of range of the particles and size of the showers at 3260-m elevation. A measurement with the same apparatus has been made at 260-m elevation, in order to show the altitude variation. It is found that the showers at 3260 m contain many photons and electrons which can be detected under absorbers up to 7-inches lead. The particles penetrating more than this thickness have a very small absorption coefficient in iron, and decrease in density slowly as they traverse the atmosphere. Hence they are thought to be primarily μ-mesons.

IMPROVED measurements have been made, during the summer of 1948, of the penetrating particles present in the extensive air showers at Echo Lake, Colorado (elevation 3260 m), and at Ithaca, N. Y. (elevation 260 m). These measurements, as well as similar measurements made in the past,[1-4] yield numbers for $R(t)$, which is an effective value for the fractional number of shower particles capable of penetrating a thickness t of absorber. It was our intention to improve the precision of determination of R, to study the dependence of R on the size of the showers, and to investigate the nature of the penetrating particles by studying their absorption properties; i.e., the dependence of R on t and on the altitude above sea level.

Three unshielded counter trays, A, B, and C, each of total area S, were disposed in a triangular arrangement in a horizontal plane, with six-meter separation between counter trays at Echo Lake, four-meter separation at Ithaca. Three other counter trays, M_1, M_2, and M_3, each of area S', were placed one above another within a large block of absorber, as shown in Fig. 1. The absorber contained 9 tons of lead plus 3 tons of iron. Simultaneous records were obtained of the coincidences ABC, $ABCM_1$, $ABCM_2$, and $ABCM_3$.[5] The ratio $ABCM_i/ABC$ essentially determines the value of R for the absorber thickness above tray M_i.

The pulses from counters A, B, C were at the same time used in another experiment, on the density spectrum of the electrons in the showers. That experiment is described in an accompanying article in this issue. Further details about the apparatus and precautions taken to eliminate errors are given in that article, and so are omitted here.

DEPENDENCE OF R ON SIZE OF SHOWERS

Showers of various mean particle-densities were selected by using different areas S for the unshielded counters. It is well known that the frequency of showers of density greater than Δ follows the empirical law

$$f(\Delta)=K\Delta^{-\gamma},$$

where γ is approximately 1.5 and varies slowly both with Δ and with altitude. Therefore the contribution from showers of density between Δ and $\Delta+d\Delta$ to the coincidence rate of three counters of area S is proportional to

$$g(\Delta)d\Delta=\Delta^{-(\gamma+1)}(1-e^{-S\Delta})^3d\Delta.$$

The contribution per logarithmic unit interval of Δ (i.e., $\Delta g(\Delta)$) is shown in Fig. 2 for $\gamma=1.5$. It is apparent that the choice of a given value of S selects showers that fall in a limited density range, from about $1/10S$ to $10/S$. The slow variation of γ is unimportant over the range of densities that contribute strongly to the coincidence rate. While the present experiment was in progress, careful measurements of γ were simultaneously being carried out by G. and V. Cocconi (see accompanying paper in this issue), so the correct value of γ could be chosen for each of the counter areas S.

In Table I, the data taken at Echo Lake with fixed absorber thicknesses but variable S are presented. Above M_1 the absorber t_1+t_2 was 7 inches of lead (plus 0.15 inch of iron and brass), which is 204 g/cm² or 35 radiation lengths. The experiments with variable absorber, discussed below, show that this is sufficient to exclude essentially all the electrons and photons of the showers. Between M_1 and M_2 was 8 inches of iron ($t_3=155$ g/cm²), while between M_2 and M_3 was another 8 inches of iron, t_4. The momentum losses for mesons of mass 10^8 ev/c² that can barely traverse these absorbers are 3.4, 5.8 and 8.3×10^8 ev/c.

The ratio R for particles capable of traversing the absorbers has been found under the assumption that it is a fixed quantity, independent of the size of the shower or the distance from the shower core.

* On leave from the University of Catania, Italy.

[1] G. Cocconi, A. Loverdo, and V. Tongiorgi, Phys. Rev. **70**, 852 (1946).

[2] D. Broadbent and L. Janossy, Proc. Roy. Soc. **A191**, 517 (1947); **A192**, 364 (1948).

[3] B. Chaudhuri, Nature **161**, 680 (1948).

[4] J. E. Treat and K. Greisen, Phys. Rev. **74**, 414 (1948).

[5] In part of the experiment, the rate $ABCM_2$ was not recorded.

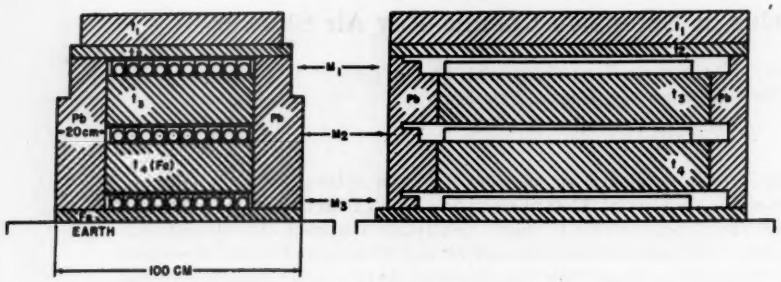

FIG. 1. Arrangement of shielded counters and absorbers.

Such an assumption seems necessary, for lack of any information on the production process or scattering of the penetrating particles in the showers. The values of R thus found are true average values only if the assumption is approximately correct; otherwise they are weighted averages, weighted according to the probabilities of detection of the showers. Under this assumption, the counting rates $ABCM$ and ABC are related by

$$\frac{ABCM}{ABC}=\frac{\int_0^\infty \Delta^{-(\gamma+1)}(1-e^{-S\Delta})^3(1-e^{-RS'\Delta})d\Delta}{\int_0^\infty \Delta^{-(\gamma+1)}(1-e^{-S\Delta})^3 d\Delta}.$$

This ratio has been plotted as a function of RS'/S for several values of γ in Fig. 3. The values of R deduced from the graph and from the experimental rates $ABCM$, ABC, are given in the last three columns of Table I. The area S' for all of the measurements was 5000 cm².

It may be noted that some sources of error have little or no effect in the above treatment of data. In fact, the data in Tables I and II have been corrected only for the small numbers of chance coincidences (the resolving time was 4 microseconds). The barometric correction has been omitted because it cancels out in the ratio $ABCM/ABC$. The inefficiency of counters A, B, and C, when these trays are composed of single counters, has no effect on the ratio. When the trays are composed of several counters (i.e., for the 1560-cm² area only), the inefficiency acts like a small reduction in the area S. The inefficiency of the trays M was very small (less than one percent), and acts as a reduction in the area S'; this, however, compensates almost exactly for the partial effectiveness of the spaces between the counters in the trays. A mixing circuit was employed so that the use of a large number of counters in parallel would not increase the inefficiency. The effective area of the trays M decreases with increasing inclination of the shower axis relative to the zenith. However, the area of the unshielded trays decreases similarly with inclination, and the ratio RS'/S, which determines the relative counting rates $ABCM/ABC$, is unaffected.

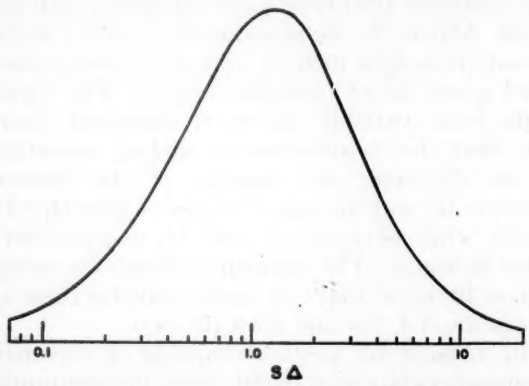

FIG. 2. Contribution to the threefold coincidence rate, made by showers of different densities, per logarithmic density interval.

The values of R_1, R_2, and R_3 in Table I indicate that the "penetrating particles" are really penetrating in character, and hence are (mostly, at least) not photons or electrons. The average ratio $R_1/R_2/R_3$ is 1.00/0.90/0.79. In this ratio the errors are smaller than one would conclude if one considered R_1, R_2, and R_3 as statistically independent, for in fact they are not so. The area of the trays was so large compared with the separation, that many of the particles crossing one of the trays crossed the other trays also.

The values of R_1 and R_3 from Table I are shown in the graph of Fig. 4, which is a logarithmic plot of R against reciprocal counter area. Since the mean electron density in the showers is proportional to $1/S$, the proportion of penetrating particles is observed to decrease as the electron density increases, going approximately as

$$\frac{\text{Pen. Part.}}{\text{Electrons}}\sim(\text{Electrons})^{-0.13}$$

or

$$\text{Pen. Part.}\sim(\text{Electrons})^{0.87}.$$

The explanation for this is probably as follows. When one selects higher densities, one selects, on the average, showers of higher primary energy. In these, the electrons are not as far beyond the maximum of the multiplication curve as in showers of lower primary energy; hence the number of electrons per unit primary energy is larger in the

TABLE I. Data for determination of R *vs.* mean density of showers at Echo Lake, elevation 3260 m. $t_1+t_2=204$ g/cm² Pb, $t_3=t_4=155$ g/cm² Fe. R_i is the fraction of the shower particles that can penetrate to the layer i of shielded counters.

Counter area S (cm²)	γ	Time (hours)	ABC	$ABCM_1$	$ABCM_2$	$ABCM_3$	$R_1\times100$	$R_2\times100$	$R_3\times100$
9	1.56	372.4	70	64	——	61	0.93±0.36	——	0.64±0.21
29	1.51	190.0	215	148	——	141	0.71±0.10	——	0.62±0.08
98	1.46	169.2	1187	602	——	537	1.08±0.07	——	0.87±0.05
500	1.39	38.5	2967	646	582	538	1.27±0.06	1.10±0.05	1.00±0.05
1560	1.34	30.6	11,520	1334	——	1076	1.56±0.05	——	1.20±0.04
1560	1.34	44.9	17,735	1888	1761	——	1.41±0.04	1.29±0.03	——

denser showers. The penetrating particles are not so strongly absorbed, so their transition curve is much more flat and they are more likely to be proportional in number to the primary energy. Hence the relative number of electrons should be greater in the denser showers.

In support of this hypothesis, Fig. 5 shows a graph of number of electrons, N, in showers at 15 radiation lengths depth, as a function of primary photon energy W_0. It is seen that over the range of N that contributes most to the counting rates (200 to 10^5, allowing for some multiplicity of the primary photons), the number of electrons is proportional to $W_0^{1.14}$. If the number of penetrating particles is proportional to W_0, we then have

$$\frac{\text{Pen. Part.}}{\text{Electrons}}\sim W_0^{-0.14}\sim(\text{Electrons})^{-0.12}.$$

The good agreement with the data of Fig. 4 lends support to the assumption that the number of penetrating particles in a shower is proportional to the primary energy.

DEPENDENCE OF R ON ABSORBER THICKNESS

In order to investigate the nature of the particles absorbed in less than 204 g/cm² lead, further data were taken at Echo Lake with constant area S (1560 cm²) but with different thicknesses and kinds of absorber in t_1 and t_3. These data, along with the deduced values of R, are given in Table II.

The results in Table II have been plotted in Fig. 6, with the abscissas equal to the momentum limits set by the absorbers for ordinary μ-mesons traveling in the vertical direction. Such a scale is similar to an ionization-loss scale for particles heavier than mesons also. It is immediately obvious from this graph that the particles that can penetrate the smaller absorbers (4 to 7 inches of lead, or 6 inches iron plus 2 to 5 inches lead) are not all mesons. Indeed, a large fraction consists of particles that are stopped much more effectively by lead than by iron. Such behavior suggests that they are high energy electrons and photons.

It is also obvious that beyond 8 inches of lead, or 8 inches iron plus 6 inches lead, the penetrating particles are *not* electrons or photons. In fact, the absorption is extremely small. The straight line drawn on the graph has a slope equal to 4×10^{-6} per g/cm² Fe, which is 3×10^{-4} relative to the intercept. In other words, if the absorption of this hard component is exponential, the mean free path is about 3600 g/cm² Fe, which is about 25 times the mean free path of high energy protons (or other heavy particles with strong nuclear interactions). The data of course do not permit the slope to be

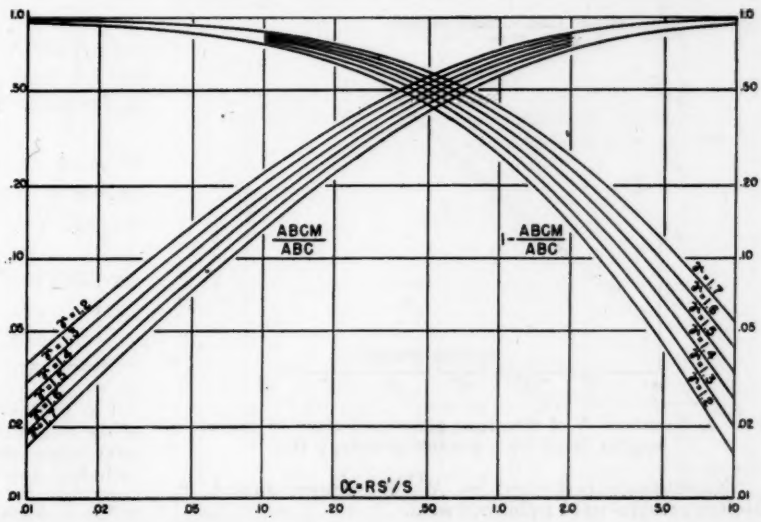

FIG. 3. $(ABCM/ABC)$ *versus* RS'/S for several values of γ.

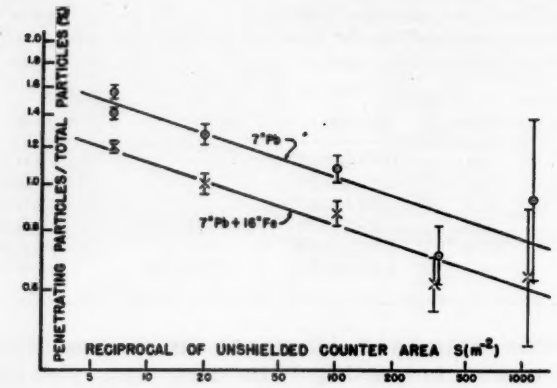

FIG. 4. *R versus* $1/S$, for penetrating particles capable of penetrating 7" Pb and 7" Pb+16" Fe.

determined with precision, but the above value can hardly be too low by as much as a factor two.

Therefore we think that the hard component of the showers is composed mainly of ordinary μ-mesons, rather than other types of heavy particles. This conclusion must be considered tentative, because the properties of the absorption curve for protons plus their secondaries are not known. A high energy proton has a relatively short mean free path for nuclear interaction, but in this act it produces further penetrating particles. These are presumably not μ-mesons, but again strongly interacting particles, that produce more nuclear interactions after short free paths. Such a process of multiplication should exhaust the primary energy rapidly, not giving an exponential absorption curve in the first two or three mean free paths (i.e., in our experiment), but yet giving a faster absorption than 3×10^{-4} per g/cm² Fe.

Pictures taken this summer with a cloud chamber under thick lead, triggered by air showers,[6] show the occasional presence of a heavy particle that produces a star, or a penetrating shower, or a local burst of cascade radiation. V. Cocconi Tongiorgi[7] has also demonstrated that heavy particles in the showers frequently produce neutrons. The heavy particles that do these things are not μ-mesons. The slow absorption in lead can be understood, however, if the strongly interacting particles are a minor fraction of the penetrating component in the showers near sea level, not more than about 25 percent.

In order to test the conclusion that the particles absorbed in less than 7 inches of lead are photons and electrons, the parts of R which were due to penetrating particles (as read from the straight line drawn in Fig. 6) have been subtracted from the values of R in Table II, and the differences have been plotted in Fig. 7 as a function of the total absorber thickness in radiation lengths (in the vertical direction). The points for iron-and-lead absorbers as well as those for the pure lead absorbers are seen to fall approximately on a single smooth curve. The slight discrepancies are in the right direction to be accounted for by the errors in the simplified cascade theory which predicts that all materials should be equivalent in radiation units. More specifically, the low energy photons have a much longer range (in radiation lengths) in lead than in iron; hence the counting rates are slightly greater under the lead absorbers than under the lead and iron.

It should be noted that all the data in Table II, taken with absorbers thin enough that some electrons and photons are included in R, were obtained with at least ten radiation units of lead directly above the counters (except for one point, which is enclosed in parentheses in the table and not plotted in the graphs of either Fig. 6 or Fig. 7). The layer of constant material above the counters ensures that the particles of low energy in the cascades always have the same spectrum. Without

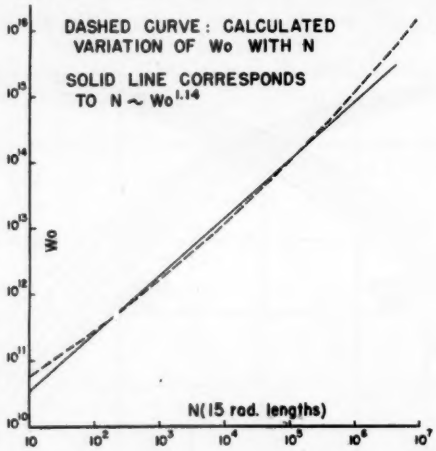

FIG. 5. Numbers N of electrons generated after 15 radiation lengths in air by a photon of energy Wo.

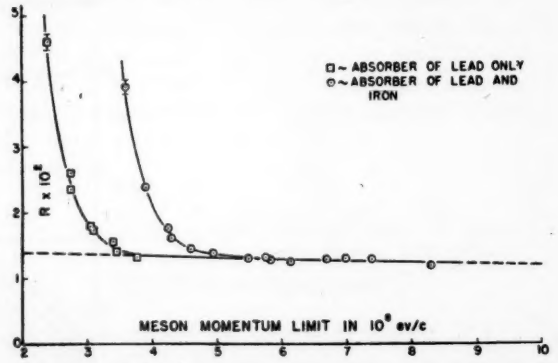

FIG. 6. *R versus* total absorber thickness, expressed in terms of the meson momentum limit. The points enclosed in squares refer to lead thicknesses from 4 to 8 inches. The least absorber including iron was 2 inches lead plus 6 inches iron.

[6] Experiments performed by W. W. Brown and A. S. McKay; results to be published soon.

[7] V. T. Cocconi, Phys. Rev. **74**, 226 (1948).

TABLE II. Data for absorption curve at Echo Lake. Areas = 1560 cm² (unshielded counters), 5000 cm² (shielded counters).

Absorbers (g/cm²)				Time	Counts recorded				Fraction of particles		
t_1	t_2	t_3	t_4	(hours)	ABC	$ABCM_1$	$ABCM_2$	$ABCM_3$	$R_1\times100$	$R_2\times100$	$R_3\times100$
57 Pb	60 Pb	60 Pb	155 Fe	23.6	8784	2279	1106	886	4.59±0.12	1.73±0.06	1.31±0.05
114 Fe	60 Pb	60 Pb	155 Fe	22.7	8465	1960	1008	847	3.91±0.11	1.62±0.06	1.30±0.05
86 Pb	60 Pb	60 Pb	155 Fe	44.9	17,735	2823	1888	1761	2.35±0.06	1.41±0.04	1.29±0.03
114 Fe	89 Pb	60 Pb	155 Fe	35.6	13,993	2256	1533	1404	2.39±0.06	1.46±0.04	1.31±0.04
86 Pb	60 Pb	41 Fe	155 Fe	47.0	18,445	3186	2349	1884	2.61±0.06	(1.76±0.04)	1.33±0.04
115 Pb	60 Pb	60 Pb	155 Fe	22.3	8631	1107	883	843	1.78±0.06	1.33±0.05	1.26±0.05
114 Fe	89 Pb	60 Pb	155 Fe	21.5	8063	1028	852	803	1.77±0.06	1.39±0.06	1.30±0.05
144 Pb	60 Pb	155 Fe	155 Fe	30.6	11,520	1334	——	1076	1.56±0.05	——	1.20±0.04

such a constant layer, absorbers of iron and lead would not be even approximately equivalent in radiation units for the cascade showers.

DEPENDENCE OF R ON ALTITUDE

The proportion of penetrating particles in air showers has also been determined at Ithaca, N. Y. (elevation 260 m), with the same apparatus as that used at Echo Lake. The separation between counters A, B, and C was 4 meters (corresponding to the 6-meter separation used at Echo Lake). The absorbers were the same as for the Echo Lake data of Table I: namely, $t_1+t_2=204$ g/cm² Pb, $t_3=t_4=155$ g/cm² Fe. The area of the unshielded counters was 1680 cm², and of the shielded counters was 5000 cm².

In 202.1 hours the following counts were recorded (corrected only for chance coincidences): ABC, 8863; $ABCM_1$, 1370; $ABCM_2$, 1251; $ABCM_3$, 1144. The value of γ appropriate to 1680-cm² area of the unshielded counters is 1.38. From these data we deduce for the relative number of penetrating particles

$$R_1\times100=2.60\pm0.09,$$
$$R_2\times100=2.31\pm0.08,$$
$$R_3\times100=2.06\pm0.07.$$

The values of R_1, R_2, and R_3 are found to be in the ratio 1.00/0.89/0.79, almost exactly the same as at Echo Lake under the same absorbers. But all three values of R are larger than at Echo Lake, which indicates that the density of the penetrating particles varies less than the density of the electrons as the showers cross the atmosphere.

Indeed, from interpolation between the data of Table I, one finds that the showers ABC recorded at Ithaca have the same frequency as the showers recorded at Echo Lake with counters A, B, C smaller in area by a factor 5.0. Hence the electron density in these showers decreases by an average factor 5.0 between Echo Lake and Ithaca. The relative density of penetrating particles, meanwhile, changes from 1.21 percent at Echo Lake to 2.60 percent at Ithaca (for particles that can traverse 7 inches Pb), or from 0.96 percent at Echo Lake to 2.06 percent at Ithaca (for particles that can traverse 7 inches Pb plus 16 inches Fe). The density of the penetrating particles in the showers, therefore, is reduced by a factor 2.33±0.1 between Echo Lake and Ithaca. This factor is found to be independent of the absorber thickness within the statistical errors (all absorbers in this comparison were thick enough to exclude practically all the photons and electrons).

These results exclude the possibility that most of the penetrating particles are locally produced in the absorbers, either by the photons in the showers or by strongly interacting heavy particles. If they were all locally produced, the number of penetrating particles should be proportional to the local intensity of the producing particles. The soft component of the showers decreases by an average factor 5.0, and the strongly interacting heavy particles must be reduced by a factor about 10 between Echo Lake and Ithaca. Both of these factors are much greater than the factor 2.3 measured for the penetrating particles.

The density-reduction factor 2.3 represents the combined effect of many possible processes: (*a*) further scattering in the air, (*b*) increase in spread due to previous angular divergence, (*c*) ionization loss, (*d*) nuclear interactions, (*e*) radioactive decay in the air, and (*f*) absorption, in the air, of the shower particles that may produce penetrating particles in the local absorbers—all of which processes tend to reduce the density—plus (*g*) further production of penetrating particles in the

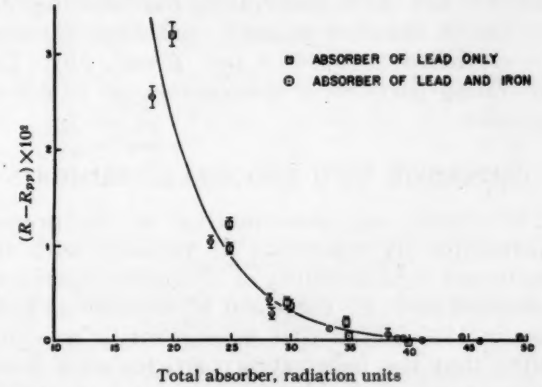

FIG. 7. The part of R not due to penetrating particles, plotted *versus* total absorber thickness, measured in radiation units.

TABLE III. Dependence of measurements on the separation of counters A, B, C. Area of unshielded counters = 1680 cm², that of shielded counters = 5000 cm². Effective value of $\gamma = 1.38$. $t_1 + t_2 = 204$ g/cm² Pb, $t_3 = t_4 = 155$ g/cm² Fe.

Mean separation of counters ABC	Time (hours)	ABC	$ABCM_1$	$ABCM_2$	$ABCM_3$	$R_1 \times 100$	$R_2 \times 100$	$R_3 \times 100$
1.3 m	206.4	11002	1588	1380	1312	2.38±0.07	1.99±0.06	1.87±0.06
4.5 m	202.1	8863	1370	1251	1144	2.60±0.09	2.31±0.08	2.06±0.07
15.0 m	231.8	8020	1313	1227	1197	2.81±0.09	2.57±0.09	2.48±0.09

air, which tends to increase the density. As pointed out above, the small net reduction factor indicates that local production is comparatively unimportant. Hence the decrease in amount of local production in the absorbers (process f) and the production in the air (process g) are small factors which approximately cancel each other and may therefore be neglected.

For the strongly interacting particles that produce penetrating showers (in general not associated with extensive showers), the reduction due to ionization loss and nuclear interactions, minus the creation in the air, is a factor 10 between Echo Lake and Ithaca (see accompanying article by G. Cocconi on penetrating showers). Hence it is inconceivable that the penetrating particles in extensive showers should be mostly of the strongly interacting type, such as high energy protons. For μ-mesons not associated with extensive showers, on the other hand, the reduction in number, arising from ionization loss and decay, minus the effect of local production, is a factor 1.74 between the two elevations. The increase in geometrical separation of the particles, caused by scattering and previous angular divergence, can easily account for a further density-reduction of $2.33/1.74 = 1.34$. Therefore the penetrating particles are probably μ-mesons, created in the air high above the apparatus.

The experimental results given above may be summarized as follows. The particles in the showers, capable of penetrating rather thick absorbers, consist (a) of electrons and photons, which are not fully absorbed until 40 radiation lengths of absorber, and (b) of penetrating particles that are very slowly absorbed in large thicknesses (absorption coefficient $\approx 3 \times 10^{-4}$ per g/cm² Fe). The penetrating particles in the showers are primarily μ-mesons.

COMPARISON WITH PREVIOUS EXPERIMENTS

The results and interpretation of the present experiments are somewhat at variance with the results and interpretation of a similar experiment performed by J. E. Treat and K. Greisen[4] at Echo Lake in 1947. From that experiment, it was concluded that the penetrating particles were about three percent of the shower particles (rather than about one percent), and were rather easily absorbed; moreover, that the penetrating particles varied in density even more rapidly than the electrons as the altitude was changed. The reason for the errors in these conclusions is now obvious: Treat and Greisen did not use quite enough lead above the counters to exclude all the electrons and photons. In their "Experiment A" the absorber was 14-cm thick; we see from the graph in Fig. 6 or 7 that under this thickness, about $\frac{1}{3}$ of the "penetrating" particles are photons or electrons. Their lead shielding was also not quite complete at the ends of the counters, so that perhaps as many as $\frac{1}{2}$ of their "penetrating" particles were soft component. When they changed the elevation, the number of high energy electrons and photons increased more rapidly than the number of low energy electrons. And when they increased the amount of absorber, the soft component was absorbed. Under their maximum absorber, 39 cm Pb, they found $R = (83 \pm 7)^{-1} = 1.20 \pm 0.10$ percent at Echo Lake, in excellent agreement with our present results.

From the experiments of Cocconi, Loverdo, and Tongiorgi,[1] one may deduce $R \times 100 = 2.2 \pm 0.2$ at 2200-m elevation under 16 cm Pb. We see now that this figure included some electrons as well as penetrating particles. Broadbent and Janossy,[2] at sea level, have found $R \times 100 = 2.0 \pm 0.5$ under very thick absorbers, with the result independent of the atomic number of the absorber. B. Chaudhuri,[3] also at sea level, has found $R \times 100 = 2.0 \pm 0.2$. The latter two results are in good agreement with those of the present experiment at sea level.

PLACE OF ORIGIN OF THE PENETRATING PARTICLES

The question has frequently been raised,[2, 8–11] whether the penetrating particles observed in extensive showers are created in the absorbers of the detecting apparatus, or arrive on the absorbers from the air. The information accumulated by now allows a fairly complete answer to this question. In the first place, production of penetrating particles in the lead plates of a cloud chamber has been seen[6] in association with air showers; hence, *some* of the penetrating particles observed under lead are locally produced. This implies that production

[8] G. Cocconi and C. Festa, Nuovo Cimento **3**, 293 (1946).
[9] D. Broadbent and L. Janossy, Proc. Roy. Soc. **A190**, 497 (1947).
[10] G. Salvini and G. Tagliaferri, Phys. Rev. **73**, 261 (1948).
[11] G. Cocconi and K. Greisen, Phys. Rev. **74**, 62 (1948).

can also occur in the air. Several experiments[8–10] have shown that the number of penetrating particles observed is independent of the atomic number of the absorber. Hence, either the particles are mostly *not* locally produced, or the amount of production is independent of atomic number. Finally, we observe that the penetrating particles have very small average absorption coefficients in lead and iron, and increase in number slowly with elevation. Therefore the particles can be produced in air, even at a great height above the apparatus, and still be observed. The number produced in the air is in general much greater than the number produced locally, because the weight of air above the apparatus is greater than the weight of absorber, and the average intensity of the producing agents is greater in the air.

The penetrating particles produced in the air, however, are separated from each other because of their initial angular divergence and their scattering, so they are only rarely found close together. If one designs a counter arrangement that exerts a strong bias in favor of close-packed groups of penetrating particles, one may record most frequently those groups of penetrating particles that are locally produced, even though these are a small fraction of all the penetrating particles in the showers. If, however, one uses a single shielded counter or a group of widely separated counters, one will detect most frequently the penetrating particles that were produced in the air above the apparatus. This explanation accounts fairly well for the differences among the experimental results in the references given above.

APPENDIX I

Dependence of the Measured Value of R on the Separation of Counters A, B, and C

The dependence of R on counter separation has been investigated experimentally at Ithaca, by repeating the measurement with different distances between the counters A, B, C. The big absorber surrounding the counters M was always located a few meters below the plane of counters A, B, C, under a point near the center of the triangle formed by those counters. The data (corrected for chance coincidences) are given in Table III, and the ratios $ABCM/ABC$ have been plotted in Fig. 8 *versus* the mean separation of counters A, B, and C. The three curves correspond to the same three absorber thicknesses as were used to obtain the data at Echo Lake, given in Table I and Fig. 4. Figure 8 also shows, on a different scale, the variation of the coincidence rate ABC with counter separation.

The coincidence rate ABC is observed to be 21 percent greater at 1.3 meters, and 21 percent less at 15 meters, than the rate with 4.5-meter separation. The decrease of ABC with separation is due to elimination of the small showers striking very nearby, which have sufficient density to discharge the counters only over a small area. The magnitude of the effect would indicate that about $\frac{1}{3}$ of the showers that discharge the counters having 1.3-meter separation strike with their cores within about 10 meters of the counters.

The ratios $ABCM/ABC$ do not change by such a large percentage, but nevertheless show a significant increase with distance between the counters. From the extrapolated values of the ratio at zero counter separation, we obtain the following values of R:

$$R_1\times 100=2.28,$$
$$R_2\times 100=1.93,$$
$$R_3\times 100=1.70.$$

These are less than the values found at 4.5-meter separation by about 15 percent. Presumably a similar difference would be found at Echo Lake between zero and 6-meters counter separation.

In computing the above values of R and the values in Table III, however, we have assumed the effective value of the exponent γ in the density spectrum to be constant at the value (1.38) measured with 4-meter counter separation. Recent data by Loverdo and Daudin[12] and by R. W. Williams[13] indicate that γ increases with counter separation. This implies that a more correct evaluation of R would show an even stronger increase with counter separation than is indicated above.

One may conclude that the following assumptions, used in our evaluation of R, are not accurate: (1) that the showers have the same density at each of the counters (this is wrong for the large fraction of showers that strike nearby), (2) that R is independent of shower size, and (3) that R is independent of distance from the shower core.

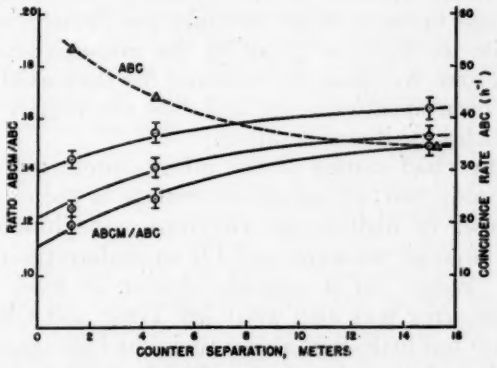

FIG. 8. ($ABCM/ABC$) and ABC *versus* separation of the unshielded counters ABC.

[12] A. Loverdo and J. Daudin, J. de phys. et rad. 9, 134 (1948).

[13] Robert W. Williams, Phys. Rev. 74, 1689 (1948). We are grateful to the author for communicating his data to us before publication.

It seems unlikely that the error in the assumption of uniform density could have produced an effect as large as that which was found. The weak dependence of R on shower size has been discussed above (Fig. 4). Since R decreases with shower size, and the average shower size increases with counter separation, this effect would make R decrease with separation of counters A, B, C. That would be opposite to the observed variation of R. Therefore it seems probable that R increases rather strongly with distance from the shower core, because the average distance to the core of the showers increases with counter separation. In other words, it seems likely that the mesons are not concentrated as strongly near the core of a shower as are the electrons.

It should not be concluded that measurements of R made with extremely small counter separation are more accurate than measurements made with several meters separation. Indeed, if counters A, B, C are placed too close to each other, they will be sensitive not only to extensive showers, but to small local showers and stars as well. Rather, it must be recognized that any values of the relative number of penetrating particles, measured as in the present experiments, are effective values, averaged over a wide range of shower sizes and distances from the shower core. R is not a constant, but in principle should be measured as a function of these parameters.

APPENDIX II

On the Existence of λ-mesons

It has been suggested[14] that the particles of the extensive showers which are absorbed in thicknesses between 3 and 7 inches of lead are too penetrating to be electrons and too soft to be μ-mesons, but must represent another particle, the λ-meson, of mass between 3 and 10 times the electron mass. While we have no proof of the non-existence of λ-mesons, we think the evidence for their existence has been misinterpreted and does not require new particles for its explanation.

The chief causes of the misinterpretation were probably two: (1) an underestimate of the relative number of high-energy electrons and photons in the large air showers, and (2) an underestimate of the "range" of a cascade shower in lead. The latter error was also what led Treat and Greisen to use too little lead above their shielded counters.

The relative abundance of high-energy particles in the extensive showers is much greater than in the smaller showers which constitute the bulk of the soft component in the atmosphere. In fact, the total soft component in the atmosphere is known to have an energy spectrum (at high energies) that goes approximately as dE/E^3. The extensive showers, on the other hand, are mostly observed only slightly beyond their maximum development. The energy spectrum under these conditions goes about as dE/E^{s+1} with $s+1\approx 2.1$ or 2.2. The relative abundance of particles above 10^{10} ev therefore is greater by a factor of order 10^2 in the extensive showers, as compared with the soft component observed independently of extensive showers.

Furthermore, the "range" of a cascade in lead, initiated by a photon or electron, is a concept almost entirely without meaning in experiments where the cascades are detected by single counters under the lead. This is because of the large number of low-energy photons produced, some of which have a mean free path greater than 4 radiation units in lead. The low-energy photons do not contribute much to the development of the cascade, but may produce a pulse in a G-M-counter at a depth far beyond what is normally considered the range of the shower. This effect is considered in an approximate quantitative calculation by Greisen in an accompanying article. The result is that at large depths, the probability of detecting a cascade particle is a rather slowly increasing (rather than abruptly increasing) function of the primary energy. This increase is counterbalanced by the relative frequency of shower particles striking the lead, which decreases with energy. The counts recorded at large depths, it is found, are mostly due to rather low-energy incident particles, whose cascades have died out but are survived by some low-energy photons. The counting rate is much greater than one would predict by ignoring the low-energy photons and considering that each cascade had a fixed range.

According to Greisen, if one detects the extensive air showers near their maximum, the number of particles (photons and electrons) detected under 6-inches Pb (30 radiation lengths), as compared with the total number of electrons in the shower, should be about 2×10^{-3}. This is in approximate agreement with the experimental value of the part of R due to soft component, as seen in Fig. 7. Hence it is not necessary to assume the existence of a new type of particle slightly more penetrating than electrons.

Perfect agreement between the calculations and the experimental values of the part of R due to soft component should not be expected, not only because of the approximations in the calculation, but because of the experimental method of determining R, which assumes R to be a fixed quantity at all points in the shower. Actually, the density of high-energy photons and electrons, relative to the low-energy

[14] P. Auger, J. Daudin, A. Fréon, and R. Maze, Comptes Rendus 226, 169 (1948); 226, 569 (1948).

electrons in the air showers, changes strongly with distance from the shower core. Hence the experimental numbers of high-energy cascade particles are strongly weighted averages and should be considered only approximate in absolute value.

The authors are grateful to the Research Corporation for a grant which covered the expense of performing the experiment described above. The cost of constructing the apparatus was provided through a Navy contract. The facilities of the Inter-University High Altitude Laboratories, and the help of Professors Cohn and Iona of Denver University, were an invaluable aid in performing the experiment. The authors thank Mr. G. Branch for assistance in the measurements made in Ithaca.

PHYSICAL REVIEW VOLUME 75, NUMBER 7 APRIL 1, 1949

Range of Cascade Showers in Lead

K. GREISEN
Cornell University, Ithaca, New York
(Received December 6, 1948)

A calculation has been made of the probability of a cascade particle being detected under large thicknesses of lead, taking into account the effect of the low energy photons produced in the lead. The low energy photons increase the probability of detection very greatly, and make the concept of "range" of a cascade shower in lead very indeterminate. The results have been applied to the case of large air showers, where general agreement is found between the calculated and experimental counting rates under large thicknesses.

IN this paper, an attempt is made to calculate the expected counting rate in a G-M counter under a large thickness of lead, when a known spectrum of photons and electrons is incident on the lead. The solution is of importance in the interpretation of many cosmic-ray experiments, and may be useful in work with high energy synchrotron beams.

If we express the incident spectrum $f(W)$ as the number of particles per logarithmic interval of energy W, the counting rate C is given by

$$C(T)=\int_0^\infty f(W)P(W,T)d(\log W) \qquad (1)$$

where $P(W, T)$ is the probability of obtaining a count under T radiation lengths of lead when a particle of energy W strikes the lead. Thus the problem is reduced to a computation of $P(W, T)$.

In this paper, we consider only large values of T, greater than about 20 radiation lengths (4 inches of Pb); and the probabilities P have been evaluated only for the case of photons striking the lead. Indeed, for energies W large compared with the critical energy of lead, the result does not depend strongly on whether the incident particle is a positron, electron or photon: while if W is less than the critical energy, the probabilities P are large only for incident photons. Also, the number of low energy photons is large compared with the number of low energy electrons, both in cosmic rays and in a beam emerging from a synchrotron.

Solutions have already been computed, according to the cascade theory, for the function $\pi(W, O, T)$, which is the average number of electrons above zero energy at a depth T in a cascade initiated by a photon of energy W. In first approximation, then, our solution for P may be written

$$P_0=1-e^{-\pi}. \qquad (2)$$

This formula assumes a Poisson form for the fluctuations in the number of shower particles, which is admittedly an underestimate of the fluctuations in the case $\pi\gg1$. But in this case P is large anyway, and the error is not serious. For $\pi<1$, the physical explanation for the long tail of the shower curve is that one of the photons may survive beyond the depth where the rest of the shower is practically exhausted, and release an electron in the neighborhood of T. This accounts for the shape of the tail, which is approximately $\pi\sim e^{-\sigma T}$, σ being the nearly constant absorption coefficient of high energy photons. In this case, which is the one of importance in the present calculations, Eq. (2) represents the fluctuations correctly.

Our problem would be completely solved by Eqs. (1) and (2) if the quantity π had been completely and correctly evaluated. This has not been done, however, for an arbitrary depth T in the shower, but only for the thickness corresponding to the maximum, or integrated over the shower length. The solutions which have been given for arbitrary T have taken the collision loss of electrons into account, but have ignored the variation of the absorption coefficient of the photons with their energy. This simplification is not serious for materials of low atomic number, in which the absorption coefficient is never much less than its asymptotic value. It is very bad, however, at large depths

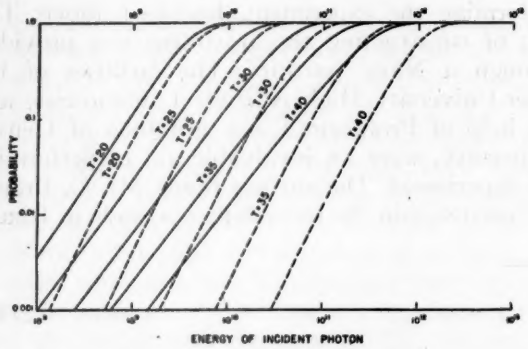

FIG. 1. Probability of detecting an incident photon by a G-M counter under various thicknesses of lead, measured in radiation units (5 rad. units = 1 inch). Dashed curves are calculated by ignoring the low energy photons produced. Solid curves include effect of low energy photons.

in materials of high atomic number like lead, in which low energy photons have a very long mean free path. But this is just the material which is most frequently used in shielding against electronic radiation.

For lead, we take Eq. (2) for P_0 as representing the contribution to P from all components of the shower except the low energy photons. The function π, calculated by Snyder and Serber, is quoted from the survey article by Rossi and Greisen,[1] whose terminology we follow. π is expressed by two equations, with a parameter s:

$$\pi(W, O, T)=\frac{1}{(2\pi s)^{\frac{1}{2}}}\frac{M\cdot K}{[\lambda_1''T+(1/2s^2)]^{\frac{1}{2}}}\left(\frac{W}{\epsilon}\right)^{s}e^{\lambda_1 t}$$
$$\log(W/\epsilon)=(1/2s)-\lambda_1'T. \qquad (3)$$

The probabilities P_0 calculated with this function are shown by the dashed curves in Fig. 1.

As low energy photons in lead, we consider the group between 1.2 and 7 Mev, which have an approximately constant absorption coefficient of about 0.23 per radiation length (see Fig. 13a, reference 1). The precise width of the group is not important, since it will enter only logarithmically in the result. Photons of energy below 1.2 Mev have a rapidly increasing absorption coefficient, and a decreasing probability of detection even if they reach the counters, so the low energy cut-off is rather well determined. Photons of energy above 7 Mev have a rapidly increasing absorption coefficient also, and moreover, their effects are already at least partially included in the probability P_0. Between 1.2 and 7 Mev, the absorption coefficient is nearly constant; the number of photons is distributed as dW/W and the efficiency of detection is proportional to W; hence all parts of the interval are about equally effective. For this group, we approximate the absorption coefficient as being exactly constant (0.23), and the efficiency of detection as constant also at 0.020. The latter figure assumes copper or brass counter walls, since the low energy photons are detected mainly by producing Compton electrons in the walls of the counters. The value of the efficiency is taken from the work of G-A. Renard,[2] and is actually the efficiency for photons of 3 Mev.

In good approximation, the absorption of a low energy gamma-ray simply removes it from the shower, and does not lead to further production of photons in the same energy interval because the electrons produced are below the critical energy and are quickly stopped by ionization. In fair approximation, the probability of production of a low energy photon of energy W to $W+dW$ is dW/W per radiation length per electron of energy above 7 Mev (the critical energy in Pb), and zero for electrons of lower energy. Hence, the photons between 1.2 and 7 Mev, produced in dt at depth t of a cascade, that survive to depth T are

$$dN_\gamma=\log(7/1.2)e^{-.23(T-t)}\pi(W, \epsilon, t)dt,$$

and the total number of low energy photons that reach T is

$$N_\gamma(W, T)=1.8e^{-.23T}\int_0^T e^{.23t}\pi(W, \epsilon, t)dt.$$

We consider only values of T far beyond the maximum of the cascade shower, therefore the upper limit of the integral can be taken as infinite, and the integral is then the Laplace transform of π with parameter $\lambda=-0.23$,

$$N_\gamma(W, T)=1.8e^{-.23T}\mathfrak{L}_\pi(W, \epsilon, -0.23). \qquad (4)$$

The Laplace transform has also been given in reference 1, calculated with consideration of the ionization loss, under approximations that are good for energies above ϵ. The parametric equations are

$$\mathfrak{L}_\pi(W, \epsilon, -.23)=-\frac{1}{s}\frac{B}{(\lambda_1-\lambda_2)\lambda_1'}\left(\frac{W}{\rho_1\epsilon}\right)^{s}\cdot$$
$$\lambda_1(s)=-.23 \qquad (5)$$

Insertion of the numerical values of the constants yields

$$N_\gamma(W, T)=1.0e^{-.23T}(W/12)^{1.29} \qquad (6)$$

with W expressed in Mev.

The probability of a counter being discharged by one of the N_γ photons is

$$P_\gamma=1-e^{-.02N\gamma}, \qquad (7)$$

and the total probability that a counter be discharged when a photon of energy W strikes the lead is

$$P=P_0+(1-P_0)P_\gamma. \qquad (8)$$

[1] B. Rossi and K. Greisen, Rev. Mod. Phys. **13**, 240 (1941).

[2] G-A. Renard, J. de phys. et rad. 9, 212 (1948).

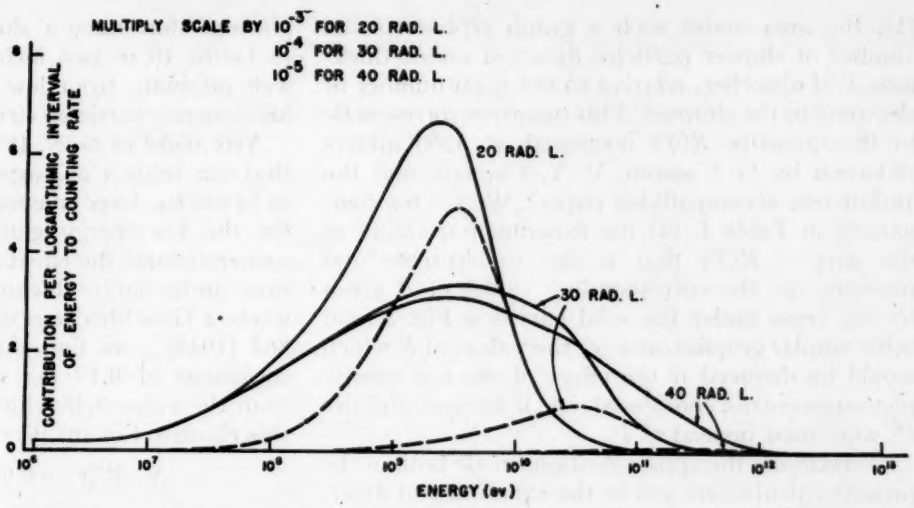
MULTIPLY SCALE BY 10^{-3} FOR 20 RAD. L.
10^{-4} FOR 30 RAD. L.
10^{-5} FOR 40 RAD. L.
CONTRIBUTION PER LOGARITHMIC INTERVAL OF ENERGY TO COUNTING RATE
20 RAD. L.
30 RAD. L.
40 RAD. L.
ENERGY (ev)

FIG. 2. Contribution to counting rate under various thicknesses of lead made by incident photons and electrons of various energies in an extensive air shower of primary energy 5×10^{13} ev, at a depth of 17 radiation lengths. Dashed curves ignore effect of low energy photons generated in the lead. Solid curves include effect of low energy photons.

In Fig. 1, P has been plotted as a function of W for $T=20$, 25, 30, 35 and 40 radiation lengths (4, 5, 6, 7 and 8 inches Pb). The values of P may be contrasted with the values of P_0, which appear as dashed curves on the same graph. The difference is not strong for a lead thickness of 4 inches, but increases with thickness and is very great at 8 inches. The probability of recording an incident photon of moderate energy (say 2.10^9 ev) is observed to decrease much more slowly with T than would be predicted if the low energy photons were ignored.

These results have been applied in the case of the extensive showers observed at 3260 meters elevation with three or four unshielded counters of 1500 cm² area in coincidence. Most of the showers recorded are slightly beyond their maximum development, considering *all* the electrons in the shower; i.e., $s\approx1.2$ in the function $\pi(E_0, O, t)$ describing the shower in the air. Most of the showers recorded probably originate about 17 radiation lengths (610 g/cm²) above the apparatus. By making use of the formulas in reference 1, we find therefore that a typical initiating energy for the recorded air showers is 5.10^{13} ev. For the spectrum of the air showers we have, therefore, computed the spectrum of photons and electrons at 17 radiation lengths depth, in a shower of 5.10^{13} ev primary energy.* Down to energies of about 2.10^8, the formulas in reference 1 have been used for deducing the spectrum. Below 2.10^8, the spectrum calculated by Richards and Nordheim[3] has been used. This should be accurate, because the shape of the low energy end of the shower spectrum does not change greatly with depth near the maximum of the shower.

The spectrum has been expressed as the number of particles (photons and electrons) per logarithmic interval of energy, relative to the total number of electrons in the shower at the same depth. The total number of electrons, for the typical shower assumed above, is 3.5×10^4. When the spectrum is expressed in this way, it is rather insensitive to the precise value assumed for the typical primary energy.

If the spectrum of the shower particles is multiplied by the probability curves of Fig. 1, graphs like those shown in Fig. 2 result.** Following Eq.

TABLE I. Comparison of experimental and calculated values of the part of R due to soft component in extensive showers. $R(T)$ is the number of particles detected under thickness T of lead, relative to the total number of electrons in the showers.

Lead thickness (inches)	Experimental value of R	Calculated value considering low energy photons	Calculated value ignoring low energy photons
	$10^{-3}\times$	$10^{-3}\times$	$10^{-3}\times$
4	31–33	25.0	14.0
5	9–13	6.1	2.2
6	3.0–4.5	2.1	0.30
7	0.5–2.0	0.65	0.036
8	0.0–0.5	0.21	0.0036

* Occasionally, the "normal spectrum" or spectrum at the maximum of a shower has been treated. It should be noted that no shower ever has the normal spectrum at any fixed depth, because the depth of the maximum is different for different energies of the secondary particles. The "normal spectrum" of a shower is of the form dW/W^{s+1} with constant s. The actual spectrum of a shower at a fixed depth is of the same form, except that s is not constant; instead, s increases logarithmically with W.

[3] J. A. Richards, Jr. and L. W. Nordheim, Phys. Rev. **74**, 1106 (1948).

** Below 10^8 ev, the Laplace transforms used to compute P were not calculable. For energies from 1.2 to 7 Mev, we ignored the electrons striking the lead and considered that the photons were equivalent to photons of the same energy generated in the lead at depth $t=0$. Only the exponential absorption, $\exp(-0.23T)$, and the efficiency of detection by the counters had to be considered for these photons. Between 7 Mev and 100 Mev, we joined the two parts of the curves smoothly. The area under the curves below 10^8 ev was small compared with the total area, hence slight errors in the smooth joining of the curves have a negligible effect. The contribution below 1.2 Mev goes very rapidly to zero because of the increase in absorption coefficient of the gamma-rays.

(1), the area under such a graph represents the number of shower particles detected under thickness T of absorber, relative to the total number of electrons in the showers. This quantity corresponds to the quantity $R(T)$ measured at 3260 meters elevation by G. Cocconi, V. T. Cocconi, and the author (see accompanying paper). We list for comparison in Table I, (a) the experimental values of the part of $R(T)$ that is due to electrons and photons, (b) the corresponding values of R given by the areas under the solid curves in Fig. 2 (and other similar graphs), and (c) the values of R which would be deduced if the effect of the low energy photons were not considered; i.e., if the probabilities P_0 were used instead of P.

Considering the approximations made both in the present calculations and in the experimental determination of the part of R due to soft component, the agreement between (a) and (b) in Table I is very good. If the low energy photons were not considered, however, it would seem that some of the shower particles were much too penetrating to be photons and electrons. Taking into account the effect of the low energy photons removes the necessity for imagining the existence of new particles.

It is apparent from Fig. 2 that when one increases the absorber thickness beyond about 5 or 6 inches (25 or 30 radiation lengths), one does not detect incident cascade particles of higher average energy. Indeed, beyond 6 inches of lead, practically the only cascade particles detected are the low energy photons that have a slow exponential absorption (a factor 10 in two inches Pb), and may equally well originate from low energy particles as from high energy particles striking the lead.

Note added in proof: It has been pointed out to us that our neglect of post-Compton photons has led us to use too *large* an effective absorption coefficient for the low-energy gamma-rays. Thus we have *underestimated* the effect of the low-energy gamma-rays under large thicknesses of lead. From the work of Hirschfelder *et al.* [Phys. Rev. **73**, 852 and 863 (1948)], we find that an effective absorption coefficient of 0.19 per radiation length is better than the value 0.23 which we have used. Applying this change, Eq. (6) becomes

$$N_\gamma(W,T)=0.9e^{-.19T}(W/12)^{1.23},$$

from which the corrected values of P_γ and P (Eq. (7) and (8)) may be calculated.

The qualitative conclusions in the above article are not affected by this change. Applying it to the air showers, the numbers in column 3 of Table I become $10^{-3}\times 31.5$, 11.0, 4.2, 1.7 and 0.68 for the calculated values of R taking into account the low-energy photons. The agreement with the experimental values is even improved by the present correction. However, such excellent agreement must be regarded as somewhat fortuitous, because the method of calculation is such that the results are only expected to be accurate within a factor of about 2.

PHYSICAL REVIEW VOLUME 75, NUMBER 7 APRIL 1, 1949

Some Properties of the Cosmic-Ray Ionizing Particles That Generate Penetrating Showers

G. Cocconi*
Laboratory of Nuclear Studies, Cornell University, Ithaca, New York
(Received December 6, 1948)

The mean free path of the ionizing particles that produce penetrating showers has been measured in various materials at 260 and 3260 m above sea level. It has been found that in both places the mean free path is much larger in Pb than in C, and that it increases with the thickness of the absorbers. Possible interpretations are discussed.

THE experiments described below have been performed in order to study the total cross section in different materials of the ionizing particles of the cosmic radiation which produce penetrating showers. The information thus far acquired concerning such phenomena seems to indicate that the shower-producing particles are likely protons and that penetrating showers are more frequently produced in materials with low atomic number.[1]

EXPERIMENTAL APPARATUS AND RESULTS

The apparatus used is drawn in Fig. 1. The G-M counters were of all-metal type, filled with alcohol-argon mixture, $1''\times 16''$ effective surface, and brass walls 0.5 mm thick. The large surface A, $16''\times 20''$ in area, was realized with 20 counters connected in parallel through the crystal diode mixing circuit described in another paper in this issue.[2] Counters B, C, and D constitute three other groups of counters, each group consisting of three counters

* On leave from the University of Catania, Italy.

[1] G. Cocconi and K. Greisen, Phys. Rev. **74**, 62 (1948); H. A. Meyer, G. Schwachheim, and A. Wataghin, Phys. Rev. **74**, 846 (1948).

[2] G. Cocconi and V. Cocconi Tongiorgi, Phys. Rev. **75**, 1058 (1949).

TABLE I. Results of measurements.

1 $\Sigma+\Sigma'$ (g/cm²)	2 P showers (h⁻¹) $A+B+C+D+1E$	3 (h⁻¹) $A+B+C+D+2E$	4 (h⁻¹) $A+B+C+D+3E$	5 $\frac{A+B+C+D+2E}{A+B+C+D+1E}$	6 $\frac{A+B+C+D+3E}{A+B+C+D+1E}$
Echo Lake					
0+0=0	9.90±0.24	2.60	4.67	0.26	0.47
115+0=115 Pb	4.95±0.24	1.61	6.94	0.32	1.40
284+0=284 Pb	2.31±0.15	0.74	5.52	0.32	2.40
284+116=460 Pb	1.32±0.10	0.595	5.25	0.45	4.00
284+321=605 Pb	0.892±0.07	0.455	4.68	0.51	5.25
200+0=200 Fe	2.72±0.15	0.68	6.50	0.25	2.40
200+200=400 Fe	1.18±0.09	0.48	5.38	0.40	4.55
46+0=46 C	6.41±0.26	1.91	8.07	0.30	1.26
46+51=97 C	3.85±0.18	1.65	10.08	0.43	2.80
Ithaca					
0+0=0	1.04±0.045	0.26	0.51	0.25	0.49
30+0=30 Pb	0.92±0.09	0.84	0.602	0.91	0.66
147+0=147 Pb	0.66±0.06	0.166	0.753	0.25	1.14
250+0=250 Pb	0.47±0.045	0.145	0.71	0.31	1.51
250+176=426 Pb	0.32±0.04	0.09	0.54	0.28	1.69
46+0=46 C	0.708±0.04	0.235	0.685	0.33	0.97
46+64=110 C	0.52±0.03	0.213	0.925	0.41	1.78

in parallel. Coincidences $A+B+C+D$ were recorded with a resolving time of 1.2 μsec. (blocking oscillators and crystal diode coincidences) and were presumably due to penetrating showers. In fact, the lead P all around the counters B, C, and D was 6″ thick on all sides and above the counters, and each counter of the trays B, C, D was separated from the neighbors by 1″ of Pb.

The showers can be generated either in the lead P, or in the absorbers Σ, Σ', or in the roof of the room in which the experiments were performed (5 g cm^{-2} in all stations), or in the atmosphere. In order to select only the showers generated in the lead P, 20 counters were placed in E, and their pulses were fed into a circuit able to discriminate how many counters E were simultaneously discharged, within 10 μsec. Actually this discriminating circuit was able to select coincidences $A+B+C+D$ accompanied by the discharge of either one, or two, or more than two of the counters E. We consider the coincidences $A+B+C+D$ accompanied by the discharge of only *one* of counter E (coincidences $A+B+C+D+1E$) as due to penetrating showers generated by a single ionizing particle in the lead P (showers P).

Of course, the distance of Σ from the counters was chosen large enough so that any shower generated in Σ would have to strike more than one of the counters E in order to strike B, C, and D. Chance coincidences were always negligible. The rate of the P showers had been measured, varying the amount and the nature of the absorbers Σ and Σ' both at Ithaca (260 m above sea level, mean pressure 1007 g cm^{-2}) and at Echo Lake (3260 m, 708 g cm^{-2}). The results are reported in Table I. Column 2 refers to P showers (coinc. $A+B+C+D+1E$), column 3 to showers which discharged two of the counters E (coinc. $A+B+C+D+2E$), and column 4 to showers which discharged three or more counters E (coinc. $A+B+C+D+3E$). The frequencies of P showers *versus* the thickness of absorbers $\Sigma+\Sigma'$ are plotted on a logarithmic scale in Figs. 2 and 3. From Fig. 2 one observes:

(a) At 3260 m, the initial slopes of the absorption curves correspond to the following mean free path of the shower-producing particles for absorption and production of penetrating showers:

$$\begin{aligned} &\text{In Pb} && \lambda_{Pb}=160\pm15 \text{ g cm}^{-2},\\ &\text{in Fe} && \lambda_{Fe}=135\pm15 \text{ g cm}^{-2},\\ &\text{in C} && \lambda_{C}=100\pm5 \text{ g cm}^{-2},\end{aligned} \qquad (1)$$

$$\lambda_{Pb}/\lambda_{C}= \quad 1.60\pm0.17.$$

(b) The absorption curves for Pb and Fe, which are continued up to large thicknesses, are not purely exponential; the mean free paths increase with the thickness, so that under about 500 g cm^{-2} of absorber they become:

$$\begin{aligned} &\text{In Pb} && \lambda_{Pb}=380\pm60 \text{ g cm}^{-2},\\ &\text{in Fe} && \lambda_{Fe}=310\pm60 \text{ g cm}^{-2}.\end{aligned} \qquad (2)$$

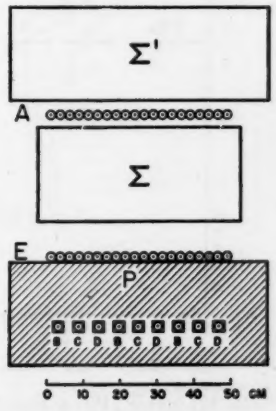

FIG. 1. Arrangement of counters and absorbers.

From Fig. 3 one finds:

(c) At 260 m above sea level the mean free path of the shower-producing particles are:

$$\begin{array}{ll} \text{In Pb} & \lambda_{Pb}=310\pm30 \text{ g cm}^{-2}, \\ \text{in C} & \lambda_C=140\pm20 \text{ g cm}^{-2}, \end{array} \qquad (3)$$

$$\lambda_{Pb}/\lambda_C=2.20\pm0.45.$$

(d) From the ratio of the intensity of the P showers observed at Echo Lake and at Ithaca with lead absorber, one deduces, assuming in air an exponential decrease:

$$\begin{array}{lll} \text{With} & 0 \text{ g cm}^{-2} & \lambda_a=133\pm7 \text{ g cm}^{-2}, \\ \text{with} & 200 \text{ g cm}^{-2} & \lambda_a=169\pm10 \text{ g cm}^{-2}, \\ \text{with} & 400 \text{ g cm}^{-2} & \lambda_a=191\pm15 \text{ g cm}^{-2}. \end{array} \qquad (4)$$

Before discussing the meaning of these results, we wish to point out that no other phenomena, except penetrating showers, seem to be recorded by our apparatus. It might be supposed that an appreciable percentage of knock-on electrons, by the meson component, notwithstanding the complete screenings of the counters with lead, may discharge the counters A, B, C, D, and that their number, decreasing with the thickness of the absorber less than the number of the penetrating showers, may vary the slope of the absorption curve and increase, at the greater thickness, the apparent free path of the radiation which produces penetrating showers. If this happened, one would have to expect, increasing Σ, a decrease of the ratio $(A+B+C+D+2E/A+B+C+D+1E)$ as well as of the ratio $(A+B+C+D+3E/A+B+C+D+1E)$, because no electron shower able to discharge A, B, and C can be produced in the absorber Σ. From columns 5 and 6 of the table, one observes, instead, the opposite behavior, which indicates, on the other hand, that the number of showers created in Σ increases with its thickness. Furthermore, if such an effect existed, the difference between λ_{Pb} and λ_C would decrease at sea level, and here too we observed the opposite.

Another strong argument in favor of the reliability of our results is the following. Consider the absorption curves in Pb; the frequency of the P showers at Echo Lake with $\sim$550 g cm^{-2} (see Fig. 2) is 1.04 h^{-1}; the same frequency we observed at Ithaca with $\Sigma+\Sigma'=0$. If we continue the curve of Fig. 2 with the curve of Fig. 3, beginning the second at 550 g cm^{-2}, we obtain the smooth curve of Fig. 4, which demonstrates that the variation in slope observed at Echo Lake is real, since the same behavior is found after 300 g cm^{-2} of air.

Finally, we observe that the mean free path (4) deduced for the air with $\Sigma+\Sigma'=0$ is well in agreement with the mean free path measured by other authors.[3] The question naturally arises as to why the frequency of the penetrating showers decreases exponentially with the thickness of the atmosphere, over thicknesses of air corresponding to many mean free paths, while in lead it does not decrease exponentially. We may only observe that in the case of the measurements taken in the atmosphere the λ deduced does not represent a mean free path for absorption of the shower producing radiation, because it may happen, as it is shown by many cloud-chamber pictures, that some of the particles in the penetrating showers generated in the air have energy big enough for generating another penetrating shower, and hence are not eliminated; this cannot happen in our measurement because, if the incoming particle generates a penetrating shower in Σ or Σ', very likely more than a single particle reaches counters E, and the eventual secondary shower is not recorded. A second alternative is the possibility of radioactive decay in the atmosphere, which is unlikely to occur in our apparatus because of the short path.

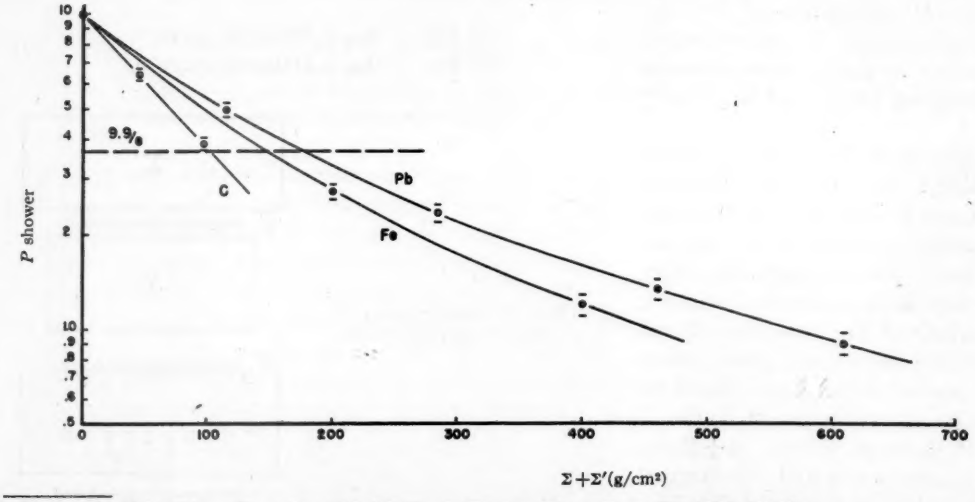

FIG. 2. P showers *versus* thickness $\Sigma+\Sigma'$ at Echo Lake.

[3] G. Wataghin, Phys. Rev. **71**, 453 (1947); J. Tinlot, Phys. Rev. **73**, 1476 (1948).

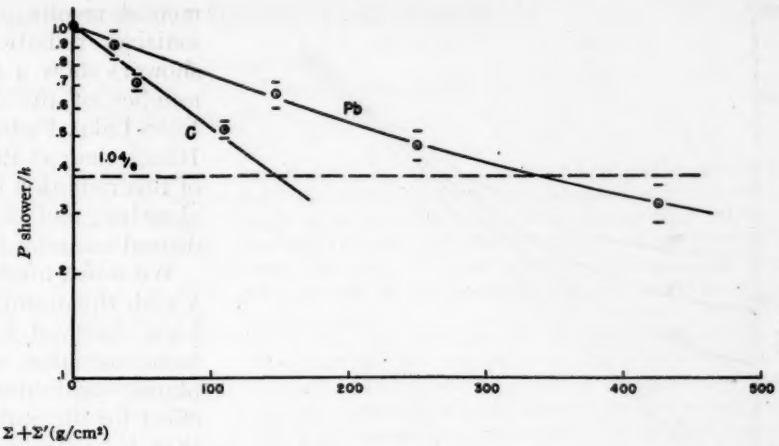

FIG. 3. P showers *versus* thickness $\Sigma+\Sigma'$ at Ithaca.

DISCUSSION

We may begin by discussing the mean free paths (1) deduced from the initial slopes of the curves at Echo Lake. The obvious explanation for the decrease of λ with atomic number is that the primaries generating penetrating showers interact with the nucleons with a cross section of the order of magnitude of the geometrical cross section of the nucleons. In this case, in heavy nuclei the number of inside nucleons screened by the nucleons on the surface is larger than in light nuclei (packing effect), and the heavy nuclei have a smaller stopping power, per nucleon, then the light ones. If the nuclei were completely opaque, the mean free path λ_0 of the penetrating shower producing radiation in a substance of atomic number A would be:

$$\lambda_0=(A/\pi R^2N)\text{ g cm}^{-2}, \tag{5}$$

where N is Avogadro's number and R is the radius of the nucleus. Assuming $R=rA^{\frac{1}{3}}$, one finds immediately the well-known $A^{\frac{2}{3}}$ law.

If instead the nucleus is not completely opaque, the mean free path becomes:

$$\lambda_A=\lambda_0/(1-P_A), \tag{6}$$

where P_A is the probability for the penetrating shower-producing radiation to cross the nucleus without being absorbed. If α is the mean free path *in nuclear matter* of the shower-producing radiation,

$$P_A=\int_0^R(2\pi x/\pi R^2)\exp[-(2(R^2-x^2)^{\frac{1}{2}}/\alpha)]dx$$
$$=(\alpha^2/2R^2)[1-(1+(2R/\alpha)/\exp(2R/\alpha))]. \tag{7}$$

With

$$R=rA^{\frac{1}{3}}=1.5\times10^{-13}\times A^{\frac{1}{3}}\text{ cm}, \tag{8}$$

one deduces the curves of Fig. 5. The values (1) for λ, fit quite well the calculated ones, if one assumes $\alpha=\sim4r$.

Following this scheme, the increase of λ_{Pb} with the thickness of $\Sigma+\Sigma'$ may be interpreted as due to a decrease of the cross section of the penetrating shower-producing radiation due to a hardening of the filtered radiation (perhaps as a result of a change in the average energy). But as a consequence

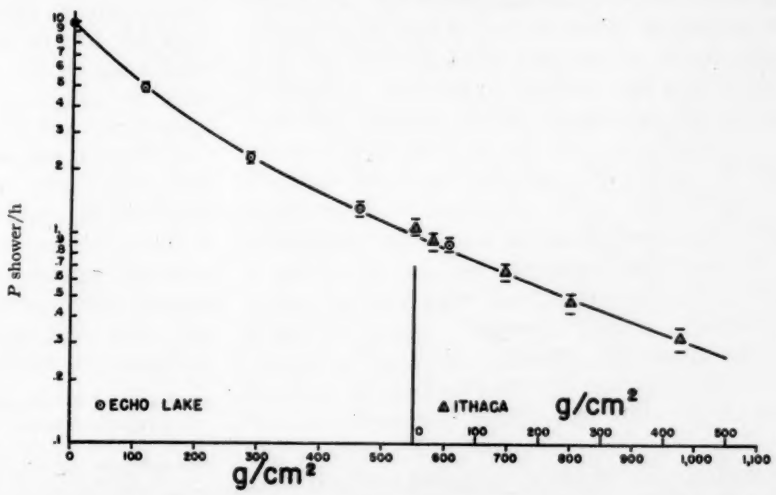

FIG. 4. Absorption curve in P showers at Echo Lake, continued with the absorption curve at Ithaca.

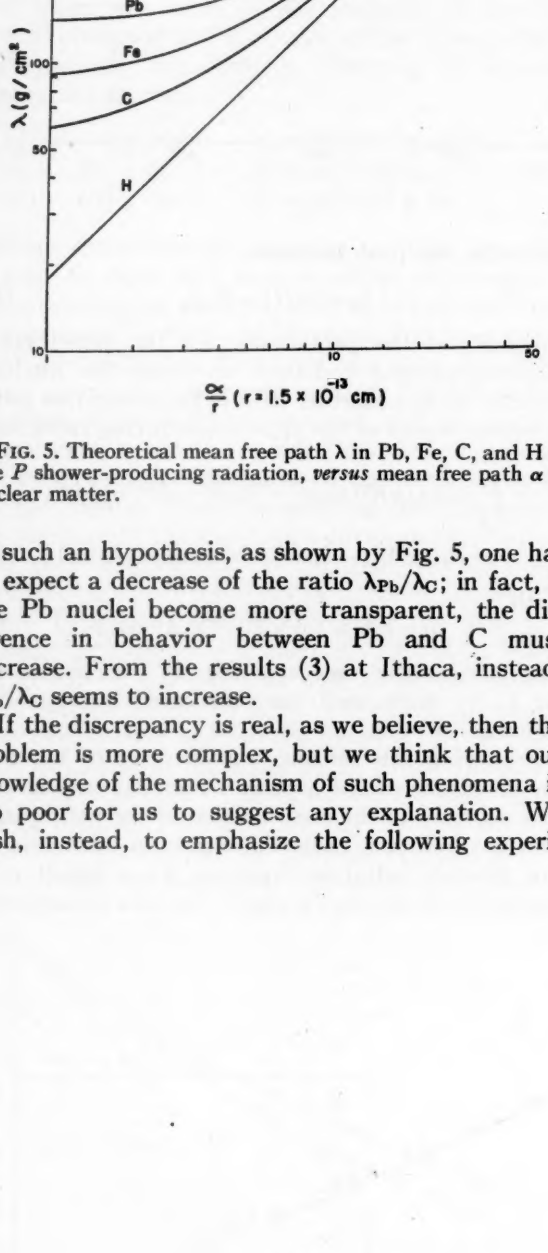

FIG. 5. Theoretical mean free path λ in Pb, Fe, C, and H of the *P* shower-producing radiation, *versus* mean free path α in nuclear matter.

of such an hypothesis, as shown by Fig. 5, one has to expect a decrease of the ratio λ_{Pb}/λ_C; in fact, if the Pb nuclei become more transparent, the difference in behavior between Pb and C must decrease. From the results (3) at Ithaca, instead, λ_{Pb}/λ_C seems to increase.

If the discrepancy is real, as we believe, then the problem is more complex, but we think that our knowledge of the mechanism of such phenomena is too poor for us to suggest any explanation. We wish, instead, to emphasize the following experimental results: (a) The mean free paths of the ionizing radiation which produces penetrating showers show a strong dependence on the atomic number of the absorber both at Ithaca and at Echo Lake. Perhaps this dependence is stronger at Ithaca than at Echo Lake. (b) The mean free path of this radiation increases with the thickness of the absorber, and this has been proved both for condensed material (Pb) and for air.

We want, finally, to point out that a decrease of λ with the atomic number of the absorber has also been observed for a quite different kind of phenomenon—the stars observed in photographic plates[4]—and interpreted as an indication of packing effect for the particles which produce stars. Besides that, it has been shown[5] that neutrons of few Mev, and very likely stars, are associated with penetrating showers. As pointed out in reference 5, it is possible that the two phenomena are more closely related than it was thought before, and that the variation of λ observed for stars must really be ascribed to the variation of λ for the radiation which produces penetrating showers.

The author wishes to thank Professors K. Greisen and H. Bethe for many helpful suggestions and discussions. He is very grateful to the Research Corporation for a grant which covered the expenses of performing the experiment at Echo Lake. The cost of constructing the apparatus was provided through a Navy contract. The facilities of the Inter-University High Altitude Laboratories, and the help of Professors Cohn and Iona of Denver University were an invaluable aid in performing the experiment.

[4] E. P. George, Nature **162**, 333 (1948); G. Bernardini, C. Cortini, and A. Manfredini, Phys. Rev. **74**, 845 (1948).
[5] G. Cocconi, V. Cocconi Tongiorgi, and K. Greisen, Phys. Rev. **74**, 1876 (1948).

PHYSICAL REVIEW VOLUME 75, NUMBER 7 APRIL 1, 1949

On the Quantization of a Unitary Field Theory

R. J. FINKELSTEIN
Institute for Advanced Study, Princeton, New Jersey
(Received September 20, 1948)

In a unitary field theory particles appear not as singularities but as small volumes in which energy and charge of the field are concentrated. In a theory of this nature, which is necessarily non-linear, all properties of the particles, such as their equations of motion, follow from the field equations. It is pointed out in this paper that the non-linearity present in the usual classical field theories is sufficient to permit the existence of particle-like solutions under certain conditions and that it is therefore possible to derive a class of classical unitary theories by postulating that solutions of the usual classical theories are physically admissible only if they are free from singularities. We have studied the quantization of such a theory without specializing the Lagrangian. Momentum (G_α) and angular momentum ($M_{\alpha\beta}$) appear naturally and a relativistic definition of the position (X_α) of a particle may be given in terms of $M_{\alpha\beta}$ and G_α. The commutators of these particle observables (X_α, G_α, $M_{\alpha\beta}$) with each other are calculated and found similar to those postulated in the Snyder formalism which quantizes space-time; these commutators reduce to the usual ones for non-relativistic velocities. (The quantized Born-Infeld theory did not agree with the usual quantum theory of particles even in the non-relativistic limit, because it was not strictly unitary.) The connection between velocity and momentum, and the equation of motion of particles which follow from the field equations are the usual ones. Operators for mass and charge may be defined; these mutually commute and permit the usual classification of the elementary particles according to mass and charge. Magnetic moment and charge commute with the total electromagnetic field. Particle observables and observables describing the external field may not commute in general.

INTRODUCTION

CURRENT theories of matter are based on the concept of elementary particles, which are described either as point singularities or as extended sources of field. The point source models lead to infinities which must be removed by subtraction formalisms; they are unsatisfactory in their present forms either because of the arbitrariness associated with the subtraction recipes or because of their reliance on a future theory which is expected to permit the calculation of certain "infinite" integrals.[1] On the other hand, the extended source models, which correspond to cut-off and strong coupling theories, are not relativistically covariant. We are here interested in a theory which avoids, at least at the classical level, the difficulties characteristic of both the point and extended source particles. In the theory to be discussed the field is everywhere finite, single-valued, and continuous. The particles appear only as small regions where energy-momentum and charge current of the field are concentrated. The particles, being no longer associated with singularities, do not have an independent existence. Such a theory is for this reason termed unitary and ascribes to the elementary particles a finite extension whenever the concept of particle is adequate. On the other hand, in this kind of theory one must abandon the particle concept in certain situations such as a high energy collision, in which the interaction is so intimate that charge, spin, and rest energy are exchanged, and the number of product particles need not be equal to the number of colliding ones; for it is certainly meaningless to speak of the existence of extended and distinct particles during such a collision. It is, however, still possible to describe collisions of this sort in terms of the energy-momentum and charge current densities in the space where the interaction occurs. Of course, it is likely that such a detailed description of the interaction is not physically meaningful; in that case it can be hoped that investigations along these lines will reveal which elements are essential and which may be omitted. In a similar spirit one may interpret the structure which a field theory ascribes to the elementary particles: only those structural details which are observable, such as mass and charge, should be taken seriously.

In a unitary theory the equations of motion of the particle follow from the field equations; in this respect it differs from a theory in which the particles are represented by singularities in the field, for in that case the field equations break down at the singularities, and therefore cannot in general determine the motion of the particles. A unitary theory is necessarily non-linear, for one particle could not influence another if the equations were linear. A second essential role of the non-linearity is to stabilize the concentrations of energy which are interpreted as particles. Since the current field theories are non-linear before field quantization, one is led to investigate the possibilities which arise, when one takes over the Lagrangians of the usually accepted fields—Maxwell, Dirac, Yukawa and Einstein—and the usually discussed couplings between them, and adds the postulate that a solution is physically admissible only if it has no singularities. The coupling between these fields leads to a non-linearity in the field equations which

[1] Mass and charge renormalization appears to be a unique procedure, but (1) the replacement of infinite integrals by finite quantities needs to be justified by the "future theory," and (2) mass and charge are associated with the singularities in a semi-empirical way.

permits in the one case which has been investigated the existence of static and spherically symmetric solutions, which can be interpreted as particles, since they concentrate charge and energy in a small region. The Lagrangian which has been investigated is

$$L=-\tfrac{1}{4}F_{\mu\nu}F_{\mu\nu}+(D_\mu\psi)(D_\mu^*\psi^*)+\sigma^2\psi\psi^*, \quad (1)$$

where

$$D_\mu\psi=(\partial_\mu-i\epsilon\varphi_\mu)\psi, \quad \mu=1\cdots4,$$
$$D_\mu^*\psi^*=(\partial_\mu+i\epsilon\varphi_\mu)\psi^*, \quad x_4=ict. \quad (1a)$$

This case was considered by Rosen,[2] who was led to it as the simplest modification of the Maxwellian Lagrangian which contains the potential explicitly and is still gauge invariant. Except for a sign difference, however, this Lagrangian represents simply the usual Maxwell field coupled in the ordinary way to the usual scalar (or pseudoscalar) mesic field. The signs are so chosen that the energy of the free electromagnetic field is positive, as it should be, while that of the free mesic field is negative. This choice of signs is physically meaningful if the net energy of a particle constructed out of this mixture is positive; we return to this question later.

Before considering the Lagrangian (1) in more detail, we wish to point out that the Maxwell-Dirac case, which is the most thoroughly investigated field from the standpoint of quantum perturbation theory, has not yet been considered from this point of view. Other combinations of known fields are possible, and it is possible that if a field theory of matter exists at all, one can approach it by considering simple combinations of fields already believed to exist. The cases to be discussed in the next paragraph are only illustrative and have no physical application as they stand; we wish to point out mainly that there is a class of unitary theories which are very close to the current theories and which may be arrived at by rejecting singular solutions and rigorously satisfying the self-consistency conditions of current theory.

THE MAXWELL-YUKAWA AND THE SCALAR-SCALAR FIELD

The Lagrangian (1) leads to the field equations

$$(D_\lambda D_\lambda-\sigma^2)\psi=0, \quad (2)$$

and

$$F_{\mu\lambda,\lambda}=S_\mu, \quad (3)$$

where

$$S_\mu=i\epsilon(\psi^*D_\mu\psi-\psi D_\mu^*\psi^*) \quad (3a)$$

is the current. We look for solutions of the type

$$\psi=\theta(r)e^{i\omega t}, \quad \varphi_\mu=(0, i\varphi).$$

Then the field equations become

$$r^{-2}\frac{d}{dr}r^2\frac{d\theta}{dr}+\left(\frac{\omega}{c}+\epsilon\varphi\right)^2\theta-\sigma^2\theta=0, \quad (4a)$$

$$r^{-2}\frac{d}{dr}r^2\frac{d\varphi}{dr}+2\epsilon\left(\frac{\omega}{c}+\epsilon\varphi\right)\theta^2=0. \quad (4b)$$

Change to dimensionless variables

$$z=\sigma^{-1}(\omega/c+\epsilon\varphi), \quad y=\sqrt{2}\sigma^{-1}\epsilon\theta, \quad x=\sigma r, \quad (5a)$$

and take

$$\eta=xy, \quad \zeta=xz. \quad (5b)$$

Then the non-linear equations

$$\eta''+(\zeta^2/x^2-1)\eta=0, \quad (6a)$$

$$\zeta''+\eta^2x^{-2}\zeta=0, \quad (6b)$$

must be satisfied simultaneously subject to the boundary conditions

$$z, y \text{ finite at } x=0,$$

$$\frac{dz}{dx}=\frac{dy}{dx}=0 \text{ at } x=0,$$

or

$$\zeta(0)=\eta(0)=0, \quad \zeta'(0)=z(0), \quad \eta'(0)=y(0). \quad (7a)$$

These conditions exclude a discontinuity in slope of θ and φ and a corresponding discontinuity in the electric field at $x=0$. In addition we require

$$\lim_{r\to\infty}\begin{cases}\varphi=0\\ \theta=0\end{cases} \text{ or } \lim_{x\to\infty}\begin{cases}\zeta/x=\omega/c\sigma\\ \eta/x=0.\end{cases} \quad (7b)$$

If one of the slopes $\zeta'(0)$ or $\eta'(0)$ is assigned arbitrarily, the other is fixed by the condition of finiteness at $x=\infty$.

Thus there is a one parameter family of solutions to (6) and (7). The value of this parameter may be assigned as follows. Asymptotically one has by (6b)

$$\zeta=\epsilon Q+Bx,$$

where Q and B are integration constants. To satisfy (7) we take $B=\omega/c\sigma$. We may regard Q as the parameter to be fixed. One sees that $\phi=Q/r$ at large distances, and also that

$$\int S_0 d\mathbf{r}=4\pi Q. \quad (8)$$

Hence the constant of integration, Q, corresponds to the charge of the particle, and may be fixed by assigning the charge. It may now be shown that (6) and (7) possess nodeless solutions[2] depending on the four physical constants (c, σ, ϵ, Q); the frequency ω has a corresponding eigenvalue.

[2] Nathan Rosen, Phys. Rev. **55**, 94 (1939). The particle-like solutions corresponding to this Lagrangian were independently found by H. Jehle whose calculations have, however, not been published.

The energy momentum tensor follows uniquely from the equation

$$\delta L = -\tfrac{1}{2}\int \theta_{\mu\nu}\delta g^{\mu\nu}(-g)^{\frac{1}{2}}d\tau, \tag{9a}$$

where δL is the variation in the Lagrangian when only the $g^{\mu\nu}$ are varied. In the simple case considered here one finds

$$-\theta_{\mu\nu} = 2\frac{\partial L}{\partial g^{\mu\nu}} - Lg_{\mu\nu}. \tag{9b}$$

According to this definition of $\theta_{\mu\nu}$ the integral, $-\int\theta_{44}d\tau$ is equivalent to the gravitational rest mass. The canonical tensor,

$$-\sum\frac{\partial L}{\partial(D_\mu\psi)}(D_\nu\psi)+Lg_{\mu\nu}=T_{\mu\nu}$$

in general must be corrected to agree with (9a). One finds here

$$\begin{aligned}-\theta_{\mu\nu} = {}& \tfrac{1}{4}F_{\lambda\sigma}F_{\lambda\sigma}g_{\mu\nu} - F_{\alpha\mu}F_{\alpha\nu} \\ & +(D_\mu^*\psi^*)(D_\nu\psi)+(D_\nu^*\psi^*)(D_\mu\psi) \\ & -[(D_\mu^*\psi^*)(D_\mu\psi)+\sigma^2\psi^*\psi]g_{\mu\nu}.\end{aligned} \tag{9c}$$

This leads to the rest mass

$$Mc^2 = -\int\theta_{44}d\tau. \tag{10}$$

M is a function of the four physical quantities (c, ϵ, σ, Q). For example, if ϵQ is small, $Mc^2\sim -\epsilon^{-1}Q\sigma$. The sign of M is negative for the Lagranian (1); it cannot be made positive by adding a divergenceless tensor to $\theta_{\mu\nu}$ without violating (9a) which relates θ_{44} to the density of gravitational mass. The sign of M is a fundamental defect of the theory just described, but there are ways of avoiding this difficulty. For example, consider the Lagrangian describing a scalar-scalar field with pair coupling

$$L = -(\partial_\lambda\psi)(\partial_\lambda\psi^*)-\sigma^2\psi\psi^*-(\partial_\lambda\varphi)(\partial_\lambda\varphi)+g\psi\psi^*\varphi^2, \tag{1}'$$

where $g>0$. This leads to the equations of motion

$$\begin{aligned}\nabla^2\theta+(\omega^2/c^2-\sigma^2)\theta &= -g\theta\varphi^2, \\ \nabla^2\varphi &= -g\theta^2\varphi,\end{aligned} \tag{4}'$$

where $\psi=\theta e^{i\omega t}$ and $\partial\varphi/\partial t=0$. These may be brought to the form (6) by the substitutions

$$\eta=g^{\frac{1}{2}}r\theta;\quad \zeta=g^{\frac{1}{2}}r\varphi;\quad x=ar;\quad a^2=\sigma^2-\omega^2/c^2.$$

The boundary conditions at infinity are $\zeta/x=\eta/x=0$. These correspond to (7b) if we put $\omega=0$. Since the boundary value problem described by Eqs. (6) and (7) has a solution when $\omega=0$, it may be concluded that (4)′ also have particle-like solutions.[3] It is easily shown that the energy of such a particle is positive (the energy density is positive), and so it is possible to display at least one unitary theory which leads to particles of positive mass.[4]

A unitary theory also has the following property: if the charge, Q, is fixed, a discrete spectrum of rest masses follows uniquely, and one can hope to identify the masses of the elementary particles with this spectrum.[2] On the other hand, in the unquantized theory which we have described there is no condition to fix the charge; it will be shown later that the field quantization imposes a relation between the minimum value of Q and the coupling constant, ϵ, namely: $\epsilon=Q_{\min.}/\hbar c$. It is not clear whether the number $Q_{\min.}{}^2/\hbar c$ is also determined.

If one limits himself to classical theory, it is natural to consider other Lagrangians, in particular, the Maxwell-Dirac case, and to study solutions for which $\varphi\neq 0$.[5] However, one would expect major changes to be introduced by the field quantization, and we therefore turn to this question. The theory corresponding to the Lagrangians (1) and (1)′ has been given because it is the only unitary theory which, as far as we know, has been carried to a point where the existence of particle-like solutions could be ascertained. It should be emphasized, however, that the work to be given in the remainder of this paper has not been specialized to a particular Lagrangian, and so is not vulnerable to criticism directed specifically against the forms (1) and (1)′.

QUANTIZATION

Since the field operators are fundamental and all particle observables are derived in a unitary scheme, the quantum theory of particles is already contained in the quantized field theory; or in more formal terms, the commutation relations between the particle observables are already determined by the postulated commutators of the field operators. On the other hand, all the commutators of the new theory must agree with those of the current theory in the correspondence limit. Hence in this limit the new theory must postulate the field commutators of current theory and derive the particle commutators which are now known to be valid. It was one of the defects of the quantized Born-Infeld theory that this condition was not met; in particular the position and momentum of a particle were commutable. The cause of this failure can be traced to the fact that the corresponding classical theory was

[3] N. Rosen and A. Menius, Phys. Rev. 62, 436 (1942). Solutions are found for which $\omega=0$.

[4] I wish to thank D. Bohm for the remark that one can expect to form a particle of positive mass by locking the Dirac field to a scalar Yukawa field, and that one could perhaps get a useful theory of the nucleon in this way.

[5] In unpublished calculations H. Jehle has found that the Maxwell-Yukawa Lagrangian, with the *usual* choice of signs, leads to particles of positive mass for the case of $\varphi\neq 0$.

not strictly unitary insofar as particles were still associated with field singularities. Since the positions of the singularities did not follow from the field equations, it was necessary to regard their coordinates, which were also the particle coordinates, as independent of the field observables. But since the theory was unitary insofar as momentum resided exclusively in the field, it followed that the momentum, depending on the field observables only, commuted with position, which was independent of the field variables. An attempt to overcome the difficulty was made by Pryce,[6] who ascribed to the particles an intrinsic momentum which did not reside in the field; but after this amendment the theory was no longer unitary in even a restricted sense. It will be shown here that the quantization of a classical theory which is strictly unitary does not lead to such difficulties. This is a general fact which does not depend on either the Lagrangian or the commutation relations obeyed by the fields.

COMMUTATORS FOR FIELD VARIABLES

The field may be quantized according to either Einstein-Bose or Fermi-Dirac rules. The former are

$$[\pi^{(\sigma)}(x), \psi^{(\sigma')}, (x')]_- = -i\hbar\delta_{\sigma\sigma'}\delta(x-x'),$$
$$[\pi^{*(\sigma)}(x), \psi^{*(\sigma')}(x')]_- = -i\hbar\delta_{\sigma\sigma'}\delta(x-x'). \tag{11a}$$

All other commutators vanish. The latter are

$$[\psi^{(\sigma)}(x), \psi^{*(\sigma')}(x')]_+ = \delta_{\sigma\sigma'}\delta(x-x'),$$
$$[\psi^{(\sigma)}(x), \psi^{(\sigma')}(x')]_+ = [\psi^{*(\sigma)}(x), \psi^{*(\sigma')}(x')]_+ = 0. \tag{11b}$$

In the following Einstein-Bose rules are to be understood unless the contrary is explicitly stated.

MOMENTUM AND ANGULAR MOMENTUM

The density of energy-momentum in space is defined as $(-iT_{4\nu}/c)$, where

$$T_{\mu\nu} = -\sum_\alpha \left[\frac{\partial L}{\partial(D_\mu\psi^{(\alpha)})}(D_\nu\psi^{(\alpha)}) + \frac{\partial L}{\partial(D_\mu{}^*\psi^{(\alpha)*})}(D_\nu{}^*\psi^{(\alpha)*}) \right] + Lg_{\mu\nu}. \tag{12}$$

The sum over α means the sum over all components of all fields assumed to be present, but D_μ is to be replaced by ∂_μ in those terms corresponding to the Maxwell field. A symmetrizing term must be added to $T_{\mu\nu}$ if (12) does not agree with (9a). The density of angular momentum is similarly defined as $(-iM_{4\mu\nu}/c)$, where[7]

$$M_{\lambda\mu\nu} = T_{\lambda\mu}x_\nu - T_{\lambda\nu}x_\mu + \sum_{\alpha,\beta} \frac{\partial L}{\partial(D_\lambda\psi^{(\alpha)})} S_{\mu\nu}{}^{(\alpha\beta)}\psi^{(\beta)} + *, \tag{13}$$

where

$$\delta\psi^{(\alpha)} = \sum_{\lambda<\mu}\sum_\beta S_{\lambda\mu}{}^{(\alpha\beta)}\delta\omega_{\lambda\mu}\psi^{(\beta)},$$

and

$$\delta x_\lambda = \sum_\mu \delta\omega_{\lambda\mu}x_\mu$$

is an infinitesimal Lorentz transformation. The third term in (13) can be interpreted as the density of spin angular momentum. One has $T_{\lambda\nu,\lambda}=0$, $\theta_{\lambda\nu,\lambda}=0$, and $M_{\lambda\mu\nu,\lambda}=0$. Then if $\theta_{\mu\nu}$ and $M_{\lambda\mu\nu}$ vanish outside a 3-dimensional volume, the integrals

$$icG_\nu = \int T_{4\nu}d\mathbf{x} = \int \theta_{4\nu}d\mathbf{x},$$

$$icM_{\mu\nu} = \int M_{4\mu\nu}d\mathbf{x} = \int (\theta_{4\mu}x_\nu - \theta_{4\nu}x_\mu)d\mathbf{x}$$

over that volume have the transformation properties of a 4-vector and an antisymmetric tensor, respectively. Hence if there are solutions free from singularities for which $\theta_{\mu\nu}$ and $M_{\lambda\mu\nu}$ are concentrated in a small volume, then this small region behaves like a particle whose momentum is G_ν and whose angular momentum is $M_{\mu\nu}$.

In canonical variables the momentum now is

$$G_\mu = \int \theta_\mu d\mathbf{x} \tag{14}$$

and the angular momentum

$$M_{\mu\nu} = \int (g_\mu x_\nu - g_\nu x_\mu)d\mathbf{x} + \int S_{\mu\nu}{}^{(\alpha\beta)}\pi^{(\alpha)}\psi^{(\beta)}d\mathbf{x}, \tag{15}$$

where

$$g_k = -\sum_\sigma(\pi^{(\sigma)}D_k\psi^{(\sigma)} + D_k{}^*\psi^{*(\sigma)}\pi^{*(\sigma)}), \tag{16a}$$

$$g_4 = -ic^{-1}L - \sum_\sigma(\pi^{(\sigma)}D_4\psi^{(\sigma)} + D_4{}^*\psi^{*(\sigma)}\pi^{*(\sigma)}), \tag{16b}$$

where

$$ic\pi = \partial L/\partial(D_4\psi) = \partial L/\partial(\partial_4\psi).$$

The "true" density of momentum, i.e., the density agreeing with gravitational theory, is, on the other hand, $\theta_\alpha \equiv -i\theta_{4\alpha}/c$, where $\theta_{\alpha\beta}$ is the symmetric energy momentum tensor. In terms of θ_α the angular momentum is

$$M_{\mu\nu} = \int (\theta_\mu x_\nu - \theta_\nu \mathbf{x}_\mu). \tag{15a}$$

The momentum and angular momentum so defined are obviously gauge invariant. The density

[6] M. H. L. Pryce, Proc. Roy. Soc. **159**, 355 (1937).

[7] Wolfgang Pauli, Rev. Mod. Phys. **13**, 204 (1941). The notation for $T_{\mu\nu}$ and $M_{\lambda\mu\nu}$ is slightly different here.

of momentum can be written

$$g_\mu = p_\mu + \rho\varphi_\mu, \tag{16c}$$

where p_μ is the form of g_μ when no electromagnetic field is simultaneously present, and ρ is the charge density operator:

$$\rho = -i\epsilon \sum_{(\sigma)} (\pi^{(\sigma)}\psi^{(\sigma)} - \psi^{*(\sigma)}\pi^{*(\sigma)}). \tag{16d}$$

From these definitions and the commutation rules (11) one finds

$$[G_k, f(x)] = i\hbar \frac{\partial f}{\partial x_k} + \int \varphi_k'[\rho', f]d\mathbf{x}',$$

where ρ' means $\rho(x')$. If f is gauge invariant, then

$$[\rho', f] = 0$$

and the integral vanishes. In the applications to be made here f is gauge invariant. The commutator with respect to G_4 is similarly the x_4 derivative but this last relation, giving the equations of motion, is not a consequence of the commutation relations (11). One may write

$$[G_\alpha, f] = i\hbar(\partial f/\partial x_\alpha) \quad \alpha = 1 \cdot\cdot 4. \tag{17}$$

Similarly one shows that the space components of G_α commute among themselves; and if $T_{\mu\nu}$ vanishes outside the volume of the particle, i.e., if there is no external field, then $[G_i, G_4] = 0$ also. Hence in this case

$$[G_\alpha, G_\beta] = 0 \quad \alpha, \beta = 1 \cdot\cdot 4. \tag{18}$$

The angular momentum $(M_{\mu\nu})$ consists according to (15), of two parts

$$G_{\mu\nu} = \int (g_\mu x_\nu - g_\nu x_\mu)d\mathbf{x}, \tag{19a}$$

and

$$s_{\mu\nu} = \int S_{\mu\nu}{}^{(\alpha\beta)}\pi^{(\alpha)}\psi^{(\beta)}d\mathbf{x}. \tag{19b}$$

$G_{\mu\nu}$ and $s_{\mu\nu}$, the orbital and spin contributions, are not separately tensors although their sum is.

One now shows by the rules (11) that

$$[G_{ij}, G_{jk}] = i\hbar G_{ik}, \quad [G_{ij}, G_{kl}] = 0,$$
$$[s_{ij}, s_{jk}] = i\hbar s_{ik}, \quad [s_{ij}, s_{kl}] = 0,$$
$$[G_{ij}, s_{kl}] = 0, \text{ including the case } k = j.$$

For example

$$[s_{ij}, s_{jk}] = \sum_{\alpha\beta\gamma\delta} \int\int S_{ij}{}^{(\alpha\beta)} S_{jk}{}^{(\gamma\delta)} [\pi^{(\alpha)}\psi^{(\beta)}, \pi^{(\gamma)\prime}\psi^{(\delta)\prime}]d\mathbf{x}d\mathbf{x}'$$

$$= i\hbar \sum_{\alpha\lambda\delta} \int (S_{ij}{}^{(\alpha\lambda)} S_{jk}{}^{(\lambda\delta)} - S_{jk}{}^{(\alpha\lambda)} S_{ij}{}^{(\lambda\delta)})\pi^{(\alpha)}\psi^{(\delta)}d\mathbf{x}$$

$$= i\hbar s_{ik}.$$

It follows that the total angular momentum obeys the rules

$$[M_{ij}, M_{jk}] = i\hbar M_{ik}, \quad i, j, k = 1, 2, 3.$$

Now by making a Lorentz transformation on this equation one can show that the same rules are also valid for the $i4$ components.

All of these commutators can be summarized in the tensor equation:

$$[M_{\alpha\beta}, M_{\gamma\delta}] = (g_{\alpha\delta}M_{\beta\gamma} + g_{\beta\gamma}M_{\alpha\delta} - g_{\alpha\gamma}M_{\beta\delta} - g_{\beta\delta}M_{\alpha\gamma})i\hbar. \tag{20}$$

Likewise one finds

$$[M_{\alpha\beta}, G_\gamma] = (G_\alpha g_{\beta\gamma} - G_\beta g_{\alpha\gamma})i\hbar. \tag{21}$$

Equations (20) and (21) depend simply on the facts that G_α is a displacement operator and that $M_{\alpha\beta}$ is an infinitesimal representation of the Lorentz group. The Eqs. (18), (20), (21) show that the momentum and angular momentum associated with a small volume of space according to the definitions (14) and (15) indeed obey the commutation laws *ordinarily assumed for the corresponding properties of particles.*

NON-RELATIVISTIC DEFINITIONS OF POSITION

According to the last paragraph, the momentum and angular momentum of the derived particles appear very naturally in a field theory. The concept of position is less fundamental. We give two illustrations of non-relativistic definitions before considering the relativistic case. If the particle results from the locking of a Maxwell field to a Yukawa field, or to some other field, in the way discussed earlier, a simple definition of position X_i, suggests itself, namely:

$$X_i \int \rho d\mathbf{x} = \int x_i \rho d\mathbf{x}. \tag{22}$$

For ρ one can take the charge density (Eq. 16d). It then follows from the commutation rules (11a) that

$$[G_k, X_i] \int \rho d\mathbf{x} = -i\hbar\delta_{ki} \int \rho d\mathbf{x}. \tag{23}$$

One can put $\int \rho d\mathbf{x} = 1$ when (as for the Lagrangian (1)) this integral is a constant of the motion. One can also get (23) by taking $\rho = \psi^*\psi$.

To prove (23) we calculate

$$J_{ik} = \int\int x_i[\rho, g_k']d\mathbf{x}d\mathbf{x}'.$$

Note that $[\rho, g_k'] = [\rho, p_k'] = [\rho, (\pi'\partial_k\psi' + (\partial_k\psi^*)'\pi^{*\prime})]$,

$$\int\int x_i[\rho, \pi'(\partial_k\psi)']d\mathbf{x}d\mathbf{x}' = e\hbar \int\int x_i\{\pi(\partial_k\psi)'\delta(x-x') - \pi'\psi\partial_k'\delta(x-x')\}d\mathbf{x}d\mathbf{x}'$$

$$= e\hbar \int x_i\partial_k(\pi\psi)d\mathbf{x},$$

$$\int\int x_i[\rho, \pi^{*\prime}(\partial_k\psi^*)']d\mathbf{x}d\mathbf{x}' = -e\hbar \int x_i\partial_k(\pi^*\psi^*)d\mathbf{x}.$$

Hence

$$J_{ik}=i\hbar\delta_{ik}\int\rho d\mathbf{x}.$$

Likewise if one considers a particle built out of the Dirac-Maxwell field, a natural definition of position is

$$X_i\int(\psi^*1\psi)d\mathbf{x}=\int x_i(\psi^*1\psi)d\mathbf{x}. \tag{24}$$

The weighting function in (24) is again the charge density. Let us take a Dirac-Lagrangian[8] unsymmetric in ψ and ψ^*, such that $\pi^*=0$ and $\pi=i\hbar\psi^*$. Then (24) is a special case of (22) and (16d), and (23) is, of course true if one quantized the Dirac field according to the canonical rules. Equation (23) is moreover still true if one quantizes according to the anticanonical rules (11b).

To show this one finds

$$\left[\int x_i'\rho'd\mathbf{x}', G_k\right]=\left[\int x_i'\rho'd\mathbf{x}', p_k\right],$$

since $[\rho, \rho']=0$. The hermitized momentum density is

$$p_k=(i\hbar/2)[\psi^*\partial_k\psi-(\partial_k\psi)^*\psi]. \tag{25}$$

One therefore calculates

$$J_{ik}=-(i\hbar/2)\sum_{\alpha,\beta}\int\int x_i'[\psi_\alpha^{*\prime}\psi_{\alpha'}, \psi_\beta^*\partial_k\psi_\beta]d\mathbf{x}d\mathbf{x}',$$

and the hermitian conjugate term. The following identity may be used

$$[ab, cd]_-=a[c, b]_+d-c[a, d]_+b+ca[b, d]_+-[c, a]_+bd.$$

Then by (11b)

$$J_{ik}=-(i\hbar/2)\sum_\alpha\int\int x_i\{\psi_\alpha^{*\prime}\delta(x-x')\partial_k\psi_\alpha - \psi_\alpha^*\psi_{\alpha'}\partial_k\delta(x-x')\}d\mathbf{x}d\mathbf{x}'$$

$$=(i\hbar/2)\delta_{ik}\sum_\alpha\int\psi_\alpha^*\psi_\alpha d\mathbf{x}.$$

Since $J_{ik}^*=J_{ik}$, the total commutator is $2J_{ik}$.

Thus, starting from the non-relativistic definition of position (22), one arrives at the usual commutators whether one quantizes according to F. D. or E. B. brackets.

RELATIVISTIC DEFINITION OF POSITION (CLASSICAL)

One can give a relativistic definition of position (X_μ) in terms of G_μ, $M_{\mu\nu}$, and a new tensor, $m_{\mu\nu}$, in the following way

$$M_{\mu\nu}=G_\mu X_\nu-G_\nu X_\mu+m_{\mu\nu}. \tag{26}$$

Here $m_{\mu\nu}$ is to be interpreted as the intrinsic spin of the particle. Let us first consider (26) as a classical equation; then if one assigns X_4, there are six relations to determine (X_1, X_2, X_3) and the six components of $m_{\mu\nu}$. It is hence necessary to have three other relations; these may be chosen as follows. We require that in the proper system ($G_i=0$),

$$m_{i4}=0. \tag{27a}$$

The motivation for the choice (27a) is the following. One can put the definition (26) in a different form by starting from

$$M_{i4}=G_iX_4-G_4X_i+m_{i4}.$$

In the proper system this becomes

$$M_{i4}=-G_4X_i.$$

By (15a)

$$M_{i4}=G_ix_4-\int\theta_4x_id\mathbf{x}$$

$$=-\int\theta_4x_id\mathbf{x}.$$

Hence

$$X_i=(G_4)^{-1}\int\theta_4x_id\mathbf{x}. \tag{28}$$

That is, in the proper system (26) reduces to a center of mass definition[9] since θ_4 is just the energy density. This simple interpretation of (28) indicates that the choice of the auxiliary conditions (27a) is a natural one. These three conditions on $m_{\mu\nu}$ can be written in tensor form

$$G_\mu m_{\mu\nu}=0. \tag{27b}$$

Equation (26) may be solved for X_μ in any coordinate system by multiplying by G_ν and summing on ν.

$$X_\nu=G^{-1}(G_\mu M_{\mu\nu}+G_\nu T), \tag{29}$$

where

$$G\equiv G_\mu G_\mu,\quad T\equiv G_\mu X_\mu=G_4{}^pX_4{}^p=G^{\frac{1}{2}}X_4{}^p,$$

where the index p refers to the proper system. It is still necessary to connect $X_4{}^p$ with the field time; we do this by identifying $-iX^p{}_4$ with the field time in the proper system. Hence

$$T=iG^{\frac{1}{2}}\tau, \tag{29a}$$

where τ is proper field time.

The Eqs. (29) and (29a) define the X_μ explicitly. The $m_{\mu\nu}$ now follow from (26) and (29).

$$m_{\mu\nu}=M_{\mu\nu}+G^{-1}(G_\nu G_\alpha M_{\alpha\mu}-G_\mu G_\alpha M_{\alpha\nu}). \tag{30}$$

If there is no spin angular momentum in the field, $s_{\mu\nu}=0$, but it does not follow that $m_{\mu\nu}=0$. Equations (26) are consistent with $m_{\mu\nu}=0$ only if

$$\epsilon_{\alpha\beta\gamma\delta}G_\beta M_{\gamma\delta}=0. \tag{31}$$

[8] G. Wentzel, *Quantentheorie der Wellenfelder* (Frany Deuticke, Wein, 1943), Chap. V.

[9] Møller has also used a similar definition in a paper to appear soon (Communications of Institute for Advanced Study, Dublin).

The conditions (31) are in general not satisfied for extended particles, even if $s_{\mu\nu}=0$.

RELATIVISTIC DEFINITION OF POSITION AFTER FIELD QUANTIZATION

Let us now regard (29) and (30) as operator equations defininining the operators X_μ and $m_{\mu\nu}$ in terms of $M_{\mu\nu}$, G_μ, and T. It is assumed that these equations have been hermitized. $M_{\mu\nu}$ and G_μ are defined as operators in (14) and (15). It is now necessary to define T as an operator and, just as in the classical case, to connect it with the field time. We therefore postulate the following connection between T and the field time

$$T=iG^{\frac{1}{2}}\tau, \tag{32}$$

where τ is the field time in the coordinate system for which the expectation values of the G_i vanish.

$$\langle G_i\rangle=0. \tag{32a}$$

The operator Eq. (32) agrees with the corresponding classical equation in the limit $\hbar\to 0$.

From (32) it follows that T obeys the following commutation rules

$$[T, G_\alpha]=0. \tag{33}$$

Further, since T is an invariant (for Lorentz rotations) it commutes with the angular momentum

$$[T, M_{\alpha\beta}]=0. \tag{34}$$

One can now calculate from (21), (29), and (33)

$$[G_\alpha, X_\beta]=-i\hbar(g_{\alpha\beta}-G_\alpha G_\beta G^{-1}). \tag{35}$$

Using also (34) one finds

$$\begin{aligned}[X_\alpha, X_\beta]&=[G^{-1}G_\mu M_{\mu\alpha}, G^{-1}G_\sigma M_{\sigma\beta}]\\&\quad+[G^{-1}G_\mu M_{\mu\alpha}, G^{-1}G_\beta T]\\&\quad+[G^{-1}G_\alpha T, G^{-1}G_\mu M_{\mu\beta}]\\&=[G^{-1}G_\mu M_{\mu\alpha}, G^{-1}G_\sigma M_{\sigma\beta}]\\&=G^{-2}[G_\mu M_{\mu\alpha}, G_\sigma M_{\sigma\beta}].\end{aligned}$$

And by (20)

$$[X_\alpha, X_\beta]=i\hbar G^{-1}M_{\alpha\beta}, \tag{36}$$

and using (26) one gets

$$[m_{\alpha\beta}, G_\gamma]=0, \tag{37a}$$

$$\begin{aligned}[m_{\alpha\beta}, m_{\gamma\delta}]=i\hbar(&m_{\beta\gamma}g_{\alpha\delta}'+m_{\alpha\delta}g_{\beta\gamma}'\\&-m_{\alpha\gamma}g_{\beta\delta}'-m_{\beta\delta}g_{\alpha\gamma}'),\end{aligned} \tag{37b}$$

where $g_{\alpha\beta}'=g_{\alpha\beta}-G_\alpha G_\beta G^{-1}$. According to Eqs. (37) the $m_{\alpha\beta}$ do not quite obey the commutation laws of a spin angular momentum. The Eqs. (18), (35), and (36) are very similar to commutation rules appearing in a recently proposed formalism which quantizes space.[10] According to our view, however, these new uncertainty relations, stemming from the commutation rules for the underlying fields, describe the particles rather than space itself. The fundamental length appearing in (35) and (36), corresponding to limits of observability for position, is simply the Compton wave length of the particle. For the electron this length is rather large but is not in disagreement with Dirac electron theory where position is uncertain in the region of the *zitterbewegung*.

We note that these results also apply to the case in which there are several particles in the volume for which the momentum and the angular momentum are considered. In this situation Eq. (26) is a center of mass definition for the set of particles, and (35) and (36) then apply to the coordinates of the center of mass.

Although we wish to interpret G_α and $M_{\alpha\beta}$ as the momentum and angular momentum of a particle-like field, it should be noted that the commutators (35) and (36) depend only on general properties of the momentum and angular momentum, and the definition of position in terms of them.

EQUATIONS OF MOTION

The angular momentum of a free particle is conserved

$$\frac{dM_{ij}}{dt}=\frac{\partial M_{ij}}{\partial t}+\frac{1}{\hbar}[G_4, M_{ij}]$$

because $\partial M_{ij}/\partial t$ and $[G_4, M_{ij}]$ vanish separately. The M_{i4} components are also conserved since

$$\begin{aligned}\frac{dM_{i4}}{dx_4}&=+G_i-\int\frac{dg_4}{dx_4}x_i=G_i+\int\frac{\partial g_j}{\partial x_j}x_i\\&=G_i-G_j\delta_{ij}=0.\end{aligned}$$

We now show that the relativistic connection between velocity and momentum of a free particle is preserved by the definition (29). By (29)

$$dX_i/dt=(dT/dt)G_iG^{-1}, \tag{38}$$

since dG_μ/dt and $dM_{\mu\nu}/dt$ separately vanish and by (32) this becomes

$$\langle dX_i/dt\rangle=\langle G_iG_4^{-1}\rangle \tag{39}$$

as was to be shown.

One of the important advantages of a unitary theory over a dualistic one is that the equations of motion of the particle are in the unitary case deducible from the field equations. This has been shown in the classical limit.[2,6] One can show that

[10] Hartland S. Snyder, Phys. Rev. 71, 38 (1947).

the equations of motion also follow from the field equations in the quantum theory. For this purpose assume that there is a weak external field. Then one must add an interaction term, H^{int}, which depends on the external field, to the Hamiltonian. The change of momentum is caused by this term alone.

$$\frac{dG_i}{dt}=\frac{i}{\hbar}[H^{\text{int}}, G_i]=\frac{i}{\hbar}\int[\eta', G_i]d\mathbf{x}',$$

where $\eta'=\eta(x')$ is the density of the interaction Hamiltonian

$$\frac{i}{\hbar}[\eta, G_i]=\sum_{(\sigma)}\frac{\partial\eta}{\partial\psi^{(\sigma)}}\frac{\partial\psi^{(\sigma)}}{\partial x_i}+\frac{\partial\eta}{\partial\pi^{(\sigma)}}\frac{\partial\pi^{(\sigma)}}{\partial x_i}$$

$$=\frac{d\eta}{dx}-\left(\frac{d\eta}{dx}\right)_{\text{ext}},$$

where $(d\eta/dx)_{\text{ext}}$ is the partial gradient associated with the dependence of η on the external field. Then

$$\frac{dG_i}{dt}=\int\left[\frac{d\eta}{dx_i}-\left(\frac{d\eta}{dx_i}\right)_{\text{ext}}\right]d\mathbf{x}=-\int\left(\frac{d\eta}{dx_i}\right)_{\text{ext}}d\mathbf{x} \quad (40)$$

since the first term can be removed by an integration. This is the equation of motion: the rate of change of momentum is the integral of the force over the volume of the particle.

MASS AND CHARGE

We define the rest mass by the operator

$$-M^2=G_\alpha G_\alpha=G_4{}^2+\mathbf{G}^2. \quad (41)$$

Then

$$\hbar\dot{M}=[G_4, M]=0. \quad (42a)$$

Similarly,

$$[G_i, M]=0, \quad (42b)$$

and

$$[M_{\alpha\beta}, M^2]=0. \quad (43)$$

Hence the rest mass is a constant of the motion and can be specified simultaneously with the momentum and angular momentum. From Eq. (35) it follows that M^2 also commutes with position

$$[M^2, X_\alpha]=0. \quad (44)$$

It is possible to ascribe a charge to the particle. Although $\int S_\alpha d\mathbf{x}$ is not a 4-vector, $\int S_4 d\mathbf{x}$ is a scalar since $\partial S_\alpha/\partial x_\alpha=0$. This is defined to be the charge

$$Q=\int s_4 d\mathbf{x}.$$

In general

$$S_\alpha=-i\epsilon\sum_{(\sigma)}\left[\frac{\partial L}{\partial(\partial\psi^{(\sigma)}/\partial x_\alpha)}\psi^{(\sigma)}-\frac{\partial L}{\partial(\partial\psi^{(\sigma)*}/\partial x_\alpha)}\psi^{*(\sigma)}\right] \quad (45)$$

so that the operator for the charge is

$$Q=-i\epsilon\sum_{(\sigma)}\int(\pi^{(\sigma)}\psi^{(\sigma)}-\pi^{*(\sigma)}\psi^{*(\sigma)})d\mathbf{x}. \quad (46)$$

The charge is conserved; it also commutes with the momentum and angular momentum, since they are gauge-invariant and as one may verify by the use of (46).

$$[Q, G_\alpha]=0, \quad (47)$$

$$[Q, M_{\alpha\beta}]=0, \quad (48)$$

and by (41)

$$[Q, M^2]=0. \quad (49)$$

Since Q and M are commuting observables, the usual classification of the elementary particles according to charge and mass remains valid.

The charge current vector of the particle may be defined in the customary way

$$J_\mu=Q(dX_\mu/dS) \quad (50)$$

although $\int s_\mu d\mathbf{x}$ cannot be used for this purpose.

CONNECTION BETWEEN CHARGE AND COUPLING CONSTANT

The solutions of Eqs. (4) contain two constants, Q and ϵ. Q is defined as the integral of the charge density (Eq. (8)), whereas ϵ is a constant appearing in the Lagrangian in the combination $\partial_\nu-i\epsilon\varphi_\nu$. In the classical theory Q and ϵ are unrelated, but we shall now show that the field quantization imposes a connection between them. The charge after field quantization is given by Eq. (46).

By the usual transformation

$$\psi=(\hbar/2)^{\frac{1}{2}}(\alpha+\beta^*), \quad \pi=i(\hbar/2)^{\frac{1}{2}}(\alpha^*-\beta). \quad (51)$$

Equation (46) may be rewritten as

$$Q=(\epsilon\hbar/2)\int[\alpha\alpha^*+\alpha^*\alpha-\beta\beta^*-\beta^*\beta]d\mathbf{x}, \quad (52)$$

where

$$[\alpha(x), \alpha^*(x')]=\delta(x-x'),$$
$$[\beta(x), \beta^*(x')]=\delta(x-x'), \quad (52a)$$
$$[\alpha(x), \beta(x')]=0.$$

The transformation (51) is usually made in momentum space but it is also useful in configuration space since the charge operator contains no gradients. Now replace the continuum by a discrete set of points, each commanding the volume, v. Then $\delta(x'-x)\to v^{-1}\delta_{ij}$ where the indices i, j replace

x and x'; and by the usual argument

$$Q=(\epsilon\hbar/2)\sum\{(2N_a+1)-(2N_b+1)\} =\hbar\epsilon\sum(N_a-N_b), \quad (53)$$

where the sum extends over all lattice points. If e is defined to be the minimum positive value of Q, then

$$\epsilon=e/\hbar. \quad (54)$$

Hence the connection between the coupling constant ϵ and the elementary charge cannot be imposed on the theory in an arbitrary way, since it follows from the field quantization. In particular the connection $\epsilon=1/e$ suggested by Rosen[2] in an interpretation of the Lagrangian (1), is not consistent with the field quantization.

ELECTRIC FIELD, MAGNETIC MOMENT, AND CHARGE

The electromagnetic field commutes with the charge and magnetic moment of a particle. This may be shown as follows. The commutators of the field with itself are

$$[F_{\alpha\beta}, F_{\gamma\epsilon}']=-i\hbar c^2\{\delta_{\beta\epsilon}\partial_{\alpha\gamma'}+\delta_{\alpha\gamma}\partial_{\beta\epsilon'}-\delta_{\beta\gamma}\partial_{\alpha\epsilon'} -\delta_{\alpha\epsilon}\partial_{\beta\gamma'}\}D(x-x', t-t'),$$

where

$$\partial_{\alpha\gamma'}=\partial^2/\partial x_\alpha\partial x_\gamma'.$$

If s_γ is the current density one has, since $F_{\gamma\epsilon,\epsilon}=s_\gamma$

$$[F_{\alpha\beta}, S_\gamma']=-i\hbar c^2\{\partial_{\alpha\gamma'\beta'}-\delta_{\beta\gamma}\partial_\alpha\Box'-\partial_{\alpha'\beta\gamma'} +\delta_{\alpha\gamma}\partial_\beta\Box'\}D(x-x', t-t')$$

$$=i\hbar c(\partial_{\alpha\gamma'\beta'}-\partial_{\alpha'\beta\gamma'})D(x-x', t-t'),$$

since $\Box D=0$. Since also $\partial=-\partial'$, it follows that

$$[F_{\alpha\beta}, S_\gamma']=0.$$

Hence

$$[F_{\alpha\beta}, Q]=\left[F_{\alpha\beta}, \int S_4'd\mathbf{x}\right]=0. \quad (55)$$

Since the magnetic moment is

$$\mu_{ij}=\int(x_is_j-x_js_i)d\mathbf{x},$$

one also has

$$[F_{\alpha\beta}, \mu_{ij}]=0, \quad (56)$$

REPLACEMENT OF CLASSICAL DIFFERENTIAL EQUATIONS BY OPERATOR EQUATIONS

Since the G_α are displacement operators according to (17), the classical wave equation, for example, can be replaced by the quantal equation

$$[G_\alpha, [G_\alpha, \psi]]=0.$$

Maxwell's equations have been similarly rewritten in terms of commutators by Snyder[10] and Yukawa.[11] The rule $i\hbar\partial_\alpha F\rightarrow[G_\alpha, F]$ was proposed by the former in order to define differentiation in a lattice space. In a unitary scheme, however, this substitution is not an additional rule but an elementary consequence of the theory.

EXTERNAL FIELDS

In the usual dualistic theory the following relations are satisfied

$$[X_\alpha^p, A]=0, \quad (57a)$$

$$[G_\alpha^p, A]=0, \quad (57b)$$

where X_α^p and G_α^p are the position and momentum of a particle and A is any field quantity: Markow[12] has proposed a modified theory which replaces (57a) by a non-vanishing commutator, and Yukawa has suggested a scheme in which the second relation becomes $[G_\alpha^p, A]=i\hbar\partial_\alpha A$. Both of these proposals can be regarded as consequences of a unitary theory since the particle observables there become function of the field observables, and hence the relations (57) may not hold. The precise form of these commutators depends on the way the external field is defined. We hope to discuss this question in a later paper.

I wish to thank Professor C. Møller for having pointed out an error in (37b) as it appeared in the manuscript. The remaining differences between our commutators stem from the fact that he takes t to be a c-number, whereas in this paper the proper time is taken to be a c-number.

[11] H. Yukawa, Prog. Theor. Phys. 2, 209 (1947).
[12] M. Markow, J. Phys. U.S.S.R. 2, 453 (1940).

On the Canonical Reduction of Quadratic Forms

R. G. HELSEL
Department of Mathematics, The Ohio State University, Columbus, Ohio
(Received December 13, 1948)

The standard method for simultaneously reducing two quadratic forms in n variables to sums of squares depends upon finding a set of n independent eigenvectors. The same method is applicable to the reduction of a hermitian matrix to diagonal form by a unitary matrix, as is done in quantum mechanics. This method is based on the following fundamental theorem concerning eigenvectors: If A and B are two hermitian matrices of order n, A being positive definite, and if λ_i is a k-fold root of the secular equation $|B-\lambda A|=0$, then the equation $(B-\lambda_i A)\xi=0$ has k independent solutions. In other words, there are k independent eigenvectors corresponding to a k-fold root of the secular equation. A proof is given for this theorem which is concise and at the same time quite elementary.

I. INTRODUCTION

THE theory of small vibrations of a dynamical system is based on the determination of a set of so-called normal coordinates, for which the two real quadratic forms representing the kinetic and potential energies of the system reduce simultaneously to sums of squares. Also in the matrix approach to problems in quantum mechanics it is often necessary to reduce a single hermitian matrix to diagonal form by means of a unitary transformation.

The standard method[1,2] for accomplishing reductions such as those mentioned above involves the determination of a set of eigenvectors corresponding to the roots of the secular equation. In order to discuss simultaneously both the reduction of a pair of real quadratic forms and the reduction of a single hermitian matrix, it is convenient to consider the reduction of a pair of hermitian matrices. If A and B are two hermitian matrices of order n, A being positive definite, it is necessary to find a set of n eigenvectors which are orthonormal with respect to A, that is, a set of vectors ξ_i, $i=1, \cdots, n$, satisfying the equations

$$(B-\lambda_i A)\xi_i=0 \tag{1}$$

and the orthonormality relations[3]

$$\xi_i' A \xi_j=\delta_{ij}, \tag{2}$$

where λ_i, $i=1, \cdots, n$, are the roots (not necessarily distinct) of the secular equation $|B-\lambda A|=0$. If such a set of eigenvectors can be determined, the non-singular matrix

$$X=[\xi_1, \cdots, \xi_n], \tag{3}$$

whose columns are the eigenvectors, reduces both A and B to diagonal matrices. In fact it follows from (2) that $X'AX=I$ and subsequently from (1) that $X'BX=\Lambda$, where Λ is a diagonal matrix with the roots of the secular equation along its diagonal. In view of (2), if $A=I$ the matrix X as defined in (3) is unitary and, therefore, the above method is applicable to the problem of finding a unitary matrix which transforms a given hermitian matrix into a diagonal matrix. Of course the method also applies to the reduction of a pair of real symmetric matrices.

If the roots of the secular equation are all distinct, it is easy to verify that a set of n orthonormal eigenvectors does exist[1,2] and, hence, for that case the procedure just described actually constructs a non-singular matrix which simultaneously reduces both A and B to diagonal matrices. In case some of the roots of the secular equation are repeated, it is not obvious that a set of n orthonormal eigenvectors does exist. To establish the existence of such a set it is sufficient[1,2] to show that *if a root λ_i has multiplicity k then the equation $(B-\lambda_i A)\xi=0$ has k independent solutions* or, in other words, *if λ_i is a k-fold root of the secular equation then the rank of the matrix $B-\lambda_i A$ is exactly $n-k$.* This fact is well known and is a consequence of the theorem (usually proved by induction) which states that if A and B are hermitian matrices of order n and A is positive definite, then a simultaneous reduction to diagonal form is always possible. It seems desirable, however, since the practical method of reducing a pair of hermitian matrices is based on eigenvectors, to have a simple and direct proof of the rank theorem stated above in italics. Attempts in this direction have been made by Routh,[4] Todd,[5] and others. Although some of the existing proofs are brief, particularly Todd's, none of them seems suitable for presentation to beginning students in mathematical physics. It is the purpose of this note to give a proof which is not only short but

[1] H. and B. S. Jeffreys, *Methods of Mathematical Physics* (University Press, Cambridge, 1946), p. 124 *et seq.*
[2] W. L. Ferrar, "The simultaneous reduction of two real quadratic forms," Quarterly Journal of Mathematics (Oxford series) **18**, 186–192 (1947).
[3] A prime on a matrix denotes the conjugate transpose.
[4] E. J. Routh, *Advanced Rigid Dynamics* (MacMillan Company, Ltd., London, 1884), fourth edition, p. 36.
[5] J. A. Todd, "A note on real quadratic forms," Quarterly Journal of Mathematics, Oxford series, **18**, 183–185 (1947).

also well suited for presentation to students who possess a limited knowledge of the theory of determinants and matrices.

II. PROOF OF THE THEOREM

Theorem. *If A and B are hermitian matrices of order n, A being positive definite, the rank of the matrix $B-\lambda_i A$ is exactly $n-k$, where k is the multiplicity of the root λ_i of the secular equation $|B-\lambda A|=0$.*

Let the rank of $B-\lambda_i A$ be $n-r$. Then the equation

$$(B-\lambda_i A)\xi=0 \tag{1}$$

has r independent solutions, say $\xi_1, \cdots, \xi_r$. These solutions can be so chosen[1,2] that they also satisfy the orthonormality relations

$$\xi_i' A \xi_j=\delta_{ij}. \tag{2}$$

By selecting arbitrarily $n-r$ additional vectors,[6] say $\xi_{r+1}, \cdots, \xi_n$, so that the entire set of n vectors is orthonormal in the sense of (2), one obtains a non-singular matrix $X=[\xi_1, \cdots, \xi_n]$ such that $X'AX=I$. In view of this relation and the fact that the first r columns of X satisfy (1), the matrix $X'BX$ has the form

$$\begin{bmatrix} \lambda_i & & & & & \\ & \ddots & & & & \\ & & \lambda_i & & 0 & \\ & & & \ddots & & \\ & & & & \ddots & \\ & & 0 & & & B_1 \end{bmatrix},$$

where B_1 is hermitian and of order $n-r$. It follows that $X'(B-\lambda A)X$

$$=\begin{bmatrix} \lambda_i-\lambda & & & & & \\ & \ddots & & & & \\ & & \lambda_i-\lambda & & 0 & \\ & & & \ddots & & \\ & & & & \ddots & \\ & & 0 & & & B_1-\lambda I \end{bmatrix}. \tag{3}$$

Since the roots of the equation $|X'(B-\lambda A)X|=0$ are the same as the roots of the secular equation and, in view of (3), λ_i is a root of the equation $|X'(B-\lambda A)X|=0$ of multiplicity r at least, it follows that r cannot exceed the multiplicity k of the root λ_i for the secular equation. But if r is less than k then λ_i is necessarily a root of the equation $|B_1-\lambda I|=0$. This is impossible since the rank of $X'(B-\lambda_i A)X$ is equal to the rank of $B-\lambda_i A$, which is $n-r$ by assumption, and by (3) the rank of $X'(B-\lambda_i A)X$ is also equal to the rank of $B_1-\lambda_i I$, which is less than $n-r$ if $|B_1-\lambda_i I|=0$. It follows that $r=k$ and the rank of $B-\lambda_i A$ is $n-k$ as asserted.

[6] This device has been used by other authors to prove similar theorems. See, for example, P. R. Halmos, "Finite dimensional vector spaces," *Annals of Mathematics Studies* (Princeton University Press, Princeton, 1942), No. 7, pp. 125–126.

PHYSICAL REVIEW VOLUME 75, NUMBER 7 APRIL 1, 1949

Remarks on the Evolution of the Expanding Universe*,†

RALPH A. ALPHER AND ROBERT C. HERMAN
Applied Physics Laboratory, The Johns Hopkins University, Silver Spring, Maryland
(Received December 27, 1948)

The relativistic energy equation for an expanding universe of non-interconverting matter and radiation is integrated. The above result, together with a knowledge of the physical conditions that prevailed during the element forming process in the early stages of the expansion, is used to determine the time dependences of proper distance as well as of the densities of matter and radiation. These relationships are employed to determine the mean galactic diameter and mass when formed as 2.1×10^8 light years and 3.8×10^7 sun masses, respectively. Galactic separations are computed to be of the order of 10^9 light years at the present time.

I. INTRODUCTION

WITH the experimental and theoretical information now available it is possible to give a tentative description of the structure and evolution of the universe. Investigations of cosmological models of various types have been carried out which explain many of the features of the observed

* The work described in this paper was supported by the Bureau of Ordnance, U. S. Navy, under Contract NOrd-7386.
† A preliminary account of this work was given at the New York meeting of the American Physical Society, January, 1949.

universe.[1] It does not appear to have been possible to complete these speculations principally for lack of sufficient physical data. Recent studies of the origin and relative abundances of the elements have yielded new information concerning the physical state of the universe at the very early time during which the elements were apparently formed.[2-9] According to this theory the ylem (the primordial substance from which the elements were formed) consisted of neutrons at a high density and temperature. Protons were formed by neutron decay, and the successive capture of neutrons led to the formation of the elements. In order to predict the observed relative abundances of the elements, it is necessary to stipulate the magnitude and the time dependence of the temperature, and density of matter during the period of element formation.

On the basis of a simplified version of the neutron capture theory, namely, one which involves the building up of deuterons only, Gamow[8] has examined the state of the universe at early times and traced the evolution of the universe through the formation of galaxies. For reasons which will be discussed later, Gamow's formulation gives rise to certain difficulties.

We have reformulated this problem from a somewhat different point of view, following some of Gamow's basic ideas.[4,8] This reformulation, which is the main purpose of this paper, involves the use of the general non-static relativistic cosmological model together with knowledge of the physical conditions of matter and radiation which prevail now and also those which are required to predict the observed relative abundances of the nuclear species formed during the very early stages of the universe. As a consequence, it is possible to obtain the functional dependence of both the density of matter and radiation on time. On the basis of the foregoing, the formation of galaxies and other cosmological consequences are considered.

II. FORMULATION OF THE PROBLEM

The model of the expanding universe that we shall discuss is one in which there is a homogeneous and isotropic mixture of radiation and matter, assumed to be non-interconverting. This mixture is treated as a perfect fluid. If the pressure due to matter is neglected, one may write the relativistic energy equation for the non-static model in the following form:[1]

$$d[\exp(\tfrac{1}{2}g(t))]/dt=\pm[(8\pi/3)\rho\exp(g(t))-R_0^{-2}]^{\frac{1}{2}}, \quad (1)$$

which is in relativistic units. The cosmological constant Λ is taken equal to zero. In Eq. (1), ρ is the density of mass and the radius of curvature, R, is given by $R=R_0\exp(g(t))$, where $\exp(g(t))$ is the time-dependent factor in the spatial portion of the line element. Now,

$$\exp(\tfrac{1}{2}g(t))=l/l_0=R/R_0, \quad (2)$$

where l is any proper distance, and l_0, the unit of length, together with R_0, must be determined from the boundary conditions for Eq. (1). It should be pointed out that solutions of Eq. (1) involve l/l_0 and not l alone. The density of mass ρ, which determines the geometry of the space, is the sum of the density of matter, ρ_m, and the density of radiation, ρ_r. If matter is to be conserved we must have

$$\rho_m l^3=A=\text{constant}. \quad (3a)$$

Furthermore, if the universal expansion is adiabatic, the temperature, T, must vary[1] as l^{-1}. If one assumes that the universe contains blackbody radiation, then

$$\rho_r l^4=B=\text{constant}. \quad (3b)$$

It is to be noted that energy is not conserved in models of this type. Equations (3a) and (3b) obviously may be written as

$$\rho_r\rho_m^{-4/3}=\text{constant}. \quad (4)$$

It is clear that this relationship must hold throughout the universal expansion and that the density of mass at any time is

$$\rho=\rho_m+\rho_r=Al^{-3}+Bl^{-4}, \quad (5)$$

providing, as stated earlier, there is no interconversion of matter and radiation. If we substitute Eqs. (2) and (5) into Eq. (1), and convert to c.g.s. units, we obtain

$$dl/dt=+[(8\pi G/3)(Al^{-3}+Bl^{-4})l^2-c^2l_0^2/R_0^2]^{\frac{1}{2}}, \quad (6)$$

where the positive sign is taken to indicate expansion and c and G are the velocity of light and the gravitational constant, respectively. Equation (6) can be integrated and the result given in the form

$$t=K_1+K_2^{-1}[\gamma\rho_{r''}+\gamma\rho_{m''}L+K_2L^2]^{\frac{1}{2}}-(\gamma\rho_{m''}/2K_2^{\frac{1}{2}})\ln\{[\gamma\rho_{r''}+\gamma\rho_{m''}L+K_2L^2]^{\frac{1}{2}}+K_2^{\frac{1}{2}}L+(\gamma\rho_{m''}/2K_2^{\frac{1}{2}})\}, \quad (7)$$

where

$$K_1=(\gamma\rho_{m''}/2K_2^{\frac{1}{2}})\ln[(\gamma\rho_{r''})^{\frac{1}{2}}+(\gamma\rho_{m''}/2K_2^{\frac{1}{2}})]-(\gamma\rho_{r''}/K_2)^{\frac{1}{2}}. \quad (8)$$

[1] R. C. Tolman, *Relativity, Thermodynamics and Cosmology* (Clarendon Press, Oxford, 1934).
[2] G. Gamow, Phys. Rev. **70**, 572 (1946).
[3] R. A. Alpher, H. A. Bethe, and G. Gamow, Phys. Rev. **73**, 803 (1948).
[4] G. Gamow, Phys. Rev. **74**, 505 (1948).
[5] R. A. Alpher, R. C. Herman, and G. Gamow, Phys. Rev. **74**, 1198 (1948).
[6] R. A. Alpher, Phys. Rev. **74**, 1577 (1948).
[7] R. A. Alpher and R. C. Herman, Phys. Rev. **74**, 1737 (1948).
[8] G. Gamow, Nature, **162**, 680 (1948).
[9] R. A. Alpher and R. C. Herman, Nature **162**, 774 (1948).

In Eqs. (7) and (8), $L=l/l_0$, $\gamma=(8\pi G/3)$, $K_2=(c^2/|R_0^2|)$, and $\rho_{m''}$ and $\rho_{r''}$ are the densities of matter and radiation when $L=1$. In order to integrate Eq. (6) and evaluate the integration constant, it is necessary to specify the parameter R_0 and consequently l_0, which gives the units in which R_0 is measured. Examination of Eq. (6) indicates that R_0 can be determined only if it is possible to specify $[(dl/dt)/l]_{l=l_0}$, ρ_m, and ρ_r at any given time. Since $[(dl/dt)/l]_{l=l_0}$ is the expansion rate of space as determined by Hubble[10] and known, therefore, only at the present time, since ρ_m is also known now, and if we assume that $\rho_m \gg \rho_r$ now, one may evaluate R_0 and K_2. Introducing the value of the present expansion rate of the universe $[(dl/dt)/l]_{l=l_0}=1.8\times10^{-17}$ sec.$^{-1}$, taking $\rho_{m''}=10^{-30}$ g/cm^3 and $l=l_0=10^{10}$ cm, i.e., l_0 is the side of a cube containing one gram of matter now, one obtains $R_0=1.7\times10^{27}(-1)^{\frac{1}{2}}$ cm and $K_2=3.2\times10^{-34}$ sec.$^{-2}$. The constants appearing in Eqs. (7) and (8) involve the present densities of matter and radiation. Clearly, in utilizing Eqs. (7) or (8) one may introduce the density values at any other time providing one specifies a value of L at that time which leads to the present value of the density of matter. For convenience we have chosen l_0 to be the side of a cube containing one gram of matter at the present time, so that $L=1$ now. Furthermore, we have again for convenience assumed that $L=0$ at $t=0$. While Eq. (6) has a singularity at $t=0$ which is physically unreasonable, we have employed the solutions in such a manner that the singularity is of no consequence.

For purposes of computation it is convenient to employ an approximate form for Eq. (7) which is valid for early t, i.e., when

$$L[(\rho_{m''}/\rho_{r''})+(K_2/\gamma\rho_{r''})L]<1. \tag{9}$$

The expansion of Eq. (7) which satisfies the above inequality is

$$t=(4\gamma\rho_{r''})^{-\frac{1}{2}}L^2+(\rho_{m''}/6\gamma^{\frac{1}{2}}\rho_{r''}^{\frac{1}{2}})L^3+(8\gamma^{\frac{1}{2}}\rho_{r''}^{\frac{1}{2}})^{-1}\times[(3\gamma\rho_{m''}^2/4\rho_{r''})-K_2]L^4+\cdots. \tag{10}$$

The validity of Eqs. (7) or (10) is questionable for very early times, i.e., in the vicinity of the singularity at $t=0$, when the energy of light quanta was comparable to the rest mass of elementary particles. In fact, Einstein[11] has pointed out that there is a difficulty at very early times because of the separate treatment of the metric field (gravitation) and electromagnetic fields and matter in the theory of relativity. For large densities of field and of matter, the field equations and even the field variables which enter into them will have no real significance. However, since we do not concern ourselves with the "beginning" this difficulty is obviated. In addition to the fact that the relativistic energy equation is not valid for very early times, there are the problems of angular momentum of matter in the universe, as well as certain physical factors involved in the formation of the elements, which we cannot handle satisfactorily at present.

In order to utilize the above equations, it is necessary to specify $\rho_{m''}$, $\rho_{r''}$, and K_2. While it may appear that one need specify the matter and radiation densities at the present time only, because of Eq. (4), specifying $\rho_{m''}$ and $\rho_{r''}$ is equivalent to specifying $\rho_{m'}$ and $\rho_{r'}$, these being the densities at a time during the period of element formation. This time is to be specified later. (The primed quantities should not be confused with the running variables.) It must be remembered that the value of R_0 employed is that calculated from the present value of dL/dt.

III. PHYSICAL CONDITIONS DURING THE EXPANSION

Some information is available regarding the values of the matter and radiation densities at the present time and, recently, studies of the relative abundances of the elements have indicated values for these densities prevailing very early in the universe during the period of element formation. Because of Eq. (4) a knowledge of $\rho_{m'}$ and $\rho_{r'}$ during the element forming period together with $\rho_{m''}$ fixes a value for $\rho_{r''}$, the present radiation density, which is perhaps the least well-known quantity.

In a recent paper Gamow,[8] by considerations which are different than those we have employed, found a set of physical conditions which prevailed during the early stages of the universe. He studied the formation of deuterons only, by the capture of neutrons by protons, taking into account the universal expansion. Equations for the formation of deuterons were integrated from $t=0$, subject to the condition that there were neutrons at the start (unit concentration by weight) and that the final concentration by weight of protons and deuterons was 0.5. This solution determined a parameter α which in turn defined the magnitude of the matter density,[12] $\rho_m=\rho_0 t^{-\frac{3}{2}}$.

[10] E. P. Hubble, *The Observational Approach to Cosmology* (Clarendon Press, Oxford, 1937).

[11] A. Einstein, *The Meaning of Relativity* (Princeton University Press, Princeton, 1945).

[12] The expression for the parameter α, as given by Gamow in reference 8, has been found to be incorrect (see reference 9). We find that $\alpha(=\rho_m v\sigma t/m$, where $\rho_m=\rho_0 t^{-3/2}$ is the density of matter, v is the mean velocity of particles of mass m, and σ is the capture cross section of protons for neutrons) is correctly given by

$$\alpha=\frac{2^{9/4}\pi^{5/4}G^{1/4}a^{1/4}e^2\hbar}{3^{1/4}m^{9/2}c^{11/2}k}(|\mu_P|+|\mu_N|)^2(\epsilon^{1/2}+\epsilon_0^{1/2})\epsilon^{3/2}\rho_0.$$

In this expression all the quantities have been defined by Gamow in reference 8 except μ_P and μ_N, the magnetic moments in nuclear magnetons of proton and neutron, respectively, ϵ_0,

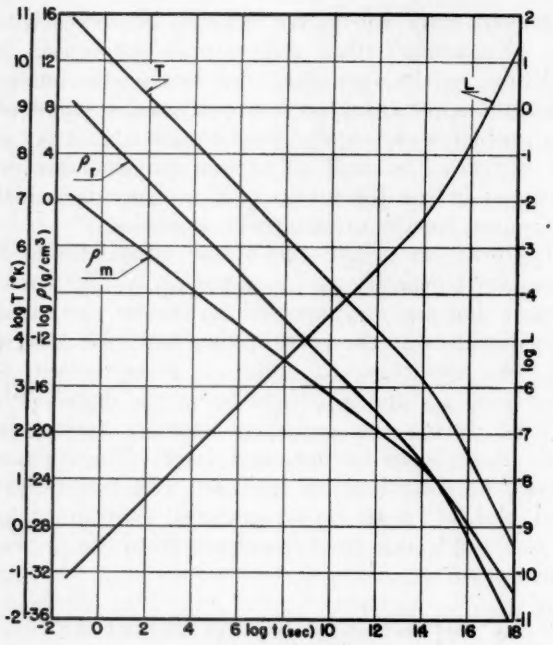

FIG. 1. The time dependence of the proper distance L, the densities of matter and radiation, ρ_m, and ρ_r, as well as the temperature, T, are shown for the case where $\rho_{m''} \leqq 10^{-30}$ g/cm³, $\rho_{r''} \leqq 10^{-32}$ g/cm³, $\rho_{m'} \leqq 10^{-6}$ g/cm³, and $\rho_{r'} \leqq 1$ g/cm³. [See Eq. (12).]

We believe that a determination of the matter density on the basis of only the first few light elements is likely to be in error. Our experience with integrations required to determine the relative abundances of all elements[6,7] indicates that these computed abundances are critically dependent upon the choice of matter density. Furthermore, all formulations of the neutron capture process which have been made thus far neglect the thermal dissociation of nuclei, which is one of the important competing processes during the element forming period if elements are formed from a very early time.

In order to clarify the difficulties associated with the singularity at $t=0$, we digress here for an examination of the equations employed to describe the formation of the elements. These equations, recently given by the authors,[7] include neutron decay and universal expansion but do not take into account the effects of nuclear evaporation or any processes other than radiative capture of neutrons. In terms of concentrations by weight, $x_j = m_j n_j/\rho_m$, rather than particle concentrations, n_j, Eqs. (6)–(8) of reference 7 may be written as

$$dx_0/dt = -\lambda x_0 - \sum_{j=1}^{J} (p_j \rho_m/m_j) x_j x_0, \qquad (11a)$$

$$dx_1/dt = \lambda x_0 - (p_1 \rho_m/m_1) x_1 x_0, \qquad (11b)$$

and

$$dx_j/dt = j(p_{j-1}\rho_m/m_{j-1})x_{j-1}x_0 - j(p_j\rho_m/m_j)x_j x_0, \quad j=2, 3, \cdots, J, \qquad (11c)$$

where x_0, x_1, and x_j are the concentrations by weight of neutrons, protons, and nuclei of atomic weight $2 \leqq j \leqq J$, respectively, m_j the nuclear mass, ρ_m the density of matter, λ the neutron decay constant, and p_j the effective neutron capture volume swept out per second by nuclei of species j. Gamow[8] has solved Eqs. (11a) and (11b) numerically, taking $J=1$, and thereby describing the building up of deuterons only. In general, Eqs. (11) have a singularity at the origin because when $t \to 0$, $\rho_m \to \infty$ as $t^{-\frac{1}{2}}$. In the approximation used by Gamow this singularity is reduced because a relation for the capture cross section of protons for neutrons is employed which makes $p_1\rho_m (= \sigma_1 v \rho_m)$ vary as t^{-1}.

It may be seen readily that Eq. (11c) can be written in the form

$$dx_j/dz = (p_{j-1}/\lambda m_{j-1})x_{j-1} - (p_j/\lambda m_j)x_j, \quad j=2, 3, \cdots, J, \qquad (11d)$$

where

$$z = \int_{\tau_0}^{\tau} j\rho_m(\tau) x_0(\tau) d\tau, \qquad (11e)$$

and

$$\tau = \lambda t.$$

In general, the integrand in Eq. (11e) is singular at $\tau=0$, so that one must take $\tau_0 > 0$. This implies the choice of an initial time at which the element forming process started. Physically, one may not speak of an initial time because there were competing processes which became unimportant as the neutron capture process became important. Competing processes such as photo-disintegration and nuclear evaporation fall off approximately exponentially with time so that neutron capture would become significant rather rapidly, say in a time of the order of 10^2 seconds. The inclusion of this type of competing process in principle could be handled and would yield a better estimate of the relative abundances of the elements. However, without a better knowledge of cosmology at very early t it does not appear to be possible to avoid the above-mentioned difficulty. Finally, if Eqs. (11a), (11b), and (11c) are solved simultaneously for $J=4$, the remaining equations for $j>4$ are given by Eq. (11d) which is a simple first-order linear differential equation with constant coefficients. Nevertheless, Eqs. (11a) and (11b), which are the controlling equations for the process, are not reduced to a simple form and must still be solved in their present form. Because of the above difficulties we find it necessary to introduce the concept of a starting

the binding energy of the virtual triplet state of the deuteron, and the radiation density constant $a = 7.65 \times 10^{-15}$ erg cm^{-3} deg.$^{-4}$. Our expression differs from that originally given by Gamow because of algebraic errors contained in his results and because he neglected the magnetic moment factor.

time for the element forming process. Equations (11) have not yet been solved but are given to illustrate the singularity. So far as we know, any formulation of a theory of element building which includes the type of cosmology discussed will reflect these same difficulties.

In what follows we continue the discussion of the physical conditions employed in the solutions of the relativistic energy equation. The mean density of matter in the universe at the present time has been determined by Hubble[10] to be

$$\rho_{m''} \leqq 10^{-30} \text{ g/cm}^3. \tag{12a}$$

An estimate of the density of matter, $\rho_{m'}$, prevailing at the start of the period of element formation is obtained by integration of the equations for the neutron capture theory of the formation of the elements. Integrations in which neutron decay is explicitly included, but in which the expansion of the universe is not included, yield a matter density of 5×10^{-9} g/cm^3. Preliminary investigations of the equations, including the universal expansion, indicate that this density should be increased by a factor roughly of the order of 100 in order that one may correctly determine the relative abundance of the elements with the universal expansion taken into account. In fact, we have numerically integrated for the light elements the complete equations (see Eqs. (11)) with an "initial" density about 100 times the density used in obtaining solutions without the universal expansion.[7] We find that the above factor of $\sim$100 is roughly what might be required. Accordingly, we have taken

$$\rho_{m'} \leqq 10^{-6} \text{ g/cm}^3. \tag{12b}$$

As discussed elsewhere,[6,7] the temperature during the element-forming process must have been of the order of 10^8–10^{10}°K. This temperature is limited, on the one hand, by photo-disintegration and thermal dissociation of nuclei and, on the other hand, by the lack of evidence in the relative abundance data for resonance capture of neutrons. For purposes of simplicity we have chosen

$$\rho_{r'} \leqq 1 \text{ g/cm}^3, \tag{12c}$$

which corresponds to $T \leqq 0.6\times10^{9}$°K at the time when the neutron capture process became important.

In accordance with Eq. (4), the specification of $\rho_{m''}$, $\rho_{m'}$, and $\rho_{r'}$ fixes the present density of radiation, $\rho_{r''}$. In fact, we find that the value of $\rho_{r''}$ consistent with Eq. (4) is

$$\rho_{r''} \leqq 10^{-32} \text{ g/cm}^3, \tag{12d}$$

which corresponds to a temperature now of the order of 5°K. This mean temperature for the universe is to be interpreted as the background temperature which would result from the universal expansion alone. However, the thermal energy resulting from the nuclear energy production in stars would increase this value.

Since we have $\rho_{r'} \gg \rho_{m'}$ at early time the energy relation given in Eq. (6) may be integrated in a simpler form, with the result

$$T = [(32\pi Ga)/(3c^2)]^{-\frac{1}{4}} t^{-\frac{1}{2}} \text{°K} = 1.52\times10^{10} t^{-\frac{1}{2}} \text{°K}. \tag{13a}$$

The density of radiation, ρ_r, may be found from $\rho_r = (a/c^2)T^4$, or

$$\rho_r = 4.48\times10^{5} t^{-2} \text{ g/cm}^3. \tag{13b}$$

These expressions for T and ρ_r at early time are the consequence of the assumption of an adiabatic universe filled with blackbody radiation. It can also be shown that with the densities chosen in Eq. (12) we have for early time

$$\rho_m = 1.70\times10^{-2} t^{-\frac{3}{2}} \text{ g/cm}^3. \tag{13c}$$

Using l and l_0 as already defined, we may determine the constants A and B in Eq. (3). With the densities discussed above we find $A = 1$ g and $B = 10^8$ g cm. These values of A and B fix the dependence of ρ_m and ρ_r on time through $L(=l/l_0)$. Using these values of A and B, we have computed L, ρ_m, ρ_r, and T. These quantities are plotted on a logarithmic scale in Fig. 1. It should be noted in Fig. 1 that all the quantities plotted bear simple relationships with the time to within several orders of magnitude

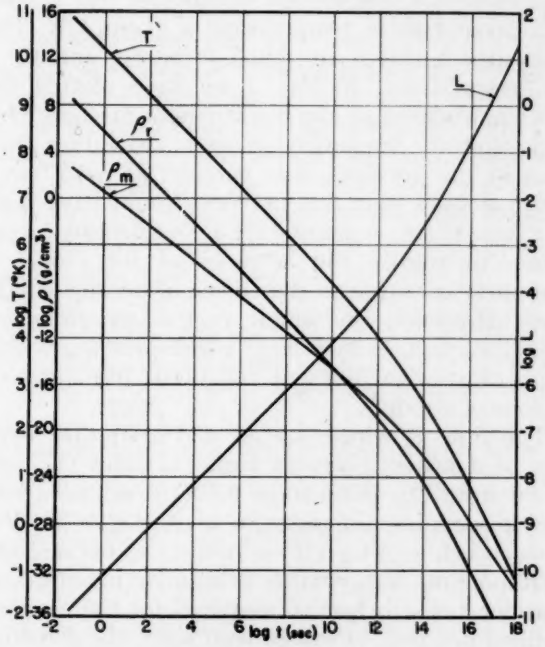

FIG. 2. The time dependence of the proper distance L, the densities of matter and radiation, ρ_m, and ρ_r, as well as the temperature, T, are shown for the case where $\rho_{m''} \leqq 10^{-30}$ g/cm^3, $\rho_{r''} \leqq 10^{-35}$ g/cm^3, $\rho_{m'} \leqq 1.8\times10^{-4}$ g/cm^3, and $\rho_{r'} \leqq 1$ g/cm^3. [See Eq. (15).]

of the time when the universal expansion changes from one controlled by gravitation to one of free escape. This transition occurs in the region of about 10^{13}–10^{14} sec. Following this transition the quantities L, ρ_m, ρ_r, and T again are simple functions of the time. The relations for large t are as follows:

$$\begin{aligned} L &= K_2^{\frac{1}{2}}t, \\ \rho_m &= (\rho_{m''}/K_2^{\frac{1}{2}})t^{-3}, \\ \rho_r &= (\rho_{r''}/K_2^{2})t^{-4}, \end{aligned} \tag{14}$$

and,

$$T = (c^2\rho_{r''}/aK_2^{2})t^{-1}.$$

It is to be noted that in the region of transition to free escape the densities of matter and radiation become equal so that, in fact, prior to the transition the expansion is controlled chiefly by radiation and subsequent to the transition by matter. The universe is now in the freely expanding state, and, since the radius of curvature is imaginary, is of the open, hyperbolic type.

In order to study how sensitive this model is to the choice of densities, we have considered the following additional set of density values which satisfy Eq. (4):

$$\begin{aligned} \rho_{m'} &\cong 1.78\times10^{-4}\ \text{g/cm}^3, \\ \rho_{r'} &\cong 1\ \text{g/cm}^3, \\ \rho_{m''} &\cong 10^{-30}\ \text{g/cm}^3, \end{aligned} \tag{15}$$

and

$$\rho_{r''} \cong 10^{-35}\ \text{g/cm}^3.$$

The value obtained for $\rho_{r''}$ in this case corresponds to a present mean temperature of about 1°K. The constants A and B are found to be 1 g and 10^5 g cm, respectively. In Fig. 2 we have plotted the time dependence of the quantities of interest. One finds that the transition occurs at an earlier time than in the previous case, namely, at $\sim10^{10}$ sec., which implies that this universe would have been in a state of free expansion for a considerably longer time. Apparently the behavior of the model is extremely sensitive to the choice of density conditions. However, the simple type of relations for L, ρ_m, ρ_r, and T that were given previously still apply, but with different constants and different regions of validity.

The time at which $\rho_m=\rho_{m'}$ and $\rho_r=\rho_{r'}$ for both sets of densities given in Eqs. (12) and (15) are found from Eq. (13b) to be 6.7×10^2 seconds, with a corresponding temperature of 0.59×10^9°K. We have chosen $\rho_{r'}\cong1$ g/cm³ in both cases because the corresponding temperature is seen by independent considerations to be that required for the element forming process. As will be seen later, the densities given in Eq. (15) with $\rho_{m'}\cong1.78\times10^{-4}$ g/cm³ do not yield a satisfactory description of the size and mass of galaxies. On the other hand, as already stated a density $\rho_{m'}\cong100(5\times10^{-9}$ g/cm³) is apparently enough to overcome the effect of the universal expansion and give the correct relative abundances of the elements. Thus, on the basis of these considerations one is led to the conclusion that when $t\cong6.70\times10^2$ sec., and $\rho_{r'}\cong1$ g/cm³ we have

$$5.0\times10^{-7}\ \text{g/cm}^3 \gtrsim \rho_{m'} \gtrsim 1.8\times10^{-4}\ \text{g/cm}^3.$$

While it is not particularly germane to the study reported in this paper, it is interesting to note that one may find the dependence of the universal expansion rate on the time in this type of model. This rate is the percentage change in proper distance per unit time determined by Hubble[10] from the red-shift in spectra of nebulae, and is given in $V=Hd$, where V is the velocity of recession of a nebula at a distance d. In our notation, we have, in general,

$$H=(dL/dt)/L=L^{-1}(\gamma\rho L^2+K_2)^{\frac{1}{2}}. \tag{16}$$

For early time this reduces to

$$H=(2t)^{-1}, \tag{16a}$$

and, for late time, to

$$H=t^{-1}. \tag{16b}$$

For early and late t, the value of H does not depend upon the choice of densities. However, in the transition region where the functional form of H changes, the manner of change does depend on the existing density conditions. The universal expansion rate is the reciprocal of the age of the universe if measured during the period of free expansion.

IV. THE FORMATION OF GALAXIES

In his discussion of the evolution of the universe, Gamow[8] suggested that galactic formation occurred at the time when the densities of matter and radiation were equal. He assumes that the Jeans' criterion of gravitational instability may be applied at this time and as a consequence derives expressions for the galactic diameter and mass.[13] We have carried out calculations[9] based on Gamow's formulation using the corrected expressions for D and M given in footnote 13. We find that $\rho_m=\rho_r$ when $t_e\cong0.86\times10^{13}$ sec., which is greater than the age of the universe. This arises out of the fact that, in addition to the difficulties with density determinations mentioned earlier, there is involved an extra-

[13] Using the corrected form of α described in footnote 12, we find for the galactic diameter, D, and mass, M, the following corrected expressions according to Gamow's formulation:

$$D^2=\frac{10\pi^2e^2\hbar}{3Gm^{11/2}c^5\alpha}(|\mu_P|+|\mu_N|)^2(\epsilon^{1/2}+\epsilon_0^{1/2})\epsilon^{3/2}t_e,$$

and

$$M\cong\rho_mD^3=\frac{5^{3/2}\pi^{7/4}e\hbar^{1/2}k}{2^{3/4}3^{5/4}G^{7/4}a^{1/4}m^{15/4}c^2\alpha^{1/2}}(|\mu_P|+|\mu_N|)(\epsilon^{1/2}+\epsilon_0^{1/2})\epsilon^{3/4},$$

where t_e is the time at which the densities of matter and radiation were equal.

polation of relations valid only for early t past their region of validity. It is evident from our choice of densities that the densities of matter and radiation must be equal at a time t_c which is earlier than now. We have retained Gamow's basic idea of galactic condensation at t_c and have applied the Jeans' criterion,[14]

$$D^2=(5\pi kT_c)/(3Gm\rho_{m,c}), \tag{17}$$

where T_c and $\rho_{m,c}$ are taken at $t=t_c$. We may write

$$D=KB^{9/8}, \tag{18}$$

where

$$K=[(5\pi kc^{\frac{1}{2}})/(3a^{\frac{1}{2}}Gm)]^{\frac{1}{4}}, \tag{18a}$$

$$B=\rho_r\rho_m^{-4/3}, \tag{18b}$$

and

$$M\cong\rho_m D^3=K^3B^{3/8}. \tag{19}$$

For the set of density conditions as given in Eq. (12), we obtain for D and M the values 2.1×10^3 light years and 3.8×10^7 sun masses, respectively. When the densities of matter and radiation were equal, $t_c\cong3.5\times10^{14}$ sec.$\cong10^7$ years, $\rho_{m,c}\cong10^{-24}$ g/cm^3 and $T_c\cong5.9\times10^{2}$°K. For the set of densities given in Eq. (15) we obtain $D\cong1$ light year, $M\cong2.8\times10^5$ sun masses, $t_c\cong1.8\times10^{10}$ sec.$\cong6\times10^2$ years, $\rho_{m,c}\cong10^{-15}$ g/cm^3, and $T_c\cong10^5$°K. In the former case we find values for the galactic mass, diameter and density which are roughly of the order of magnitude observed for the average nebula. In the latter case the values differ by many orders of magnitude. Thus, the values one obtains for the galactic mass and diameter appear to be extremely critical to the choice of densities. One might interpret the large discrepancy in the latter case as arising from the fact that the density conditions chosen appear to be incompatible with the neutron-capture theory of the formation of the elements.

The Jeans' criterion of gravitational instability was derived by the consideration of an acoustic wave propagating in a static medium. If the Jeans' criterion is satisfied, regions of condensation whose size is of the order of D, D being the acoustic wavelength, would have separated and would have been gravitationally stable. The separation between condensations would then also have been of the order of D. The separation distance would increase with time, however, because of the universal expansion, whereas the condensations, being gravitationally stable units, would not expand. Subsequently, stars would evolve in these condensations and nebular configurations would be established.[14] From the time variation of proper distance the separation between galaxies is computed to be about 10^6 light years at the present time, in general agreement with observed separations.

The applicability of Jeans' criterion of gravitational instability to this situation must be seriously questioned since it does not contain the possible effects of universal expansion, radiation, relativity, and low matter density. However, it seems reasonable to attach some significance to the time at which radiation and matter densities are equal, because beyond this time the expansion is free and it would become increasingly difficult to form condensations.[15] It should be mentioned that Lifshitz[16] has considered the problem of gravitational instability associated with infinitesimal perturbations of an arbitrary nature in a general relativistic expanding universe and has found that the system is stable and the perturbations do not grow. Until such time as a physically satisfactory criterion for the formation of galaxies is found, it does not appear to be profitable to delve further into such questions as the variation in galactic mass and size with time of formation.

V. ACKNOWLEDGMENTS

Our thanks are due Dr. G. Gamow for his interest in this work and for many stimulating discussions. We wish to express our appreciation to Dr. R. B. Kershner for his interest and invaluable aid concerning some mathematical questions. We wish also to thank Drs. J. W. Follin, Jr., and F. T. McClure for valuable discussions, and Miss S. Thomas for her aid during the preparation of the manuscript.

[14] J. H. Jeans, *Astronomy and Cosmogony* (Cambridge University Press, London, 1929). Except for a numerical factor, Jeans' criterion may be obtained by equating the average thermal energy of a particle with the gravitational potential energy of this particle on the surface of a sphere of diameter D.

[15] See G. Gamow and E. Teller, Phys. Rev. **55**, 654 (1939). In this paper it is shown that if galaxies were formed during a period of free expansion then

$$G\rho_m[(4\pi/3)(D/2)^3]/(D/2)\geqq(H^2/2)(D/2)^2,$$

where H is Hubble's expansion rate and D is the diameter of the condensation. This condition sets a lower limit to ρ_m, namely $\rho_m\geqq(3H^2/8\pi G)=0.6\times10^{-27}$ g/cm^3 and is satisfied by the density value we obtain for galaxies at the time of formation.

[16] E. Lifshitz, J. Phys. U.S.S.R. **10**, 116 (1946).

Relation Between Half-Life and Energy in Alpha-Decay

I. PERLMAN, A. GHIORSO, AND G. T. SEABORG
Department of Chemistry and Radiation Laboratory, University of California, Berkeley, California
(Received February 21, 1949)

THE great number of new alpha-particle emitters has recently made possible the observation of new and interesting systematics in the alpha-decay process. For example, a plot of alpha-energy *versus* mass number for about 90 alpha-emitters has led to interesting conclusions as to the nature of the energy surface in the region of the heavy elements.[1] The present note contains some correlations between alpha-energy and half-life which have resulted in some new conclusions regarding the effect of nuclear type on this relationship.

Figure 1 shows a plot of the logarithm of the half-life *versus* the alpha-energy for the nuclear species of the even-even type. Berthelot[2] had previously treated a more limited amount of alpha-decay data in this manner and reached some of the same deductions that will be noted here. It is not possible to give references for the many recently prepared isotopes which are shown here but, with a few exceptions, the information which is used here may be found in a review article covering all of the isotopes.[3] All of the even-even alpha-emitters for which both the alpha-half-life and the energy are known are included in Fig. 1 while those species which exhibit branching decay with an unknown proportion of orbital electron capture are excluded.

It will be seen that all of the even-even species as reported in Fig. 1 fall on seven nearly parallel lines corresponding to the seven elements polonium, emanation, radium, thorium, uranium, plutonium, and curium. (The three exceptions, Po^{206}, Po^{208}, and Po^{210}, will be discussed below.) The positions of these lines are such as to indicate an average decrease of about a factor of ten in the probability for alpha-emission with an increase of two in atomic number. This displacement is in agreement with the effect attributed to Z in the Gamow formula.[4]

Other nuclear types, even-odd, odd-even, and odd-odd have not been entered in Fig. 1 because the large number of points would obscure the regularities of the even-even isotopes. However, keeping as reference the positions of the lines for the even-even isotopes it is possible to observe some definite departures for the other nuclear types.

Even-odd nuclei (even protons, odd neutrons) of an element lie above the curves for the even-even isotopes of that element signifying abnormally long half-life. As an example Pu^{239} with its 5.15-Mev alpha-particle would cut the line joining Pu^{238} and Pu^{240} at a half-life of 3000 years whereas its actual half-life is 24,000 years. On the average the even-odd nuclei have longer half-lives by a factor of about five over what might be predicted on the basis of the even-even nuclei. The greatest deviation noted was a factor of 10, the least was a factor of 2.

If one draws lines midway between each pair of lines in Fig. 1 to signify hypothetical half-life-energy curves for the odd Z elements, it is found that the odd-even isotopes have longer half-lives than would be predicted. The half-life deviation from prediction for the 15 odd-even isotopes is about fivefold on the average.

In examining the odd-odd species of which six are known, it is found that the deviations are much greater than for the even-odd or odd-even types. On the average these isotopes have longer half-lives by a factor of some 10 to 20 than indicated by predictions from the hypothetical curves.

In all of these correlations, in the cases of isotopes with more than one alpha-group, partial alpha-half-lives have been calculated and the deviations noted are for the least forbidden group. As an example the short-range alpha-group of Pa^{231} has a half-life three times too long while the long range group is thirty times too long.

The above correlations do not include At^{211}, polonium isotopes below 212, and all naturally occurring bismuth alpha-emitters. In all of these cases half-lives are abnormally long and this includes the even-even nuclei. Since these are just the nuclei whose alpha-energies are explained by a depression in the energy surface[1] it is suggested that the decreased probability of alpha-emission is due to the attendant shrunken nuclear radius. If we attempt to dissociate the effect of decrease in radius from the effects due to odd protons and neutrons for bismuth isotopes by making corrections based on regularities observed in the other elements, it is found that a discontinuity in radius of about 10 percent is required for these bismuth isotopes.

It is remarkable that all nuclei with odd protons or odd neutrons have abnormally long half-lives

[1] I. Perlman, A. Ghiorso, and G. T. Seaborg, Phys. Rev. **74**, 1740 (1948).
[2] A. Berthelot, J. de Physique (Ser. VIII) **3**, 52 (1942).
[3] G. T. Seaborg and I. Perlman, Rev. Mod. Phys. **20**, 585 (1948).
[4] G. A. Gamow, *Structure of Atomic Nuclei and Nuclear Transformations* (Clarendon Press, Oxford, 1937).

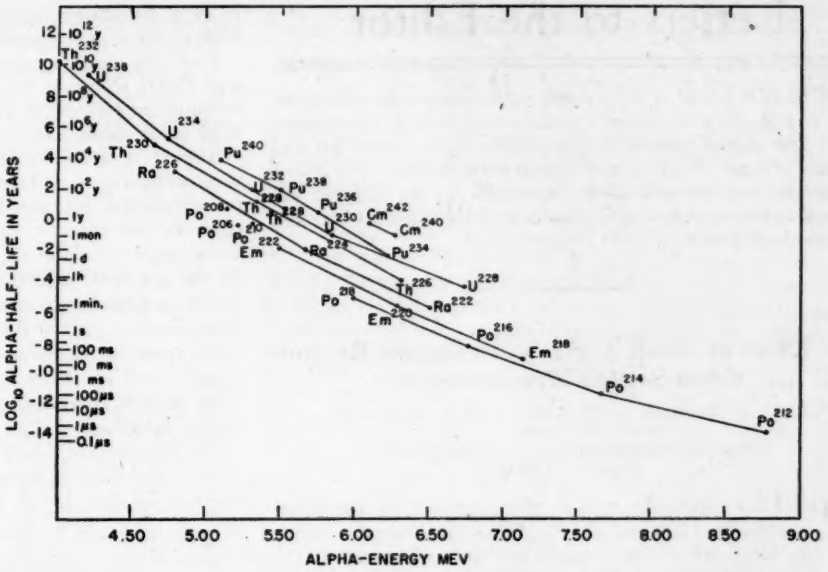

FIG. 1. Plot of log of alpha-half-life *versus* alpha-energy for even-even nuclei.

with the apparent exceptions At^{217}, Po^{215}, and Po^{213}. It is perhaps noteworthy that all of these have high decay energies, 7 Mev or greater. In addition the "normal" for comparison is the line connecting Po^{216}, Po^{214}, and Po^{212}, and it cannot be known for sure that these nuclei are not already beginning to show the effect which becomes so pronounced for Po^{210} and thus are themselves abnormally long-lived.

The generally lengthened half-life for any isotope with odd neutron, odd proton, or both is probably not explicitly explained by existing alpha-decay theory. The occurrence of abnormally long half-lives has been generally attributed to an actual abnormal decrease in nuclear radius (as is no doubt the important factor for At^{211}, the light polonium isotopes, and the bismuth isotopes as mentioned above) and to changes in spin between parent and product nuclei in which the alpha-particle is emitted with angular momentum. Although spin changes of this kind may contribute in some cases it is probably impossible to explain all of the forbidden transitions in this way. In the first place this would demand regular alternation of large and small spin numbers down a decay series. Furthermore in a case like U^{235} alpha-decay, the ground state transition would require a spin change of the order of some 10 units according to Gamow's relationship[3] while the measured values[5,6] for U^{235} and Pa^{231} are 5/2 (or 7/2) and 3/2, respectively, corresponding to a change of only 1 unit (or 2 units). To explain the apparent forbidden nature of all alpha-decay processes in which there is an odd neutron, odd proton, or both it may be necessary to turn to the coefficient of the exponential term and connect the prohibition with a greater difficulty in assembling the components of the alpha-particle in these cases. In this sense one may consider that the existence of one or more unpaired nucleons presumably in the highest quantum states will hinder the formation and emission with full energy of an alpha particle since it must be made up of two neutrons and two protons each pair having antiparallel spins.

All of the data on alpha-emitters will be presented in a forthcoming paper in which will be included further discussion of the regularities.

This work was performed under the auspices of the AEC.

[5] O. E. Anderson and H. E. White, Phys. Rev. **71**, 911 (1947).

[6] H. Schüler and H. Gollnow, Naturwiss. **22**, 511 (1934).

Letters to the Editor

PUBLICATION of brief reports of important discoveries in physics may be secured by addressing them to this department. The closing date for this department is five weeks prior to the date of issue. No proof will be sent to the authors. The Board of Editors does not hold itself responsible for the opinions expressed by the correspondents. Communications should not exceed 600 words in length.

The Effect of Small Angle Scattering on Neutron Cross-Section Measurements

H. H. A. KRUEGER, D. MENEGHETTI, G. R. RINGO, AND L. WINSBERG
Argonne National Laboratory, Chicago, Illinois*
February 11, 1949

DURING neutron cross-section studies of powdered crystalline CaO and ZnO with the mechanical velocity selector, large scattering components were observed in the region below 0.003 ev.[1] Work reported below indicates this effect to be due to the scattering of neutrons into small angles by substances in a highly divided state.

Transmission measurements were made with the mechanical velocity selector in the energy regions 0.001 to 0.0025 ev, 0.005 to 0.01 ev, and 0.045 to 0.09 ev on a variety of materials in various states of subdivision. The neutron beam used was from the thermal column of the Argonne heavy-water-moderated pile. In these measurements, the total cross sections were determined with the samples in positions far from and near to the neutron detector. The angles subtended at the center of the samples by the smaller dimension of the 1.7-cm $\times$10.0-cm slit in the shield of the BF_3 counter were 0.9° at the far position ($\sim$112-cm distance) and 3.8° at the near position (26 cm). The angles subtended by the 10-cm dimension of the detector slit were 5.9° and 21.7°, respectively. In the case of a few samples, slightly different dimensions were used.** Thus, at the shorter distance more of the neutrons scattered into angles of a few degrees were detected by the counter. This resulted in a lower cross section. In the case of single crystals, solids consisting of large crystals, and solid metals, no appreciable difference in cross section at the two positions was noticed. On the other hand, for almost all the powdered and porous substances the cross sections at the near positions were markedly smaller indicating large amounts of small angle scattering. In several cases the effect was very large, and seems to be a decreasing function of the particle size (determined from electron micrographs). The data are given in Table I.

From the data on grain size given in Table I, for lampblack and Cr_2O_3, it might be argued that grain size does not determine the amount of scattering; however, more information is certainly needed on this point.

The effect of the sample thickness on the total cross-section measurements is indicated in Fig. 1, which shows these measurements for powdered lampblack. With the sample close to the counter the two different sample thicknesses have equal values of cross section, showing that essentially all the scattered neutrons were detected. In the far position the thicker sample has a smaller cross section than the thinner sample, although the thicker sample scattered more neutrons away from the detector. This suggests that the scattering is largely multiple, even in the thinnest sample studied. The cross section resulting from this effect decreases as neutron energy increases.

To observe the small angle scattering more directly, intensity distributions were measured by moving the counter in the narrow direction of the beam. With lampblack in place, the width of the transmitted beam is a decreasing function of energy (Fig. 2) in agreement with the data reported above.

The phenomena observed here have obvious analogs in x-ray scattering. It is to be expected that a quantitative explanation can be derived along the lines of x-ray scattering theory.[2,3]

TABLE I. Experimental data.

Material	Particle size by electron micrograph	Grain size by x-ray diffraction	g/cm²	Total cross section in barns for 0.0016-ev neutrons: Far position	Near position
Al powd.	$\sim$2.0μ	0.1μ–10μ	17.3	1.72	1.44
$CaCO_3$ powd.	$\sim$0.15μ	0.1μ–10μ	4.2	38.2	20.0
CaO powd.	$\sim$0.5μ	0.1μ–10μ	13.9	5.4	2.8
Lampblack	$\sim$0.3μ	0.1μ or less	0.97 2.03	32.8 29.0	18.5 18.5
Cr_2O_3 powd.	$\sim$0.15μ	0.1μ–10μ	5.61	150.0	94.0
Sulfur powd.	$\sim$2.0μ	0.1μ–10μ	7.4	2.8	2.7
ZnO powd.	$\sim$1.5μ	0.1μ–10μ	32.0	7.4	5.0
Al solid		0.1μ–10μ	8.17	1.25	1.25
Bi large crystals		•	50.0	2.4	2.4
Calcite crystal			18.1	3.9	3.9
Graphite		0.1μ–10μ	3.08	4.2	1.3
Pb pellets		10μ or larger	31.6	1.7	1.7
Pb single crystal			55.7	1.5	1.5

FIG. 1. The effect of small angle scattering on the total cross-section measurement as a function of neutron energy for various sample thicknesses of powdered lampblack.

FIG. 2. The broadening of the neutron beam due to small angle scattering by powdered lampblack.

We are indebted to Professor S. S. Sidhu of the University of Pittsburgh for the x-ray grain size determinations and to Mr. J. Sayre of this laboratory for the electron micrographs.

* Research work carried out under the auspices of the AEC.
[1] L. Winsberg, D. Meneghetti, and S. S. Sidhu, Phys. Rev. **75**, 975 (1949).
** Calcite: narrow dimension 0.45° and 17°, wide dimension 5.9° and 112° CaO: narrow dimension 0.96° and 7.6°, wide dimension 5.6° and 43.6°
[2] R. von Nardroff, Phys. Rev. **28**, 240 (1926).
[3] A. Guinier, Ann. de Physique **12**, 161 (1939).

Angular Distribution of Protons from Photo-Disintegration of the Deuteron

N. O. LASSEN
Institute for Theoretical Physics, University of Copenhagen, Denmark
February 21, 1949

IN an earlier letter[1] experiments were reported in which the angular distribution of protons from the photo-disintegration of the deuteron by ^{24}Na γ-rays (2.76 Mev) was measured by means of a battery of porportional counters arranged in parallel. The counters were filled with deuterium to such a pressure that the range of the protons was about four times the counter diameter.* By this arrangement, protons moving parallel to the axis of the counters produce much higher pulses than do protons moving perpendicular to the axis, since the latter traverse only part of their range before hitting the walls of the counters. Hence, by counting pulses of maximum size we get the number of protons moving in directions almost parallel to the counter axis, and the angular distribution is obtained by a series of countings for various values of the angle between the direction of the incident γ-rays and the counter axis.

The result of the experiments was given in the earlier letter[1] as $\sigma_0/\sigma_{90}=0.18$, but a closer consideration has shown that the influence of the finite solid angles was somewhat underestimated. The author is indebted to Mr. Kofoed-Hansen for pointing out that, if the differential cross section follows the relation

$$\sigma_\theta=(a+b\sin^2\theta)\sigma_{90°},$$

the number of protons counted directly will obey a similar law, in which θ is replaced by the angle between the axis of the counters and the axis of the γ-ray beam, and the values of the constants are slightly altered. Actually, the proton number was found to follow such a law and, by taking the corrections into account, we finally get

$$\sigma_\theta=(0.15+0.85\sin^2\theta)\sigma_{90°}$$

and

$$\sigma_0/\sigma_{90°}=0.15\pm0.03.$$

This value gives for the ratio between the cross sections of the photomagnetic and the photoelectric effect

$$\sigma_m/\sigma_e=0.26.$$

These results agree, within the limits of error, with the theoretical expectations. For example, from the Møller-Rosenfeld theory L. Hulthén,[2] when using the value of 2.18 Mev for the threshold of the process, finds $\sigma_0/\sigma_{90°}=0.126$ for the γ-rays of the frequency used in the experiments. When the new value for the threshold,[3] 2.24 Mev, is used, the ratio is calculated to be $\sigma_0/\sigma_{90°}=0.14$, in close conformity with the experimental value. The present measurements, however, are not sufficiently accurate to discriminate between the results to be expected from various assumptions regarding the type of nuclear forces. In order to obtain a greater accuracy further experiments with an improved arrangement are in preparation.

[1] N. O. Lassen, Phys. Rev. **74**, 1533 (1948).
* By a misprint in the letter (reference 1), the range was given as ¼ of the counter diameter instead of 3–4 times the counter diameter.
[2] L. Hulthén, private communication.
[3] E. E. Bell and L. G. Elliott, Phys. Rev. **74**, 1552 (1948).

Gamma-Rays from Na^{24} and V^{48}

J. EUGENE ROBINSON, MICHEL TER-POGOSSIAN, AND C. SHARP COOK
Physics Department, Washington University, St. Louis, Missouri
February 8, 1949

IN connection with some other investigations in this department, the gamma-radiations from Na^{24} and V^{48} have been measured on a 14-cm radius of curvature semicircular beta-ray spectrometer.[1] Since the other measured values of these radiations have been obtained using lens spectrometers,[2–4] the confirming evidence herein offered is perhaps of interest. In the present work the K and L lines of all gamma-rays are distinctly visible, and the gamma-ray energies obtained from the K lines are in very good agreement with previously reported values (see Fig. 1).

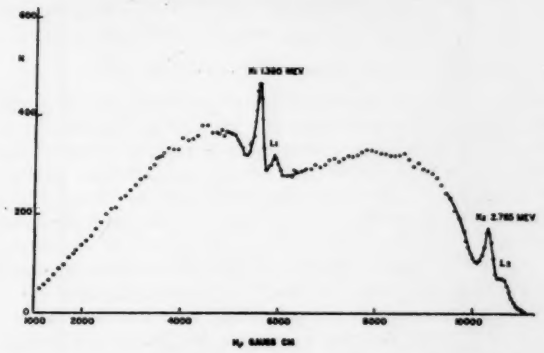

FIG. 1. The Compton and photoelectron spectrum produced from a 50 mg/cm² uranium radiator by the gamma-rays from Na^{24} in a semicircular magnetic spectrometer. Both K and L peaks are visible. Energies of 1.380 Mev and 2.765 Mev are derived from measurements on the K lines of the spectrum.

Calibration of the smaller multi-layer flip coil used to determine the magnetic field was made with a large single-layer flip coil whose total effective area was known quite accurately. It gives good agreement with the accepted value for the annihilation radiation, as can be seen in Fig. 2.

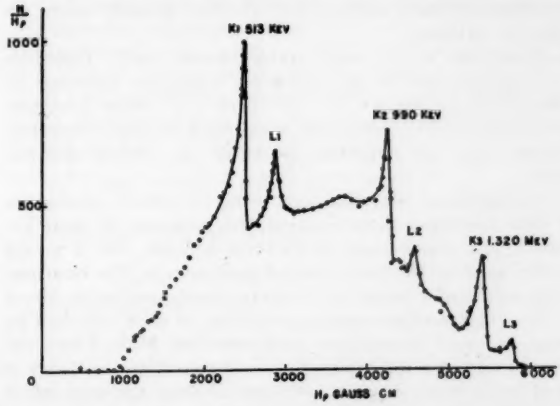

FIG. 2. The Compton and photoelectron spectrum produced from a 50-mg/cm² uranium radiator by the gamma-rays from V^{48}. Gamma-ray energies are 0.990 Mev and 1.320 Mev. The energy of 0.513 Mev given to the annihilation is that derived from the absolute calibration of the instrument mentioned in the text, and is within experimental error of the theoretical value.

This work was supported partly by the joint program of the ONR and AEC.

[1] F. N. D. Kurie and M. Ter-Pogossian, Phys. Rev. **74**, 677 (1948); M. Ter-Pogossian, J. E. Robinson, and C. S. Cook, Phys. Rev. **75**, 995 (1949).
[2] L. G. Elliott, M. Deutsch, and A. Roberts, Phys. Rev. **63**, 386 (1943).
[3] K. Siegbahn, Phys. Rev. **70**, 127 (1946).
[4] W. C. Peacock and M. Deutsch, Phys. Rev. **69**, 306 (1946).

Radioactive Thallium Isotopes Produced from Gold

D. A. ORTH, L. MARQUEZ, W. J. HEIMAN,* AND D. H. TEMPLETON
Department of Chemistry and Radiation Laboratory, University of California, Berkeley, California
February 14, 1949

WE have observed three radioactive isotopes of thallium formed by bombardment of gold metal with 38-Mev helium ions accelerated in the Berkeley 60-inch cyclotron. Mercury and thallium carriers were added to a solution of the gold target and then separated by various chemical schemes. In every case the major portion of the radioactivity was found in the thallium fractions. A composite decay curve for the radioactivity of one of these purified thallium fractions is shown in Fig. 1. It was constructed by normalization

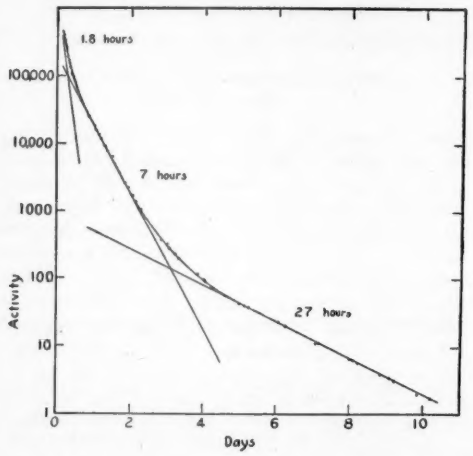

FIG. 1. Decay curve of a mixture of 1.8-hour Tl^{198}, 7-hour Tl^{199}, and 27-hour Tl^{200}.

of data from several unequal portions of the material, counted under the same conditions. The curve was resolved into three components with half-lives 1.8 hours, 7 hours, and 27 hours. Chemical separations made at various intervals subsequent to the bombardment showed that all three periods belong to isotopes of thallium.

Gold consists of the single stable isotope Au^{197}. Therefore (α, n), $(\alpha, 2n)$, and $(\alpha, 3n)$ reactions, which are expected at 38 Mev, will give only Tl^{200}, Tl^{199}, and Tl^{198}. Since these isotopes are neutron deficient and are isobaric to stable mercury isotopes, they are expected to decay by orbital electron capture.

Examination of the radiations using beryllium, aluminum and lead absorbers demonstrated the presence of particles, L x-rays, and gamma-rays in all three periods. The K x-rays were obscured by the electrons and gamma-rays. The electrons in each case had a range in aluminum corresponding to about 0.4 Mev. The most energetic gamma-ray in each case had an energy (by lead absorption) well over one Mev. From the character of these radiations it is probable that the decay is indeed by electron capture, as expected from the position of the isotopes. None of these activities decayed to a radioactive mercury daughter which could be observed. This fact rules out Tl^{197} as one of these activities, since it should decay to one or both of the 23-hour and 64-hour Hg^{197} isomers.[1] Each of these thallium isotopes probably has sufficient energy to decay to the 43-minute mercury isomer of unknown mass number[1,2,3] if the latter belongs to the corresponding daughter, but a search for this activity failed.

Some excitation function data were obtained by irradiation of stacks of 0.004-cm gold foils. This thickness corresponds to an energy loss of about 7 Mev in each foil. The maximum yields of 1.8-hour, 7-hour, and 27-hour thallium were obtained at 38 Mev, 28 Mev, and 20 Mev, respectively. The thresholds were in the same decreasing order but were not well defined by these experiments. These data suggest $(\alpha, 3n)$, $(\alpha, 2n)$, and (α, n) reactions leading to Tl^{198}, Tl^{199}, and Tl^{200}, respectively.

We failed to obtain any evidence in these bombardments for the 4-minute and 3.8-hour activities reported from helium ions on gold[4] and the 10.5-hour and 44-hour periods reported from deuterons on mercury.[3] A 3-minute activity present in some of our targets was demonstrated by chemical separations not to be due to thallium, mercury, or gold.

We are indebted to Mr. B. Rossi and the crew of the 60-inch cyclotron for their cooperation in making the irradiations. Some of the equipment used in this investigation was provided by the AEC.

* Present address: Institute for Atomic Research, Iowa State College, Ames, Iowa.

[1] G. Friedlander and C. S. Wu, Phys. Rev. **63**, 227 (1943).
[2] Marcellus L. Wiedenbeck, Phys. Rev. **68**, 1 (1945); N. Hole, Arkiv. Mat. Astron. Fysik **34B**, No. 19 (1947).
[3] R. S. Krishnan and E. A. Nahun, Proc. Camb. Phil. Soc. **36**, 490 (1940).
[4] L. D. P. King, W. J. Henderson, and J. R. Risser, Phys. Rev. **55**, 1118 (1939).

On the Hole Current in the Germanium Transistor

KURT LEHOVEC
Signal Corps Engineering Laboratories, Fort Monmouth, New Jersey
February 7, 1949

WHEN the transistor was announced by Bell Telephone Laboratories,[1] it was stated that the interaction of the emitter circuit on the collector circuit was the result of a hole current from the emitter to the collector. Consequently, interest focuses on (a) the lifetime of the holes in comparison to their transit time, and (b) the production of the holes at the emitter. The table below is a compilation of some data which has reference to (a). The basic values assumed under 1, 2, and 5 may be considered as representative for the order of magnitude, encountered in high resistivity n-type germanium samples as used for high back voltage rectifiers and transistors. The capture cross section given under six is a tentative value taken in analogy to findings on alkalihalides. All numerical data refer to room temperature.

(1) Mobility of electrons	$v_e = 2000$ cm²/volt sec.
(2) Mobility of holes	$v_h = 1200$ cm²/volt sec.
(3) Diffusion coefficient of holes	$D = (kT/e) \cdot v_h = 30$ cm²/sec.
(4) Distance x, diffused by a hole in time t	$x(\text{cm}) = (2Dt)^{\frac{1}{2}} = 7.7(t(\text{sec.}))^{\frac{1}{2}}$.
(5) Density of free electrons in a n-type sample of resistivity $\rho = 10$ ohm cm	$n^0 = 1/\rho e v_e = 3.10^{14}$ cm^{-3}
(6) Capture cross section of an electron for a hole	$q = 10^{-15}$ cm².
(7) Mean total way of a hole in n-type germanium of the resistivity 10 ohm cm before being captured	$L = (1/qn^0) = 3.3$ cm.
(8) Thermal velocity of a hole	$u = ((3kT/m_n))^{\frac{1}{2}} 7.10^6$ cm/sec.
(9) Mean lifetime of a hole in n-type germanium of the resistivity 10 ohm cm	$\tau = L/u = 5.10^{-7}$ sec.
(10) Mean diffusion lengths in 5.10^{-7} sec.	$x = 55.10^{-4}$ cm.
(11) Distance R from the collector, from which a hole can reach the collector in the mean lifetime τ	$\tau = \int_0^R (1/v_n F)dr$.
($F = (\rho I_e)/(2\pi r^2)$ is the field intensity in the bulk germanium near the collector due to the "spreading resistance.")	$R^3 = (3/2\pi) \cdot \rho v_n I_e \tau$ $R(\text{cm}) \approx 10^{-3}(I_e(mA))^{\frac{1}{3}}$

Emphasis should be laid on the lifetime τ and the distance R. An experimental value for τ derived from pulse-resistivity measurement on bulk germanium samples,[2] is 5–10μsec. The discrepancy between that value and 0.5μsec. given in the table, indicates that either the capture cross section of an electron with a hole is much smaller than 10^{-15} cm², or the recombination of an electron with a hole leads to an intermediate state (exciton) from which a much larger probability for thermal dissociation exists than for the final recombination. Since only the third root of τ enters into the determination of R, the value given in the table may still be considered as

representative for the order of magnitude, and corresponds to the maximum distance between the catwhiskers, emitter and collector, where still a transitor interaction may be found. Incidentally, the high quantum yield observed by S. Benzer[3] at illuminated high back voltage germanium detectors, may result from the fact that there is a large probability for the holes released within R (and not only for those released within the barrier layer) to reach the collector before recombination.

The production of holes near the emitter can be understood by the following considerations. The extent of decrease of electron density toward the electrode, which is characteristic of the barrier layer, is large enough so that the hole density, which is negligible in the bulk germanium, becomes higher than the electron density.[1] Thus the current will be carried mostly by holes in the region very close to the electrode, whereas practically only by electrons, in the bulk germanium at sufficient distance from the electrode. The transition of hole current into electron current requires an excess of the recombination of holes with electrons over the rate of production by thermal agitation in the lattice, if a current passes in the forward direction (holes near the electrode and electrons of the bulk germanium move in direction together to each other). On the other hand, there is an excess of formation of holes and electrons if a current flows in the blocking direction (holes near the electrode and electrons of the bulk germanium move in direction apart from each other). Excess of recombination necessitates a density of holes and electrons higher than in thermal equilibrium. Thus the current in the forward direction shifts the equilibrium of holes and free electrons in the neighborhood of the catwhisker in a similar way as a temperature rise would do.

Finally, it should be mentioned that the density of excitons increases with the densities of holes and free electrons. Thus, holes and electrons may find their way as excitons from the emitter area to the collector base field, and they may contribute to current amplification if they dissociate there.

[1] J. Bardeen and W. H. Brattain, Phys. Rev. **74**, 230 (1948).
[2] Quoted by W. Shockley at the meeting of the Am. Phys. Soc., January 27, 1949, in discussion of his presented paper: "Electronic Theory of the Transistor."
[3] S. Benzer, Phys. Rev. **70**, 105 (1946).

On the Difficulty of the Meson Theory of Nuclear Forces

GENTARO ARAKI
Department of Industrial Chemistry, Kyoto University, Kyoto, Japan
January 20, 1949

IT has generally been believed that the meson theories of nuclear forces involve a difficulty of r^{-3}. Mixtures of two fields were considered first by Møller and Rosenfeld[1] and later by Schwinger[2] in order to eliminate such a term. Furthermore, a divergence difficulty was noticed by the present author, and another mixture was proposed by him.[3] It will be shown in the following, however, that these difficulties are merely apparent so far as the pseudoscalar theory is concerned. Consequently it seems that they have no connection with the general defect of the contemporary field theory.

In the meson theory the matrix element of the two-nucleon potential, W, is given by

$$W_{BA}=\Sigma_I H_{BI}'H_{IA}'/(E_I-E_A)-\Sigma_I H_{BI}'H_{IBA}'/(E_I-E_A) \quad (1)$$

where H' is the interaction between mesons and nucleons. We can find W itself by the Fourier theorem as follows:

$$W=\Sigma_B W_{BA}\exp(i\mathbf{kx}), \quad (2)$$

where $\mathbf{x}$ is the relative position vector between two nucleons, $\hbar\mathbf{k}$ is the momentum of a meson in the intermediate state, I, and matrix elements of the charge and spin operators are suitably converted to the operators themselves.

If we adopt the pseudoscalar meson theory, H' is given by

$$H'=-(f/\kappa^2)\int\psi^\dagger\tau\boldsymbol{\sigma}\,\mathrm{grad}\,U\psi dV+\text{its adjoint} \quad (3)$$

in the non-relativistic approximation where ψ is the wave function of nucleons, U is the pseudoscalar wave function of mesons, and the other notations have the usual meaning. Matrix elements of H' in (1) should be calculated in the non-relativistic approximation, for W is required only in such an approximation. In this approximation we have

$$(1/\kappa)\boldsymbol{\sigma}\,\mathrm{grad}\,U=(2M/\mu)\rho_3 U, \quad (4)$$

where M and μ are masses of a nucleon and a meson, respectively. This identity can easily be shown for every one of their matrix elements with respect to eigenstates of the nucleon momentum on the basis of Dirac's equation. Such a relation was first suggested by Nelson[4] and was later derived by Dyson[5] according to a method of a transformation.

Making use of the relations (1), (2), (3), and (4) we have

$$W=-(2M/\mu)^2(f^2/r)\exp(-\kappa r)T\rho_2^{(1)}\rho_2^{(2)}, \quad (5)$$

where $T=(\tau_1^{(1)}\tau_1^{(2)}+\tau_2^{(1)}\tau_2^{(2)})/2$ (charged theory) or $\boldsymbol{\tau}^{(1)}\boldsymbol{\tau}^{(2)}/2$ (symmetrical theory). At first sight it seems as if this potential vanishes in the non-relativistic approximation, but this is not the case because of the first factor and of the peculiar properties of ρ_2 and Dirac's Hamiltonian. This two-nucleon potential has neither an r^{-3} term nor a divergent integral (especially it has no term of δ-function type). This verifies what was said at the beginning of this letter.

The potential given by (5) seems to be quite different from a usual one, but it is just the same as a hitherto well-known expression, as will be shown in the following. The Hamiltonian of a two-nucleon system with the interaction (5) is given by

$$H=\rho_1^{(1)}\boldsymbol{\sigma}_1\mathbf{p}_1+\rho_1^{(2)}\boldsymbol{\sigma}_2\mathbf{p}_2+(\rho_3^{(1)}+\rho_3^{(2)})Mc^2+W, \quad (6)$$

where $\mathbf{p}$ is equal to $-i\hbar c\nabla$. We expand the eigenfunction of H as follows:

$$\psi=\psi^{++}\chi^+(1)\chi^+(2)+\psi^{+-}\chi^+(1)\chi^-(2)+\psi^{-+}\chi^-(1)\chi^+(2)+\psi^{--}\chi^-(1)\chi^-(2), \quad (7)$$

where χ^+ and χ^- are eigenfunctions of ρ_3 belonging to its eigenvalues $+1$ and -1, respectively. If we substitute (6) and (7) into $H\psi=E\psi$, this equation becomes a system of simultaneous equations for ψ^{++}, ψ^{+-}, ψ^{-+}, and ψ^{--}. In the non-relativistic case ψ^{++} is largest. If we eliminate ψ^{+-}, ψ^{-+}, and ψ^{--} on an assumption that $\phi\ll 1$, we have $H''\psi^{++}=(E-2Mc^2)\psi^{++}$ in the non-relativistic approximation where H'' is a non-relativistic Hamiltonian given by $H''=-(\hbar^2/2M)\times(\Delta_1+\Delta_2)+W'$. W' and ϕ are given by

$$W'=f^2T\exp(-\kappa r)/(1+\phi)(1+2\phi)r\{\tfrac{1}{3}\boldsymbol{\sigma}_1\boldsymbol{\sigma}_2+(\tfrac{1}{3}+1/\kappa r+1/\kappa^2r^2)\Lambda\}, \quad (8)$$

$$\phi=(M/\mu)(f^2/\hbar c)(|a|/\kappa r)\exp(-\kappa r), \quad (9)$$

and

$$\Lambda=3(\boldsymbol{\sigma}_1\mathbf{x})(\boldsymbol{\sigma}_2\mathbf{x})/r^2-\boldsymbol{\sigma}_1\boldsymbol{\sigma}_2, \quad (10)$$

where a is the eigenvalue of T.

ϕ in the expression of W' should be omitted, for W' is derived in the non-relativistic approximation. If we put $\phi=0$ in Eq. (8) it is just the same as the well-known potential of the pseudoscalar meson theory. Equation (8) is correct only for large r as is seen from the assumption for its derivation (compare (9) and $\phi\ll 1$). When ϕ becomes comparable with or larger than unity, Eq. (8) does not hold. If such a region of small r does not play any role for the behavior of the system, the expression (8) can be used as a non-relativistic approximation of W given by (5) for all values of r because of involving no r^{-3} term. Such a possibility was once imagined by Bethe,[6] but finally discarded by him.

From this consideration we find that a r^{-3} term and divergent integrals are due to the unsuitable non-relativistic form

of W_{BA} in the customary method. In the actual calculation, the sum in (2) includes relativistic states whereas W_{BA} is non-relativistic. Therefore the non-relativistic form of W_{BA} should be so determined that the contribution from a relativistic region in the sum of (2) does not play any role. The method of the present letter satisfies this requirement, whereas the customary method does not. The difficulties of the latter come from the relativistic region in the sum of (2).

[1] C. Møller and L. Rosenfeld, Kgl. Danske Vid. Sels. Math.-Fys. Medd. 17, No. 8 (1940).
[2] J. Schwinger, Phys. Rev. 61, 387 (1942).
[3] G. Araki, Phys. Rev. 74, 985, 986 (1948).
[4] E. C. Nelson, Phys. Rev. 60, 830 (1941).
[5] F. J. Dyson, Phys. Rev. 73, 929 (1948).
[6] H. A. Bethe, Phys. Rev. 57, 260 (1940).

Microwave Spectrum of Methyl Bromide

A. Harry Sharbaugh and John Mattern
General Electric Research Laboratory, Schenectady, New York
February 16, 1949

We have measured and analyzed the $J=0\rightarrow1$ rotational transition of $C^{12}H_3Br^{79}$ and $C^{12}H_3Br^{81}$ and found the molecular and nuclear constants to be in good agreement with those reported by Gordy, Simmons and Smith[1] for the corresponding $J=1\rightarrow2$ transition. The measurements were made with a 2K33 Klystron whose low frequency range was extended by increasing the diameter of the external resonant cavity peculiar to this tube. The Wilson-Hughes stark-modulation scheme was used for detection of the lines. Frequency measurements were made to an accuracy of ± 0.1 Mc by using harmonics of a crystal-controlled oscillator which was zero beat with the Bureau of Standards Station WWV.

Table I. Observed and calculated absorption frequencies for J, $K=(0,0)\rightarrow(1,0)$ transition of methyl bromide. Ground vibrational state.

$F\rightarrow F\pm1$	Frequency Observed For $C^{12}H_3Br^{79}$	Calculated* $\nu_0=19136.73$
3/2→1/2	18992.36 mc/sec.	18992.41
3/2→3/2	19252.13	19252.19
3/2→5/2	19107.97	19107.87
	For $C^{12}H_3Br^{81}$	$\nu_0=19064.40$
3/2→1/2	18943.77	18943.80
3/2→3/2	19160.82	19160.88
3/2→5/2	19040.32	19040.28

* $eQ(\partial^2V/\partial Z^2)=577.3$ Mc for $C^{12}H_3Br^{79}$
$eQ(\partial^2V/\partial Z^2)=482.4$ Mc for $C^{12}H_3Br^{81}$

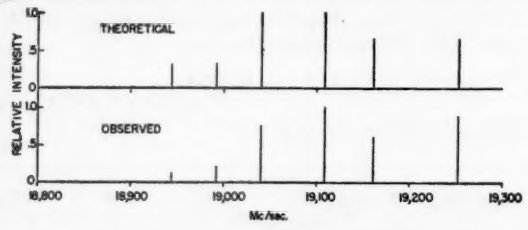

Fig. 1. Microwave absorption spectrum of methyl bromide, $J=0\rightarrow1$ transition.

Table II. Frequencies of unsplit rotational lines and calculated moments of inertia.

Molecule	Transition	ν_0(mc/sec.)	$I_B\times10^{40}$ (g-cm²)	$eQ(\partial^2V/\partial Z^2)$
$C^{12}H_3Br^{79}$	0→1	19136.73	87.68_{11}	577.3
$C^{12}H_3Br^{79a}$	1→2	38272.40	87.68_{35}	577.0
$C^{12}H_3Br^{81}$	0→1	19064.40	88.01_{57}	482.4
$C^{12}H_3Br^{81a}$	1→2	38126.97	88.01_{80}	482.0

[a] See reference 1.

In Table I are listed the experimentally observed and calculated absorption frequencies together with the assigned quantum numbers. Second-order quadrupole corrections[2] were of the same order of magnitude as the experimental error and were neglected. Figure 1 shows graphically the comparison between the observed and calculated spectrum.

The frequencies of the unsplit lines (ν_0), moments of inertia (I_B), and quadrupole coupling constants $eQ(\partial^2V/\partial Z^2)$ are compared with those obtained by Gordy *et al.* for the $J=1\rightarrow2$ transition[1] in Table II. The agreement is seen to be quite satisfactory.

[1] W. Gordy, J. W. Simmons, and A. G. Smith, Phys. Rev. 74, 243 (1948).
[2] J. Bardeen and C. H. Townes, Phys. Rev. 73, 627 (1948).

Erratum: Screening and Relativistic Effects on Beta-Spectra

[Phys. Rev. 75, 264 (1949)]

C. Longmire and H. Brown
Pupin Physics Laboratories, Columbia University, New York, New York

Just prior to publication of this article we noted that in our calculations concerning the screening effect, we had overlooked the energy dependence of the free-electron S wave function at the origin. When this is considered, the radicals in Eqs. (4) and (6) must be inverted, i.e., the correct expression is

$$F_e^{\pm}(Z,W)=F(Z,W\pm D_0)\left(\frac{W-mc^2\pm D_0}{W-mc^2}\right)^{\frac{1}{2}}.$$

Therefore, the numbers in the second column of Table I should be *divided* by the numbers in the third column to obtain the fourth column. This modification approximately interchanges the electron and positron corrections. Thus the positron correction is actually the larger of the two. The screening correction for electrons is almost negligible, because of almost complete cancellation of the two factors involved. Even for *RaE* the correction in the Kurie plot amounts to less than (−) one percent at 20 kev. Thus curve (*b*) in Fig. 4 ought to be a horizontal line. The smallness of the effect for electrons was noted correctly long ago by M. E. Rose,[1] with whose result we are now in accord.

We wish to emphasize that correction of this error *improves* the over-all agreement between the Cu^{64} spectra obtained by Wu and Albert[2] and the theoretical allowed spectra because of the increased magnitude of the screening correction for positrons, particularly at the higher energies. It is nevertheless true that the relative smallness of the deviations found by Wu and Albert, compared to those previously reported, does not depend to an appreciable extent on whether the screening correction is applied, as may be seen from the uncorrected curves of these authors.

[1] M. E. Rose, Phys. Rev. 49, 727 (1936).
[2] C. S. Wu and R. D. Albert, Phys. Rev. 75, 315 (1949). See also C. S. Wu and R. D. Albert, this issue.

Electronic Eigenfunctions in Ionic Crystals

Reikichi Nosawa
Physics Department, Tokyo Institute of Technology, Tokyo, Japan
January 26, 1949

The Wigner-Seitz method of approximation, developed further by Slater and others, has proved very useful when applied to the problem of valence-electrons in metals. It must be noted, however, that the approximation thus far used is valid only in the case where the contribution of surrounding cells to the potential can be assumed zero on account of high symmetry and essentially neutral electrical nature, as in metals having cubic structure. The method is, therefore, applicable strictly neither to the ionic crystal where the neutral nature of surrounding cells is lost, nor to the

metallic crystal having a cell shape and symmetry departing widely from that of a sphere.

The writer has essentially improved and extended the method by using and generalizing Von der Lage and Bethe's Kubic Harmonics.* The points where the present method differs from the previous ones are as follows: (1) The electron-potentials have been assumed to have the crystal symmetry within a lattice cell. While the Schroedinger equation is then not separable, the eigenfunction can still be expanded in terms which are products of spherical solid harmonics and solutions to a set of simultaneous radial equations.

As in Von der Lage and Bethe's treatment, eigenfunctions belonging to special wave vectors are constructed by suitable linear combinations of spherical harmonics so as to satisfy symmetry requirements. (2) Boundary conditions have been satisfied more exactly than in their treatment by using a different average fitting and, in consequence, the arbitrariness in choosing the fitting points on the cell surface is removed. (3) Essentially different features of the present treatment from preceding ones, such as Shockley's, Ewing and Seitz's and Tibbs', result from the electron-potential adopted. Starting from the picture of point charges, the classical Madelung's field in ionic crystals belonging to the cubic system has been obtained in terms of Kubic Harmonics. This has further been modified by superposing the Hartree fields of nearest neighboring ions. The resulting potential is naturally continuous throughout the crystal except at the lattice points and has the full cubic symmetry. (4) Lastly, reasonable joining of the wave functions at the cell boundaries has been achieved in virtue of this potential. Thus, the only assumptions made in our article are that in the ionic crystal the inner shells of ions are not altered from their form in the free ions and that the contribution of nearest neighboring ions to the potential is given by superposition of the Hartree fields arising from them. The method is being applied to NaCl and CsCl to find the ground state of the valence-electron in both crystals and of the additional electron in rock salt. The results will be published shortly.

* F. C. Von der Lage and H. A. Bethe, Phys. Rev. **71**, 612 (1947).

Approximate Densities of Liquid He^3 between 1.27° and 2.79°K*

E. R. Grilly, E. F. Hammel, and S. G. Sydoriak
Los Alamos Scientific Laboratory, Los Alamos, New Mexico
February 14, 1949

THE pure He^3 used in these experiments was the same as used in vapor pressure measurements.[1] The principal apparatus consisted of a gas buret-manometer combination connected to a narrow soft glass tube (hereafter called "the capillary") in which the He^3 was liquefied. Around the capillary was a bath of liquid He^4, then liquid air, both Dewars having unsilvered strips. The capillary dimensions were: 1.656-mm I.D., 2.95-mm O.D., 90 mm long. It was fused to another glass capillary (0.687-mm I.D., 4.83-mm O.D.) which connected to the buret. Although this thick-walled section introduced an undesirable temperature gradient, it was necessary in order to conserve volume and yet provide sufficient rigidity. The liquid levels were observed by means of a cathetometer, suitable illumination being obtained from a 2-watt neon lamp on the opposite side.

Liquefied He^3 was observed in the capillary to be clear and colorless. The meniscus was sharp, and moved markedly when the capillary was tapped. At one temperature, 1.7°, sudden reduction of He^3 pressure caused a violent boiling[2] similar to that in He^4 (*I*).

During measurements the capillary immersion in the bath was kept constant by raising the Dewars. The procedure used follows: He^3 was liquefied in the capillary to a height of several mm, then most of this was evaporated by loweringthe mercury in the buret. Since the evaporated liquid was replaced by vapor at the same temperature, the data gave the difference between liquid and vapor densities:

$$\rho_L-\rho_v=\frac{3.02\times 273 P\Delta V_{bur}}{22400\times 760 T_{bur}\Delta V_L},$$

where ΔV_{bur} = buret volume change at P(mm Hg) and T_{bur}°K. And ΔV_L = liquid volume change due to change in liquid height. The results are given in Table I along with

TABLE I. Differences between liquid and vapor densities of He^3.

T	1.27	1.73	2.26	2.52	2.79°K
$\rho_L-\rho_v$	0.0783	0.0781	0.0698	0.0661	0.0542 g/cc
Uncertainty	±2	±3	±2.5	±2.5	±5%

estimated uncertainties in ΔV_L, by far the most significant. After completion of the measurements, an examination of the Dewar windows showed that refractive errors varied considerably with the height of observation.

In the absence of saturated vapor density data, absolute values of liquid densities were estimated, using the law of rectilinear diameters. For both He^3 and He^4, critical densities ρ_c were calculated from critical pressures and temperatures[3] by means of the Dieterici and van der Waals equations of state. For He^4 ρ_c from the law of rectilinear diameters, using vapor and liquid densities measured at Leiden,[4,5] is about 0.4 of the way between Dieterici and van der Waals values of ρ_c (see Table II and Fig. 1). Assuming a corresponding situa-

TABLE II. Critical densities of He^3 and He^4 by various methods.

	Dieterici	van der Waals	Rectilinear diameters	De Boer
He^3	0.0460	0.0360		0.041–0.046
He^4	0.0780	0.0564	0.0693	

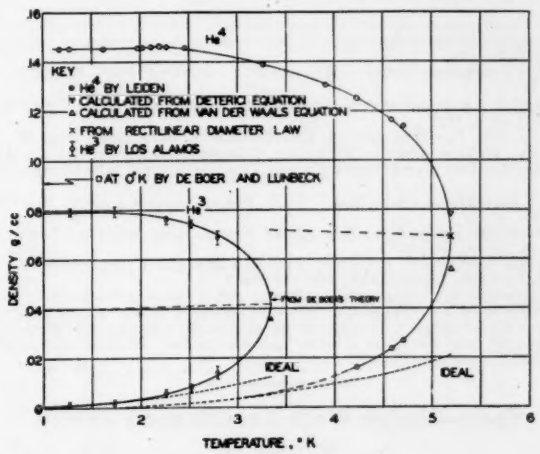

FIG. 1. Density of helium *vs.* temperature.

tion for He^3, $\rho_c=0.0420$ was taken to fix one point of the mean density line. The other point used was taken from our data at 1.27°, where the vapor density is small and close to ideal:

$$\tfrac{1}{2}(\rho_L-\rho_v)+(MP/RT)=0.0401.$$

Our data were then plotted so that $\rho_L-\rho_v$ was divided equally above and below the mean density. The resulting vapor and

TABLE III. Smoothed densities of liquid and vapor He^3.

T	1.0	1.5	2.0	2.5	2.8	3.1	3.34°K
Liquid	0.0792	0.0792	0.0784	0.0744	0.0700	0.0618	0.0420 g/cc
Vapor	0.0005	0.0016	0.0036	0.0084	0.0132	0.0220	0.0420 g/cc

liquid density curves are shown in Fig. 1 and the smoothed values in Table III. The density for condensed He^3 at 0°K was calculated by De Boer and Lunbeck[6] to be 0.091; and ρ_e was calculated by us, from De Boer's theory,[7] to be in the range 0.041–0.046 g/cc.

Using $\Delta H_{vap} = T\Delta V(dP/dT)$ with our density and vapor pressure[1] data, heats of vaporization as a function of temperature were calculated and are presented in Fig. 2. The reliability of the results is insufficient for establishment of anything but

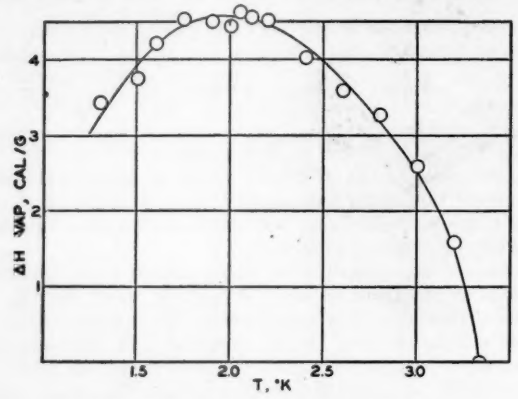

FIG. 2. Heat of vaporization for He^3 *vs.* temperature.

a smooth curve which has a maximum of 4.5 cal./g between 1.7° and 2.2°.

It is recognized that greater precision is imperative for establishing a lambda-transition such as exists for He^4. To improve density and vapor pressure measurements[8] and to reach lower temperatures, we are making major design changes in our apparatus.

We acknowledge helpful discussions with Dr. F. G. Brickwedde and Dr. J. E. Kilpatrick.

* This document is based on work performed at the Los Alamos Scientific Laboratory of the University of California under government contract W-7405-Eng-36.

[1] S. G. Sydoriak, E. R. Grilly, and E. F. Hammel, Phys. Rev. **75**, 303 (1949).

[2] Such observations at various temperatures might be useful for detecting a phase *II* in He^3.

[3] For He^4, $P_e = 1718$ mm Hg and $T_e = 5.20$°K were taken from W. H. Keesom, *Helium* (Elsevier Publishing Company, Inc., New York, 1942), p. 191. For He^3, $P_e = 875$ mm Hg and $T_e = 3.34$°K were taken from reference 1.

[4] H. Kamerlingh Onnes and J. D. A. Boks, Commun. Leiden, No. 170b (1924).

[5] Mathias, Crommelin, Kamerlingh Onnes, and Swallow, Commun. Leiden, No. 172b (1925).

[6] J. De Boer and R. J. Lunbeck, Physica **XIV**, No. 7 (September, 1948).

[7] J. De Boer, Physica **XIV**, 139–148 (1948).

[8] In reference 1, we noted the vapor pressure excess in the stainless steel capillary when it contained He^4. We have obtained similar results using the present glass capillary. This excess was independent of capillary immersion depth and was the same whether the surrounding Dewars were wholly silvered or strip-silvered.

Space-Charge Wave Amplification Effects

V. A. BAILEY
School of Physics, University of Sydney, Sydney, Australia
February 21, 1949

IN a letter under the title given above,[1] which has just come to my notice, A. V. Haeff reports on "an entirely new method (of amplification of microwave energy) based on space-charge amplification effects occurring as a result of interaction between streams of charged particles" and states that "this mechanism of interaction between particles and the associated space-charge waves plays an important part in many natural phenomena" such as bursts of solar noise associated with sunspot activity and the excess noise in electron-beam tubes.

The theoretical and experimental results obtained by him are clearly of wide interest, and it is, therefore, of some importance to consider how they are related to certain other work on these topics.

Haeff considers first-order perturbations of the form

$$V = V_0 \exp(\Gamma z + j\omega t),$$

where Γ is the propagation constant corresponding to a frequency ω, in a medium composed of k streams of particles, each of charge e and mass m, of which the typical ith component stream has a particle density ρ_i and velocity v_i (presumably directed along the z axis). He states that Γ is determined by the following equation:

$$\Sigma_1^k \omega_i^2/[(\omega + j\Gamma v_i)^2] = 1, \qquad (1)$$

where

$$\omega_i^2 = e/m \cdot \rho_i/\epsilon.$$

In this way, for the special case $k=2$, and $\omega_1 = \omega_2$, he finds that spatial amplification occurs over a limited range of values of the factor $\omega(v_1 - v_2)/\omega_1(v_1 + v_2)$. Apparently, the corresponding field wave has no magnetic component, no transverse electric component, and no associated Poynting flux.

This mechanism may be compared with two other mechanisms of plane wave-amplification which were published about seven months previously by J. R. Pierce[2] and V. A. Bailey,[3] respectively.

In Pierce's theory of fluctuations in a stream of electrons, he considers the perturbations which can arise through the presence of a second stream of charged particles, namely, positive ions, and obtains an equation for determining Γ which is formally very similar to Eq. (1). This theory yielded plane wave-amplification even when the stream velocity of the positive ions was neglected.

Bailey's theory of spontaneous waves in discharge tubes and in the solar and other atmospheres is based on the general investigation of plane waves in an ionized gas which is pervaded by static electric and magnetic fields $\mathbf{E}_0$ and $\mathbf{H}_0$, respectively. It was found that, in general, over several ranges of frequency, the ionized medium acts as an amplifier for one or more of the eight possible types of wave, of a given (real) frequency, which can travel through it, and that through this mode of wave-amplification almost any initial random fluctuation can grow into electric noise. The presence of a static electric field was found to be essential and that of a static magnetic field to be favorable to such amplification. The fundamental equations of this theory (when the vibrations of the positive ions are neglected) were given in a paper read to the Royal Society of New South Wales on June 2nd, 1948, and published in its Journal.[4] It was there shown that the (complex) wave number[5] l is related to ω by a dispersion equation equivalent to

$$X(Y^2 - \Omega_1^2 Z^2) + U_T^2 l^2[Y(R - i\nu) - \Omega_1^2 Z] - RY\Omega_T^2 Z - 2lRZ\Omega_1 \boldsymbol{\Omega}_T \cdot \mathbf{U}_T = 0 \qquad (2)$$

where

$X = R^2 - \tau l^2 - 1 - i\nu R$, $\quad Y = RZ + R - i\nu Z$,
$Z = l^2 - \omega^2$, $\quad R = \omega - U_1 l$,
$\mathbf{U}_0$ = the mean drift velocity of the electrons,
$\boldsymbol{\Omega}_0 = -\mathbf{H}_0 e/mc$, (using Gaussian units),
ν = the collision-frequency of an electron with molecules,
τ = one-third of the mean square velocity of agitation of the electrons,

the subscripts 1 and T, respectively, denote components along, and transverse to, $0z$, the direction of wave-propagation, and the units of velocity $\mathbf{U}_0$ and frequency ω, are taken as equal, respectively, to c, the velocity of light and p, the electron plasma frequency.

It can be deduced from Eq. (2) that, when ν is not too large, wave-amplification exists in certain frequency-bands under any one of the following three simple conditions:

1. $\mathbf{U}_0$ and $\mathbf{H}_0$ are parallel to $0z$ and $\tau = 0$.
2. $\mathbf{U}_0$ is oblique to $0z$, $\mathbf{H}_0 = 0$ and $\tau = 0$.
3. $\mathbf{U}_0$ is parallel to $0z$, $\tau > U_0^2$ (approx.) and $\mathbf{H}_0 = 0$.

These offer simple examples of wave-amplification occurring (in Haeff's phrasing) "without the presence of any field-supporting resonant or wave-guiding structures." Moreover, in some of these examples there is an associated Poynting flux.

It will thus be seen that in order to explain solar and other electric noise it is not *necessary* to postulate (with Haeff) interaction of two or more different components of the stream. It is, however, important to note that the superposition, on a single stream of charged particles, of other streams or of a static magnetic field or of random motions of the particles—each and all increase the existing capacity of the medium to amplify plane waves.

These considerations do not however diminish the importance of Haeff's contributions to the subject of wave-amplification.

[1] A. V. Haeff, Phys. Rev. **74**, 1532 (1948).
[2] J. R. Pierce, J. App. Phys. **19**, 231 (1948).
[3] V. A. Bailey, Nature **161**, 599 (1948).
[4] J. Roy. Soc. of New South Wales, Vol. LXXXII, p. 107 (1948). The more complete theory, including the motions of the positive ions, is given in the Australian Journal of Scientific Research **1**, 351 (1948).
* Here equivalent to $i\Gamma$.

Alpha-Radioactivity in Elements Lighter than Bismuth

N. E. Ballou
Naval Radiological Defense Laboratory, San Francisco, California
February 16, 1949

An examination has been made of the possibility of existence of alpha-emitting nuclides of elements below bismuth in atomic number. The liquid-drop model of the nucleus[1] and the effects of closed shells in nuclei[2] are utilized in obtaining the following conclusions. Some experimental work has been done to test these conclusions, and the results obtained to date are summarized at the end of this note.

According to the liquid-drop theory the energy for alpha-particle emission increases with decreasing mass number for a given element. Consequently, the possibility of alpha-emission competing significantly with beta-emission is greatest with those isotopes on the light side of stability. Of course, the most favorable case for alpha-particle emission is that in which the energy for beta-disintegration is zero or very small. If such a nuclide of low beta-disintegration energy differs in composition from that of a closed shell nuclide by an alpha-particle, it is postulated that alpha-disintegration may be the important mode of decay.

A thorough analysis of stability of nuclei has been made by Kohman.[3] He lists twenty-one unknown nuclides on the neutron deficient side of stability which are of low beta-disintegration energy and some of which may be beta-stable. These are the nuclides which should be examined for alpha-radioactivity. Even though some of them may be beta-unstable, alpha-branching may occur to an extent large enough to be detectable. Others may be beta-stable but alpha-unstable with half-lives short enough to allow their detection. Such instability would then be the cause of their non-existence on earth.

Of especial interest are the nuclides Ti^{44}, Sm^{146}, and 61^{145}. Alpha-decay in these results in the formation of Ca^{40}, Nd^{142}, and Pr^{141}; these latter are all closed shell nuclei. The possibility of 61^{145} being an alpha-emitter and the experiments in progress to prepare it by neutron irradiation of samarium have been described previously.[4] In this neutron irradiation of samarium there is some Sm^{146} formed by neutron capture in Sm^{144}; measurable amounts of Sm^{146} may be produced due to the long half-life of Sm^{145} [5] and the probability that its neutron capture cross section is large since it is an odd-odd nucleus.

Attempts to produce Ti^{44} by irradiations of Sc^{45} with 19-Mev deuterons have been made.[6] As yet no alpha- (or beta-) activity due to this isotope has been detected; its half-life must then either be less than about a minute or greater than several hundred years. Although Zr^{88} would not go to a closed shell nucleus by alpha-decay, it was also examined for alpha-radioactivity since its beta-disintegration energy is calculated to be small and it is on the neutron deficient side of stability. Production of this nuclide was attempted by irradiation of Y^{89} with 19-Mev deuterons. The same results and conclusions were obtained for Zr^{88} as for Ti^{44}. More extensive deuteron irradiations of Sc^{45} and Y^{89} are in progress in an effort to produce detectable amounts of Ti^{44} and Zr^{88}.

[1] N. Bohr, and J. A. Wheeler, Phys. Rev. **56**, 426 (1939); E. Feenberg, Rev. Mod. Phys. **19**, 239 (1947).
[2] M. G. Mayer, Phys. Rev. **74**, 235 (1948).
[3] T. P. Kohman, Phys. Rev. **73**, 16 (1948); T. P. Kohman, AEC Document AECD-2060 (1948).
[4] N. E. Ballou, Phys. Rev. **73**, 630 (1948).
[5] M. G. Inghram, R. J. Hayden, and D. C. Hess, Jr., Phys. Rev. **71**, 643 (1947).
[6] This portion of the work has been done at the Radiation Laboratory, University of California, Berkeley, with the support of the AEC.

The Determination of the Mass of N_7^{16} by Means of Interpolation

Tibor Z. Szelenyi
Budapest, Hungary
December 29, 1948

It has not yet been possible to determine the exact nuclear mass of N_7^{16}. This is due to the fact that one does not know either the energy maximum of its beta-spectrum, nor did one succeed to determine its reaction energies. It is only possible to indicate the limits between which the exact mass must be. The limits are the following: 16.0065–16.011 MU.[1] In Mattauch's Tables we find the value: 16.00645 MU, and according to Barkas' computations[2] the mass of N_7^{16} coincides with the given upper limit, namely it is 16.0114 ± 0.0020 MU.

With the aid of a simple interpolation method which is accurate enough, we are able to determine the mass which we are in search of. We plot the mass defect (md) differences of the isobars $X_{Z-1}^{A} - Y_Z^A = \Delta E_{4n}$ as functions of A. ($A = 4, 8, 12, \cdots 36$, and $Z = A/2$.) (See Fig. 1.)

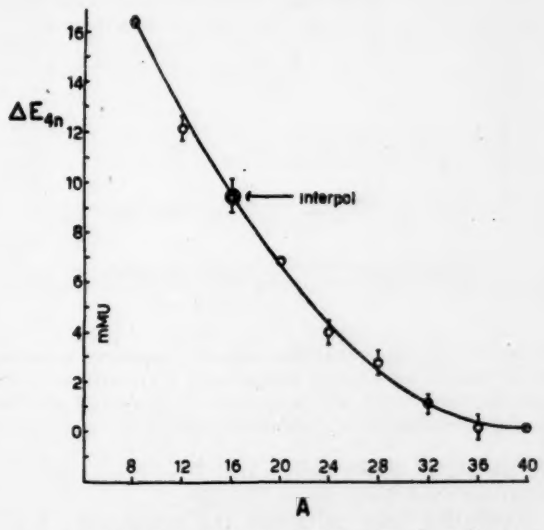

Fig. 1. Mass defect differences of isobars $X_{Z-1}^{A} - Y_Z^A$ as a function of A.

Interpolating now we also find the md difference of the $N_7^{16} - O_8^{16}$ isobars. Since the md of O_8^{16} is known we obtain the md and mass of N_7^{16}.

Seeing that the values of the md's themselves are of a higher order than their differences, the precision of the conclusions drawn from the differences is reliable.

If we interpolate on the curve ΔE_{4n} we get for the 16 isobars the value: 9.4±0.6 mMU. (The possible mean error was estimated from the graph.)

Subtracting this from the md of $O_8^{16}=136.61\pm0.2$ mMU, we get 127.2±0.7 for the md, and finally 16.0102±0.0007 MU for the mass of N_7^{16}.

[1] Hans A. Bethe, *Elementary Nuclear Theory* (John Wiley and Sons, Inc., New York, 1947).
[2] Walter H. Barkas, Phys. Rev. **55**, 691 (1939).

Energy of Beta-Rays from K^{40}

J. J. Floyd and L. B. Borst
Brookhaven National Laboratory, Upton, New York*
February 21, 1949

A NEW enriched sample of K^{40} prepared by the Electromagnetic Division of the Carbide and Carbon Chemical Corporation, Oak Ridge, Tennessee,[1] has been examined to redetermine the maximum β-ray energy, previously reported as $E_m=1.9\pm0.2$ Mev.[2] The new sample is enriched about 100-fold in K^{40} and has the following analysis: K^{39} 76.6±0.5 percent, K^{40} 1.31±0.05 percent, K^{41} 22.1±0.5 percent. 233 mg of KCl were mounted on thin aluminum (7 mg/cm²) using a sample thickness of 33 mg/cm². The same counting geometry previously described[2] was used. Figure 1 shows the

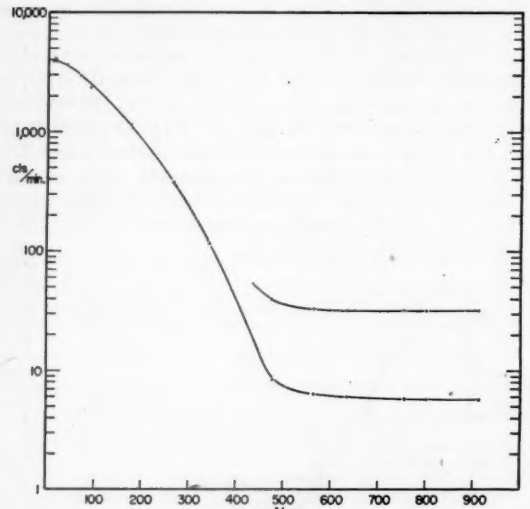

FIG. 1. Counting rates for different absorber thicknesses. Upper curve, measured counting rates; lower, rates with background counts subtracted.

absorption curve, the upper data give the measured counting rates, the lower, less counter background. Examination of the original data shows the end point to be between 625 and 700 mg/cm² corresponding to a maximum energy $E_m=1.45\pm0.15$ Mev.

The sample previously investigated is being reinvestigated to determine the basis of the earlier value.

A penetrating γ-ray component (5.7 counts/min.) is observed. In the geometry used the ratio of γ-counts to β-counts is $I_\gamma/I_\beta=0.0014$. Using a thin sample of Na^{24} in the same geometry $I_\gamma/I_\beta=0.046$. Since Na^{24} is known to have one 1.38-Mev and one 2.76-Mev γ-ray for each β-ray,[3] about 60 percent of the disintegration rate is due to the 1.38-Mev component $I_{1.38}/I_\beta=0.028$. The ratio of these values gives an approximate ratio of disintegration constants for γ- and β-emission in K^{40}. The value so obtained is $\lambda_\gamma/\lambda_\beta=0.05\pm0.01$.

A new determination of the β-ray disintegration constant was made using a thin sample (6 mg/cm²) of KCl weighing 19.7 mg. The counting rate at 21 percent geometry corrected to zero absorber was 350 counts/min. The disintegration constant for β-decay is therefore $\lambda_\beta=4.3\pm0.4\times10^{-10}$ yr.$^{-1}$. The disintegration constant for γ-ray emission is correspondingly $\lambda_\gamma=0.21\pm0.05\times10^{-10}$ yr.$^{-1}$.

* Research work carried out under auspices of the AEC.
[1] Obtained through the Stable Isotope Division, Atomic Energy Commission, Oak Ridge, Tennessee.
[2] L. B. Borst and J. J. Floyd, Phys. Rev. **74**, 989 (1948).
[3] Marcellus L. Wiedenbeck, Phys. Rev. **72**, 429 (1947).

Exchange Moments of H^3 and He^3

R. Avery* and E. N. Adams II**
Department of Physics, University of Wisconsin, Madison, Wisconsin
February 14, 1949

IT has been shown that the assumption of an interaction between nucleons which involves a space exchange operator implies the existence of exchange currents which may give a non-vanishing contribution to the magnetic moment of a nucleus.[1] In the expression for the exchange moment of the H^3 nucleus, obtained when using a Gauss potential and Gauss wave function, the major contribution to the exchange moment is proportional to the strength of the tensor interaction and to the amplitude of the ^4D part of the wave function. Since the value of the H^3 exchange moment was found to be much smaller than the H^3 moment anomaly,[2] it was concluded that this exchange moment is inadequate to account for the anomaly.

Recent work[3] on interactions with the Yukawa radial dependence has had the result that a relatively large amount of tensor interaction is required to fit the low energy deuteron data, particularly if the tensor and central ranges are taken to be the same. A stronger tensor interaction would be expected to favor a correspondingly larger exchange moment, so it seemed worth while to reinvestigate the magnitude of the exchange moment using Yukawa potentials. Several interactions were considered:[4] they were similar in that they all had "symmetrical" exchange properties and range of ordinary forces equal to the Breit range ($M\sim326m_e$); they differed in the strength and range of the tensor force.

The wave function used was the simple mixture of ^2S and ^4D used by Gerjuoy and Schwinger.[5] Since particularly accurate wave functions did not seem necessary, simple Gauss radial functions were considered in the beginning. A variational calculation to minimize the energy showed the Gauss radial functions to be completely unsatisfactory, inasmuch as no binding was obtained even on the assumption of an all central interaction;[6] consequently, the radial dependence $\exp\{-a(r_{12}+r_{23}+r_{31})\}$ was adopted. With this radial dependence one easily finds 200 percent binding of H^3 on the assumption of all central forces.[7]

When the interactions involving a tensor force are introduced into the variational calculation, no binding is obtained unless the tensor range is taken to be longer than that of the central forces.[8] As a consequence the interaction finally adopted[9] had a tensor range appreciably longer ($M\sim245m_e$) than the Breit range. The minimum of energy (60 percent of the experimental binding energy) was found for a choice of the parameters:

$$a_S=2.70/r_0, \quad a_D=5.22/r_0, \quad D^2=2.6 \text{ percent},$$

where D^2 is the ^4D probability and r_0 is e^2/m_ec^2.

The calculated exchange moment of H^3 was 0.016 n.m., to be compared with 0.035 n.m. obtained with the Gauss potential.[1] This reduction comes about directly as a conse-

quence of the long range of the tensor interaction. With a long tensor range a weaker tensor force suffices to give account of the deuteron quadrupole moment, and with a weaker tensor force the ^4D probability in H^3 is reduced. The exchange moment, which is proportional to both the ^4D amplitude and the strength of the tensor forces, is thus doubly reduced. Since it seems unlikely that an interaction which involves very strong tensor forces will give enough binding for H^3, we can probably conclude that this exchange moment will not make a major contribution to the H^3 moment anomaly.

Parallel calculations with inclusion of the Coulomb energy were made for He^3 in order to estimate the effects of the small difference between the H^3 and He^3 wave functions on the sums of the ordinary and exchange moments;[1,10] these effects are completely negligible.

This problem was suggested by Professor R. G. Sachs, who gave us much helpful advice; we were materially aided by information supplied us by Professor Herman Feshbach.

* Work supported by Wisconsin Alumni Research Foundation.
** AEC Predoctoral fellow.
[1] R. G. Sachs, Phys. Rev. **74**, 433 (1948).
[2] R. G. Sachs, Phys. Rev. **72**, 312 (1947).
[3] G. F. Chew and M. L. Goldberger, Phys. Rev. **73**, 1409 (1948).
[4] Reference 3, also W. Rarita, (priv. comm.); J. Eisenstein and F. Rohrlich (priv. comm.).
[5] E. Gerjuoy and J. Schwinger, Phys. Rev. **61**, 138 (1942).
[6] R. G. Sachs and M. Goeppert-Mayer, Phys. Rev. **53**, 991 (1938).
[7] Huang, Frohlich, and Sneddon, Proc. Roy. Soc. **A191**, 61, who investigated the binding of light nuclei using the Møller-Rosenfeld potential, found that such functions are a very good approximation to the exact solution of the Schroedinger equation for the problem in the absence of tensor forces.
[8] H. Primakoff, Phys. Rev. **72**, 118 (1947).
[9] Eisenstein and Rohrlich. The use of this interaction was suggested to us by H. Feshbach.
[10] R. G. Sachs, Phys. Rev. **69**, 611 (1946).

Radioactivity of K^{40}*

ROBERT W. STOUT
Massachusetts Institute of Technology, Cambridge, Massachusetts
February 7, 1949

A DETERMINATION of the beta-radioactivity of K^{40} has been made by an internal calibration of KCl sources with standardized amounts of Na^{24}. If the near identity of the absorption curves of the spectra of Na^{24} and K^{40} reported by Hirzel and Wäffler[1] is assumed, the method of internal calibration of the potassium source eliminates the need of corrections for differences in self-absorption, geometry, back-scattering, and intrinsic counter efficiency for the two activities. Fortunately, the short half-life of Na^{24} (14.8 hours) makes the method experimentally practical, for the sodium can be "removed" after it has been used for calibration by simply allowing it to decay.

A Co^{60} standard prepared by the National Bureau of Standards was used to calibrate an approximately equal activity of impurity-free Na^{24} on both a platinum and copper cathode gamma-counter. The ratio of the efficiency of the platinum counter for the detection of the gamma-rays of Co^{60} to its efficiency for the detection of the gamma-rays of Na^{24} was taken as 0.664, and the corresponding ratio for the copper counter as 0.584. These values are from coincidence measurements by Peacock.[2] Small corrections of the order of 2 percent were made in each case for the difference in absorption of the gamma-rays from the two activities in traversing quarter-inch aluminum and sixteenth-inch lead shields surrounding the counters. The statistical error in counting and the uncertainty in the assumed efficiency ratios amounted to about 4 percent in each case, while the value of Na^{24} activity measured on the copper counter agreed with that measured on the platinum to within 3 percent. A small aliquot of the Na^{24} solution, measured by pipetting and checked gravimetrically, was added to about 4 grams of KCl in solution. The mixture was brought to dryness in a nickle crucible and ground to insure homogenous distribution of the sodium activity throughout the KCl.

Eighth-inch thick aluminum slides with the active material held in circular depressions of $\frac{3}{32}$" depth and 5.7 square centimeters area served as source holders. The slides were held rigidly in a channel provided in the counter support, with the KCl directly beneath the 10-micron mica window of a bell-shaped beta-counter. Reproducibility of geometry and constancy of the counter efficiency were checked regularly with a thick standard source of potassium chloride. The slides were counted periodically from the original measurement, when the beta-activity of the sodium was about thirty times that of the K^{40}, until all but a negligible amount of the sodium had decayed—a total of seven measurements for each source. During the first two counting periods, an experimentally determined correction of about 3 percent was made for the effect of the Na^{24} gamma-rays, this correction being applied to all later measurements. The seven resulting counting rates for each slide gave points on the decay curve of Na^{24}, with the activity of the K^{40} present as a constant background.

From these data a best value for the counting rates of the potassium and the sodium at some initial time was calculated for each of the sources. Over the range of source thicknesses used, the ratio of the counting rates, and therefore the ratio of the net efficiencies of the counter for the two spectra, was independent of source thickness to within the statistical error of 2 percent. (See Table I.)

TABLE I. Ratio of counting rates for various thicknesses of sources.

Source thickness in milligrams/cm²	Na^{24} betas/K^{40} betas
43	32.2
63	33.2
74	32.8
79	32.9
97	33.0

If the absorption curves of the two spectra are identical, then their net counting efficiencies may be taken as equal. The ratio of the known activity of the sodium in each source to the activity of the potassium is then equal to the ratio of the counting rates of the two. An average of the data from the five sources gives the specific activity of potassium as 30.6 ± 2.0 betas/second/gram of ordinary potassium.

I should like to express my appreciation to Professor M. Deutsch for suggesting the method employed and to Dr. R. K. Osborne for his constant advice during the course of this research.

* Supported in part by the joint program of the ONR and the AEC.
[1] O. Hirzel and H. Wäffler, Phys. Rev. **74**, 1553 (1948).
[2] W. C. Peacock, Ph.D. Thesis, Massachusetts Institute of Technology (1944).

The Beta-Ray Spectra of Cu^{64} and the Ratio of $N+/N-$

C. S. WU AND R. D. ALBERT
Columbia University, New York, New York
February 14, 1949

IN a previous Letter to the Editor[1] reporting the investigations on the negatron and positron spectra of Cu^{64}, we pointed out that a gradual but consistent reduction of deviation *versus* the source thickness at low energy region has been observed and with the thinnest ($\sim$0.1 mg/cm²) and most uniform source prepared, the deviation was found to be much less than previously reported in other laboratories.[2–4] Since the theoretical interpretation of the experimental results involves the Coulomb correction factor which is particularly sensitive for positrons in the low energy region, the screening and relativistic corrections calculated by Longmire and Brown[5]

were used. In carrying out the calculations, they had overlooked one factor which is of importance to this comparison. When this is considered, their results are in good agreement with the corrections calculated by M. E. Rose[6] for negatrons which are indeed negligible. However, the corrections for positrons turn out to be considerably larger than those for negatrons. These small corrections do not account for all the deviations observed in the low energy region where the true distribution of electrons is susceptible to distortion due to the finite source thickness and backing. Nevertheless these corrections improve the over-all agreements. In Fig. 1, we have re-

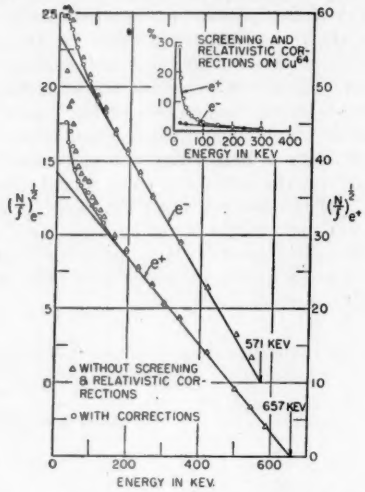

FIG. 1. Kurie plots of Cu^{64} negatron and positron spectra.

plotted the Kurie plots of Cu^{64} negatron and positron spectra. In the upper right corner of Fig. 1 is an insert of the revised screening and relativistic corrections for Cu^{64}. With these corrections, the negatron curve now starts to deviate from the straight line in the Kurie plot around 130 kev, and the positron curve begins to deviate around 140 kev. Even at 50 kev the deviation from the Kurie plot for negatrons is less than 6 percent, for positrons not more than 8 percent. In Fig. 2, the

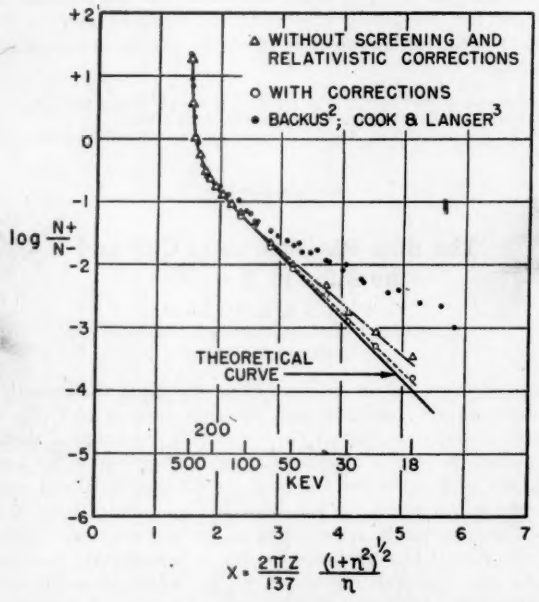

FIG. 2. The ratio of the number of positrons to the number of negatrons as a function of energy.

logarithm of the ratio of the positrons to negatrons is plotted against x. The theoretical curve is drawn according to the approximation formula where $Z_{Ni}=Z_{Zn}=Z_{Cu}$. If the exact equation is used, the theoretical curve will be rotated upward approximately one degree in Fig. 2. This figure illustrates that even without screening and relativistic corrections, the experimental value of the ratio of positrons to negatrons is less than twice the theoretical value at 18 kev. However, when the corrections are applied, the agreement between the experimental and theoretical values is excellent. The dotted curve in Fig. 2 shows the data of Backus[2] and Cook and Langer[3] adjusted to our data in the high energy region.

If there is distortion due to elastic backscattering or change of detector efficiency with energy, this should affect the electron and positron curves equally, and thus the ratio $N+/N-$ should remain unaffected. On the other hand, the inelastic scattering effects must be small here. Otherwise, they would tend to affect the positrons more than the electrons at low energies due to the sharper low energy "cut-off" of the positron momentum distribution curve and, thus, increase the $N+/N-$ ratio at low energies.

The good agreement between the theoretical and experimental curves in Fig. 2 indicates that the Fermi theory probably does approximate the true distributions for negatrons and positrons at low energies. In any event, any remaining true deviations must be much smaller than has been previously suggested.[2,3]

[1] C. S. Wu and R. D. Albert, Phys. Rev. 75, 315 (1949).
[2] John Backus, Phys. Rev. 68, 59 (1945).
[3] C. S. Cook and L. M. Langer, Phys. Rev. 73, 601 (1948).
[4] G. E. Owen and H. Primakoff, Phys. Rev. 74, 1406 (1948).
[5] C. Longmire and H. Brown, Phys. Rev. 75, 264 (1949).
[6] Morris E. Rose, Phys. Rev. 49, 727 (1936).

The Fundamental Band of Carbon Monoxide at 4.7μ in the Solar Spectrum*

MARCEL V. MIGEOTTE**
Mendenhall Laboratory of Physics, The Ohio State University, Columbus, Ohio
February 17, 1949

DURING 1948 high dispersion spectrograms of the sun were obtained in Columbus, Ohio using a prism-grating infra-red spectrograph designed by Dr. R. Noble under the direction of Professor H. H. Nielsen (instrument of the Pfund type, focal length of the parabolic mirrors: 100 cm, aperture: f/5). The installation was equipped with a rapid response Perkin-Elmer thermopile, an electronic amplifier of the same firm, and a Brown recorder. In particular, the region extending from 2250 cm^{-1} (4.44μ) to 1990 cm^{-1} (5.02μ) was mapped with an echelette grating ruled with 7200 lines per inch. Spectral lines 0.5 cm^{-1} apart are clearly separated.

The new solar spectrograms have been compared with measurements published in 1947 on the fundamental bands of $C^{12}O^{16}$ and $C^{13}O^{16}$ situated in the 4.7μ region.[1] In this publication the wave numbers of 51 rotational lines are given for the fundamental band of $C^{12}O^{16}$. It is stated that the positions of the lines are reliable to about ±0.07 cm^{-1}.

In the solar spectrum part of the CO band (from R_{15} to R_{28}) falls in a region of stong absorption due to the 4.5μ band of N_2O^2 and to the 4.3μ band of CO_2. Of the 38 remaining lines, twenty correspond within ±0.10 cm^{-1} to sharp lines observed in the solar spectrum while the eighteen others are masked by stronger lines or may be found in the wings of such lines. The distribution of intensities also corresponds to that observed in the laboratory. Hence, it may be stated that the fundamental band of $C^{12}O^{16}$ is present on the observed solar spectrograms. Because of the complexity of these spectrograms it has not been possible to decide with certainty about the identification of the fundamental band due to $C^{13}O^{16}$.

A striking change in intensity was observed for the band identified as CO when the solar spectrum was observed on different days. On April 25, May 26, and May 31, 1948 this band was intense; for example, the line noted R_3 by Lagemann, Nielsen, and Dickey[1] had a central absorption of about 50 percent on a spectrogram taken at 4 P.M. on May 31. On records obtained on June 16 and 17, 1948 the CO band was weak; for example, the central absorption of R_3 was observed to be about 15 percent on a spectrogram taken at 9 A.M. on June 16. For the same days an intensity change of the same order was also noted, in the same spectral region for several lines due to CO_2, while no appreciable change was observed for the 4.5μ band of N_2O. Hence, it may be concluded that the absorption by CO and CO_2 was enhanced in the atmosphere of Columbus, Ohio during April and May, 1948. CO may also be expected in the solar atmosphere. However, it is believed that the solar contribution to the band observed at 4.7μ is negligible.

Details on our observations of the solar spectrum will be published in the Astrophysical Journal.

* This work was carried out, in part, under contract between the Air Materiel Command Wright Patterson Air Force Base and the Ohio State University Research Foundation.

** Now at the Institut d'Astrophysique, University of Liege, Belgium.

[1] R. T. Lagemann, A. H. Nielsen, and F. P. Dickey, Phys. Rev. **72**, 284 (1947).

[2] M. Migeotte, The Astronomical Journal **54**, 45 (1948); J. H. Shaw, G.B.B.M. Sutherland, and T. W. Wormell, Phys. Rev. **74**, 978 (1948).

Shape of the Beta-Spectrum of the Forbidden Transition of Yttrium 91

LAWRENCE M. LANGER AND H. CLAY PRICE, JR.
Indiana University, Bloomington, Indiana
February 16, 1949

THE momentum distribution of the negatrons emitted in the 57-day disintegration of $_{39}Y^{91}$ has been determined as being different from the spectrum expected for an allowed transition. The exact shape of the spectrum gives confirmation for the shell structure model of the nucleus and for the validity of Gamow-Teller selection rules.

The measurements were made in the large, high resolution, magnetic spectrometer.[1] The activity, obtained carrier-free from Oak Ridge, was further separated from the alkaline earths. The source had a thickness of about 0.15 mg/cm^2 and was uniformly deposited on a plastic (LC-600) backing of 0.02 mg/cm^2 and held at ground potential. Both mica and thin Zapon window counters were used in appropriate and overlapping energy regions, and the data were adjusted to the same intensity level at one point.

Figure 1 shows a conventional Fermi plot of the data. The Coulomb function, F_B was evaluated by means of Bethe's approximation,[2] which was found to be in very good agreement with that calculated by expanding the complex Γ-function. It is obvious from Fig. 1 that the Fermi plot is not the straight line which is characteristic of allowed transitions and which has also been found for many presumably forbidden transitions.[3] It is instead, definitely curved, being convex toward the energy axis near the end point.[4] The maximum energy release is 1.53 Mev.

According to its "comparative lifetime" ($f=4.7\times10^8$), this transition would be empirically classified as twice-forbidden. However, Feenberg and Hammack's[5] analysis of the shell structure in nuclei leads to the prediction of a spin change of 2 units, together with a parity change. Such a transition is theoretically classified as once-forbidden under Gamow-Teller selection rules. According to the theory of forbidden spectra,[6] it also has the special property that only one type of nuclear matrix element fails to vanish for it. This means that a unique energy dependence is predicted, differing from the allowed shape by the factor

$$a\sim[(W^2-1)+(W_0-W)^2],$$

where W is the electron's energy in mc^2 units, and $W_0=4.01$ is the end point.

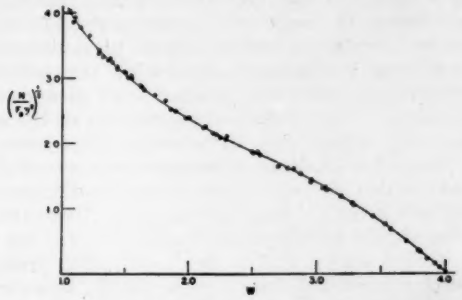

FIG. 1. Conventional Fermi plot for Y^{91} beta-spectrum.

When the ordinates of the curve in Fig. 1 are divided by a, a straight line should be obtained if the above outlined theory is correct. The actual result is shown in Fig. 2. The striking agreement with the theoretical expectations furnishes good evidence for the reliability of the shell model. It also provides the first piece of evidence for the validity of the Gamow-Teller rules based on a spectrum shape.

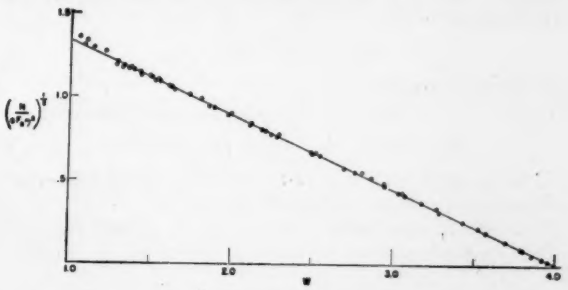

FIG. 2. Forbidden Fermi plot for Y^{91} beta-spectrum. Here the ordinates are divided by the additional factor,

$$a^{\frac{1}{2}}\sim[(W^2-1)+(W_0-W)^2]^{\frac{1}{2}}.$$

This work has been assisted by a grant from the Frederick Gardner Cottrell Fund of the Research Corporation and by the joint program of the ONR and AEC.

[1] L. M. Langer and C. S. Cook, Rev. Sci. Inst. **19**, 257 (1948).

[2] H. A. Bethe and R. F. Bacher, Rev. Mod. Phys. **8**, 194 (1936).

[3] Kai Siegbahn, Phys. Rev. **70**, 127 (1946).

[4] A similar non-allowed shape has been obtained for the spectrum of Cs^{137} by C. L. Peacock and confirmed by the authors. Because of the low energy of the end point, the presence of strong internally converted gamma-radiation and a weak second group of electrons, the interpretation in this case is less definitive. A full report of this work will be published later.

[5] E. Feenberg and K. C. Hammack, private communication.

[6] E. J. Konopinski and G. E. Uhlenbeck, Phys. Rev. **60**, 308 (1941); Emil J. Konopinski, Rev. Mod. Phys. **15**, 226 (1943).

Threshold Energy for Meson Production

WALTER H. BARKAS
Office of Naval Research, San Francisco, California
February 14, 1949

THE threshold energy for the production of mesons by colliding systems of elementary particles can be calculated by a simple relativistic extension of the principles employed in deducing the "Q" and the threshold beam energy for ordinary nuclear reactions. This calculation does not re-

quire a knowledge of the internal dynamics of the participating systems; only their mass energies are required in order to set a rigorous lower limit on the beam energy for single or multiple production of mesons.

The most convenient coordinate frame for the analysis of the threshold is that in which the center of gravity of the colliding systems is at rest. The net momentum then vanishes, and when the kinetic energy of all products also vanishes, the threshold for the reaction leading to these particular products has been reached. Furthermore, the absolute threshold for the production of any particular product, such as a meson, is reached when all other products of the reaction are left in their combined state of lowest energy (often a single system in its ground state). For example, when protons bombard C^{12} the threshold reaction yielding positive mesons is the one simultaneously producing C^{13} in its ground state. Above threshold resonances should be observable in which C^{13} is left in its various excited states, and at any bombarding energy the meson spectrum should show a corresponding structure near the upper energy limit. On the other hand, the threshold production of negative mesons, when neutrons bombard Li^7, yields in addition two alpha-particles of zero kinetic energy.

For a quantitative treatment suppose that in laboratory coordinates a moving system, mass m, of kinetic energy T' bombards a target system, mass M, at rest. The sum of their kinetic energies, T, in the center-of-gravity system is then:

$$(m+M)c^2\{[1+(2MT'/(m+M)^2c^2)]^{\frac{1}{2}}-1\}. \quad (1)$$

For a reaction leading to particular products of mass m_1 and other products of total rest mass M_1 in their ith discrete energy state, we have:

$$(m+M)c^2=(m_1+M_1)c^2+Q_i, \quad (2)$$

as the defining equation for Q_i.

We set $T=-Q_i$ and thus obtain as a general theorem:

$$T_i'=[(m_1+M_1)^2-(m+M)^2]c^2/2M, \quad (3)$$

T_i' being the kinetic energy of the beam in the laboratory system at which the ith resonance occurs.

The absolute thresholds of a number of typical reactions leading to single meson production are given in Table I.

TABLE I. Thresholds for typical reaction leading to single meson production.

Beam	Target	Meson produced	Other products	Threshold Mev
γ	p	Pos.	n	159
γ	C^{12}	Pos.	B^{12}	161
γ	C^{12}	Neg.	N^{12}	165
p	p	Pos.	d	301
p	C^{12}	Pos.	C^{13}	155
p	C^{12}	Neg.	$N^{12}+p$	178
n	p	Neg.	$2p$	301
n	p	Pos.	$2n$	306
n	C^{12}	Neg.	N^{13}	156
n	C^{12}	Pos.	B^{13}	168
d	C^{12}	Pos.	C^{14}	162
d	C^{12}	Neg.	O^{14}	166
α	C^{12}	Neg.	F^{16}	207
α	C^{12}	Pos.	N^{16}	202

Masses of bare nuclei have been used in the calculations, the coupling to electronic systems being quite negligible in the energy range where mesons are produced. The meson mass used was 286 electron masses.

This type of threshold calculation invokes the over-all conservation of momentum and energy. The internal kinetic energies[1] of the reacting systems and the Coulomb barriers will enter only if one undertakes further to estimate cross sections for such reactions. A deficiency of internal kinetic energy, as in the deuteron, may increase the *observable* threshold if mesons can be produced only by the energetic collisions of pairs of nucleons, but lower thresholds than those here calculated cannot be obtained consistent with energy and momentum conservation. However, when one compares the threshold energy (3) with that calculated by the admittedly approximate theory of McMillan and Teller, their result often is considerably *lower*. The discrepancy arises because their formulation is inexact in the following details:

(a) The meson is supposed to be produced by the collision of a beam nucleon with a target nucleon, which at that instant is approaching the beam nucleon. The velocities then compound to raise the available energy. In order for the momentum of the target nucleus to remain zero, however, the remaining nucleons of the target must instaneously have a net momentum in the direction of the beam. The corresponding kinetic energy term, which will usually be small, has been omitted. Furthermore, the velociy of the remainder of the nucleus makes it necessary to calculate the kinetic energy of the product nucleons in the moving reference frame of the assemblage before equating their kinetic energies to the Fermi energy. McMillan and Teller neglected this effect.
(b) Errors are introduced by their use of non-relativistic mechanics.
(c) In the light nuclei, especially, the binding energy[2] of a nucleon to the nucleus may deviate widely from 8 Mev, and as they note the kinetic energy may be poorly approximated by the Fermi energy.
(d) The threshold state is not, as assumed, that in which the meson has zero kinetic energy in the laboratory coordinates, but one in which it has the velocity of the center of gravity of the reacting systems.

The valuable comments of Professor Robert Serber in discussions with the writer on this subject are much appreciated.

[1] W. G. McMillan and E. Teller, Phys. Rev. **72**, 1 (1947).
[2] W. H. Barkas, Phys. Rev. **55**, 692 (1939), Fig. 1.

Erratum: On the Numerical Calculation of the Internal Conversion in the *K*-Shell—The Electric Dipole Case

[Phys. Rev. **75**, 534 (1949)]

B. A. GRIFFITH AND J. P. STANLEY
University of Toronto, Toronto, Canada

IN the above letter,

(1) The formula for I_K should read as follows:

$$I_K=\frac{\gamma^{3+2\beta}\{[1+\beta+(1/\theta)]^2-1\}^{-(1+\beta)}e^{b\pi}|\Gamma(1+\beta-ib)|^2}{24(137)(2+\beta)\Gamma(3+2\beta)|(-z)^{-(1+\beta-ib)}|^2}\times[2|P|^2+|Q|^2].$$

(2) The explanation of $2I_K$ given in the note below Table I is based on Hulme's simplified model of the system considered. This is now known to be incorrect. Accordingly, the first paragraph of this note should read as follows:

In the above table, $2I_K$ represents the ratio of observed K-electrons to observed photons of energy $h\nu$. No allowance for screening effects has been made.

For further details, see N. F. Mott, and I. N. Sneddon, *Wave Mechanics and Its Applications* (Oxford University Press, London, 1948).

Alpha-Particle Ionization in Argon and in Air and the Range-Energy Curves

WILLIAM P. JESSE AND JOHN SADAUSKIS
Argonne National Laboratory, Chicago, Illinois
February 17, 1949

WE have recently compared by a method already described[1,2] the relative ionization for individual samarium and polonium alpha-particles in argon and in air. We find the ionization for samarium relative to polonium about 5 percent less in air than in argon. These preliminary measurements would indicate what has long been suspected,[3] that, while in hydrogen and the noble gases the total alpha-ionization is fairly well proportional to the particle energy, air is distinctly anomalous in this respect. Thus, should we assume the above relation fulfilled in each gas, we get for a computed

TABLE I. Derived values of $(n-H^1)$ mass difference.

Range-energy curve	$(n-H^1)$ from $N^{14}(n,p)C^{14}$ (measured range =0.991 cm)	$(n-H^1)$ from $He^3(n,p)H^3$ (range =0.980 cm)	Mean of $(n-H^1)$ from the two determinations
Uncorrected Bethe-Livingston	0.751 Mev	0.754 Mev	0.753 Mev
Corrected Bethe-Livingston	0.771	0.782	0.777
Parkinson, Herb, Bellamy, Hudson	0.822	0.845	0.833

energy for the Sm alpha (Po = 5.298 Mev) 2.18 Mev from our argon comparison and only 2.07 Mev in air, a distinct discrepancy far above the experimental error.

If air behaves in the anomalous manner which these preliminary measurements would indicate, the effect of such behavior on the alpha-range-energy curves in current use is at once apparent. The energy-range curve derived from the very careful measurements of Holloway and Livingston,[4] for instance, is in reality an ionization in air-range curve. The authors have themselves explicitly stated that the validity of their relative energy values depends upon an assumed proportionality between the alpha-particle energy and the total ionization in air produced by it. If this condition is not fulfilled, as our preliminary measurements would indicate, then corrections to their energy values must be made, particularly in the region of lower alpha-energies.

Such corrections in the region from 1 to 3 Mev we have attempted to make from our measurements above. This results in raising the energy values of the Holloway-Livingston curve in this region by amounts varying from 60 to 130 kev. The maximum correction appears to fall at about 1.5 Mev. This is the region where the present curve is known to give much too low energy values for the measured ranges, as for example in the (n,α) reaction for B^{10}. From a compilation of data by L. H. Gray[5] based on the original ionization measurements of Gurney we have computed corrections to the range-energy curve almost identical with our own. Finally, we have found in the literature a limited number of reactions where alpha-ranges in air have been determined and elsewhere reaction energies independent of range measurements. The plotted points in all such cases are in better agreement with the corrected curve than with the original.

It should be emphasized that our energy values still rest upon the assumption of the proportionality between alpha-energy and alpha-ionization in argon. We have merely assumed that argon is a gas much superior to air in this respect—an assumption we think, well justified by our own experience and that of others.

We have also attempted to correct the proton[6] range-energy curve from the corrected alpha-curve. This would seem logical, since in the region above about 0.3 Mev the proton curve was apparently derived from the alpha-curve by use of the equation $R_H(E)=1.0072R_\alpha(3.971E)-c$ where R and R_H denote, respectively, the corresponding alpha- and proton-ranges and $c=0.20$ cm is an empirical constant introduced by Blackett to account for the difference in behavior of protons and alpha-particles at low energies. Obviously, a change in the alpha-curve necessitates a change in the proton curve. The energies for the corrected Livingston-Bethe proton curve are slightly higher than in the original (about 20 kev at range 1 cm) but still much lower than in the curve derived from the data of Parkinson, Herb, Bellamy, and Hudson.

Perhaps the most interesting aspect at the moment of the corrected proton range-energy curve is the effect it will have upon the energies derived from the proton range determinations by Hughes and Eggler[6] in the (n,p) reactions for N^{14} and He^3 and their bearing upon the now uncertain $(n-H^1)$ mass difference. Table I shows the derived values for $(n-H^1)$ from the three possible range-energy curves. The beta-end points have been taken as 155 kev and 19 kev for C^{14} and H^3, respectively. It will be seen that the use of the corrected curve raises the $(n-H^1)$ value derived from the proton ranges from a value in good agreement with the formerly accepted value of 0.755 Mev to a value 0.777, about halfway between the former value and the new Chalk River[7] value of 0.804 Mev. Probably the greatest uncertainty in the value 0.777 Mev lies in the uncertainty in the empirical Blackett constant c, which uncertainty affects equally the corrected and uncorrected L and B curves. A minor uncertainty may lie in the assumption mentioned above as to the energy-ionization relation in argon for alpha-particles.

[1] W. P. Jesse and H. Forstat, Phys. Rev. **73**, 926 (1948).
[2] W. P. Jesse and H. Forstat, Phys. Rev. **74**, 1259 (1948).
[3] L. H. Gray, Proc. Camb. Phil. Soc., **40**, 95 (1944).
[4] M. G. Holloway and M. S. Livingston, Phys. Rev. **54**, 18 (1938).
[5] M. S. Livingston and H. A. Bethe, Rev. Mod. Phys. **9**, 245 (1937).
[6] D. J. Hughes and C. Eggler, Phys. Rev. **73**, 809 (1948).
[7] R. E. Bell and L. G. Elliot, Phys. Rev. **74**, 1552 (1948).

Radiative Corrections to the Klein-Nishina-Formula

R. SCHAFROTH
Swiss Federal Institute of Technology, Zurich, Switzerland
February 21, 1949

IT is well known that the new developments in quantum electrodynamics allow the computation of the radiative corrections to various first-order effects.[1] We have applied these methods to the scattering of light by a charged particle of spin ½.[2] The calculation was first carried through using the older methods of perturbation theory in momentum space. After subtraction of the photon and particle self-energy-operators,[3] one can interpret the remaining divergencies (for high momenta) as a charge renormalization.[4] This charge renormalization must take place in such a fashion that in the extreme non-relativistic limiting case the corrections disappear (compare reference 2). In addition, one obtains integrals which diverge for small photon momenta, and which in a known way are compensated by the scattering cross section for the double Compton effect.[5] The formulas can then be transformed into x space where they are seen to be gauge and Lorentz invariant. Since these formulas are very long, we reserve their publication for a later detailed paper. The evaluation leads to the same uniqueness difficulties as in the case of the Lamb-Retherford shift and the anomalous magnetic moment of the electron.[6] The investigation of these difficulties is now under way. The detailed calculation for the non-relativistic limiting case (that is, limiting our results to terms $\propto k^2\log k$, but neglecting terms $\propto k^2$ where k is the momentum of the photon in the rest system of the particle) gives for the correction to the differential cross section:[7]

$$d\sigma_6=(r_0^2/137)(d\Omega/4\pi)(k/m)^2\{[1+\cos^2\vartheta][2\log(k/m)+(8/3)\log(\omega/m)]-(8/3)[1+\cos^2\vartheta]\cos\vartheta\log(\omega/m)-(4/3)[1-\cos^2\vartheta]\cos\vartheta\log(k/m)\},$$

where k is the momentum of the photon, m the mass of the electron, r_0 the classical electron radius,[8] ϑ the scattering angle, $d\Omega$ the solid angle element, and ω the cut-off radius of the double Compton effect. Thus $d\sigma_6$ is the cross section for a process in which, in addition to the scattered photon (ϑ), at most one of momentum $\leqq\omega$ is emitted.

I am very grateful to Professor Pauli for his kind interest in this work and also to Dr. Res Jost, who suggested this

topic and helped by many stimulating and valuable discussions.

[1] J. Schwinger, Phys. Rev. 73, 415 (1948); H. W. Lewis, Phys. Rev. 73, 173 (1948); S. T. Epstein, Phys. Rev. 73, 177 (1948); J. Schwinger, Phys. Rev. 74, 1439 (1948); J. Schwinger, papers in press; S. Tomonaga, Phys. Rev. 74, 224 (1948); S. Tomonaga, Prog. Theor. Phys. Vol. 1, 2, 3.
[2] E. Corinaldesi and R. Jost, Helv. Phys. Act. 21, 183 (1948).
[3] J. French and V. Weisskopf, in press.
[4] D. Feldman and J. Schwinger, Bull. Am. Phys. Soc. 23, No. 7, 17 (1948), have also noticed the fact that the divergencies can be written as mass and charge renormalization. See also Z. Koba & G. Takeda, Prog. Theor. Phys. 3, 202 (1948).
[5] F. Bloch and A. Nordsieck, Phys. Rev. 52, 54 (1937); R. Jost, Phys. Rev. 72, 815 (1947).
[6] A typical result of this lack of uniqueness is to be found in the work of G. Wentzel, Phys. Rev. 74, 1070 (1948), on the photon self-energy.
[7] This formula has been reported by Professor Pauli at the 1948 Solvay congress.
[8] These notations agree with the notations of Jost and Corinaldesi (reference 2), except that these authors define the classical electron radius in Heaviside units; that is, in our notation their result is to be multiplied by $16\pi^2$.

Local Production of the Penetrating Particles in Extensive Showers

G. SALVINI AND G. TAGLIAFERRI
Institute of Physics, University of Milan, Milan, Italy
February 7, 1949

IN a previous letter[1] we reported that associations occur in the side distribution of the penetrating particles of extensive showers, and we inferred therefrom that the penetrating particle are partly produced in the absorbers, and in groups. A similar result was obtained by Broadbent and Jànossy,[2] while Cocconi and Greisen[3] and Treat and Greisen[4] have recently disagreed with our conclusion.

Further examination of our data confirms our earlier belief, and suggests some explanation for resolving the disagreement.

Indeed, the experimental layouts were rather different: the results of Broadbent and Jànossy, and ours, are obtained with a large amount of absorber above the counters (30 cm lead, and 30 cm lead or 10 cm lead +30 cm iron, respectively); moreover, Broadbent and Jànossy used a large unshielded counter area, so that extensive showers with low mean density had a very high probability of being detected (e.g., for a shower of 10 particles/m^2 the probability was ~0.9). On the contrary, Treat and Greisen employed a comparatively small unshielded counter surface (e.g., for a shower of 10 particles/m^2 the probability was $\sim 10^{-3}$), and only a 15.5-cm lead absorber.

TABLE I. An example from our experimental results of the dependence of associations on the extensive shower density. The same notations of our previous letter are used, and only the shielded counters P_1, P_2, F_1, F_2 are taken into account. Column (1): order of the coincidences between the unshielded counters. Column (2): number of coincidences between at least the two counters F_1, F_2 and the showers of column (1). Column (3): number of coincidences between at least the two counters P_1, P_2 and the showers of column (1). Column (4): sum of column (2)+column (3). Column (5): number of coincidences between one counter in the set X+one counter in the set Y, and the showers of column (1). In column (4) and (5) are considered the implications of all complex events: for instance, a coincidence $F_1+F_2+P_1+P_2$ contributes two events to column (4) and four events to column (5). Column (6): ratio column (4)×2/column (5); obviously this ratio indicates the degree of association: its value would be the unity for no association. The factor 2 takes in account the different probability of obtaining the coincidences of column (4) and column (5).

(1)	(2)	(3)	(4)	(5)	(6)
$A_1+A_2+B+C+D+L+M+N$	21	15	36±6	53±8	1.36
A_1+A_2+at least one of the counters B, C, D, L, M, N	41	40	81±9	85±10	1.91
Time (minutes)		20,690			

Cocconi and Greisen had an intermediate experimental arrangement at sea level.

Our disposition,[1] which employed self-recording counters, points out a dependence of the associations on the extensive shower density. We have observed (see Table I) that the associations occur essentially in the showers of low average density. This result may explain the observed experimental differences.

Several arguments confirm the opportunity of employing large unshielded counter surfaces and thick absorbers in these measurements.

A complete report is being submitted to the "Nuovo Cimento."

[1] G. Salvini and G. Tagliaferri, Phys. Rev. 73, 261 (1948).
[2] D. Broadbent and L. Jànossy, Proc. Roy. Soc. A192, 364 (1948).
[3] G. Cocconi and K. Greisen, Phys. Rev. 74, 62 (1948).
[4] J. E. Treat and K. Greisen, Phys. Rev. 74, 414 (1948).

Nuclear Moments of Silver

M. F. CRAWFORD, A. L. SCHAWLOW, W. M. GRAY,* AND F. M. KELLY**
McLennan Laboratory, University of Toronto, Toronto, Canada
February 14, 1949

THE AgI resonance line $5s^2S_{\frac{1}{2}}-5p^2P^0_{3/2}$ (3281A) has been excited in an atomic beam light source and its hyperfine structure resolved with an aluminium-coated Fabry-Perot etalon. The structure observed agrees with that reported by Jackson and Kuhn[1] from absorption measurements.

Spectrograms were taken with 2-, 4-, and 5-cm etalons. The pattern obtained with the 2-cm etalon showed two components due to magnetic h.f.s. with the isotopic components unresolved. The 4-cm pattern showed two strong components just resolved and two weak ones well resolved. With the 5-cm etalon the resolution of the strong components was better, but as expected the magnetic structure due to the $^2P_{3/2}$ level was not resolved. The relative wave numbers of the four components in decreasing order are: (a) 0.000, (b) −0.013, (c) −0.055, (d) −0.077 cm^{-1}. The relative intensities of these components, corrected experimentally for self-absorption in the atomic beam are: $(a):(b)=1.00:1.05\pm0.03$; $(c):(d)=1.05\pm0.03:1.00$; $(a)+(b):(c)+(d)=1.00:0.33\pm0.02$. These values and the recent abundance ratio[2] of the silver isotopes agree with the assignment of components (a) and (d) to Ag^{109} and components (b) and (c) to Ag^{107}, and show that $I=\frac{1}{2}$ for each isotope. The isotope shift is very small, 0.004 cm^{-1}, in agreement with the conclusions of Jackson and Kuhn.

The nuclear magnetic moments of the two isotopes have been evaluated using the Goudsmit[3] formula with the addition of the Fermi-Segrè[4] correction factor determined from a Rydberg-Ritz formula. This correction which was not applied by Jackson and Kuhn is 23 percent. The nuclear magnetic moments are negative and $\mu(\mathrm{Ag}^{107})=-0.084$ and $\mu(\mathrm{Ag}^{109})=-0.155$ nuclear magneton.

A correction for the finite size of the nucleus[5] raises these values about 2 percent, giving finally $\mu(\mathrm{Ag}^{107})=-0.086$ and $\mu(\mathrm{Ag}^{109})=-0.159$ nuclear magneton. This correction will be discussed in a forthcoming paper by two of the authors.

The structure of the $5s^2S_{\frac{1}{2}}-^2P_{\frac{1}{2}}$ transition (3383A) confirms these conclusions.

* Holder of a fellowship from the Research Council of Ontario.
** Holder of a fellowship from the National Research Council of Canada.
[1] D. A. Jackson and H. Kuhn, Proc. Roy. Soc. A158, 372 (1937).
[2] J. R. White and A. E. Cameron, Phys. Rev. 74, 991 (1948).
[3] S. Goudsmit, Phys. Rev. 43, 636 (1933).
[4] E. Fermi and E. Segrè, Zeits. f. Physik 82, 729 (1933) and Reale Accad. D'Italia—Scieze Fisiche, Mat. E. Naturali Memorie 4, 131 (1933).
[5] J. E. Rosenthal and G. Breit, Phys. Rev. 41, 459 (1932).

Proceedings of the American Physical Society

MINUTES OF THE MEETING OF THE OHIO SECTION AT COLUMBUS, FEBRUARY 19, 1949

THE 1949 Mid-Winter Meeting of the Ohio Section of the American Physical Society was held in the Mendenhall Laboratories of The Ohio State University at Columbus on Saturday, February 19, 1949, with an attendance of one hundred and fifty. The program consisted of an invited paper by M. L. Pool "Nuclear Physics since the New York Meeting;" a contributed paper by Thomas Phillips "An Attempt to Define Temperature," and five other contributed papers of which the abstracts are appended.

LEON E. SMITH, *Secretary*

New Measurements of the Infra-Red Fundamental Bands of NH_3. DARWIN L. WOOD, *The Ohio State University.*—The four fundamental bands of the ammonia molecule have been measured with better resolution than formerly attainable. The perpendicular band ν_4 at 1627 cm^{-1} was measured in a vacuum grating spectrograph using an interrupted radiation beam and a thermocouple detector. The strong water vapor band at 1595 cm^{-1} has made it difficult to obtain good resolution in this region in the past,[1] but in the present work this difficulty was practically eliminated. The parallel band ν_2 near 10μ was measured in an open spectrograph with a 2-meter focus. A Golay pneumatic detector was used with an interrupted radiation beam. It was possible also in this band to improve somewhat on previous resolution of the fine structure.[2] In the 3μ region (ν_1 and ν_3) the results obtained with the vacuum spectrograph were substantially the same as those of Dennison and Hardy.[3] It is believed that with the improved resolution of the fine structure of the bands it will be possible to fit the theory of the tetrahedrally symmetric molecule to the observed spectra with more satisfaction than in the past.

[1] E. F. Barker, Phys. Rev. **55**, 657 (1939).
[2] Sheng, Barker, and Dennison, Phys. Rev. **60**, 786 (1941).
[3] D. M. Dennison and J. D. Hardy, Phys. Rev. **39**, 938 (1932).

The Measurement and Analysis of Some Infra-Red Bands of HCN. I-SHAN CHEN AND E. E. BELL, *The Ohio State University.*—Previous high resolution work on HCN by Choi and Barker[1] yielded complete rotational resolution only for the perpendicular vibration band ν_2 and partial resolution of the band $2\nu_2$. The rotational structure of the vibration bands ν_3, $2\nu_3$, $2\nu_2$, and $\nu_1+\nu_2$ have now been completely resolved with the vacuum grating spectrometer described by Bell, Noble, and Nielsen.[2] By use of the combination principles, the band centers and rotational constants have been determined as follows:

Band	Frequency cm^{-1}	$(B'-B'')$ cm^{-1}	B'' cm^{-1}
$2\nu_2$	1411.42	+0.0065	1.4776
$\nu_1+\nu_2$	2804.2	−0.0096	(1.4693)
ν_3	3311.68	−0.0102	1.4763
$2\nu_3$	6520.7	−0.0211	(1.4670)

By making measurements in an evacuated spectrometer the interference of water vapor in the $2\nu_2$ band was eliminated. Gratings of 7500, 7200, and 3600 lines per inch were used, and a chopped beam Perkin-Elmer thermocouple detection system was used for all bands except $2\nu_3$. The $2\nu_3$ band was obtained in an unevacuated spectrometer with a PbS photo-conductive detection system. The Contour and positions of the bands $\nu_1+\nu_3$ and $\nu_2+\nu_3$ were also obtained.

[1] K. N. Choi and E. F. Barker, Phys. Rev. **42**, 777 (1932).
[2] Bell, Noble, and Nielsen, Rev. Sci. Inst. **18**, 48 (1947).

The Performance of a Simple Helium Liquefier. J. G. DAUNT, C. V. HERR AND A. A. SILVIDI, *Ohio State University.*—A simple helium liquefier working on the Simon expansion principle has been in operation in the Mendenhall Laboratory for some time and details of its construction and performance are given. It enables the liquid helium to be transferred into exterior Dewar vessels in which experimental equipment can be maintained at 1°K for many hours.

The Physical Significance of the Reciprocal Lattice. ALFRED LANDÉ, *The Ohio State University.*—A crystal may be characterized by its lattice structure as well as by its reciprocal lattice. Whereas the space lattice is the basis of the wave theory of diffraction according to Laue and Bragg, the reciprocal lattice forms the background of a particle theory of diffraction, as first proposed by P. Duane. The Ewald sphere construction of the diffracted rays by means of the reciprocal lattice is but a construction in momentum space for the quantized momenta given out by the crystal and transferred to the incident particles.

A Proposed Loading of Piano Strings for Improved Tone. FRANKLIN MILLER, JR., *Kenyon College.*—An ideally stiff string has overtones ν_n which are sharper than multiples of the fundamental, the inharmonicity being proportional to n^2. This well-known theoretical result has been verified by Schuck and Young[1] for some typical strings. It is proposed to improve the tone of a piano string by attaching a small mass, thus lowering the frequency of each normal mode except those for which the mass is at a node. It turns out that for an ideally stiff string approximate correction of a large number of overtones can be obtained with a single mass suitably located. In the limit of a large mass close to an end of the string, the correction is exact for all overtones. A mass of the order of 0.1 g placed a few cm from an end of a typical string adjusts the first eight overtones to within a few hundredths of a semitone, a negligible inharmonicity. Improved tone is expected since the subjective fundamentals derived from difference tones between adjacent partials will have greatly reduced dispersion. The effect of the loading upon tuning would reduce the observed stretching of the octaves to a negligible amount. Deviations from ideal stiffness and the effect of adding 2 masses are also considered.

[1] O. H. Schuck and R. W. Young, Jr., Acous. Soc. Am. **15**, 1 (1943).

THE AMERICAN INSTITUTE OF PHYSICS

INCORPORATED

57 East 55 Street New York 22, N.Y.

MEMBER SOCIETIES:

American Physical Society
KARL K. DARROW, *Secretary*, Columbia University, New York 27, New York.

Optical Society of America
ARTHUR C. HARDY, *Secretary*, Massachusetts Institute of Technology, Cambridge 39, Massachusetts.

Acoustical Society of America
WALLACE WATERFALL, *Secretary*, 57 East 55th Street, New York 22, New York.

Society of Rheology
EARL K. FISCHER, *Secretary*, Institute of Textile Technology, Charlottesville, Virginia.

American Association of Physics Teachers
R. F. PAUSH, *Secretary*, University of Illinois, Urbana, Illinois.

AFFILIATED SOCIETIES:

American Society for X-Ray and Electron Diffraction
Electron Microscope Society of America
Physical Society of Pittsburgh
Physics Club of Chicago
Physics Club of Philadelphia
Cleveland Physics Society
Physics Club of the Lehigh Valley

ASSOCIATES:

Over seventy-five leading industrial enterprises and other institutions which contribute to the support of the Institute.

JOURNALS:

The Physical Review
JOHN T. TATE, *Editor*, University of Minnesota, Minneapolis, Minnesota.

Reviews of Modern Physics
J. W. BUCHTA, *Editor*, University of Minnesota, Minneapolis, Minnesota.

Journal of the Optical Society of America
GEORGE R. HARRISON, *Editor*, Massachusetts Institute of Technology, Cambridge, Massachusetts.

The Journal of the Acoustical Society of America
FLOYD A. FIRESTONE, *Editor*, 3312 Forrester Street, N.W., Washington, D. C.

American Journal of Physics
THOMAS H. OSGOOD, *Editor*, Michigan State College, East Lansing, Michigan.

The Review of Scientific Instruments
GAYLORD P. HARNWELL, *Editor*, Randal Morgan Laboratory of Physics, University of Pennsylvania, Philadelphia, Pennsylvania.

The Journal of Chemical Physics
JOSEPH E. MAYER, *Editor*, Kent Chemical Laboratory, University of Chicago, Chicago 37, Illinois.

Journal of Applied Physics
ELMER HOUTERMANS, *Editor*, Case Institute of Technology, Cleveland 6, Ohio.

Physics Today
DAVID A. SAXON, *Editor*, American Institute of Physics, 57 East 55 Street, New York 22, New York.

OFFICERS

GEORGE R. HARRISON, *Chairman*
Massachusetts Institute of Technology

WALLACE WATERFALL, *Secretary*
The Celotex Corporation

GEORGE B. PEGRAM, *Treasurer*
Columbia University

JOHN T. TATE,
Adviser on Publications
University of Minnesota

GOVERNING BOARD

LUIS W. ALVAREZ
J. W. BEAMS
WALLACE R. BRODE
E. U. CONDON
W. F. FAIR, JR.
HARVEY FLETCHER
GEORGE R. HARRISON
W. V. HOUSTON
PAUL KIRKPATRICK
PAUL E. KLOPSTEG
F. W. LOOMIS
PHILIP M. MORSE
J. R. OPPENHEIMER
GEORGE B. PEGRAM
HAROLD K. SCHILLING
JOHN T. TATE
WALLACE WATERFALL
M. W. WHITE
A. G. WORTHING

Consultant on Printing
MELVIN LOOS

ADMINISTRATIVE STAFF

HARRY A. BARTON, *Director*

THEODORE VORBURGER,
Business Manager

RUTH F. BRYANT,
Publication Manager

BETTY HOVSTADTER, *Office Manager*

EILEEN B. NEUBERGER,
Circulation Manager

THE American Institute of Physics was founded in 1931 as a federation of leading societies in the field of Physics. It combines into one operating agency those functions on behalf of physics which can best be done by the Societies jointly. Its purpose is the advancement and diffusion of physics and its applications to human welfare. To this end it publishes for itself or the Societies the nine journals listed on this page; promotes unity and effectiveness of effort among all who are interested in physics; renders numerous direct services to physicists and to the public; and cooperates with government agencies, national associations, educational institutions, technical industries, and others in such manner as to realize the opportunities and fulfill the responsibilities of physics as an important and constructive human activity.

CONTENTS

THE PHYSICAL REVIEW SECOND SERIES, VOL. 75, NO. 7 APRIL 1, 1949

Disintegration of Sb^{122}. MICHEL TER-POGOSSIAN, J. EUGENE ROBINSON, AND C. SHARP COOK 1041
Some Excitation Functions of Bismuth . . . . . E. L. KELLY AND E. SEGRÈ 1043
Experimental Determinations of Stopping Powers Using Alpha-Particles of 15 to 37 Mev . . . . . E. L. KELLY 1047
Neutron Diffraction Studies of Order-Disorder in Alloys . . C. G. SHULL AND SIDNEY SIEGEL 1051
New Measurement of the Binding Fractions of the Nickel Isotopes . . . . . A. E. SHALY 1061
Microwave Investigations of Methyl Fluoride, Fluoroform, and Phosphorus Trifluoride . . . . . O. R. GILLIAM, H. D. EDWARDS, AND WALTER GORDY 1066
Characteristic Radiations of Francium (142) . . . . . C. E. MANDEVILLE 1077
Radioactive Isotopes of Platinum and Gold . . . . . GEOFFREY WILKINSON 1089
Boundary Conditions and Range of Force for ^3S State of Two Protons . . . . . G. BREIT AND W. G. BOUWKAMP 1092
Separation of Gas Mixtures Flowing through a Long Tube at Low Pressure . . . . . R. D. PRESENT AND A. J. DEBETHUNE 1099
Density Spectrum of Extensive Air Showers of Cosmic Rays . . . . . G. COCCONI AND V. COCCONI TONGIORGI 1100
Penetrating Particles in Extensive Cosmic-Ray Air Showers . . . . . G. COCCONI, V. COCCONI TONGIORGI, AND K. GREISEN 1104
Range of Cascade Showers in Lead . . . . . K. GREISEN 1117
Some Properties of the Cosmic-Ray Ionizing Particles That Generate Penetrating Showers . . . . . G. COCCONI 1124
On the Quantization of a Unitary Field Theory . . . . . R. J. FINKELSTEIN 1128
On the Canonical Reduction of Quadratic Forms . . . . . R. G. HELMBERG 1138
Remarks on the Evolution of the Expanding Universe . . . . . RALPH A. ALPHER AND ROBERT C. HERMAN 1143
Relation between Half-Life and Energy in Alpha-Decay . . . . . I. PERLMAN, A. GHIORSO, AND G. T. SEABORG 1144

Letters to the Editor:

Effect of Small Angle Scattering on Neutron Cross Section Measurements . . . . . H. H. A. ENDICOTT, D. MINERBRETTI, G. R. RINGO, AND L. WIENSTEIN 1145
Angular Distribution of Protons from Photo-Disintegration of the Deuteron . . . N. C. LANGER 1147
Gamma-Rays from Sn^{117} and Sn^{119} . . . . . J. EUGENE ROBINSON, MICHEL TER-POGOSSIAN, AND C. SHARP COOK 1148
Radioactive Tantalum Isotopes Produced from Gold . . . . . D. A. ORTH, L. MARQUEZ, W. J. HERMAN, AND D. H. TEMPLETON 1149
On the Hole Theory of the Quantum Transistor . . . . . KURT LEHOVEC 1150
On the Difficulty of the Meson Theory of Nuclear Forces . . . . . GERTRUD ARAKI 1151
Microwave Spectrum of Methyl Bromide . . . . . A. HARRY SHARBAUGH AND JOHN MATHIEU 1152
Erratum: Screening and Radiative Effects on Beta-Spectra . . . C. LONGMIRE AND H. BROWN 1154
Electronic Eigenfunctions in Ionic Crystals . . . . . RISHIGHI NOZAWA 1154
Approximate Relation between Liquid He^4 Between 1.27° and 2.79°K . . . . . E. R. GRILLY, E. F. HAMMEL, AND S. G. SYDORIAK 1155
Space-Charge Wave Amplification Effects . . . . . V. A. BAILEY 1156
Alpha-Radioactivity in Bismuth: Lighter Gas Bismuth . . . . . N. E. BALLOU 1157
Determination of the Energy of Ir^{192} by Means of Interpolation . . . . . TIBOR Z. SZEKELY 1158
Energy of Beta-Rays from Ir^{192} . . . . . J. J. FLOYD AND L. B. BORST 1159
Exchange Measurements on the Odd Electron . . . . . R. AVERY AND R. N. ADAMS II 1160
Radioactivity of Ir^{192} . . . . . ROBERT W. STOUT 1160
Beta-Ray Spectra of Co^{60} and the Ratio of $K+/K-$ . . . . . C. S. WU AND R. D. ALBERT 1161
Fundamental Band of Carbon Monoxide at 4.9μ in the Solar Spectrum . . MARCEL V. MIGEOTTE 1162
Shape of the Beta-Spectrum of the Forbidden Transition of Yttrium 91 . . . . . LAWRENCE M. LANGER AND H. CLAY PRICE, JR. 1167
Threshold Energy for Photon Production . . . . . WALTER H. BARKAS 1169
Erratum: On the Relativistic Correction of the Internal Conversion in the K-Shell; the Electric Dipole Case . . . . . B. A. GRIFFITH AND J. P. STABLER 1170
Alpha-Particle Scattering by Argon and in Air and the Range-Energy Curves . . . . . WILLIAM P. JESSE AND JOHN SADAUSKIS 1170
Radiative Corrections in the Weiss-Nishina Formula . . . . . H. SCHAFROTH 1171
Local Production of Penetrating Particles in Extensive Showers . . . . . G. SALVINI AND G. TAGLIAFERRI 1172
Nuclear Moments of Gallium . . . . . M. F. CRAWFORD, A. L. SCHAWLOW, W. M. GRAY, AND F. M. KELLY 1173

Proceedings of the American Physical Society

Minutes of the Meeting of the Ohio Section in Columbus, February 24, 1949 1175

LANCASTER PRESS, INC., LANCASTER, PA.